Chapter 1

Literature review

1.1 Background

The requirement for bone graft substitutes in today's world is expanding rapidly. Demand for such alternative treatments is driven by issues with current products (autografts, allografts and xenografts), an aging population, an increase in the frequency of injuries and changes in patient care strategies (Lauzon *et al.* 2012). Tissue engineering and regenerative medicine markets in Europe were shown to be worth €1.25 billion in 2008 and are projected to reach €2.6 billion by 2013. Within tissue engineering, bone replacement graft product sales were valued at €588 million in 2007 and are projected to reach €807 million by 2014 (Frost and Sullivan 2011). Currently the synthetic materials used in bone tissue engineering include but are not limited to polymers, bioceramics, polymer composites, growth factors and stem cells. In light of this, the market for bone graft substitutes will continue to expand making synthetic bone graft substitutes using hydrogels and hydrogel based composites a more viable and attractive option for bone regeneration.

1.2 Tissue engineering

The word ***tissue*** refers to a collection of cells within an extracellular matrix (ECM) that play a key role in cell structural support and act as a regulator of cell behaviour. ***Engineering*** refers to the design and building of structures. It is therefore unsurprising that tissue engineering involves the fundamental understanding of structure-function relationships in normal and diseased tissues, as well as the development of biological substitutes that restore, maintain and improve tissue function (Langer and Vacanti 1993). In the case of *in vitro* tissue engineering, cultured cells are grown on scaffolds that provide physical and chemical cues to guide differentiation and assembly into three dimensional structures. Tissue regeneration takes place by replicating the original tissue through cellular migration, inhibitory interactions, proliferation/apoptosis, differentiation and tissue patterning/morphogenesis. The basic principles behind the process of tissue engineering are illustrated in Figure 1.1.

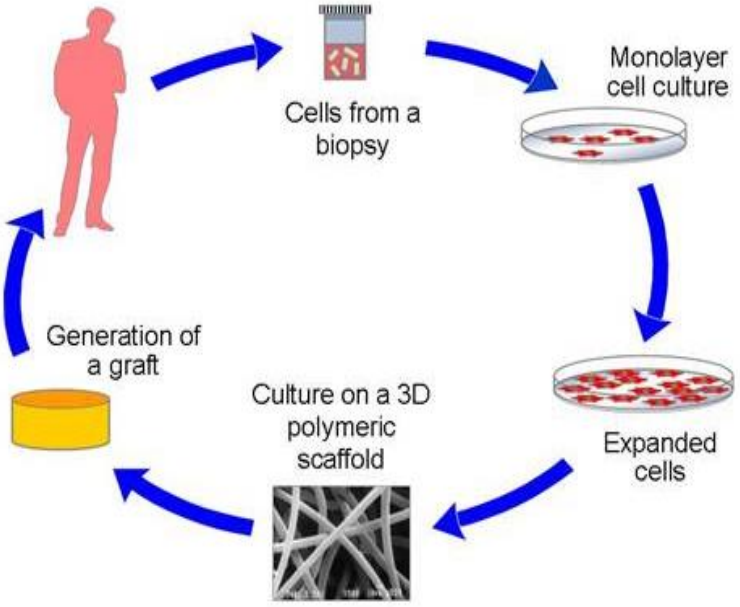

Figure 1.1 *Basic illustration of tissue engineering process* (Mayorga *et al.* 2010)

Tissue engineering can involve a wide range of tissue types, such as ectodermal, endodermal and mesodermal derived tissues (Ratner *et al.* 2002).

- *Ectodermal derived tissues*: nervous system, cornea and skin.
- *Endodermal derived tissues*: liver, pancreas and kidneys.
- *Mesodermal derived tissues*: cartilage, bone, muscle, blood vessels, heart valves and blood.

1.3 Bone

1.3.1 Structure and material properties

Bone plays an essential mechanical role by providing structural support to muscles and tendons. It also provides physical protection to the inner organs. It is a unique type of connective tissue that is strong, lightweight, anisotropic and structurally organised into several hierarchical levels. The remodelling of bone takes place along local stress field lines in order that the mechanical properties of the tissue be optimised (Bertram and Swartz 1991). Bone is a natural composite material consisting of 50-60wt% inorganic components (mainly calcium and phosphate, Ca/P ratio of 1.67), 20-30wt% organic components (mainly ECM

consisting of several proteins, with the main ECM being collagen type 1 >90%) and 10-20wt% water (Oyen 2008). The organic component collagen is highly crosslinked due to both intermolecular and intramolecular crosslinks. This causes a low level of solubility (Barone *et al.* 2011). Collagen orientates the deposition of minerals and promotes cell attachment to the bone. The mechanical properties of different bone types can be seen in Table 1.1.

Table 1.1 *Mechanical properties of cortical and trabecular bone (Boyan et al. 1999)*

Bone Type	Compressive strength (MPa)	Elastic modulus (GPa)	Flexural strength (MPa)	Flexural modulus (GPa)
Cortical bone	170	7-30	180	20
Trabecular bone	40-60	0.05-0.5	-	2
Adult mandible	90-140	2-10	-	5-12
Adult vertebra	-	0.1-0.25	-	-

Bone can be separated into two types based on structural composition: cortical and trabecular bone (Figure 1.2):

- *Cortical bone*: or compact bone, is composed of highly organised concentric rings (lamellae) of densely packed collagen fibrils in perpendicular planes. This structure gives rise to its strength considering the porosity of cortical bone is approximately 5-10%. The mechanism causing the formation of compact bone is known as endochondral ossification (Ulici *et al.* 2009). This process involves mineralisation of cartilage at the centre, which is replaced by bone through the introduction of osteoblast cells.
- *Trabecular bone*: or cancellous bone, is the inner layer of long bones, the same site that is the storage house for bone marrow and has a porosity ranging from 30-90% (Amirfeyz and Bannister 2009). The mechanism of

trabecular bone differs from cortical bone as it's based on intramembranous ossification, whereby the bone is formed directly.

The main cells contained within bone are osteoblasts, osteocytes and osteoclasts.

- *Osteoblasts*: They synthesise and deposit uncalcified new bone matrix (or osteoid). Osteoblasts are active in bone development and also in bone remodelling.
- *Osteocyctes*: multinucleate cells that secrete acids and enzymes in order to dissolve bone matrix.
- *Osteoclasts*: These cells secrete acids and enzymes to break down the mineralized bone matrix. Osteoclasts remove pre-existing bone.

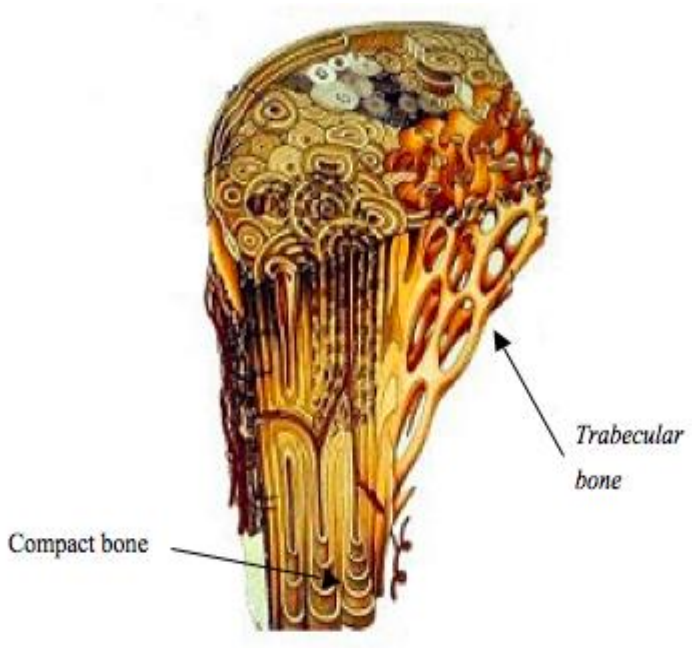

Figure 1.2 *Cortical and trabecular bone (Fr 2012)*

1.3.2 Bone regeneration

The formation of new bone, or bone remodelling, is a continuous process throughout an individual's lifetime. Remodelling takes place in response to various loadings, i.e. tension, torsion and compression. It is estimated that humans remodel approximately 10% of their bone volume each year. The rate of

remodelling is based on the function and coordination of osteoclasts and osteoblasts in the resorption and formation of new bone as shown in Figure 1.3. Osteoblasts produce factors that recruit, stimulate, proliferate, and activate osteoclasts. This is a balanced system where bone resorption stimulates bone formation. In most cases, if given sufficient time and in the presence of the appropriate environment, the natural process of bone regeneration allows bone to be restored back to its original functionality, i.e. microcracks. However, if a defect becomes too large to heal on its own, surgical measures through manipulation or augmentation are required to restore the natural healing mechanism (Cypher and Grossman 1996).

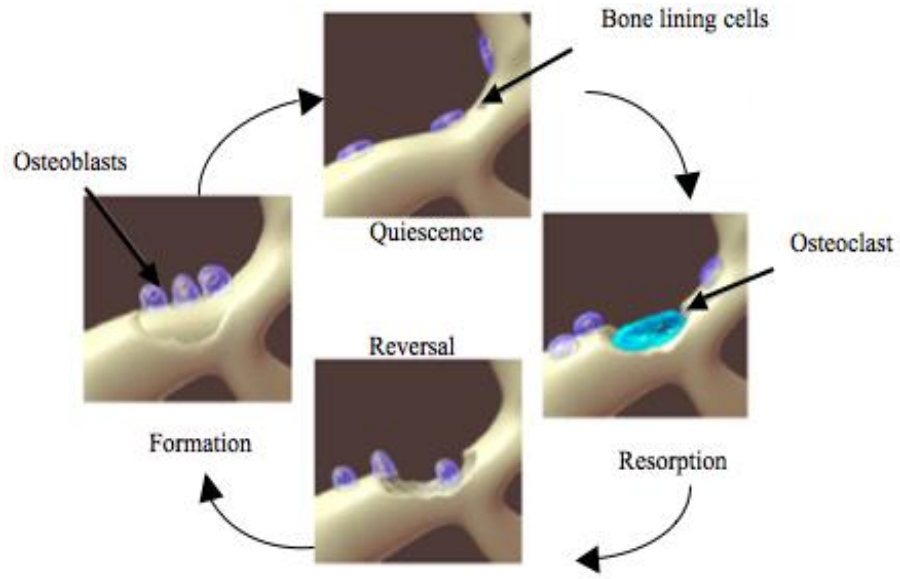

Figure 1.3 *Bone remodelling cycle (Coxon et al. 2004)*

1.3.3 Bone repair

In 2006 it was estimated that 36 million Americans suffered from bone related diseases. In the same year, three million of these people were diagnosed with fracture related injuries (Calori *et al.* 2007). Studies have approximated that 5–10% of fractures result in impaired healing, which can cause a delayed union or non-union in the bone tissue engineering (Tzioupis and Giannoudis 2007). The most serious kind of bone defect is a critical size defect (CSD). A CSD is the diameter of a bone beyond which complete calcification of the defect will not

occur during the lifetime of the injured animal (Schmitz and Hollinger 1986). Some situations such as severe trauma, defects in specific parts of the skeleton, defects in elderly patients, or defects in the presence of metabolic diseases, result in CSDs that may require additional stimulations in order to heal completely. In general, biological activities attributed to bone repair enhancers are classified as either osteogenic, osteoconductive or osteoinductive (Bauer and Muschler 2000). The most frequently used strategies to stimulate bone healing are bone-grafts, biomaterial implants (Sowmya *et al.* 2011), growth factors (Vo *et al.* 2012) and cell therapy (Albrektsson 2001).

1.3.3.1 Biological bone grafts

Bone grafting is a common surgical procedure which can solve the problem of delayed union or non union. It has been estimated that 2.2 million grafting procedures are performed worldwide each year. Currently there are three main types of biological grafts: autografts, allografts and xenografts.

1. *Autografts*: An autograft involves harvesting bone from one location in the patient's body and transplanting it into the defect of the same patient, i.e. a self-transplant of tissue. This biological graft represents 58% of current bone substitutes. Autografts are the gold standard of bone grafts because they avoid most issues related to transfer, infection or rejection. The bone is often harvested from the iliac crest and can be either trabecular or cortical tissue (Barone *et al.* 2011). Advantages of using autografts include clinical experience and their osteoconductivity, osteoinductivity and osteogenicity. Autografts do however have some limitations including a painful harvesting procedure, the possibility of donor site morbidity, chronic donor shortages and dependency on donor quality (Giannoudis *et al.* 2005).
2. *Allograft*: This type of grafting procedure differs from autografts in that the bone is harvested from one human and implanted into another. The harvesting comes from processing bone from a cadaver and transplanting it into the patient’s defect. Thus, there is a risk of

immune response and possible disease transmission with allografts (McGuire and Hendricks 2007). In order to minimise this risk, prior to placing the allograft into the patient, the graft must be thoroughly sterilised. The quality of allografts is inferior to that of autografts. Allografts have a poor degree of cellularity, there is less revascularisation than with autografts, and they have a higher resorption rate compared to autografts. These factors collectively result in a slower rate of new bone tissue formation (Goldberg and Stevenson 1987; Bullens *et al.* 2009).

3. *Xenografts*: The bone tissue from this type of biological graft is harvested from a different species prior to implantation into the patient's defect. One advantage of these grafts is the ability to create them in various shapes and sizes. However, they do present the risk of immunological reactions and infections, handling issues and poor initial strength (Calori *et al.* 2011).

1.4 Scaffold design requirements

Scaffolds effectively provide a platform for tissue formation. Oftentimes various cell types and growth factors are incorporated into the scaffold prior to implantation. To date, countless scaffolds have been synthesised using an array of biomaterials in an effort to regenerate tissues (such as bone) that have been damaged. Every specific tissue type has a number of design requirements that affect the appropriateness of any particular scaffold or material for the use in tissue engineering. Below, the defined scaffold requirements for bone tissue engineering are briefly summarised. They are: biocompatibility, mechanical properties, vascularisation, degradation, sterilisation, bioactivity and manufacturing technology.

1.4.1 Biocompatibility

The first and one of the most important scaffold requirements, is that of biocompatibility. Williams (1987) described biocompatibility as "...the ability of a material to perform with an appropriate host response in a specific

application". The key aspects of biocompatibility for scaffolds in tissue engineering are shown in Figure 1.4. Hydrogels and other synthetic scaffolds used in bone regeneration require comprehensive biocompatibility testing as they are intended for implantation and subsequent interaction with host cells and tissue. Previous investigations into the biocompatibility of hydrogels have shown that common sources of toxicity include photoinitiators, chemical crosslinkers, unreacted monomers, stabilisers and organic solvents (Geever *et al.* 2008). However, improvements can be made by optimum selection of photoinitiators as well as photoinitiator concentration and use of macromolecular monomers. Karaca *et al.* (2010) showed that minimisation of oxygen inhibition by photoinitiator selection promotes biocompatibility of the hydrogel while Studer *et al.* (2003) showed that minimisation of photoinitiator concentration leads to improved biocompatibility.

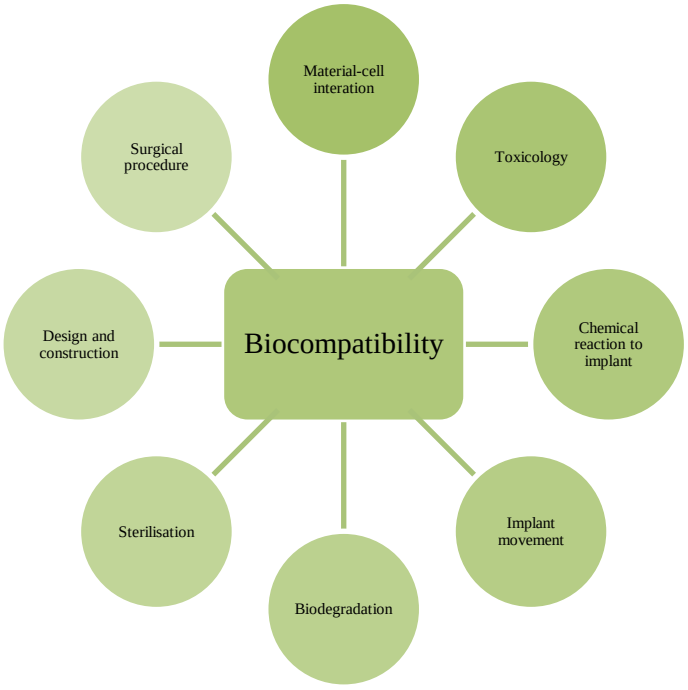

Figure 1.4 *Biocompatibility aspects between implant and the body*

1.4.2 Mechanical properties

Mechanical properties play a vital role in the success of the scaffold. Scaffolds must provide mechanical stability within the defect until full

regeneration of tissue has occurred. The mechanical forces affect the remodelling and homeostasis for tissues that are load-bearing, i.e. bone and cartilage (Horan *et al.* 2005; Puppi *et al.* 2010). In the case of hydrogels, the mechanical properties can be controlled by alternating the methods of crosslinking and the length of the polymer chain.

Stiffness of the underlying surface has been shown to affect cellular behaviour; it is believed that when the compressive modulus of the underlying substrate matches the tissue modulus *in vivo*, cells exhibit behaviour that more closely mimics physiological behaviour (Hutmacher 2001). A study by Chung *et al.* (2006) showed that in 2D culture, proliferation of osteoblasts was enhanced on stiffer poly(N-isopropylacrylamide-co-acrylic acid) gels when compared to softer gels. Gel stiffness was also shown to influence the differentiation of cardioprogenitor 3D cell constructs in PEG hydrogels (Kraehenbuehl *et al.* 2008). Chatterjee *et al.* (2010) studied the response of osteoblasts to variation in 3D hydrogel modulus (accomplished by varying the PEGDA composition, without the use of bioactive factors). It was found that osteoblasts preferentially differentiated on scaffolds where the compressive modulus matched that of mineralised bone tissue *in vivo*. It was also shown that hydrogels of modulus 225kPa or higher were required for induction of significant mineralisation.

1.4.3 Vascularisation

The majority of all tissues in the human body are vascularised. Vascularisation (formation of new blood vessels in adult tissue) is a key requirement for scaffold design because it supplies a base for nutrient exchange and elimination of waste by perfusion (Slaughter *et al.* 2009). A scaffold thus should contain a porous surface and microstructure. This allows in-growth *in vitro* cell adhesion and reorganisation for adequate vascularisation *in vivo* (Puppi *et al.* 2010). Pore interconnectivity directly influences the diffusion of physiological nutrients to cells. It also assists in the removal of metabolic waste and by-products from cells (Vacanti *et al.* 1988; Mikos *et al.* 1993). If a scaffold has a too high a degree of porosity, this will have a detrimental effect on its mechanical properties. Therefore, there is a need for a balance between these two

important properties when considering the design of a successful scaffold (O'Brien 2011).

1.4.4 Degradation

Degradation is necessary in tissue regeneration applications. Ideally, in bone regeneration, the rate at which a scaffold degrades in the defect should mimic the rate of new bone formation, allowing cells to produce their own extracellular matrix. In addition, as the scaffold degrades, the by-products should be non-toxic. In the case of hydrogels, there are two methods in which degradation can occur: hydrolysis and enzymatic cleavage. In most cases, synthetic hydrogels degrade through hydrolysis of ester linkages (Drury and Mooney 2003; Chwalek et al. 2011). Scaffolds can also be made degradable by incorporating cleavable groups into the backbone of the polymer.

1.4.5 Bioactivity

Bioactivity or biomineralisation refers to the interaction of cells or tissues on the surface of an implant by activating a specific response (Vallet-Regí *et al.* 2008). Biomineralisation is a biological process that occurs in virtually all living organisms. In biomineralisation, the scaffold has the ability to deposit a mineral layer onto the surface of the substrate. In the case of bone repair, this deposit mineral can be composed of hydroxyapatite $Ca_{10}(OH)_2(PO_4)_6$ or hydrocarbonate apatite layer. Studies have shown that this mineralisation layer allows cells to stimulate new bone formation through the process of adhesion, proliferation and differentiation. Hench and West (2006) identified two classes (A and B) of bioactive materials for bone regeneration. Class A, are bioactive materials in which the scaffold materials have osteoproduction and osteoconduction at the implant surface. The second category, Class B, occurs when only bioactivity of osteoconduction results (Hench and West 2006). Biomineralisation *in vitro* can be attained using different methods such as simulated body fluid, urea-mediated solution mineralisation, enzymatic method, alternative soaking in calcium and phosphate solutions and direct incorporation of hydroxyapatite into polymers.

The three main factors associated with bioactivity which are essential for bone growth are osteoinductivity, osteogenicity and osteoconductivity (Demirkiran *et al.* 2010). Osteoinductivity refers to the scaffolds ability to activate bone formation in a non-bony site. Osteogenicity is the ability of bone cells, i.e. osteoblasts to mineralise and form a calcified extracellular matrix. Osteoconductivity is the ability of the scaffold to continue the process of mineralisation by providing a substrate where cells can adhere, proliferate and differentiate.

1.4.6 Sterilisation

Medical devices or implants introduced into the human body temporally or permanently must be sterile to avoid subsequent infection. Sterilisation is the process by which living cells are killed or removed to the extent that they are no longer detectable in standard cultured media in which they had previously been found to proliferate. Material scientists consider sterilisation related issues early in the developmental process so that the final product can be readily sterilised and have an acceptable shelf life. There are three sterilisation techniques currently used and each has their own advantages and drawbacks:

- *Autoclaving*: This technique involves exposing the implantable material to saturated steam under pressure at 121°C. The advantages of this system are efficacy, speed and low cost, however most implants are non-metallic and depending on polymer melt temperature, they cannot be sterilised by this method.
- *Ethylene oxide (EtO):* In this sterilisation process EtO gas infiltrates the material to kill existing micro organisms. EtO is very efficient at low temperatures and has high penetration capabilities, but the formation of EtO residues can occur in the product subsequent to the process, limiting EtO sterilisation for *in vivo* applications.
- *Radiation:* This method of sterilisation utilises ionising radiation, which can be divided into two separate processes: gamma and electron-beam radiation. Gamma radiation uses Cobalt(60) and Cesium(127) radioisotopes while electron-beam radiation uses high-

energy electrons ranging between 3-10 million volts. Gamma radiation is a straightforward process that can be easily measured and controlled through dosimetry. The drawback of this technique is that the process time is very long. On the other hand, electron-beam radiation provides much shorter exposure time (<1min), but has limited effectiveness depending upon the penetration thickness of the products and can cause chain scission and crosslinking within the material affecting its mechanical properties (Murray *et al.* 2013).

1.4.7 Manufacturing technology

The manufacturing of a scaffold for tissue engineering presents many major challenges. When considering scaffolds for bone tissue engineering this is especially true, largely because of the necessary porous architecture of the materials. The main challenges involved in the manufacturing of scaffolds include the synthesis of a material and the process by which the material can be formed into a three-dimensional device (Hollister 2009). After solving these problems in the laboratory, the scaffold must be scaled up to manufacturing conditions, while still maintaining its material parameters and its cost effectiveness. Synthetic bone graft substitutes that have successfully made it to market include:

- Orthograft (Depuy, 1985) composed of β-TCP bioceramic.
- INFUSE Bone Graft, Medtronic 2002 composed of type 1 collagen soaked in growth factor.
- Vitoss Scaffold FOAM, Orthovita 2004 composed of collagen type 1 porous foam and β-TCP.
- FortrOss, Pioneer Surgical 2008 composed of nanocrystalline hydroxyapatite and porcine collagen polymerised with dextran.
- IngeniOs (Zimmer, 2012) composed of 100% non-biologic pure phase hydroxyapatite.
- Novabone putty (Novabone, 2012) composed of bioactive glasses mixed with synthetic binders.

1.5 Biomaterials

A biomaterial is a manufactured synthetic or natural material that is used to replace part of a living system or provide intimate contact with living tissue for a significant period of time. The main function of biomaterials is to interact with biological systems to evaluate, treat, augment or replace a tissue, organ or function of the body. A number of definitions for biomaterials have been developed over the years and modified with rapid advancement in technology. In the United States, the legal definition for biomaterials is "*...a systemically, pharmacologically inert substance designed for implantation within or incorporation with a living system.*" This definition was developed by the Clemson Advisory Board (Black 1981). Later this definition was updated to "*...any pharmacologically inert material, viable or non viable, natural product or manmade, that is a part of or is capable of interacting in a beneficial way with a living organism*". The most commonly accepted definition for biomaterials was developed by Williams (1987) and it states that a biomaterial is "*...any nonliving materials used in medical devices intended to interact with biological systems*".

Following implantation of a biomaterial into the body, the tissue surrounding the implant will react in different ways. This reaction will depend on the material type and the mechanism of tissue interaction. There are three main classifications for representing the tissue response with a biomaterial: bio-inert, bioactive and bioresorbable (Jayaswal *et al.* 2010). A bio-inert response refers to a minimal interaction between material and its surrounding tissue *in vivo*. These materials in general result in being encapsulated by a fibrous tissue. A bioactive response refers to the integration of the material with the surrounding tissue. This occurs through the modification of the substrate, initiated after implantation *in vivo*. A bioresorbable response refers to the degradation of material when placed *in vivo*. Ideally, an implant will be bioresorbable and will degrade at the same rate as the new tissue is formed.

Table 1.2 *Classification of tissue response to biomaterials (Hench and Wilson 1993; Jones and Hench 2003; Hing 2005)*

Classification	Tissue Response	Implant/tissue bond	Examples
Bio-inert	Formation of fibrous membrane surrounding implant	None	Polyethylene glycol, alumina and zirconia
Bioactive	Formation of interfacial bond with implant	Chemical	Hydroxyapatite and bioactive glasses
Bioresorbable	New tissue formation replaces degrading scaffold	Chemical	Polylactide, polycaprolactone, tricalcium phosphate

1.5.1 Hydrogels

An evergrowing class of biomaterials are the polymeric hydrogels. By definition, hydrogels are polymeric networks with three-dimensional configuration capable of imbibing large amounts of water or biological fluids. Since the first publication concerning hydrogels in the 1960's (Wichterle and Lim 1960), which was based on hydroxyethyl methacrylate (HEMA) hydrogels, the number of papers published in this field has increased exponentially. A hydrogel's ability to absorb water is due to the presence of hydrophilic groups such as -OH, -CONH-, -$CONH_2$, -COOH, and - SO_3H (Peppas and Khare 1993). Due to their hydrophilic nature, they can absorb 10-20wt% in aqueous media and up to thousands of times their dry weight. Hydrogels can be tailored by varying porosity, pore size, surface to volume ratio, compressive modulus, topography and wettability which makes them a promising candidate for bone regeneration. Their advantages and limitations in tissue engineering are shown in Table 1.3.

Table 1.3 *Advantages and disadvantages of hydrogels as scaffolds in tissue engineering (Hoffman 2002)*

Advantages	Disadvantages
Aqueous environment can protect cells and fragile drugs	Can be hard to handle
Good transport of nutrient to cells and products from cells	Usually mechanically weak
May be easily modified with cell adhesion ligands	May be difficult to load drugs and cells and crosslink
Can be injected *in vivo* as a liquid that gels at body temperature	*In vitro* as a prefabricated matrix
Usually biocompatible	May be difficult to sterilise

1.5.1.1 Hydrogel crosslinking

Hydrogels maintain their structure due to the crosslinks present within their network. There are two main types of crosslinking found in hydrogels; chemical crosslinks and physical crosslinks (shown in Figure 1.5).

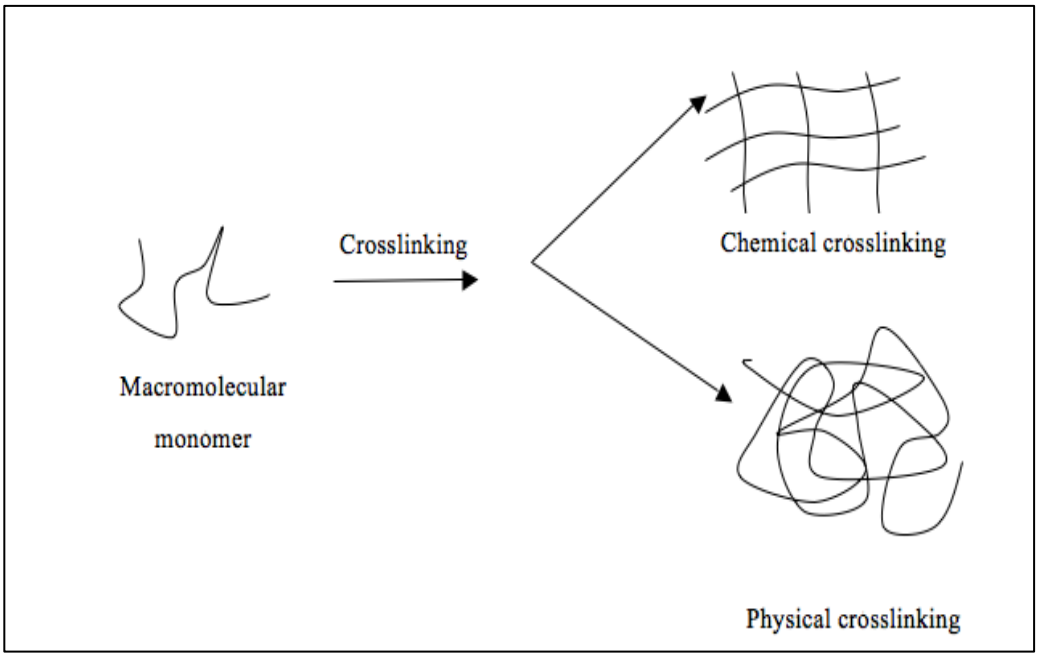

Figure 1.5 *Schematic of crosslinking methods for formation of hydrogels*

1.5.1.1.1 Chemical crosslinking

Chemical crosslinks are three-dimensional molecular networks formed from the introduction of primary covalent bonds. These hydrogels will not dissolve in aqueous solution unless chemical or physical cleavage processes can break the covalent bonds. The main methods of chemically crosslinking hydrogels are shown in Figure 1.6 and they include:

1. *Radical polymerisation* through monomers in the presence of crosslinking agent (Geever *et al.* 2008).
2. *Chemical reaction of complementary groups*: covalent linkages between chains can be established by the reaction of functional groups with complementary reactivity, i.e. crosslinking by condensation reaction (Crescenzi *et al.* 2003).
3. *High energy radiation* of gamma and electron beam to polymerise unsaturated compounds (Zhao *et al.* 2003).

1.5.1.1.2 Physical crosslinking

Alternatively, physically crosslinked hydrogels are held together by molecular entanglement, and/or secondary forces. They do not require the

introduction of external crosslinking agents and this will help promote their biocompatibility. Physically crosslinked hydrogels can be formed by:

1. *Ionic interactions* such as with a polysaccharide with mannuronic and glucuronic acid residues which are crosslinked by calcium ions (Hu and Chou 1996).
2. *Crystallisation* through the process of numerous cycles of freeze thawing (Smith *et al.* 2009).
3. *Amphiphilic block and graft copolymers* which assemble in organised structures such as micelles (Förster and Antonietti 1998).
4. *Hydrogen bonding* for example between the oxygen in PEG and the carboxyl group of PMAA (Fu *et al.* 2007).

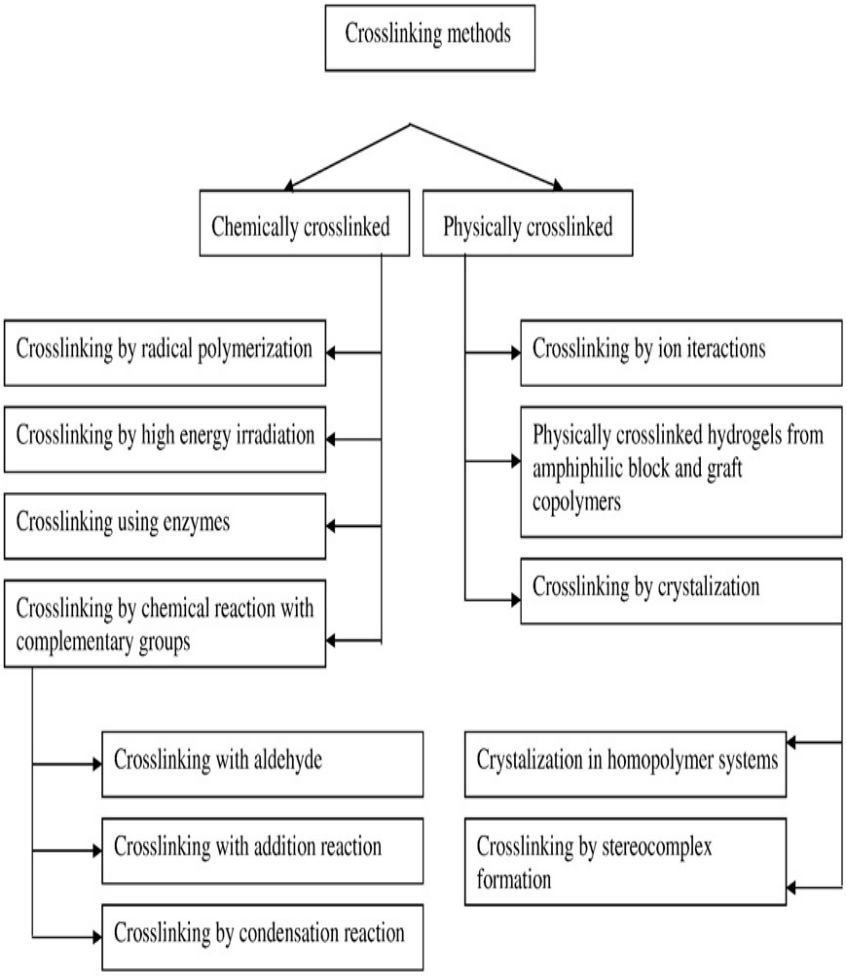

Figure 1.6 *Methods of crosslinking hydrogels (Hamidi et al. 2008)*

1.5.1.1.3 Interpenetrating networks

Hydrogels can also contain networks consisting of both chemical and physical crosslinks. These hydrogels are called interpenetrating networks (IPNs). IPNs have properties that either retain the characteristics of the single networks (chemical or physical crosslinks) or are an average of the two independent networks (Elisseeff *et al.* 2000). Lee and Kurisawa (2013) synthesised IPNs consisting of different synthetic and biological polymer combinations with mechanical properties much enhanced when compared to their independent components.

1.5.2 Hydrogels in tissue engineering

1.5.2.1 Synthetic hydrogels

Synthetic hydrogels are appealing for use in tissue engineering because their chemistry and properties are controllable and reproducible. Synthetic polymers can be fabricated with specific molecular weights, block structures, degradable linkages and crosslinking modes. These properties in turn, determine gel formation dynamics, crosslinking density and material mechanical and degradation properties (Drury and Mooney 2003). Two of the most commonly used synthetic hydrogels include poly(ethylene glycol) and poly(vinyl alcohol):

- Poly (ethylene glycol) (PEG) is US Food and Drug Administration (FDA) approved due to its biocompatibility and low toxicity. It has potential used in several tissue engineering applications including bone (Ma *et al.* 2010) and cartilage applications (Bodugoz-Senturk *et al.* 2009). PEG has excellent antifouling properties which produces resistance to protein adsorption (Csucs *et al.* 2003). PEG has been synthesised to contain in excess of 90% water. The advantage of such a high water content is the ability to create an environment suitable for cells which houses an environment that can replicate natural soft tissues (Lin and Anseth 2009). This phenomenon helps enhance biocompatibility and vascularisation, two of the key requirements for scaffold design.
- Poly(vinyl alcohol) (PVA) is obtained from poly(vinyl acetate) through aminolysis, hydrolysis or alcoholysis (Jones 1973). PVA is a hydrophilic

synthetic polymer and has been successfully used in tissue engineering because of its biocompatibility and biodegradation properties. Potential tissue engineering applications include: wound healing (Yang *et al.* 2010), heart valves (Jiang *et al.* 2004), cartilage (Ma *et al.* 2009) and bone scaffolds (Ma *et al.* 2010). PVA hydrogels may be synthesised through various techniques including incorporation of a chemical crosslinking agent, freeze/thaw synthesis and electron beam fabrication.

1.5.2.2 Natural hydrogels

Natural polymeric hydrogels have been frequently used in tissue engineering applications because they are either components of or have macro-molecular properties similar to the natural extracellular matrix (ECM) (Drury and Mooney 2003). Most natural hydrogels have been shown to have weak mechanical properties and potentially exert immunogenicity or evoke inflammatory responses due to the presence of immunogen/pathogen moieties. However, they do tend to offer various advantageous properties, such as biocompatibility and a lack of significant toxicity. Two of the main natural polymers include collagen and chitosan.

- *Collagen* is the most abundant protein found in bone tissue and is also a main component of the extracellular matrices of, skin, cartilage, ligaments and tendons. In total there are approximately 20 members of the collagen family. Of primary interest to tissue engineering are the following classes: type I (bone and skin), type II (cartilage) and type III (vasculature). Collagen can be physically crosslinked or chemically crosslinked. Physically crosslinked hydrogels have limited mechanical properties and are thermally reversible. However, if they are chemically crosslinked with the addition of a crosslinker, i.e. glutaraldehyde (Veríssimo *et al.* 2010), this can significantly improve the mechanical properties of the hydrogels. Furthermore, the mechanical properties of collagen materials are controlled by the process of purification, source of collagen, fibril formation and crosslinking type (Alina 2011).

- *Chitosan* is a natural polysaccharide and is derived by the deacetylation of shell-fish-derived chitin using alkaline solution. Chitosan has been heavily utilised in tissue engineering due to its biocompatibility, biodegradability, antimicrobial activity and its approved status by the FDA. Chitosan has been used as potential scaffolds in numerous tissue engineering applications such as nerve regeneration (Lu *et al.* 2007), drug delivery for cancer therapy (Azab *et al.* 2007), wound healing (Obara *et al.* 2003), cartilage (Jin *et al.* 2009) and bone repair (Wang and Stegemann 2010). Similarly to collagen, chitosan can be crosslinked physically or chemically with glutaraldehyde (Kandile *et al.* 2009), though it does need to overcome low solubility issues in the majority of solvents (Di Martino *et al.* 2005).

1.5.3 Existing materials for bone regeneration

As mentioned previously, hard tissues such as bone and tooth are intended to support loads. Thus these tissues must be stiffer (have a higher elastic modulus) and stronger (have a higher tensile strength) than soft tissues. Since the 1980's, numerous bone graft substitute materials have been synthesised to replace existing biological grafts. These materials are often similar in composition to the mineral phase of bone.

1.5.3.1 Polymers

Many natural and synthetic polymers have been fabricated for use in bone tissue engineering. As discussed previously (p19, Section 1.5.2.2), the demand for natural polymers has increased because of their potential as scaffolds. Their promise as scaffolds is due to two factors; the ability to allow for biological signalling and their cell adhesion properties. Natural polymers can be split into three types, proteins, polysaccharides and microbial polyesters (examples can be seen in Table 1.4). The most abundantly used natural polymer for bone repair is collagen, since 20-30wt% of bone is composed of this compound (p2, Section 1.3.1). Collagen provides the principle structural and mechanical support of bone (Lee *et al.* 2001). Additionally, it has been shown to

develop and express the phenotype of osteoblasts and the formation of mineralised tissue. Numerous fabrication techniques have been employed in the synthesis of collagen to form hydrogels, sheets, foams and scaffolds. Several commercial products have been FDA approved using collagen in bone tissue engineering such as Sunmax (Sunmax Biotechnology), Collagraft (Zimmer) and Healos (Depoy).

Alternatively, synthetic polymers are becoming more attractive since they have predictable and reproducible properties, which can be easily tailored for specific requirements. Polycaprolactone (PCL) and poly(α-hydroxyacids) are the two most investigated synthetic polymers in bone tissue engineering (Miyai *et al.* 2008; Cannillo *et al.* 2010; Sahoo *et al.* 2010; Alves *et al.* 2012). PCL has been studied using different reinforcements, i.e. phosphate glass fibers and hydroxyapatite in intramedullary pins, craniofacial repair and critical sized bone defects.

Table 1.4 *Natural and synthetic polymers used for bone tissue engineering applications*

Polymer	Characteristics	References
Natural		
Collagen	Weak mechanical properties, Good cell adhesion, Low immune response.	(Guillerminet *et al*. 2010; Murphy *et al*. 2010; Tierney *et al*. 2012)
Chitosan	Promotes osteoconduction, Antimicrobial properties.	(Zeng *et al.* 2009; Frohbergh *et al.* 2012)
Starch	Good cell adhesion, Good mechanical properties, Thermoplastic behaviour.	(Santos et al. 2007; Silva et al. 2007)
Hyaluronic acid	Minimal immunogenicity, Low mechanical properties.	(Kim *et al.* 2007; Martínez-Sanz *et al.* 2011; Zanchetta *et al.* 2012)
Synthetic		
Polycaprolactone	Degradation by bulk erosion or hydrolysis, Low chemical versatility, Slow degradation.	(Williams *et al.* 2005; Danesin *et al.* 2012)
Poly-L-lactide	Degradation by hydrolysis, Good mechanical properties.	(Morgan et al. 2007; Hu et al. 2011)

1.5.3.2 Bioceramics

Bioceramics can be defined as biomaterials of the ceramic origin. Bioceramics are biocompatible, hard, brittle materials with exceptional compressive strength; however, they have moderately weak tensile properties. Certain bioceramics can be soluble, biodegradable and resorbable (Jayaswal *et al.* 2010). Bioceramics have numerous applications throughout the body, (Mastrogiacomo *et al.* 2007; Zhai *et al.* 2012), and can be classified as either bioinert (zirconia and alumina) or bioactive (Bioglass) (Best *et al.* 2008). Applications of bioceramics include dental implants, percutaneous devices, bone graft substitutes, total joint replacements and spinal surgeries (Dorozhkin 2010). Bioceramics can be used as porous networks, microspheres and as the reinforcing phase of polymer composites (Jayaswal *et al.* 2010). Types of bioceramics include bioactive glasses and calcium phosphates, as dicussed below.

1.5.3.2.1 Bioactive glasses

This type of bioceramic is based on a random network of silica tetrahedral (Si-O-Si) bonds. The first bioactive glass was synthesised by Hench in 1970 and was composed of 45% SiO_2, 24.5% CaCO, 24.5% NaO and 6% P_2O_5. In the last forty years, various research teams have synthesised different compositions of bioactive glasses based on SiO_2 with the addition of Na_2O, $CaCO_3$ and P_2O_5, among other modifying oxides.

The mechanical properties of bioactive glasses are weaker when compared to other bioceramics, i.e. calcium phosphates. This limitation inhibits their use for load bearing applications. One of the major advantages of bioactive glasses is their ability to undergo surface reaction very rapidly. The mechanism of the surface reaction promotes integration of the scaffold with bone *in vivo* through the formation of a carbonate substituted hydroxycarbonate apatite layer (HCA) (Rahaman *et al.* 2011). This apatite layer has a similar chemical composition to hydroxyapatite of bone. This promotes a strong bond between the scaffold and the bone through the absorption of growth factors, ensued by

attachment, proliferation and differentiation of osteoprogenitor cells (Hench and Polak 2002; Rahaman *et al.* 2011).

The HCA layer results from a sequence of reactions on the surface of the scaffold, which was first described by Hench (1998). This process can be summarised in five steps:

- Step 1: A fast ion exchange occurs between bioactive glass and its network modifiers (Na_2O, $CaCO_3$ and P_2O_5) with H^* ions from the solution. This results in the formation of the silica groups (Si-OH).
- Step 2: An increase in pH causes the attack of the SiO_2 glass network, and the dissolution of silica (into the form of silica acid), $Si(OH)_4$ into the solution. This further increases the formation of silica groups on surface.
- Step 3: An amorphous SiO_2 rich layer is formed on the surface of the glass through the condensation and polymerisation of depleted Na^+ and Ca^{2+}.
- Step 4: As the glass continues to dissolve and the Ca^{2+} and PO^{2-}_4 ions continue to migrate, an amorphous calcium phosphate (ACP) layer forms on the surface of SiO_2 layer.
- Step 5: With further dissolution of bioactive glass, the ACP layer absorbs $(OH)^-$ and $(CO_3)^{2-}$ from the solution and crystallises to form a hydroxycarbonate apatite layer (Rahaman *et al.* 2011).

1.5.3.2.2 Calcium phosphate

As discussed in Section 1.3.1, the inorganic components of bone are made up of calcium and phosphate. They are the most widely used material in bone tissue engineering due to their compositional similarities to bone. There are a number of different types of calcium phosphates and the properties for each one are dependent on the proportion of calcium to phosphorus ions within the structure (Best *et al.* 2008). Different types of bioceramics include calcium phosphates such as α-tricalcium phosphate, β-tricalcium phosphate and hydroxyapatite. These calcium phosphates biodegrade at increasing rates in the following order α-TCP > β-TCP > HAP. The rate of degradation increases and the crystallinity decreases as surface area increases (powders > porous scaffold > solid scaffold).

The mechanism of formation of an apatite layer for calcium phosphates can be seen in Figure 1.7 and differs slightly from that of bioactive glasses and it can be defined in five steps:

- Step 1: The calcium phosphate scaffold surface undergoes ionic dissolution.
- Step 2: Calcium and phosphate precipitate from the external environment onto the scaffold surface.
- Step 3: Continuous ions exchange between scaffold and surround tissue.
- Step 4: An amorphous calcium-phosphate later forms on the surface of the scaffold.
- Step 5: Finally, there is amorphous crystallisation of the calcium phosphate layer which forms apatite.

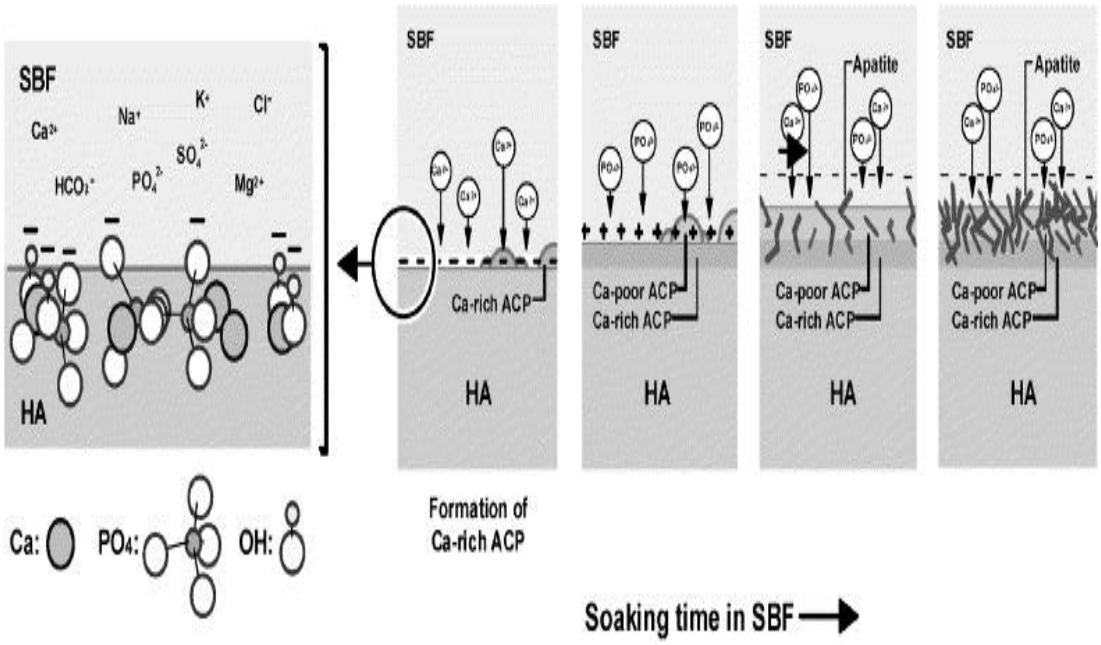

Figure 1.7 *Schematic presentations of apatite formation of hydroxyapatite in simulated body fluid (Kim et al. 2005)*

Hydroxyapatite is a bioresorbable type of bioceramic. It is the most commonly used calcium phosphate due to its chemical similarity to bone (Chu *et al.* 2002; Andronescu *et al.* 2010). Hydroxyapatite, $Ca_{10}(PO_4)_6(OH)_2$, has a theoretical composition of 39.68 wt% Ca and 18.45 wt% P, giving it a Ca/P wt

ratio of 2.151:1 and Ca/P molar ratio of 1.667. Hydroxyapatite products can be used *in vivo* as powders or porous blocks to fill bone defects.

Tricalcium phosphate is a synthetic and biodegradable bioceramic. It has been commonly used in various bone tissue engineering applications such as oral and maxilo-facial surgery (alveolar ridge and sinus augmentation). It has also been widely used for benign bone tumour filling (Yuan *et al.* 2007) and bone cements for vertbroplasty (O'Hara *et al.* 2010, O'Hara *et al.* 2012). Tricalcium phosphate $Ca_3(PO_4)_2$ has a Ca/P molar ratio of 1.5 (Bose and Tarafder 2012).

1.5.3.3 Hydrogel composites

Hydrogel composites are based on binding together a fabricated hydrogel and inorganic reinforcement materials. The composite can contain a polymer-ceramic or polymer-metallic matrix with interpenetrating network microstructures, consisting of bioceramic particles blended in with the polymer phase. Paradigm for the next generation of bone graft substitute materials is that composite hydrogels will be able to fill all the requirements of an ideal scaffold. Hydrogels tend to be over flexible and of insufficient strength to meet the mechanical requirements of bone graft subsitutes *in vivo*. On the other hand, bioceramics have high strength but are very brittle, exhibit low fracture strength, display low mechanical reliably and are difficult to fabricate (Grimm 2004, Vallet-Regi *et al*. 2008). The combination of polymers and bioceramics into hydrogel composite materials could potentially act synergistically to overcome the limitations of either individual component.

Hydrogel based composites can be designed to meet stiffness and strength requirements for hard tissue substitution. A study by Gaharwar *et al.* (2011b) incorporated silicate nanoparticles prior to photopolymerisation of the material and results showed a significant improvement in mechanical properties. The silicate particles also promoted bioadhesion of osteoblasts on the scaffold surface. A similar study by Gaharwar *et al.* (2011a) developed nanohydroxyapatite (nHAP) hydrogels for orthopaedic tissue engineering applications. The PEG-nHAP hydrogels had higher compressive strengths, fracture stresses, and toughness when compared with PEG-based hydrogels. This

improvement in mechanical properties resulted from the interactions between the polymer and nanoparticles, which interfere with the permanent crosslinking of PEG. Bioglasses can also be incorporated into hydrogels. Couto *et al.* (2009) synthesised a novel, injectable, temperature-responsive hydrogel with bioactive glass (SiO_2:CaO:P_2O_5) and chitosan for orthopaedic and tissue regenerative applications.

1.6 Fabrication techniques

A vast number of fabrication techniques have been designed to produce scaffolds for tissue engineering. The fabrication technique used to synthesise a material can greatly affect the material's structure and mechanical properties. Each technique is therefore used for specific tissue engineering applications in order to create a material with optimum scaffold properties. The main methods of scaffold fabrication are described below.

1.6.1 Photopolymerisation

Photochemical initiated polymerisation reactions are well-established techniques for many industrial applications. The field of biomedical technology is currently finding use for photopolymerisation in tissue engineering applications as well (Williams *et al.* 2005). A photoinduced polymerisation reaction takes place when a reaction's initiation step is produced by a photochemical event. Thus on exposure to UV or visible light, a liquid monomer formulation is converted into a solid polymer. If the monomer contains more than one reactive function, a crosslinked polymer network is readily produced. Initiating polymerisation by radiation curing is beneficial as it reduces the need for volatile organic solvents, allows temporal control of initiation and proceeds more rapidly than thermal polymerisation. Most monomers, oligomers, or pre-polymers commonly employed in photopolymerisation do not readily produce sufficient initiating species upon light exposure. Therefore, it is usually necessary to incorporate a photoinitiator that will begin the polymerisation process (Fouassier and Rabek 1995). As UV light energy is absorbed by the photoinitiator, it fragments into free radical or cationic reactive species. There

are also a few cases of initiators (i.e. iodonium and sulphonium salts, arene complexes), which are able to initiate polymerisations via both cationic and free radical processes. The free radical class of initiators represent greater than 90% of commercially used initiator chemistry due to their availability, high quantum yields of radical generation and monomer radical formations. Free radicals initiate the polymerisation process, attacking reactive double bonds on monomer molecules and converting them to a polymer (Moon *et al.* 2005).

Hydrogels are often fabricated using photopolymerisation. Many hydrogels are biocompatible in nature, resulting in minimal inflammatory responses and tissue damage. It is widely understood, that a variety of hydrogels from monomeric precursors require a number of time consuming washing steps to ensure the cytocompatibility of scaffolds. This is mainly due to the presence of minute levels of unreacted monomer following photopolymerisation. Due to this drawback, macromolecular monomers are being used more often because hydrogels synthesised using these materials have been reported to cause a minimal toxicological response without washing steps. Specifically for the purposes of bone regeneration, poly(ethylene glycol) derivatives have been widely investigated and reviewed and have been found to be promising scaffold materials (Zhu 2010).

1.6.2 Solvent casting and particle leaching

Particulate leaching is a very simple, easy and inexpensive fabrication technique (Dietmar 2000). This process involves dissolving a polymer in a solvent with the addition of particles, i.e. porogens. The procedure for creating these scaffolds involves casting a solution into a mould. Once the solvent has evaporated, the particulates are leached out and the empty voids left behind create a scaffold with a porous structure with uniform porosity (Liu *et al.* 2007). Solvent casting works very well with thin membranes, however if the sample cross-section is too thick, it is very difficult to remove the particles from within the polymer matrix (Mikos *et al.* 1994). The advantages of this technique include cost effectiveness, ease of fabrication and greater control of porosity (Subia *et al.*

2010). Disadvantages include the necessary step of removing the porogen, limited mechanical properties and limited thickness (Puppi *et al.* 2010).

1.6.3 Gas foaming

This fabrication method uses supercritical fluid technology to form a porous scaffold. Gas foaming technique is carried out by placing the polymer in a pressure chamber and inputting high pressure carbon dioxide into the scaffold. The carbon dioxide dissolves into the polymer, causing it to become unstable. This leads to phase separation and produces the pores within the scaffold. The advantage of using gas forming as a fabrication technique over solvent casting and particulate leaching is that it does not use any organic solvents, which enhances the biocompatibility of the resultant material. However, scaffolds produced using this technique have limited mechanical properties and poor pore interconnectivity (Ikada 2006). Salerno *et al.* (2010) synthesised a PCL/thermoplastic zein scaffold for bone regeneration using the gas forming technique.

1.6.4 Phase separation

The phase separation technique involves the thermodynamic instability of a polymer; a porous scaffold is created by the division between the polymer rich and polymer poor phases. Currently there are a number of processes used to induce phase separation in mixtures of such polymers. An example of this would be liquid-liquid phase separation. This process creates polymer rich and polymer poor phases in the polymer liquid. Once the polymer poor phase has been removed, the porous scaffold is formed (Lee *et al.* 2004a). The structure of the scaffold is controlled by phase separation conditions (Liu *et al.* 2007), however, it can be difficult to regulate the scaffold morphology (Subia *et al.* 2010). Liu *et al.* (2010) produced macroporous poly(2-hydroxyethylene) methacrylate hydrogels using this technique.

1.6.5 Electrospinning

This technique designs nonwoven fabrics consisting of extremely fine polymer fibers. The method involves applying a high electrostatic field to a capillary connected to a syringe containing a polymer solution. One electrode is placed in the collector and the other in the polymer solution (Subia *et al.* 2010). Electrospinning can produce fibers of varying lengths: from a few nanometers to hundreds of microns (Xu *et al.* 2004). The main advantage of electrospinning is that it can produce scaffolds that are appropriate for tissue and cell growth by controlling the pore size and fiber length. *N*-methylene phosphonic chitosan hydrogels and electrospun nanofibrous hydrogels have been synthesised and results show that they can be both osteoconductive and osteoinductive (Datta *et al.* 2012).

1.6.6 Rapid prototyping

Rapid prototyping technology (RP), also known as solid free form fabrication (SFF), is a computer-controlled technique. It is designed using a set of manufacturing processes capable of creating a patient-specific scaffold from a computer-aided design (CAD) package. Once the 3-D image of the tissue defect (through MRI or CT scan) has been taken and designed in CAD, the machine is ready to form the scaffold, starting with the bottom of the design and working its way up in layers (Puppi *et al.* 2010). Within rapid prototyping there are several techniques, including: stereolithography, selective laser sintering (SLS), fused deposition modeling (FDM) and 3D printing (3D-P). The advantages of RP are complete control of pore size, pore shape, interconnectivity, branching, geometry and orientation. The equipment used to fabricate these hydrogels is very expensive however, and due to the process it can only use a limited set of polymers.

1.6.7 Melt moulding

The process of melt moulding involves mixing/melting polymers in a mould, followed by heating the mould above the glass-transition temperature (T_g) or melt temperature (T_m) of the polymer. Simultaneously, pressure is applied

to the blend where the polymer is bound together. In some instances a porogen is included. Once blended, the moulding is removed and the porogen is leached out. Scaffolds produced using this technique assume the shape of the mould. This process allows independent control over the pore size and porosity, however it does require high temperatures for non-amorphous polymers (Puppi *et al.* 2010). Oh *et al.* (2003) fabricated PLGA/PVA polymer blend for potential use bone tissue engineering via melt moulding.

1.6.8 Freeze drying

Freeze drying is a technique that removes a solvent (usually water) based on the principle of sublimation: a change directly from a solid to a gaseous state, bypassing the liquid state. First the polymer is dissolved in solvent to its required concentration. The mixture is cooled down below its glass transition temperature and the polymer chains are in a frozen state resulting in the formation of ice crystals. Once frozen, the solvent is removed by applying a vacuum pressure and the sublimation cycle produces a highly porous sponge. The porosity can be controlled by the freezing rate (a faster freezing rate produces smaller pores) and pH. Wu *et al.* (2010b) prepared a porous gelatine scaffold for bone regeneration using a unidirectional freeze-drying method.

1.7 Biological considerations

One of the key issues in tissue engineering is the development of suitable materials and scaffolds for the subsequent growth of tissues. A biomaterial must have the appropriate composition and three-dimensional structure to promote cellular proliferation and differentiation, as well as the strength to provide a scaffold for tissue regeneration (Yoshikawa *et al.* 2001). Even within one tissue type, clinical problems are extremely diverse. Thus, no one approach will likely suit all potential applications. An ideal graft should mimic the living tissue from a mechanical, chemical, biological and functional point of view (Murugan and Ramakrishna 2005). In bone tissue engineering, major issues surrounding engineering scaffolds include biocompatibility and bioactivity. The inclusion of factors that signal the induction of new bone formation (an osteoinductive

environment) and supply of a scaffold conductive to new bone formation (an osteoconductive environment) are additional challenges. When using hydrogels, the matrix materials, porosity and pore characteristics, mechanical strength, degradation and surface properties can be optimised to meet the required needs for individual tissues by variation of composition, processing parameters and fabrication processes (Park 2009).

1.8 Osteomyelitis

Osteomyelitis is defined as an inflammation or an infection in the bone marrow and surrounding bone, initiated by pyrogenic bacteria or mycobateria. It can result in bone death, soft-tissue compromise, functional impairment and systemic illness and morbidity (McNally and Nagarajah 2010). Infection is one of the most serious complications resulting from bone graft implantation. When considering biological bone grafts, allografts can result in infection rates of 16% (Mankin *et al.* 1983; Bullens *et al.* 2009; Ketonis *et al.* 2011). This poses a problem with major economic impacts for the healthcare system (Brin *et al.* 2008). Osteomyelitis most commonly takes place in a single bone, but in rare instances it can occur in several bones. In cases of osteomyelitis, the infection causes the bone marrow to swell. This in turn increases pressure within the bone and constricts the blood vessels, reducing blood flow. In severe cases this process can cause parts of the bone to die. The timing and extent of treatment are critical in determining whether the infection develops and causes these complications. Osteomyelitis can be broadly classified as either *acute* or *chronic*, depending on the period of the infection or persistence of the symptoms. Acute is rapid onset of infection and is generally short lived, but chronic is persistent and long lasting (>3months). The most common symptoms of osteomyelitis include pain, swelling, warmth in the bone, drainage of pus through the skin, excessive sweating and chills. Different classifications of osteomyelitis include haematogeous, brodie's abscess, contiguous, chronic, acute and chronic sclerosing osteomyelitis (McNally and Nagarajah 2010).

Pathogens which frequently instigate osteomyelitis include *staphylococcal aureus, enterococci, enterobacteriacae, streptococci,*

propionobacterium acnes, *clostridia* and *nocardia* (McNally and Nagarajah 2010). To overcome these pathogens, drugs such as vancomycin, gentamicin, cefazolin and ciprofloxacin have been effectively used in the treatment of osteomyelitis.

The current treatments for osteomyelitis are conventional or local antibiotic administration methods. Via intravenous treatment, the drug is absorbed into the blood and distributed to various organs and tissues, so only a relatively small amount reaches the target tissue. This is especially the case for bone as it is renown for having poor perfuse properties. Consequently, treatment of osteomyelitis via intravenous methods will require extensive high dose rates which in turn can lead to increased morbidity, repeated operations and lengthy antibiotic treatment (Cheng *et al.* 2010). A new generation of controlled drug release scaffolds are under development which will help overcome the aforementioned difficulties and minimise the risk of post-surgical complications, i.e. infection and inflammation (Cheng *et al.* 2010).

1.9 Controlled drug delivery

The main modes of drug administration include oral, inhalation, parenteral, transdermal and mucosal (Perrie *et al.* 2012). The most common method of drug delivery is via conventional treatments, which require repeated administration. Repeated administration of drugs can result in inconsistent (peak and valley) drug concentrations, meaning that high levels of drug is needed to be administered to reach therapeutic levels for a sufficient period of time. Such methods have two distinct disadvantages: 1) risk of reaching toxic levels, and 2) low compliance by the patient. To overcome these problems, controlled drug delivery systems can be used. Controlled drug delivery dates back to the 1960's, when Folkman and Long first developed an implantable drug release carrier composed of silicone rubber and polyethylene (Folkman and Long 1964). Even after a half a century, today's polymer materials are the most commonly used material for drug release because of their ease of processing and tuneable chemical and physical properties during fabrication. The aim of controlled drug delivery is to deliver the correct drug at the right location, concentration and for

the right period of time. This minimises the disadvantages of conventional methods (Figure 1.8). Controlled drug delivery can be subdivided into three sections: controlled, prolonged and sustained delivery.

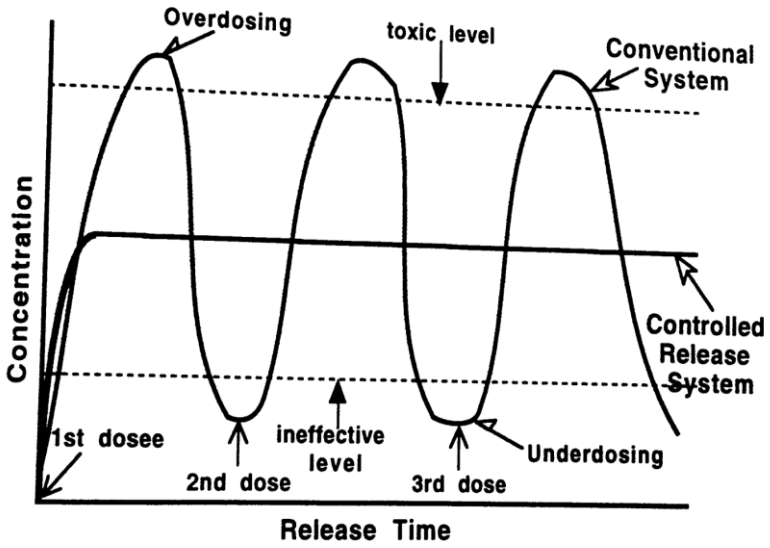

Figure 1.8 *Comparison between convention and controlled drug release systems (Wu 1996)*

1.9.1 Mechanisms of drug release

In controlled drug delivery, there are three mechanisms by which drugs are administered from the scaffold into the body:

- Diffusion of the drug in/out of the scaffold.
- Degradation/dissolution of the scaffold.
- Osmosis or swelling of the scaffold.

1.9.1.1 Diffusion controlled systems

Diffusion controlled systems are the most common mechanism of controlled release. They involve the diffusion of a drug that is embedded within the scaffold Am Ende and Brannon Peppas (1997). Diffusion can be subdivided into two main types (Figure 1.9):

- Matrix devices: these are also known as monoliths. The drug is distributed throughout the whole scaffold.

- Reservoir devices: these can be nonporous or microporous. The drug is surrounded by a rate of controlling polymer membrane.

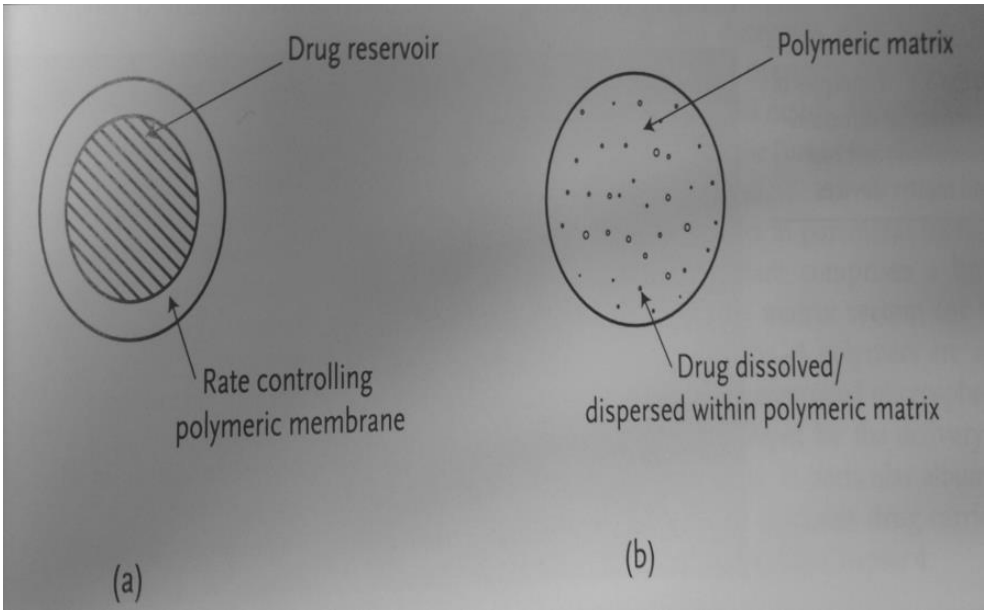

Figure 1.9 *Diffusion controlled reservoir **(a)** and matrix **(b)** systems (Hillery et al. 2001)*

In a matrix system, the polymer and the drug are mixed to form a homogeneous mixture. A typical release profile for this system can be seen in Figure 1.10. The main reason for this phenomenon is that the drug on the scaffold surface releases first (burst release), followed by the release of drug in the centre of the scaffold. The drug in the centre has a greater distance to travel to be released into the system, therefore, it has a longer diffusion time. Various factors can control the release profile for these scaffolds such as quantity of drug, mesh size of the hydrogel, solubility of the drug and molecular weight of the drug.

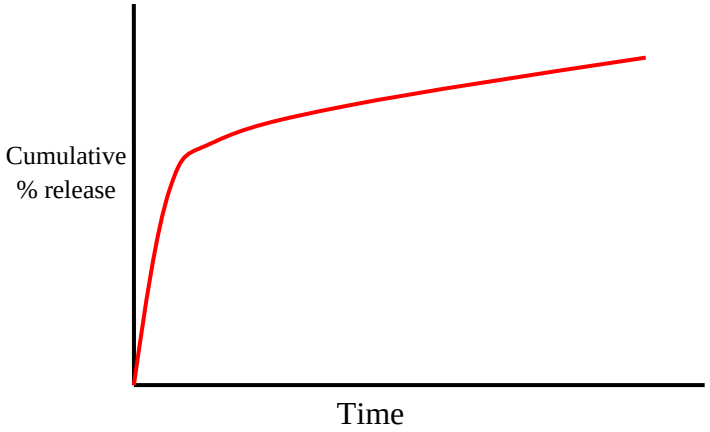

Figure 1.10 *Drug release profile by diffusion of a matrix device*

The second type of device for diffusion is a reservoir device. Reservoir devices follow a zero-order release profile (Figure 1.11). As previously mentioned, they consist of a compacted drug that is surrounded by a polymeric scaffold. Reservoir devices typically follow Fick's Law, which states, "...the rate of transfer of a drug through a material is proportional to the tissue area." Therefore, the factors that control the release profile are dependent on the diffusion coefficient of the drug in the scaffold, the scaffold thickness, the scaffold surface area and the drug concentration.

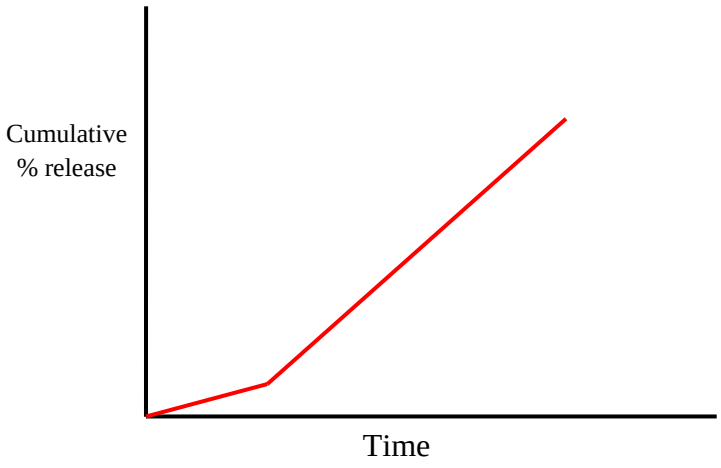

Figure 1.11 *Zero order controlled release profile of a reservoir type device*

1.9.1.2 Swelling controlled systems

The second mechanism of drug delivery is based on swelling controlled release systems of hydrophilic scaffolds. Swelling is defined as the movement of water through a semi-permeable membrane into solution. This mechanism is based on the releasing of the drug via swelling of the scaffold after being placed in biological fluids. The movement of solution into the scaffold results in an increase in pressure, known as the osmotic pressure. Osmotic pressure can be tailored to obtain a constant release rate, i.e. zero-order release. By controlling the osmotic pressure in a scaffold, the release rate is essentially independent of its environment. Hence, the drug release profiles *in vitro* are similar to *in vivo* response.

During swelling, three regions are present in hydrogel scaffolds. Within the first region ("soft rubber") is the outer most region of the hydrogel, which is highly swollen and is relatively weak in comparison to the other regions. The next region is moderately swollen ("tough rubber") and is relatively strong. The centre of the scaffold ("glass") is dry and is in a glassy state.

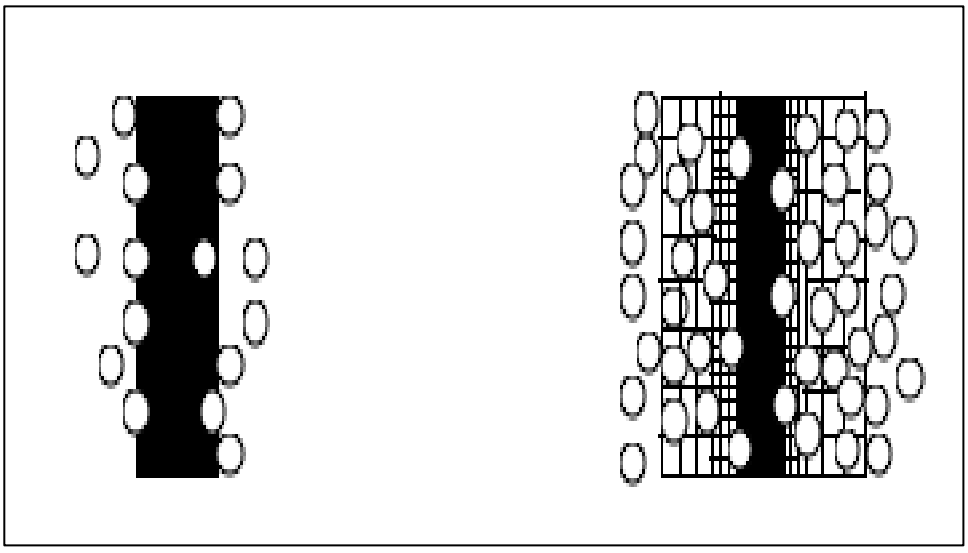

Figure 1.12 *Swelling process for chemically crosslinked hydrogels (*Kaneko *et al.* 1998*)*

1.9.1.3 Degradation controlled systems

In degradation-controlled systems, the drug release profile is influenced by the rate of erosion of the scaffold. Degradation can occur via two methods:

surface or bulk erosion. In the case of bulk erosion, degradation occurs through the whole scaffold; the rate of water penetration into the scaffold exceeds the rate at which the scaffold is transformed into water soluble material (Slaughter *et al.* 2009). Surface erosion differs in that degradation occurs solely at the exterior scaffold. This gives surface erosion an advantage over bulk erosion since the drug release is zero-order irrespective of the physiochemical properties of the drug (Mönkäre *et al.* 2012).

Similar to the diffusion mechanism, dissolution devices can be either matrix or reservoir devices. Matrix devices are scaffolds with evenly distributed drug throughout a polymeric matrix, which dissolves with time, thereby releasing the drug. Reservoir devices are scaffolds in which the drug is encapsulated with a polymer membrane. In this case, the polymer must be water soluble and/or degradable in solution. The dissolution for reservoir devices is controlled by the degradation rate of the polymer and/or thickness of the scaffold.

1.9.2 Hydrogels in drug delivery

Hydrogels are frequently used in drug delivery because of their hydrophilic, biocompatible and controllable release rates. Another advantage of hydrogels is their potential intelligence when triggered by interaction with biomolecular stimuli, i.e. pH and temperature sensitive hydrogels. The degree of swelling, crosslink density, degradation rates and delivery kinetics can be easily controlled for hydrogels. Furthermore, photopolymerisable hydrogels are especially attractive for controlled drug delivery *in vivo* because they can adhere and conform to targeted tissue when formed *in situ* (Slaughter *et al.* 2009). The loading of drugs into hydrogels can occur through three separate methods, which are shown in Figure 1.13. Each approach has its own advantages and disadvantages and the choice of which to use should be based on the hydrogel network and the nature of the drug.

- The simplest method of drug loading is permeation. This involves placing the hydrogel into a medium saturated with the drug. The drug will slowly diffuse into the hydrogel and the amount that diffuses is dependent on the

porosity of the hydrogel, size of drug and chemical properties of both hydrogel and drug. This method is useful for small molecules; however, it releases very quickly *in vivo* and takes some time for the drug to diffuse into the hydrogel.

- Another commonly used method of drug loading is entrapment. In this process, drug is mixed with the polymer prior to crosslinking. After subsequently being placed in solution and crosslinked, diffusion allows for the drug to release out of the network, which leads to an initial burst release.
- The final method is the covalent or tethering method; it limits tissue exposure to the agent but only when the hydrogel breaks down or the molecular tether is broken.

The controlled delivery of bone regeneration factors can be accomplished via biomaterial carrier systems to facilitate local repair at the defect site. The optimal carrier should provide four main functions: 1) site specific delivery of regenerative factors to the defect, 2) local regulation and retention of released factors, 3) enhanced infiltration and proliferation of cells on the three-dimensional substrate and 4) optimised biodegradation for complete tissue regeneration.

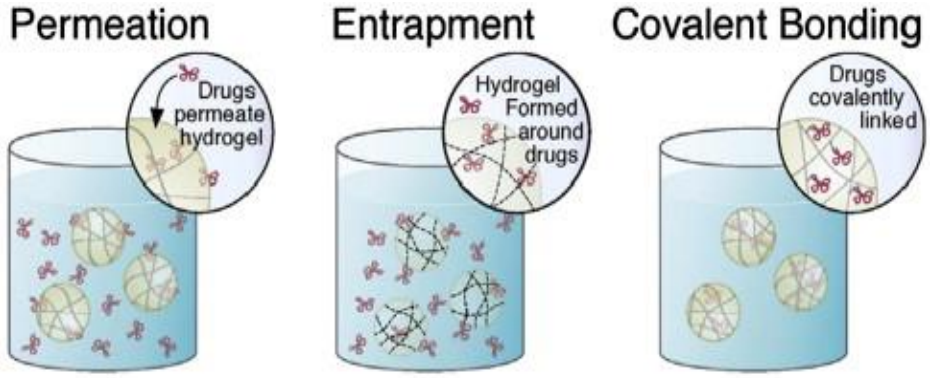

Loadable drugs		
Small molecules	Small molecules, Peptides, proteins, Micro/nanospheres	Small molecules, Peptides, proteins
Network formation		
Physical, covalently crosslinked and IPN gels	Physically and covalently crosslinked gels	Physically and covalently crosslinked gels
In situ gelation		
No	Yes	Yes
Degree of burst release		
High	Moderate	None
	Smart delivery mechanisms	
pH sensitive swelling, polymer dissolution and degradation	pH sensitive swelling, polymer dissolution and degradation	Enzyme sensitive release, polymer dissolution and degradation
Release durations		
Hours to days	Days to weeks	Days to months
Comments		
High loading efficiencies for hydrophilic drugs; Low chance of drug deactivation	Suitable for loading and hydrophobic drugs; Moderate chance of drug deactivation; Chance of toxic material leaching	Best suited for hydrophilic drugs; Possible drug deactivation during polymer bonding

Figure 1.13 *Different loading strategies for hydrogels (Bhattarai et al. 2010)*

1.10 Aims of the project

The overall aim of the research presented in this thesis is to assess novel hydrogel and hydrogel based composite scaffolds for potential use in bone tissue engineering.

The individual research aims can be summarised as follows:

- Assess the effect of the variation in molecular weight and polymer concentration of hydrogels in terms of mechanical properties.
- Photopolymerise a hydrogel that does not require numerous time consuming washing out steps.
- Determine the physical, mechanical and thermal properties of hydrogel blends.
- Synthesise a photopolymerisable material to improve the strength of the hydrogels.
- Determine the optimum bioceramic type and concentration which imparts the greatest enhancement of compressive properties of the hydrogel.
- Examine the behaviour of hydrogel based composites in simulated body fluid in terms of its bioactivity properties.
- Evaluate the antimicrobial properties and drug release profile of optimised samples.

After an extensive literature review, material candidates were selected. Various combinations of polymer blends and bioceramic loadings were investigated using different characterisation techniques, which were in accordance to the literature.

Chapter 2

Experimental details

2.1 Material selection

Previous work carried out in our laboratory involved the synthesis of polymers (using monomers) that required several washing steps to promote biocompatibility (Geever *et al.* 2008). In order to bypass this time-consuming step, the materials selected for this study were chosen based on their potential biocompatibility properties. The platform material in this study was a water soluble macromolecular monomer polyethylene glycol dimethacrylate (PEGDMA), which was selected, based on the known biocompatibility of the polyethylene glycol (PEG) component. To date, much research has been carried out using a different reactive chain end of PEG, diacrylate (DA); however, limited attention has been focused on dimethacrylate (DMA) end chains. The biocompatibility of the hydrogels synthesised was improved upon by changing the type of photoinitiator and lowering its concentration. Previous studies by our research team used 2-3wt% Irgacure 184, however this was replaced with 0.1wt% Irgacure 2959 which has been shown to be more biocompatible than Irgacure 184 (Williams *et al.* 2005).

The second material investigated in this study was polypropylene glycol (PPG), which was chosen based on its hydrophobic properties and also because it is known to be nontoxic in low concentrations. PPG based hydrogels with a series of different reactive chain ends including polypropylene glycol dimethacrylate (PPGDMA), polypropylene glycol diacrylate (PPGDA), and polypropylene acrylate (PPGA) were selected. Polyethylene glycol and polypropylene glycol are structurally identical, with the exception of the additional methyl group in the repeat unit of polypropylene glycol. Thus, this allowed the possibility to study the effect of the additional methyl group on the properties of the hydrogels composed of these materials.

Polyvinyl alcohol (PVA) was selected as the third material for investigation. PVA has potential use in different tissue engineering applications including: skin, liver, cartilage and bone. Various crosslinking methods have been employed using PVA such as freeze/thaw (McGann *et al*. 2009), gamma irradiation (Alcântara *et al*. 2012), and solvent evaporation techniques (Zhang *et al*. 2009). Very few studies have attempted to photopolymerise PVA, especially with the added modification of

attaching a maleic anhydride component in order to create a photopolymerisable material.

The next set of materials utilised were various types of bioceramics, which included one bioactive glass and two calcium phosphates. Firstly, a novel bioactive glass composed of $0.2SrO/0.2Na_2O/0.1CaO/0.1ZnO/0.4SiO_2$ (mol fraction) was synthesised, (material obtained from Dr. Daniel Boyd at the Department of Applied Oral Sciences, Dalhousie University, Halifax, Canada). The glass composition was the result of optimisation of bone graft performance from preceding studies (Murphy *et al*. 2009; Murphy *et al*. 2010). The next bioceramic was hydroxyapatite which was prepared via a wet chemical method (Murugan and Ramakrishna 2004). Finally, the last bioceramic was beta tricalcium phosphate (Sigma Aldrich, Ireland). All of the bioceramics were filtered through a sub 45µm sieve. Detailed below are the lists of the main materials used in this study and their associated chemical structures (Figures 2.1-2.8).

- Polyethylene glycol dimethacrylate with molecular weights 200, 400, 600 and 1000 (*PolySciences, Germany*).
- Polypropylene glycol dimethacrylate 425 (PPGDMA), polypropylene glycol diacrylate 600 (PPGDA) and polypropylene glycol acrylate (PPGA) 425 (*PolySciences, Germany and Sigma Aldrich, Ireland*).
- Maleic PVA synthesis: Polyvinyl alcohol medium molecular weight (M_w 89,000-98,000, 99+% hydrolysed), formamide, p-tolunesulfonic acid monohydrate, maleic anhydride, acetone, cyclohexane and sodium biocarbonate.
- Irgacure® 2959 (*Ciba Specialty Chemicals, Ireland*).
- Beta tricalcium phosphate (*Sigma Aldrich, Ireland*).
- Hydroxyapatite synthesis: Ammonium phosphate dibasic $(NH_4)_2HPO_4$, calcium chloride ($CaCL_2$) and ammonium hydroxide NH_4OH (*Sigma Aldrich, Ireland*).
- Bioactive glass synthesis: Calcium carbonate ($CaCO_3$), strontium carbonate ($SrCO_3$), zinc oxide (ZnO) and silicon dioxide SiO_2 (*Sigma Aldrich, Canada*).
- Dexamethasone (*Sigma Aldrich, USA*).

- Vancomycin (T*ullamore hospital*).
- Buffer salts: Potassium chloride (KCl), potassium biphthalate ($C_8H_5O_4K$), potassium phosphate monobasic (KH_2PO_4) and hydrochloric acid (HCl).
- Simulated body fluid: Sodium chloride (NaCl), sodium bicarbonate ($NaHCO_3$), potassium chloride (KCl), dipotassium phosphate anhydrate ($K_2HPO_4{\cdot}3H_2O$), magnesium chloride ($MgCl_2{\cdot}6H_2O$), calcium chloride ($CaCl_2$) and sodium sulphate (Na_2SO_4).

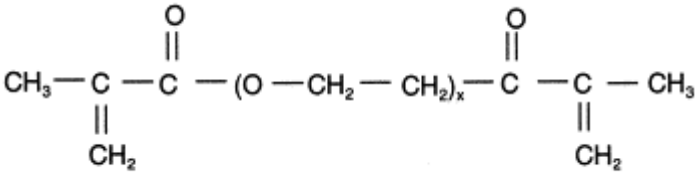

Figure 2.1 *Chemical structure of polyethylene glycol dimethacrylate (PEGDMA) (Yasmin et al. 2011)*

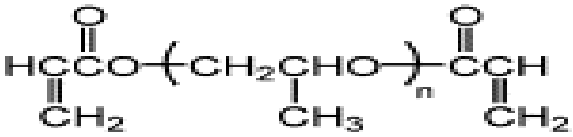

Figure 2.2 *Chemical structure of polypropylene glycol diacrylate (PPGDA)(Lee et al. 2004c)*

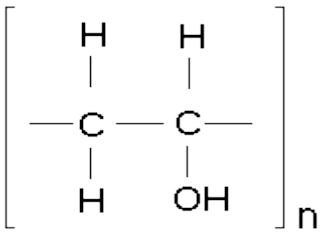

Figure 2.3 *Chemical structure of polyvinyl alcohol (PVA) (Liu et al. 2010)*

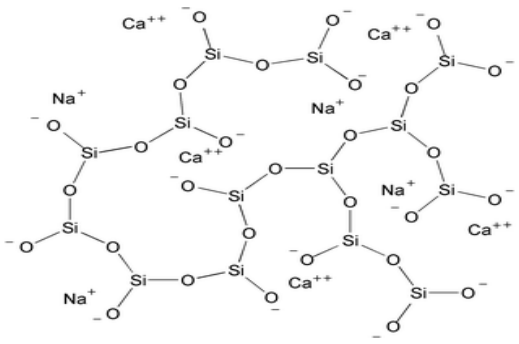

Figure 2.4 *Chemical structure of bioactive glass (BG) (Place et al. 2009)*

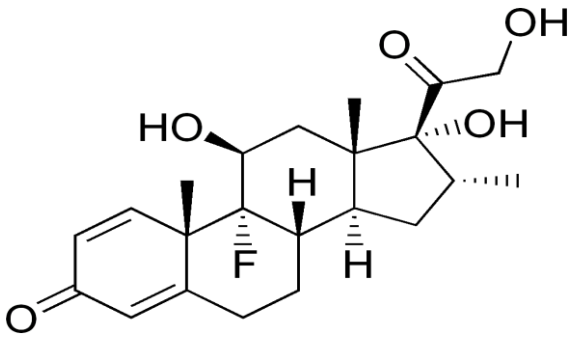

Figure 2.5 *Chemical structure of dexamethasone (Aldrich 2012a)*

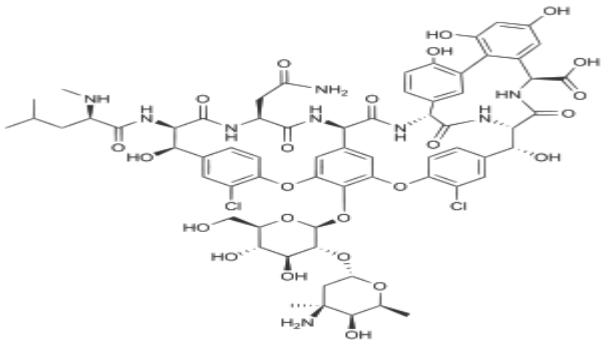

Figure 2.6 *Chemical structure of vancomycin (Aldrich 2012b)*

2.2 Photopolymerisation of samples

2.2.1 Photopolymerisation I

As mentioned above, previous monomers photopolymerised by our research group required several washing steps to promote biocompatibility. As a result, polyethylene glycol dimethacrylate (PEGDMA) was selected based on the known biocompatibility of the polyethylene glycol component, which is FDA approved. Initial studies were carried out to determine the effect of the disparity in mechanical

properties and thermal behaviour of these hydrogels by varying the molecular weight of PEGDMA (200-1000) and polymer concentration (25-75wt%). The precursor compositions can be seen in Table 2.1; they were photopolymerised using a UV chamber (Dr. Gröbel UV-Electronik GmbH). This particular irradiation chamber is a controlled radiation source with twenty UV-tubes that provides a spectral range of between 315-400nm at an average intensity of 10-13.5mW/cm^2. The solutions were pipetted into silicone moulds and photopolymerisation was carried out for 10mins, after which time gelation had occurred. These parameters are within the cytocompatible initiating conditions (Bryant *et al.* 2000).

Table 2.1 *Formulated composition of PEGDMA with distilled water prior to photopolymerisation.*

Hydrogel Code	PEGDMA 1000 (wt%)	PEGDMA 600 (wt%)	PEGDMA 400 (wt%)	PEGDMA 200 (wt%)	Distilled water (wt%)
PEG1000B	75	-	-	-	25
PEG1000C	50	-	-	-	50
PEG1000D	25	-	-	-	75
PEG600A	-	100	-	-	0
PEG600B	-	75	-	-	25
PEG600C	-	50	-	-	50
PEG600D	-	25	-	-	75
PEG400A	-	-	100	-	0
PEG400B	-	-	75	-	25
PEG400C	-	-	50	-	50
PEG400D	-	-	25	-	75
PEG200A	-	-	-	100	0

On completion of characterisation and analysis of the PEGDMA hydrogels listed in Table 2.1, subsequent studies were carried out by incorporating unique polypropylene glycol based materials into PEGDMA hydrogels in an attempt to

improve the mechanical strength, reduce percentage swelling and yet maintain biocompatibility. Initial studies were carried out using three different reactive side groups of polypropylene glycol. The optimum material to incorporate with PEGDMA was determined based on the mechanical properties of the PPG's at different concentrations. After extensive testing, PPGDMA was selected to incorporate in with PEGDMA of different molecular weights (Table 2.2). Variation in concentration of distilled water was omitted from this study due to the hydrophobic nature of the PPG.

Table 2.2 *Formulated precursor compositions of PPGDMA and PEGDMA prior to photopolymerisation*

Hydrogel Code	PEGDMA 400 (wt%)	PEGDMA 600 (wt%)	PPGDMA 425 (wt%)
PPG	-	-	100
PPG/PEG400A	75	-	25
PPG/PEG400B	50	-	50
PPG/PEG400C	25	-	75
PPG/PEG600A	-	75	25
PPG/PEG600B	-	50	50
PPG/PEG600C	-	25	75

2.2.2 Photopolymerisation II

2.2.2.1 Synthesis of maleic PVA

This research involved the synthesis of maleic polyvinyl alcohol to achieve a photopolymerisable material. Polyvinyl alcohol powder (3.5g) was added to formamide solvent (350cm^3). *p*-Tolunesulfonic acid monohydrate (3.87g) was added to the solution and stirred for 1hr at ambient temperature. Maleic anhydride solid (12.33g) was added to the solution under an inert atmosphere (N_2). The mixture was heated at 60°C for 24hr under an inert atmosphere. It was then cooled to ambient temperature and acetone was added in copious amounts followed by cyclohexane. The resultant precipitate was filtered and air-dried. The white precipitate was added to distilled water (100cm^3), which contained

dissolved sodium bicarbonate (12.43g). The solution was dialyzed against distilled water for three days (M_w cut off 12,000) to remove any excessive salts. During this period the distilled water was changed twice. The solution was lyophilised using a Virtis Freeze Drier under vacuum at -40°C for 2 days.

2.2.2.2 Photopolymerisation of hydrogels

Initial studies were carried out by photopolymerising maleic PVA samples, however, due to their limited mechanical strength, maleic PVA was incorporated with PEGDMA at different molecular weights and concentrations (Table 2.3).

Table 2.3 *Formulated precursor compositions of maleic PVA, PEGDMA and distilled water precursors prior to photopolymerisation*

Batch number	PVA concentration*	PVA ratio**	PEGDMA 1000	PEGDMA 600
PVA1000 1:0	5%	1	0	-
PVA1000 1:1	5%	1	1	-
PVA1000 1:2	5%	1	2	-
PVA1000 1:3	5%	1	3	-
PVA1000 1:4	5%	1	4	-
PVA600 1:1	5%	1	-	1
PVA600 1:2	5%	1	-	2
PVA600 1:3	5%	1	-	3
PVA600 1:4	5%	1	-	4

Table footnote:

- *PVA concentrations were based on the weight of maleic PVA dissolved in distilled water, i.e. 0.5g of maleic PVA dissolved in 10g of distilled water was equal to 5%.
- **PVA ratios were based on the weight of maleic PVA dissolved in water and the PEGDMA component. For example PVA1000 1:3 was equated to 25% of dissolved maleic PVA in distilled water and 75wt% PEGDMA1000.

2.2.3 Photopolymerisation III

2.2.3.1 Synthesis of bioactive glass

One glass was synthesised; $0.2SrO/0.2Na_2O/0.1CaO/0.1ZnO/0.4SiO_2$ (mol. fraction). Appropriate amounts of analytical grade calcium carbonate, strontium carbonate, zinc oxide and silicon dioxide (Sigma Aldrich, Canada), were weighed out in a plastic tub and homogeneously mixed in a NalgeneR plastic container (Sigma Aldrich, Canada) for 1hr. Each batch of powder was placed in platinum crucibles (50mL), then fired (1480°C, 1hr) using a Bench-Top High Temperature Muffle Furnace (EQ-KSL, MTI Corporation, USA) and shock-quenched into distilled water. The resulting glass frit was dried in an oven (120°C, one day), pulverised in an agate planetary mill (Pulverisette 7; Laval Labs Inc., Canada) and sieved to retrieve particulates of <45µm. Glass powders were subsequently stored in dry desiccators for subsequent evaluation. The glass composition in this study is the result of optimisation of bone graft performance from preceding studies (Boyd *et al*. 2009; Murphy *et al*. 2009; Murphy *et al*. 2010).

2.2.3.2 Synthesis of hydroxyapatite

Hydroxyapatite (HAP) was prepared by wet chemical method using $CaCl_2$ and $(NH_4)_2HPO_4$ as Ca and P precursors, following the procedure outlined by Murugan and Ramakrishna (2004). Specified amounts of ammonium phosphate dibasic solution was added drop-wise to a calcium chloride solution under continuous stirring at 1000rpm at 60°C for one hour while maintaining the pH above 10 by adding ammonium hydroxide. The sample was left overnight to precipitate out of solution before decanting, filtering and washing several times with distilled water to remove any residual NH_4OH. The sample was microwave irradiated for 10min and the resultant material was vacuum dried at 50mbar for 24hr at 60°C. After 24hr, the material was sieved through a micro filter with a pore size of 45µm.

2.2.3.3 Hydrogel based composites

This study involved the photopolymerisation of one bioactive glass (BG) and two different calcium phosphates, hydroxyapatite and beta tricalcium

Table 2.4 *Formulated precursor compositions of PEGDMA, distilled water and bioceramics prior to photopolymerisation*

Composite Code	PEG1000 (wt%)	PEG600 (wt%)	DI (wt%)	HAP (wt%)	BG (wt%)	β-TCP (wt%)
PEG1000A	75	-	25	0	-	-
PEG1000A H5	75	-	25	5	-	-
PEG1000A H20	75	-	25	20	-	-
PEG1000B	50	-	50	0	-	-
PEG1000B H5	50	-	50	5	-	-
PEG1000B H20	50	-	50	20	-	-
PEG600A	-	75	25	0	-	-
PEG600A H5	-	75	25	5	-	-
PEG600A H20	-	75	25	20	-	-
PEG1000A G5	75	-	25	-	5	-
PEG1000A G20	75	-	25	-	20	-
PEG1000B G5	50	-	50	-	5	-
PEG1000B G20	50	-	50	-	20	-
PEG600A G5	-	75	25	-	5	-
PEG600A G20	-	75	25	-	20	-
PEG1000A T5	75	-	25	-	-	5
PEG1000A T20	75	-	25	-	-	20
PEG1000B T5	50	-	50	-	-	5
PEG1000B T20	50	-	50	-	-	20
PEG600A T20	-	75	25	-	-	5
PEG600A T20	-	75	25	-	-	20

phosphate (β-TCP) into a polymer matrix. These bioceramics were individually incorporated into PEGDMA to determine the optimum bioceramic/PEGDMA hydrogel based composite in terms of mechanical strength and bioactive properties. The composition ratio for each individual sample can be seen in Table 2.4.

2.3 Synthesis techniques

2.3.1 Photopolymerisation

2.3.1.1 UV chamber

Hydrogels and hydrogel based composites were photopolymerised using a UV curing system (Dr. Gröbel UV-Electronik GmbH), as shown in Figure 2.7. The irradiation chamber utilised was a controlled radiation source with 20 UV-tubes that provide a spectral range of between 315-400nm at an average intensity of 10-13.5mW/cm^2. The prepolymerised mixtures were prepared by combining various combinations and concentrations of macromolecular monomers, distilled water, bioceramic powders and 0.1wt% photoinitiator (see Tables 2.1-4). The batches were placed in a 50mL beaker, mixed using a magnetic stirrer and sonicator until a homogenous mixture was achieved. The solutions were pipetted into various silicone moulds (for different characterisation techniques) and photopolymerisation was carried out for 10min, after which time gelation had occurred.

2.3.1.2 Handheld lamp

Optimised samples were photopolymerised using a SB100P 100W hand held UV curing system (Figure 2.7) for cell viability studies. The prepolymerised mixtures were prepared similar to above apart from an increase in curing time (20min). Sample preparation required a sterile environment, i.e. Class II laminar flow unit to reduce the risk of microbial contamination.

Figure 2.7 *Dr. Gröbel UV-Electronik GmbH UV box* ***(left* hand side)** *and UV handheld lamp* ***(right* hand side)**

2.3.2 Freeze drying

After synthesis, freeze drying was carried out on the maleic PVA solution to extract the liquid leaving behind pure polymer through the process of sublimation. The advantage of this solution extraction method is that it converts the solid (ice) into gas (vapour), bypassing the liquid stage which minimises the risk of damage to the structure of the maleic PVA. Prior to attaching maleic PVA solution in a round bottom flask, the sample was placed in a freezer at -40°C for 24hr. Once fully frozen the samples were attached to the freeze drier (Figure 2.8) at -40°C with a vacuum pressure of 200mtorr for 2/3 days until only pure maleic PVA was left behind. Samples were removed from the machine, ready for incorporation into batches as discussed in Section 2.2.2.2.

Figure 2.8 *Virtis Freeze Drier*

2.3.3 Preparation of aqueous salts and pH buffer solutions

Potassium chloride 0.2M (KCl) and monobasic potassium phosphate 0.2M (KH_2PO_4) were used to prepare the buffer pH 7.4. Hydrochloric acid and sodium hydroxide solutions were used to adjust the ionic strength of the solutions to 0.2M. The buffer solutions were prepared in the laboratory and filtered under vacuum using a Millipore filtration apparatus. The pH of the buffer solutions was measured using a Jenway 3520 pH meter.

2.4 Characterisation techniques

2.4.1 Swelling studies

Swelling experiments were performed on samples in buffer solution (pH 7.4). After photopolymerisation, samples with an average weight of 0.8±0.1g were placed into a petri dish. The petri dish was filled with 30ml of pH 7.4 buffer solution. The percentage swelling of the samples was calculated using the formula:

$$\textbf{Swelling}\ (\%) = \left(\frac{W_s - W_d}{W_d}\right) \times \frac{100}{1} \qquad \textbf{(Equation 1)}$$

where W_s and W_d are the weights of the hydrogels in the swelling state and the dried state, respectively. Tests were carried out in quintuplicate and data is presented as mean ± SD.

2.4.2 Distance between crosslinks and mesh size calculations

The structure of the hydrogels were characterised experimentally in terms of molecular weight between crosslinks, crosslink density, unperturbed mean-square end-to-end distance ($(r^2_0)^{1/2}$) and mesh size (ξ). All experiments were carried out on disc impressions with an aspect ratio of 0.1. The molecular weight between crosslinks can be approximated using the Peppas-Merrill equation (Peppas and Merrill 1976), which was modified from the Flory-Rehner model (Flory and Rehner 1943) as shown in Equation 2.

$$\frac{1}{M_c} = \frac{2}{M_n} - \frac{\frac{v}{V_1}[\ln(1-V_{2,s}) + V_{2,s} + \mu V^2_{2,s}]}{V_{2,r}\left[\left(\frac{V_{2,s}}{V_{2,r}}\right) - \frac{1}{2}\left(\frac{V_{2,s}}{V_{2,r}}\right)\right]} \qquad \textbf{(Equation 2)}$$

- M_c is the molecular weight between crosslinks.
- M_n is the number average molecular weight of the polymer.
- v is the specific volume of bulk PEG in amorphous state (0.893 cm^3/g).
- V_1 is the molar volume of the solvent ($18cm^3/mol$).
- μ is the Flory-Huggins polymer solvent interaction parameter (0.426 for PEG-water, as determined by Merrill *et al*. (1993)).
- $V_{2,r}$ is the volume fraction of hydrogel in relaxed state.
- $V_{2,s}$ is the volume fraction of hydrogel in equilibrium state.

The root mean squared end-to-end distance was calculated using Equation 3:

$$\left(\overline{r^2_0}\right)^{\frac{1}{2}} = l\left(\frac{2M_c}{M_r}\right)^{\frac{1}{2}} C_n^{\frac{1}{2}} \qquad \textbf{(Equation 3)}$$

- $\left(\overline{r^2_0}\right)^{\frac{1}{2}}$ is the unperturbed mean-square end-to-end distance.
- l is the average value of the bond length between C-C and C-O bonds in the PEG repeat unit [-O-CH_2-CH_2-] (1.46A)
- M_r is the molecular mass of the PEG repeat unit (44g/mol).
- C_n is the characteristic ratio of PEG (4).

Therefore, the average mesh size (ξ) of the network was calculated using Equation 4:

$$(\boldsymbol{\xi}) = \mathbf{l}\left(\frac{\mathbf{2M_c}}{\mathbf{M_r}}\right)^{\frac{1}{2}} \mathbf{c}^{\frac{1}{2}}_{\mathbf{n}} \qquad \textbf{(Equation 4)}$$

2.4.3 Gel fraction measurement

The gel fraction of all batches was measured in quintuplicate using circular discs with an average mass of 0.8±0.1g. Samples were initially dried under vacuum at 200mmHg for 24hr at 80°C to a consistent weight. The samples were allowed to swell in a sealed petri dish with 30mL of buffer solution pH 7.4 for 72hr at 21°C until equilibrium swelling was achieved. The solution was replaced with fresh buffer solution daily to ensure that the soluble fraction was completely extracted. Once equilibrium swelling was attained, samples were again dried in the vacuum oven at 80°C in the absence of water until no change in weight was observed. Gel fraction (%) was calculated using Equation 5:

$$\mathbf{Gf}\ (\%) = \left(\frac{\mathbf{W_{ex}}}{\mathbf{W_o}}\right) \times \frac{\mathbf{100}}{\mathbf{1}} \qquad \textbf{(Equation 5)}$$

where W_o and W_{ex} are the weight of the dried hydrogel after photopolymerisation and the dried weight of the sample after extraction of soluble parts, respectively.

2.4.4 Attenuated total reflectance Fourier transform infrared spectroscopy

Attenuated total reflectance Fourier transform infrared spectroscopy (ATR-FTIR) was carried out on a Perkin Elmer Spectrum One fitted with a universal ATR sampling accessory as shown in Figure 2.9. All data was recorded at 21°C, in the spectral range of 4000-520cm^{-1}, utilising a 16 scan per sample cycle and a fixed universal compression force of 80N. Subsequent analysis was carried out using Spectrum software.

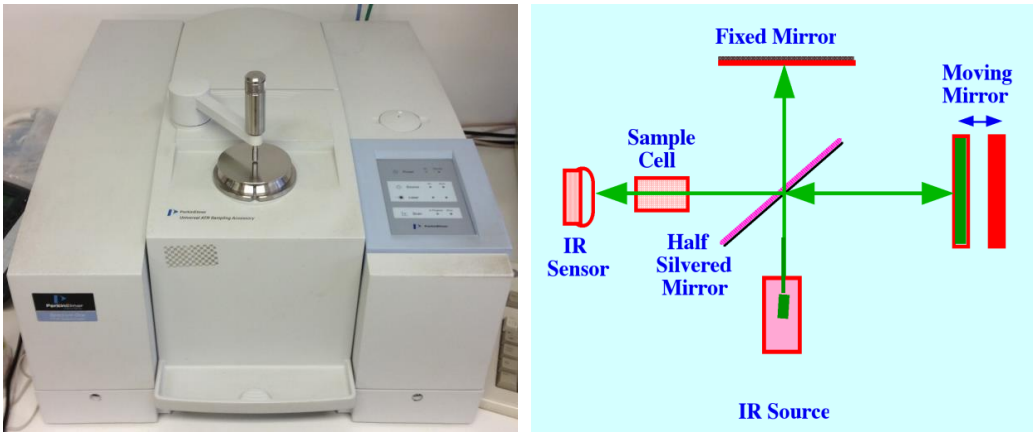

Figure 2.9 *Perkin Elmer Spectrum One ATR-FTIR* ***(left hand side)*** *and schematic diagram of FTIR* ***(right hand side)***

2.4.5 Nuclear Magnetic Resonance

Nuclear magnetic resonance spectra were measured on a JEOL LAMBDA 400MHz NMR machine. NMR samples were prepared by dissolving 0.0371g of maleic PVA in $1cm^3$ of deuterated water (D_2O). Assignments were supported by DEPT and COSY spectra. Chemical shifts are reported in parts per million (ppm) using sodium 3-(trimethylsilyl) tetradeuterio propionate as an internal standard.

Maleic PVA $\delta_H(D_2O)$ 1.48 ($-CH_2-$), 3.86 (-CH-), 5.65 (=C-H), 6.48 (=C-H). δc (D_2O) 43.4, 43.9, 44.2, 44.6, 44.8 (-CH-), 64.5, 64.7, 64.9, 66.0, 66.3, 67.7 ($-CH_2-$), 118.3, 141.6 (C=C), 162.1, 174.8 (C=O).

2.4.6 Thermal analysis

2.4.6.1 Differential scanning calorimetry

Differential scanning calorimetry (DSC) was carried out using a TA Instruments 2010 DSC as shown in Figure 2.10. Dehydrated samples of between 8-10mg were weighed out using a Sartorius scale at a resolution of $1x10^{-5}g$. These xerogels were dried in a vacuum oven (24hr, 80°C) prior to testing. All measurements were conducted in sealed non-hermetic aluminium pans. Samples were cooled to -110°C using liquid nitrogen and heated to 300°C at a rate of 10°C/min. The glass transition temperature was considered as the mid-point

temperature of the endothermic drift in the heating curves, in all cases. Volatiles were removed from the purging head using nitrogen at a rate of 30ml/min. Calibration of the instrument was performed using indium as standard. Tests were carried out in duplicate.

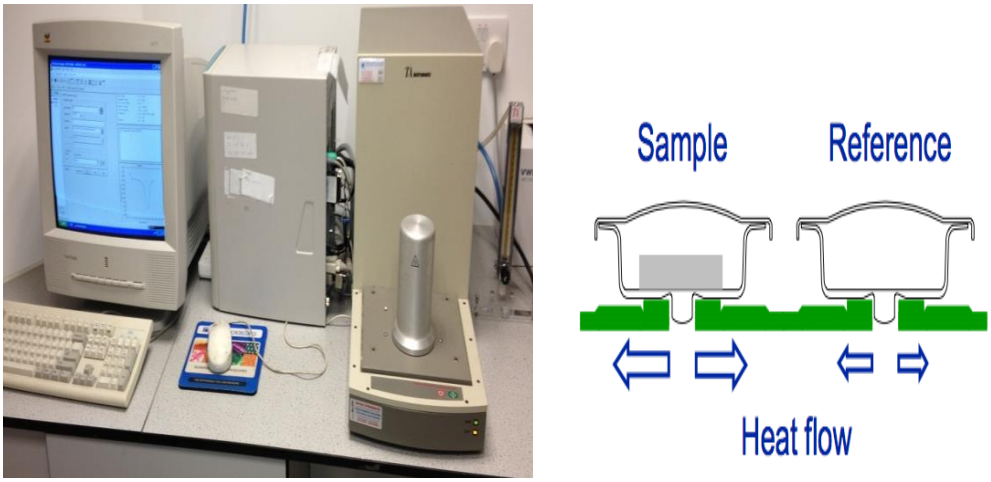

Figure 2.10 *TA Instruments 2010 DSC* ***(left hand side)*** *and DSC schematic diagram* ***(right hand side)***

2.4.6.2 Dynamic mechanical thermal analysis

Dynamic mechanical thermal analysis (DMTA) scans were carried out on samples using a Rheometric scientific mark 3 DMTA in tensile mode. The temperature profile ranged from −110 to 140°C at a 2°C/min heating rate with a frequency of 1Hz. Individual hydrogel samples were tested after photopolymerisation, where no swelling or drying was carried out.

2.4.6.3 Thermogravimetric analysis

Thermogravimetric analysis (TGA) was performed to evaluate the effective weight percentages of different bioceramics in the hydrogel based composites. Tests were conducted using a Perkin Elmer TGA 7 Thermogravimetric Analyser, coupled with a Perkin Elmer Thermal Analysis Controller TAC7/DX under nitrogen atmosphere. The tests were run from 30 to 600°C, at a heating rate of 10°C/min.

2.4.7 Rheological measurements

In all cases throughout this study, rheological measurements were performed using an Advanced Rheometer AR1000 (TA Instruments) fitted with a Peltier temperature control (Figure 2.11) to investigate the comparative strength of the samples. Samples were tested in quintuplicate (using individual samples) within 72hr of preparation at a temperature of 37°C using a 4cm parallel steel plate where the samples were in the equilibrium swollen state. Prior to testing, all samples were blotted free of water using filter paper in an attempt to minimise slippage. A compression load of 5±0.2N was exerted on the samples during testing and the mean ± SD was reported. Rheological test parameters, storage/elasticity (G') and loss (G'') modulus were obtained under dynamic conditions for these non-destructive oscillatory tests.

2.4.7.1 Rheological test I

Dynamic strain sweep test experiments were performed at a constant frequency of 1Hz with percentage strain ranging from $1.80x10^{-4}$ to $1.0x10^{-3}$.

2.4.7.2 Rheological test II

Dynamic frequency sweep test experiments were carried out at a constant strain of 0.1% (linear viscoelastic region) with frequency ranging from $1.0x10^{-1}$ to $1.0x10^{2}$ Hz.

2.4.7.3 Rheological test III

Dynamic stress sweep test experiments were performed at a constant frequency of 1Hz with oscillation stress ranging from $1.0x10^{-2}$ to $1.0x10^{2}$.

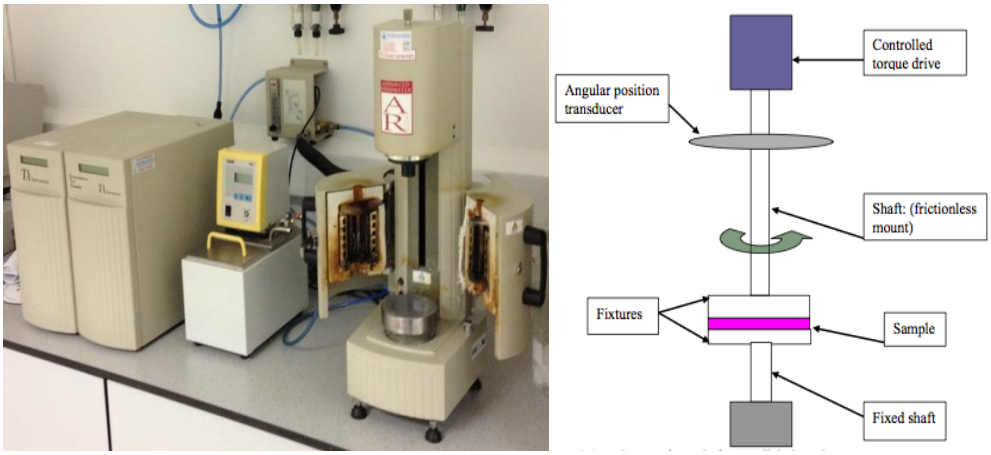

Figure 2.11 *Advanced Rheometer AR1000* ***(left hand side)*** *and schematic diagram of setup* ***(right hand side)***

2.4.8 Uniaxial tensile testing

Tensile strain to failure tests were performed on a Lloyd Lr10K Plus Series twin column materials testing apparatus using 3kN load cell. The machine was connected to a control computer with Nexygen™ software, to run appropriate testing criteria and for analysis of results. Hydrogel samples were moulded into dumbbell shape in accordance to ASTM Standard Method D638-04, and the length, breath and thickness of each sample recorded. After photopolymerisation, hydrogels were swelled to equilibrium and vacuum dried for 2hr before testing. This swelling and dehydration step was carried out to remove unreacted low molecular weight polymer from the surface so as to improve the adhesion between the hydrogel and grippers. Fixed grips were mounted onto the tensile testing machine (Figure 2.12) and a crosshead speed of 20mm/min was used. Sticky tape was placed between the hydrogel samples and the grip surface to prevent slippage during loading. Tensile testing was performed on 10 separate test specimens for each batch and mean stress at break, Young's modulus and strain at break values were calculated.

2.4.9 Compression testing

Compression measurements were performed using a Lloyd Lr10K, screw-driven testing machine fitted with a 2.5kN load cell with a bespoke 30mm diameter testing head (Figure 2.12). Samples prior to testing were equilibrated at

room temperature (21°C) for 72hr in buffer solution pH 7.4. Compression tests were carried out in quintuplicate and data is presented as mean ± SD.

2.4.9.1 Compression test I

Unconfined compression tests were carried out at a speed of 0.5mm/min and samples were strained to 60%.

2.4.9.2 Compression test II

Cyclic compression tests involved loading/unloading 10 cycles to 50% of the sample thickness at a compression speed of 0.5mm/min.

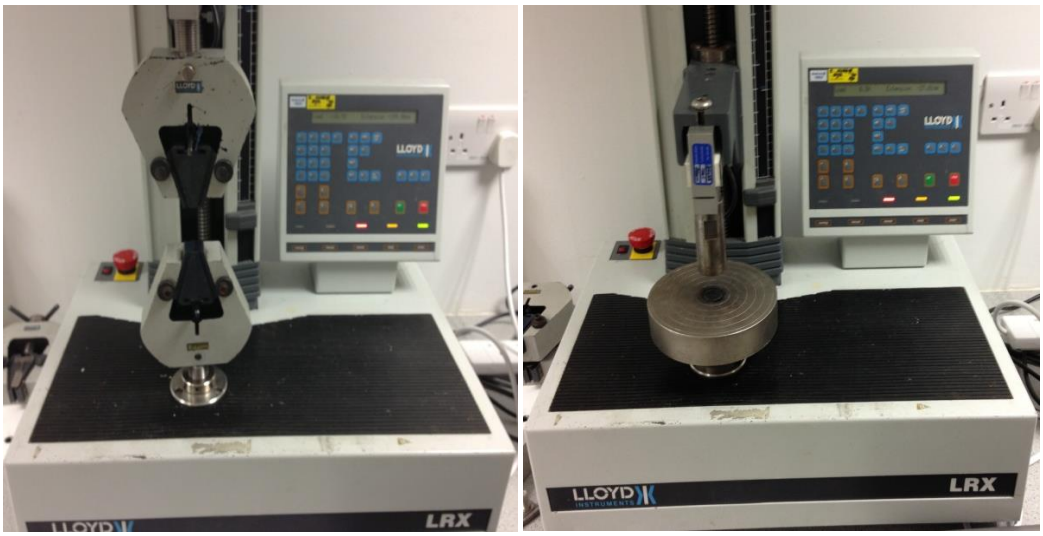

Figure 2.12 *Lloyd Lr10K Plus Series twin column machine in tensile mode* ***(left hand side)*** *and compression mode* ***(right hand side)***

2.4.10 *In vitro* biomineralisation study

A short term *in vitro* bioactivity study was carried out in simulated body fluid (SBF) as described by Kokubo and Takadama (Kokubo and Takadama 2006). Numerous methods have previously been developed (Cho *et al.* 1995; Kokubo and Takadama 2006). However, the Kukubo method was selected based on its almost exact replication of ion concentration of human plasma. Briefly, reagent grade NaCl, $NaHCO_3$, KCl, $K_2HPO_4{\cdot}3H_2O$, $MgCl_2{\cdot}6H_2O$, $CaCl_2$, and

Na_2SO_4 were dissolved (quantities can be seen in Table 2.5) in 1L of distilled water at 36.5±0.2°C and pH adjusted to 7.4 with 1.0m-HCl and Tris. Samples were immersed in SBF and kept under static conditions at 37°C for three weeks, after which they were dried at 80°C for 1 day and analysed by SEM, XRD EDX and FTIR to determine the deposition of apatite on the surface of the hydrogel based composites. SBF solution was changed twice a week to prevent saturation of the solution and ensure pH stability to replicate the physiological environment.

Table 2.5 *Comparison in ion concentration of human plasma and prepared SBF solution **(A)** and reagent masses used to formulate SBF solution **(B)***

A	Ion concentration (mmol/dm^3)		**B** SBF Formulation	
	Human plasma	SBF	Reagent	Mass (g/l)
Na^+	142	142	NaCl	8.035
K^+	5	5	$NaHCO_3$	0.355
Mg^{2+}	1.5	1.5	KCL	0.225
Ca^{2+}	2.5	2.5	$K_2HPO_4.3H_20$	0.231
Cl^-	103	147.8	$MgCl_2.6H_20$	0.311
HCO^{3-}	27	4.2	$CaCl_2$	0.292
HPO_4^{2-}	1	1	Na_2SO_4	0.072
SO_4^{2-}	0.5	0.5		

2.4.11 Scanning electron microscopy with energy-dispersive X-ray spectrometry system

Scanning electron microscopy (Sem) was performed on a Mira SEM with a magnification of 10kx (Figure 2.13). This instrument allowed the examination

of surface morphology and overall elemental uniformity through the distribution of bioceramic in the hydrogel based composite and the formation of an apatite layer. The bioceramics and polymers tested are non-conducting by nature. Therefore, samples required a coating prior to testing to increase the electrical conductivity of the sample. Sample preparation involved placing samples on the sticky surface of an aluminium stub. After sufficient time (10mins), the sample was placed in a Bal-Tec SCD sputter coater (Figure 2.13) for 110sec at 0.1mBar vacuum before testing to apply a layer of gold on the surface. The quantitative investigation of the apatite layer on the surface of the hydrogel based composites was performed with the energy-dispersive X-ray spectrometry **(**EDX) system.

Figure 2.13 *Mira scanning electron microscope **(left hand side)** and Bal-Tec SCD 005 sputter coater **(right hand side)***

2.4.12 X-ray diffraction

X-ray diffraction studies on samples were carried out using a high resolution Bruker AXS D8 DISCOVER diffractometer (Figure 2.14) in Bragg-Brentano geometry, with a CuK∝ monochromated beam (λ=0.15406A) produced at 40kV and 40mA. The scanning range was from 2 to 40^{o} (2θ) at a step size of 0.02^{o}. XRD was employed to investigate the modifications induced by the incorporation of various bioceramics into the hydrogel based composites. GADDS and Eva software packages were used to analyse the recorded results.

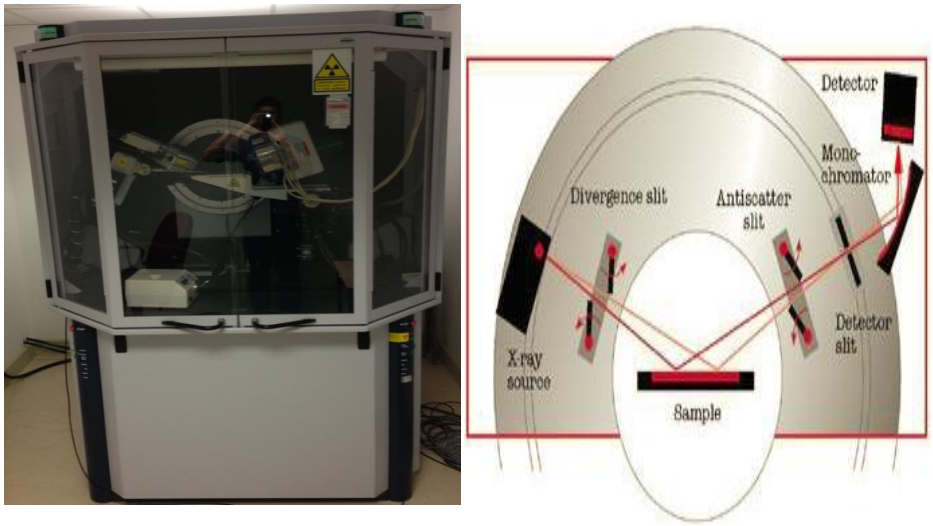

Figure 2.14 *Bruker AXS D8 DISCOVER diffractometer* ***(left hand side)*** *and schematic diagram for XRD* ***(right hand side)***

2.4.13 *In vitro* antibacterial activity (disc diffusion assay)

Antimicrobial activity of hydrogel based composites was assayed by the disc diffusion susceptibility test according to the recommendation of the National Committee for Clinical Laboratory Standards (NCCLS). The disc diffusion tests were performed on Muller-Hinton agar plates for bacteria cultures; *Escherichia coli* and *Staphylococcus aureus*. Plates were dried at 35–36°C for about 30min in an incubator before inoculation. Bacteria strains were inoculated into 25mL of Mullar–Hinton broth medium in a shaking water bath for 4–6hr until a turbidity of 0.5 McFarland (1×10^8CFU/mL) was reached. Final inocula were adjusted to 5×10^5CFU/mL using a spectrophotometer. The inoculum (50mL) from the final inocula was applied to each agar plate and uniformly spread with a sterilized cotton spreader over the surface. Absorption of excess moisture was allowed to occur for 30min before application of hydrogel discs. Hydrogel discs were incubated at 37°C for 24hr for bacteria and 48hr for fungi. The diameters of the inhibition zones were measured in millimeters.

2.4.14 Drug release studies

Drug release studies were performed using both dexamethasone (10mg/hydrogel) and vancomycin (4mg/hydrogel). Tests were carried out in triplicate on specimens with a surface area of approximately 8.168mm^2. Samples were placed into 50mL glass McCartney bottles that contained 10ml of buffer solution pH 7.4±0.1 under static conditions in an oven at 37°C. Drug release was determined by performing UV spectroscopy (Shimadzu UVmini-1240 UV-VIS Spectrophotometer) on the swelling media at predetermined time intervals: 0.5, 1, 2, 3, 4, 5 days etc., until no absorbance was detected by UV spec. The drawn solutions were analysed spectrophotometrically at 242nm and at 280nm in order to determine the amount of dexamethasone and vancomycin release. After every measurement, the solution medium was withdrawn and replaced with equal volumes of fresh buffer solution pH 7.4±0.1.

2.4.15 Toxicological assessment

The *in vitro* biocompatibility assessment of hydrogel samples was performed using a mouse embryo fibroblast (NIH/3T3) cell line. All cultures and manipulations of cells were performed within a Class II laminar flow unit in a dedicated cell culture laboratory. To ensure an adequate level of sterility, aseptic technique was strictly adhered to in accordance with standard procedures. Tissue culture plasticware was utilised at all times to ensure sterility while carbon dioxide (CO_2) incubators and laminar flow units were periodically cleaned with 70% ethanol to minimise the risk of contamination.

2.4.15.1 Preparation of complete culture media

In accordance with ATCC recommendations for cell type media selection 200ml volumes of media were aseptically prepared in 75cm^2 culture flasks and stored at 4°C for a maximum of 14 days. Table 2.6 outlines the preparation of NIH/3T3 complete culture medium. All media constituents were heated to 37°C prior to use.

Table 2.6 *Composition of NIH/3T3 complete culture medium*

Medium constituent	Volume/200ml	Final concentration (%)
Foetal calf serum (FCS)	20	10
DMEM	177	88
L-Glutamine (200mM)	2	1
Penicillin-Streptomycin (5000 U-5mg/ml)	1	0.5
Amphotericin B (200mM)	1	0.5

2.4.15.2 Cell harvesting via trypsinisation

Upon reaching 80% confluency, anchorage dependant cells must be detached from the growth substratum. Media was aspirated off aseptically and cells were rinsed with sterile PBS x2. 2ml of 0.25% trypsin-ethylenediamine tetra-acetic acid (EDTA) solution was added in order to facilitate cell removal. Cell culture flasks were incubated at 37°C for 5min. The degree of detachment was then assessed under an inverted light microscope (Olympus, Japan). Two millilitres fresh media was added in order to deactivate the trypsin upon complete cellular detachment. Cell suspensions were transferred to a sterile universal and centrifuged at 1300rpm for 5min. The supernatant was discarded and the cell pellet was resuspended in 1ml of complete culture medium. If required, a cell count was performed, otherwise the resuspended cell pellet was split equally between two cell culture flasks and incubated at 37°C in a humidified CO_2 incubator.

2.4.15.3 *In vitro* cytotoxicity testing (Sample preparation)

Cytotoxicity tests were performed in accordance with ISO 10993-5 (2009) guidelines using the elution test with MTT as an endpoint. Extracts of chemical hydrogels were prepared by placing a 250mg (±10mg) one-piece sample in a sealed container with 30ml of culture medium for 7 days at 37°C. Subsequently, eluates were poured into sterile 25ml universals and diluted in the

range of 100-1% with fresh sterile complete medium. Neat and diluted eluates were stored at 4°C until required.

2.4.15.4 Positive control cytotoxicant

A 1% solution of Triton®X-100 was prepared fresh on the day of use by adding 100µl of Triton®X-100 to 9.9ml of fresh complete medium in a sterile universal. The solution was mixed, shaken by hand, and used immediately.

2.4.15.5 Elution test (MTT endpoint)

NIH/3T3 cells were seeded at 10,000 cells per 100µl of media in 96 well microtitre plates and incubated in a humidified atmosphere of 5% CO_2: 95% air at 37°C until the desired degree of confluency was obtained. Subsequently cultures were exposed to pre-warmed test media containing 100-0% extracts from hydrogels or 1% Triton®X-100 positive control for a further 24hr at 37°C. Following removal of test media cells were washed with 100µl of warm sterile PBS. 100µl fresh culture media supplemented with 0.5mgml^{-1} MTT was added to each well and plates were incubated for a further 4hr at 37°C. The MTT media was carefully aspirated off and 100µl of DMSO was added to each well to aid in solubilisation of the crystals. Plates were shaken for 15s and incubated at room temperature for 10min prior to recording optical densities at 540nm (victor). Cell viabilities were calculated as a percentage of untreated control cells ± the standard error of the mean (SEM).

2.4.16 Statistical analysis

A statistical comparison of results were performed using a one way ANOVA with a Tukey's Honesty Significant Difference post hoc test to determine differences between individual batches. Differences were considered significant when $p \leq 0.05$. The software package used to perform statistical analysis was SPSS version 16 for Windows.

Chapter 3

Results and discussion

3.1 Evaluation of PEG and PPG based hydrogels as a potential scaffold for bone tissue engineering

3.1.1 Effect of molecular weight of PEGDMA and polymer concentration on hydrogels mechanical properties and thermal behaviour for bone tissue engineering applications

3.1.1.1 Preface

Tissue engineering is the method of replicating tissue by using principles of engineering, medicine and physical sciences (Langer and Vacanti 1993). Recently this area of research has received extensive investigation in the literature and is of particular interest for bone regeneration applications. Bone has the ability to repair itself, however the rate and amount of repair is dependent on the size of the defect (Muschler and Lane 1992). As already mentioned in Section 1.3.3, defects so large that they will not heal during an individual's lifetime have been defined as critical size defects (Schmitz and Hollinger 1986; Muschler and Lane 1992). These defects will not regenerate without intervention such as bone grafting or bone substitution. In total, 8% of all fractures, 7% of spinal disorders and 70% of cavities resulting from the removal of benign tumours require some sort of bone grafting procedure (Fitzgerald *et al.* 2002; Kahn *et al.* 2005; Muramatsu *et al.* 2006; Helms *et al.* 2007).

Given the inherent disadvantages of each of the existing techniques for repairing critical size defects, researchers have been driven to design new synthetic scaffold materials. Synthetic polymers such as poly(ε-caprolactone) and poly(α-hydroxyacids) can be easily processed and their mechanical properties altered, though they have a tendency to exhibit strong inflammatory responses (Puppi *et al.* 2010). At present, there is a demand to produce a scaffold for bone regeneration that allows high permeability of oxygen, nutrients and cell growth while at the same time providing sufficient mechanical strength.

Poly(ethylene glycol) diacrylate (Wu *et al.* 2010b) has been widely investigated as a scaffold material for bone regeneration (Zhang *et al.* 2008; Ma

et al. 2010). In this study, poly(ethylene glycol) dimethacrylate (PEGDMA) based macromolecular monomers were utilised. Hydrogels synthesised using these materials have been reported to exert minimal toxicological response and can be modified to be either bio-inert or biocompatible (Elisseeff *et al.* 1999; Lin-Gibson *et al.* 2004; Zhang *et al.* 2005). While PEGDMA has received attention in the literature in the areas of coatings, adhesives, dental and cartilage repair (Karmaker *et al.* 1997; Elisseeff *et al.* 1999; Bryant and Anseth 2003), little research has been conducted on this material specifically for bone regeneration applications.

3.1.1.2 Preparation of samples

Photopolymerisation of the hydrogels was achieved through chemical crosslinking. The presence of UV light and free radicals created by the decomposition of the photoinitiator results in the reactive chain ends of PEGDMA joining together and forming a solidified hydrogel. Photopolymerisation is an attractive *in situ* formation technique used in tissue engineering because it provides spatial and temporal control. It has been used in numerous industries in the formation of complex structures and presents a fast and cost-effective alternative to other crosslinking methods. The main advantages of this technique over other fabrication methods are the absence of organic/inorganic solvents and low processing temperatures during polymerisation. In this work, chemically crosslinked hydrogels based on PEGDMA were synthesised via photopolymerisation. Pre-polymerisation mixtures were prepared by varying PEGDMA molecular weights (200, 400, 600 and 1000) along with specified amounts of distilled water and 0.1wt% photoinitiator. Preliminary studies were carried out using both Irgacure 184 and 2959; given that no change in mechanical performance was observed between samples synthesised with either photoinitiator, Irgacure 2959 was selected due to its enhanced biocompatibility (Karaca *et al.* 2010). This was related to the hydrophobicity since permeability through the cellular membrane increases with the hydrophobicity of a compound. Irgacure 25959 is less hydrophobic due to its polar hydroxyl end groups. In addition, Irgacure 2959 minimises oxygen inhibition which also promotes biocompatibility and was previously reported to have

minimal toxicity over a broad range of mammalian cell types and species ranging from human fetal osteoblasts to bovine chondrocytes (Williams, 2005). The concentration levels of photoinitiator were kept at a minimum given that previous studies have shown that minimising photoinitiator concentration levels serves to increase biocompatibility of the hydrogel, though it also increases curing time (Studer *et al.* 2003a; Studer *et al.* 2003b). Therefore, the gelation time used for all hydrogels was 10min. This was consistent throughout the study, since variation in photoinitiator concentration and curing time can affect the crosslink density and mechanical properties of hydrogels.

Hydrogels produced with the highest concentration content of PEGDMA macromolecular monomer were colourless and transparent. Conversely, hydrogels with increasing levels of distilled water gradually became opaque after photopolymerisation. This change in colour suggests that the hydrogel underwent a polymerisation induced phase separation process as previously reported (Lin *et al.* 2006; Kang *et al.* 2008; Ju *et al.* 2009). Distilled water concentrations of 0, 25, 50 and 75wt% were utilised in the synthesis of the macromolecular monomers of all the molecular weights, with the exception of PEGDMA 200. As a result of its low molecular weight, it was not possible to form a hydrogel from this material due to the increase in inter chain distance caused by water incorporation which prohibited polymerisation. Also, due to the viscous nature of PEGDMA 1000, mixing the macromolecular monomer at a concentration of 100wt% with the photoinitiator could not be achieved.

The surface of the hydrogels contained small amounts of low molecular weight solution that was not connected to the network. Previous studies (Lin *et al.* 2006; Kalakkunnath *et al.* 2007; Ma *et al.* 2010) have reported this behaviour using various photopolymerised acrylates. FTIR confirmed that the surface solution was in fact low molecular weight polymer.

3.1.1.3 Gel fraction measurement

Gel fraction measurement was carried out on circular discs of photopolymerised hydrogels in distilled water at 21°C. The gel fraction can be used as a quantitative indicator of the efficiency of network formation (Jing *et al.*

2001; Paul *et al.* 2008; Wu *et al.* 2010b). It was found that increasing PEGDMA content during synthesis enhances the gel fraction (Table 3.1). For example PEG600A which contains 100% polymer has a gel fraction of 96.02±1.05% compared to PEG600C which contains 50% polymer which had a gel fraction of 91.37±2.20%. The incorporation of distilled water during the curing reaction causes the polymeric chains to have fewer opportunities to covalently link to the network. This observation was consistent for all molecular weights. Additionally, for hydrogels of identical macromolecular monomer concentration but varying molecular weight (PEG600A and PEG200A), gel fraction decreases with reduction in molecular weight 96.02±1.05% and 91.80±1.59%, respectively.

Table 3.1 *Gel fraction and glass transition temperature of crosslinked PEGDMA/H_2O hydrogels*

Hydrogel Code*	Gel fraction (%)	T_g DSC (°C)	T_g DMTA (°C)	Swelling (%)
PEG1000B	96.63±2.91	-48.70	-44.64	56.67±1.31
PEG1000C	95.94±2.69	-49.41	-48.88	32.25±0.81
PEG1000D	92.65±1.60	-50.13	-	16.65±0.43
PEG600A	96.02±1.05	-32.18	-	47.58±1.48
PEG600B	93.54±1.39	-35.15	-	38.43±1.26
PEG600C	91.37±2.20	-37.27	-	16.84±1.05
PEG600D	90.45±1.41	-38.06	-	12.07±.83
PEG400A	95.71±1.20	-22.41	-	27.67±.69
PEG400B	92.57±1.45	-25.37	-	11.24±.42
PEG400C	90.64±1.56	-26.85	-	8.97±.38
PEG400D	85.99±1.37	-27.23	-	4.84±.15
PEG200A	91.80±1.59	-	-	0.81±.09

** see Table 2.1*

Overall, the gel fraction was relatively high in all PEGDMA/H_2O systems. It can be concluded that water in the prepolymerisation mixture was not able to significantly disrupt the network connectivity and in all cases gel

formation occurred. Studies have showed that with the incorporation of distilled water into PEGDA at different concentrations, gel fraction was reduced from 99% to 82% (Wu *et al.* 2010b). The effect of batch-to-batch variation on the gel fraction was assessed by synthesising four different batches of hydrogel PEG600A to determine the consistency of individual batches photopolymerised. Following gel fraction calculations it was found that no significant difference was observed ($p>0.05$).

3.1.1.4 Fourier transform infrared spectroscopy

PEGDMA/H_2O hydrogels were characterised using Fourier transform infrared spectroscopy (FTIR). Prior to testing, samples were dried in a vacuum oven at 80°C for 24hr. Figure 3.1 demonstrates that the characteristic bonds for the dimethacrylate groups (C-H, C=C and C-O) have disappeared in the FTIR spectra for the PEG400A-D hydrogels when compared with non-cured PEG400A. Further indication that polymerisation had occurred was confirmed by the disappearance of peaks at 815cm^{-1} (Decker and Moussa 1987; Wu *et al.* 2010b), 1167cm^{-1} (Colthup *et al.* 1975; Wu *et al.* 2010b), and 1637cm^{-1}. This is in agreement with reports in the literature for similar PEG based macromolecular monomers (Lin *et al.* 2006; Kusuma *et al.* 2009; Sagle *et al.* 2009). The spectra for the other molecular weight samples exhibited a comparable trend (see Appendix A). Furthermore, FTIR was carried out on the excess surface solution found on the hydrogels surface after curing. Figure 3.2 verifies that this solution contained unreacted low molecular weight polymer that was not bound to the network as highlighted by the disappearance of peaks at 815cm^{-1} and 1167cm^{-1} respectively. Similar behaviour has been reported in previous studies (Lin *et al.* 2006; Kalakkunnath *et al.* 2007; Ma *et al.* 2010).

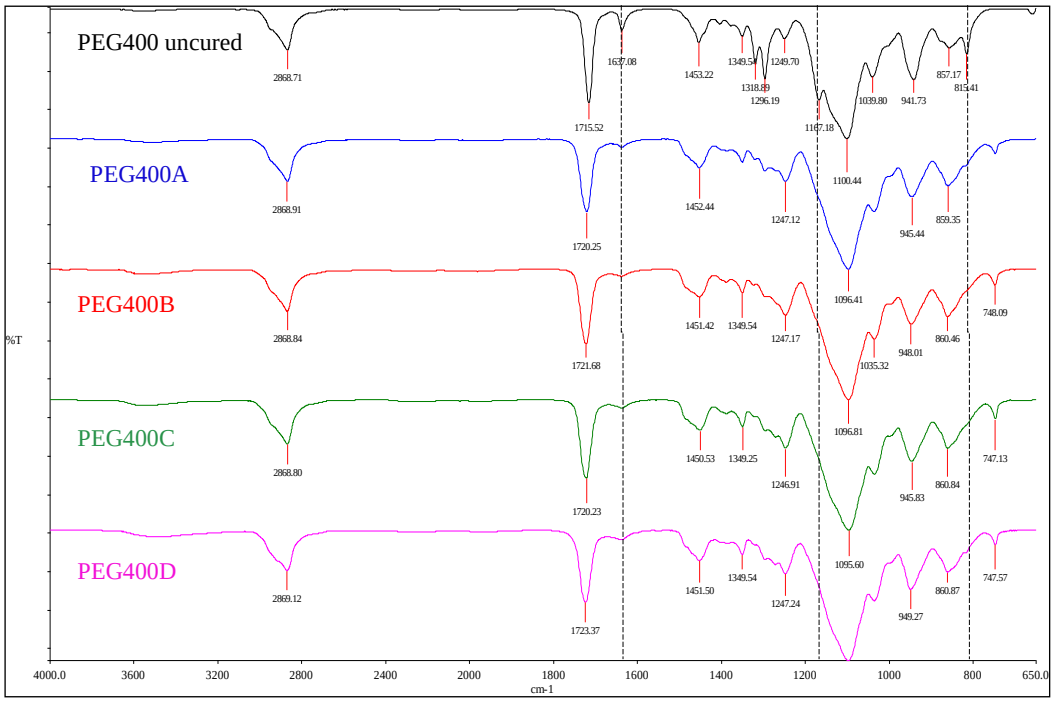

Figure 3.1 *FTIR spectra of PEGDMA 400 and its respective hydrogels*

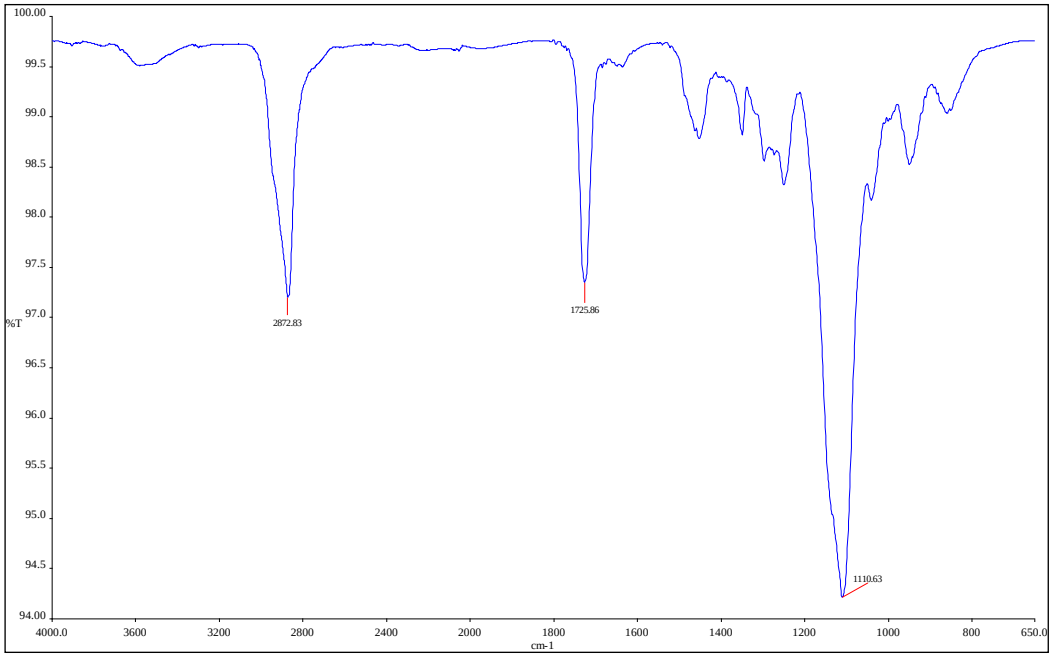

Figure 3.2 *FTIR spectrum of surface solution*

3.1.1.5 Differential scanning calorimetry

The study of the thermal properties of PEGDMA hydrogels synthesised using various molecular weights and water concentrations was carried out using

DSC analysis. A single glass transition temperature (T_g) was observed for each xerogel irrespective of the formulation used. Figure 3.3 illustrates the DSC data for PEG600A-D in the dry state where samples were vacuum oven dried at 80°C for 24hr prior to testing. Incorporation of higher levels of distilled water during the synthesis decreased T_g values (PEG600A: -32.18°C; PEG600B: -35.15°C; PEG600C: -37.27°C; PEG600D: -38.06°C), which is in agreement with reports for PEGDA hydrogels and indicates that H_2O acts as a plasticiser in the polymer (Lin *et al.* 2006). To evaluate the effect of molecular weight, the polymer to distilled water ratio (3:1) was selected. As shown in Figure 3.3, clear changes in T_g values occurred as a result of incorporation of different molecular weight PEGDMA's during the photopolymerisation (PEG1000B: -48.70°C; PEG600B: -35.15°C; PEG400B: -25.37°C). The trend seen for T_g values increasing with reduced molecular weights of PEG was expected. As polymer chain lengths are reduced (with reduced molecular weight) the material becomes less flexible (Hong *et al.* 1996; Devine *et al.* 2006). DSC thermograms on all examined networks revealed no melting transitions relating to the T_m of PEG, demonstrating an absence of crystalline PEG phases (Drumheller *et al.* 1994) and that crosslinking had hindered the polymer capacity to melt (Graham 1987). This has also been shown to be the case for other diacrylates and acrylates (Lin *et al.* 2006; Kusuma *et al.* 2009).

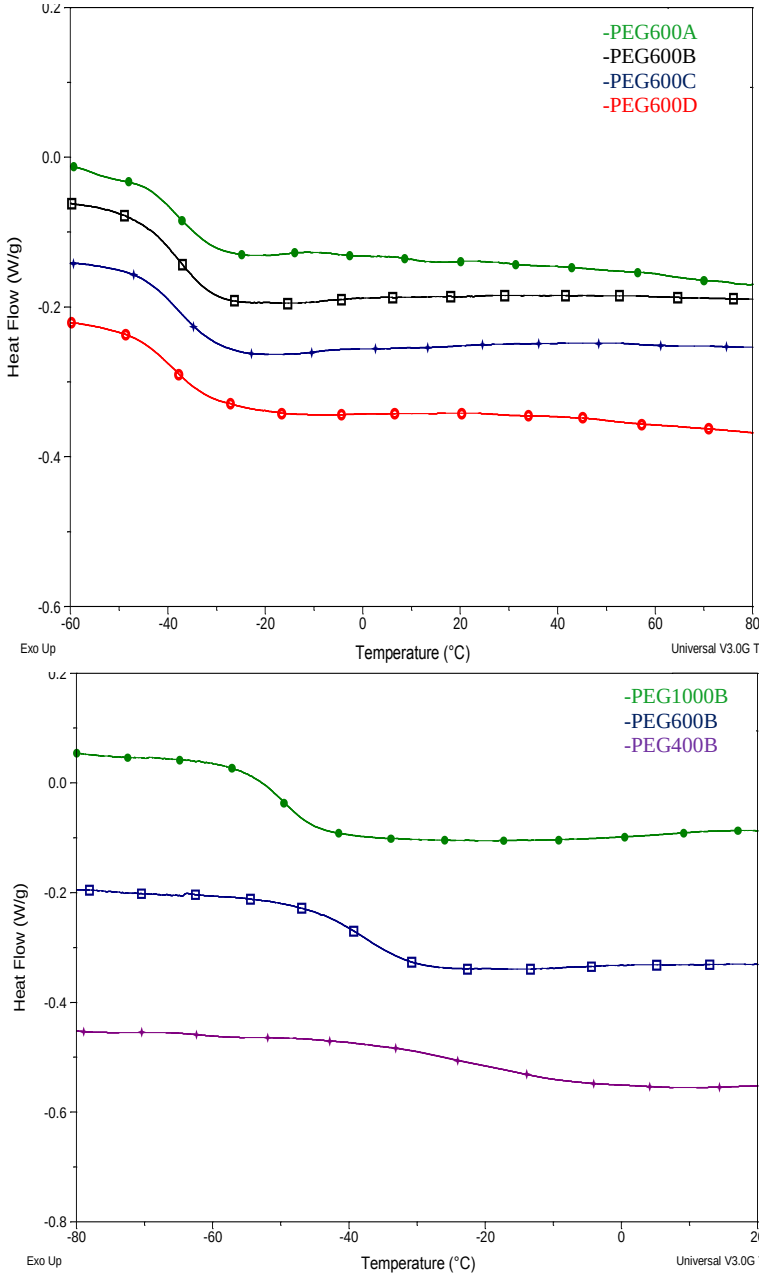

Figure 3.3 *Differential scanning calorimetry thermograms of PEG600A-D samples **(top)** and differential scanning calorimetry thermograms of PEGDMA samples at constant macromolecular monomer concentrations having various molecular weights **(bottom)***

3.1.1.6 Dynamic mechanical thermal analysis

Selected hydrogels were investigated dynamic mechanical thermal analysis (DMTA) to validate the accuracy of the DSC analysis. Dynamic mechanical results for hydrogels PEG1000B-C are plotted in Figure 3.4 as

tensile log vs. temperature at 1Hz. The data shows a step-wise drop in modulus that corresponds to the glass rubber relaxation in these networks and is accompanied by a tan delta peak as shown in Figure 3.5. Dynamic mechanical transition temperature, T_g, defined as the tan delta peak temperature at 1Hz, is shown in Table 3.1. Results detailed herein indicate that the inclusion of distilled water influences the glass transition temperature of the hydrogel network slightly which is in agreement with DSC results. It should however be noted that preparation of samples varied between DSC and DMTA testing. DMTA samples were not vacuum oven dried hence a quantity of water was contained within the materials. This may explain any degree of variation in values between both test methods highlighted in Table 3.1. The rubbery plateau modulus (E_R) from Figure 3.4 shows that an increase in distilled water concentration during synthesis causes a reduction in modulus (PEG1000B: 7.05 versus PEG1000C: 6.75). This reduction in E_R is a reflection of the reduction in the hydrogels crosslinked density and corresponds with results from mesh size analysis.

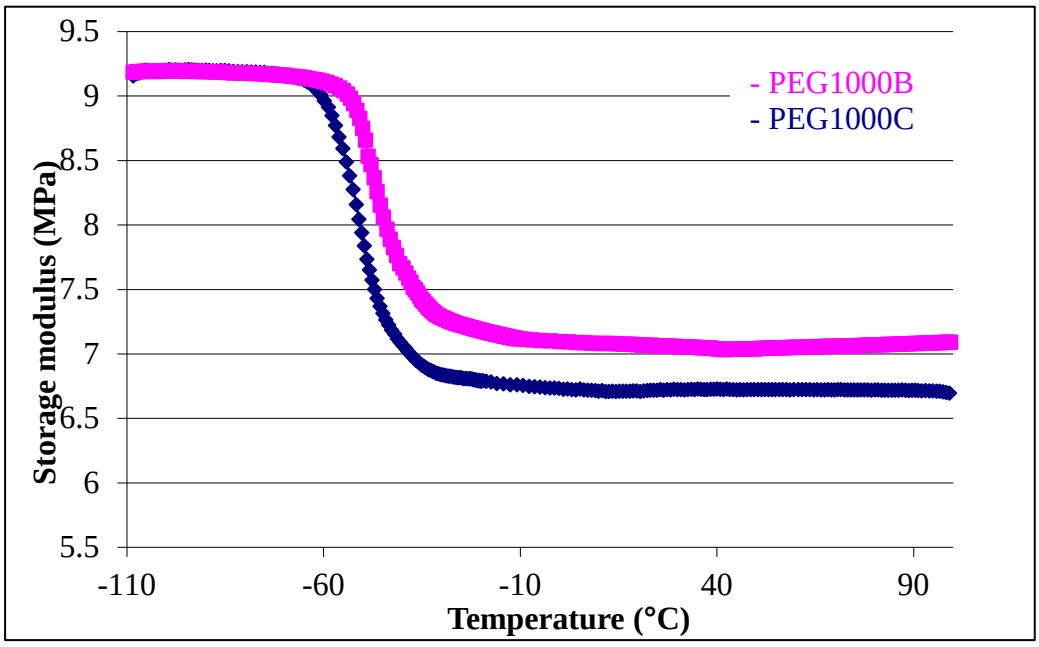

Figure 3.4 *Storage modulus vs. temperature plot at 1Hz for selected hydrogels*

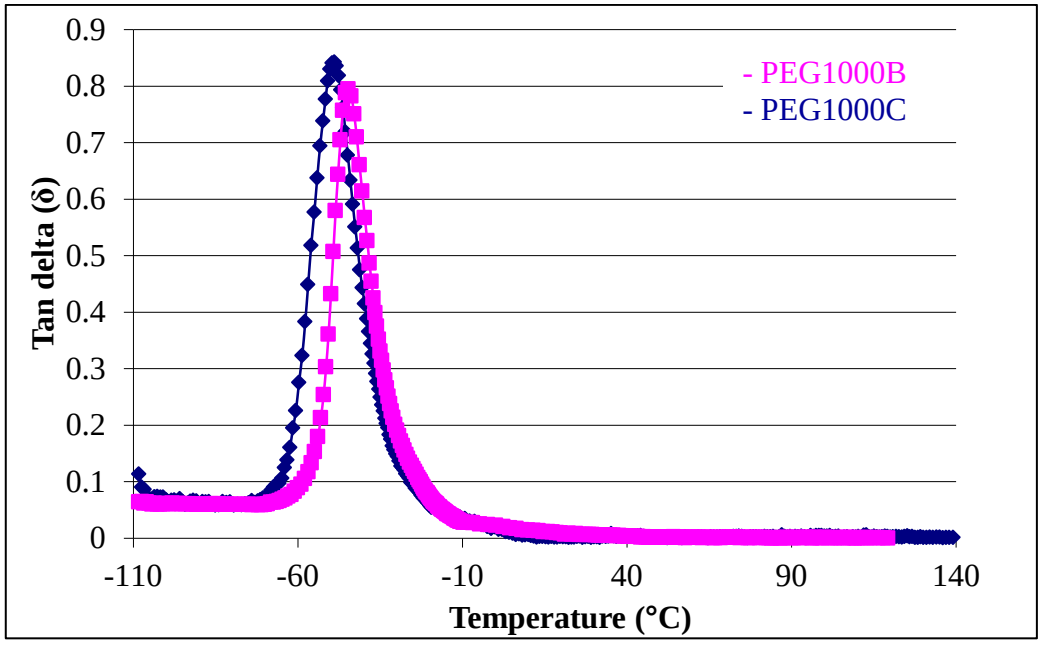

Figure 3.5 *Tan delta vs. temperature plot at 1Hz for selected hydrogels*

3.1.1.7 Swelling studies

Swelling has the ability to affect surface properties, influence solute diffusion as well as the stability of hydrogels (Panda *et al.* 2000). As shown in Figure 3.6, the PEGDMA 1000B-D hydrogels percentage swelling decreased with the incorporation of distilled water during the synthesis of the hydrogel PEG1000B: 58.64±0.89%; PEG1000C: 32.89±2.31% and PEG1000D**:** 10.48±1.74%. This sequence of results was similar for each molecular weight material analysed (see Appendix B). Therefore each of the samples had different W_d values, and this accounts for the apparent differences in equilibrium swelling. Figure 3.7 demonstrates that variation in molecular weight again has a significant effect on the equilibrium swelling properties PEG1000B: 58.64±0.89%; PEG600B: 37.28±1.01% and PEG400B: 11.04±1.32%. Similarly to gel fraction, the effect of batch-to-batch variation on the swelling was assessed using hydrogel PEG1000B which showed no significant difference ($p>0.05$).

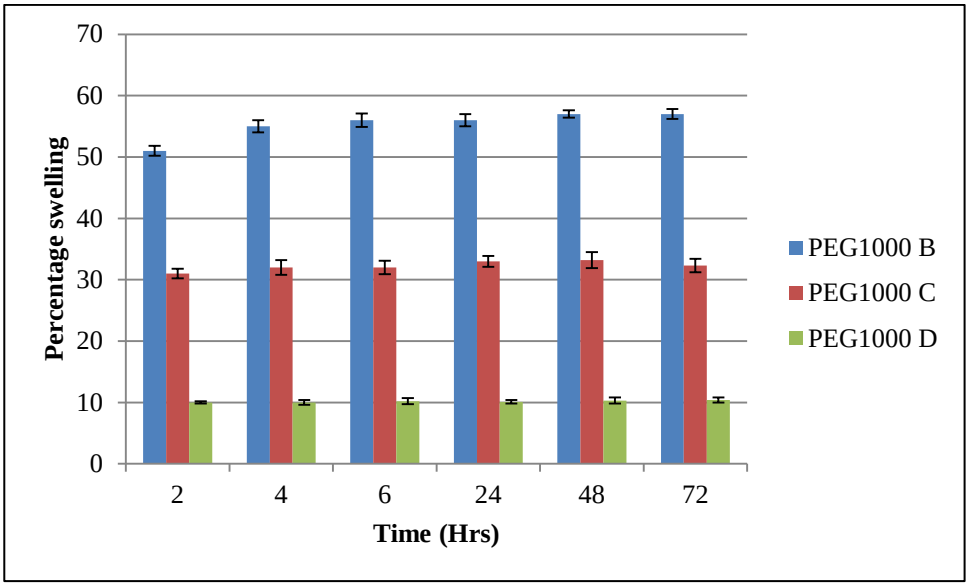

Figure 3.6 *Swelling studies for PEGDMA 1000 at various polymer concentrations*

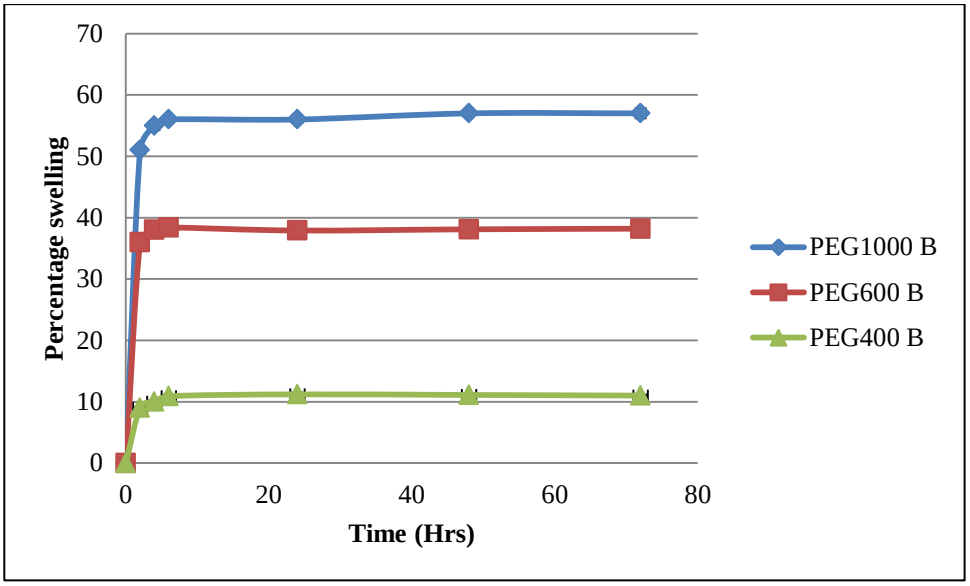

Figure 3.7 *Swelling studies showing the affect of molecular weight on hydrogels water uptake ability*

3.1.1.8 Mesh size

Mesh size is an influential factor for determining the diffusion rate of drug molecules, mechanical strength and degradation rate of a material. The required mesh size of hydrogels for tissue engineering can vary greatly

depending on its application where it can range from 5 to 100nm, in their swollen state. Experimentally, swelling studies (p78, Section 3.1.1.7) were used to calculate the corresponding distance between crosslinks and mesh size (ξ). The Peppas-Merrill model applies to systems which have solvents in their precursor; i.e. distilled water present during photopolymerisation. In this study the corresponding molecular weights between crosslinks (M_c) and mesh size (ξ) were calculated (Table 3.2). Results show that the difference in M_c and ξ values can effectively control the amount of crosslinking in the system (Figure 3.8). As the polymer volume fraction of swollen hydrogels increases, the average molecular weight between crosslinks increases. This also relates to hydrogel mesh size, where the incorporation of the distilled water acting as a spacer significantly increased mesh size for all PEGDMA molecular weights at different ratios ($p<0.001$). A similar outcome was observed for variation in molecular weight between samples, where a reduction in molecular weight caused a reduction in pore size.

However, these calculations only give an approximate result; calculations for M_c were made to quantify the changes in the nature and order of ξ, which arose as a result of changes to network parameters. This calculated value provides a minimum value for pore diameter. Free radical polymerisation rarely goes to completion. This is particularly true for the hydrogels in this study which employed minimum levels of photoinitiator and UV exposure time. The calculations for ξ thus provide a minimum value of pore dimension that directly correlates with changes to the network. Inclusion of a spacer, early termination of the reaction, side reactions, dangling end and chain entanglement can result in an increase in the pore diameter.

Table 3.2 *Molecular weight between crosslinks, crosslink density and mesh size of hydrogels*

Hydrogel code	Molecular weight between crosslinks	Crosslink density	Unperturbed mean-square end-to-end distance	Mesh size (ξ)
PEG1000B	2379	0.0004706	30.37	143.09
PEG1000C	3321	0.0003371	35.88	186.71
PEG1000D	16471	0.0000679	79.90	491.13
PEG600A	881	0.0012713	18.48	67.55
PEG600B	738	0.0015167	16.92	71.51
PEG600C	771	0.0014530	17.28	82.44
PEG600D	726	0.0015404	16.79	102.71
PEG400A	562	0.0019929	14.76	45.06
PEG400B	429	0.0026080	12.90	47.27
PEG400C	391	0.0028670	12.31	53.82
PEG400D	363	0.0030813	11.87	67.95
PEG200A	367	0.0023167	12.63	37.04

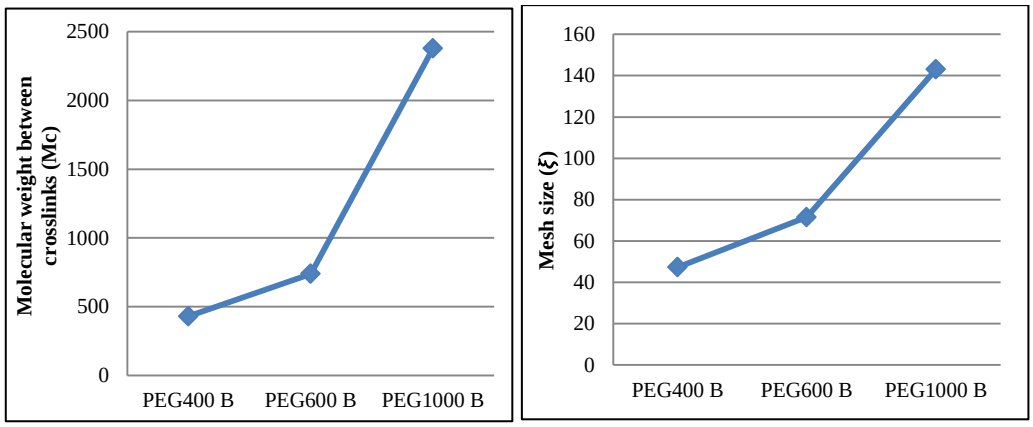

Figure 3.8 *Molecular weight between crosslinks and pore size diameter of hydrogels with variation in molecular weight*

3.1.1.9 Rheological measurement

The AR 1000 Rheometer was used to measure the stress strain relationship of the hydrogels. For all tests, storage modulus (G') values were much greater than the loss modulus (G'') values. The reason for this phenomenon is that an elastic response dominates, which is typical for hydrogels and solid like materials. Figure 3.9 shows the rheological results for all of the hydrogels analysed. In the case of the PEGDMA 1000 hydrogels, G' shifts downwards on increased water incorporation during photopolymerisation (PEG1000B: 70,491Pa; PEG1000C: 51,853Pa; PEG1000D: 14,948Pa). This is expected as the more water in the hydrogel, the weaker the sample. A similar trend was observed for the hydrogels synthesised using the other *Mw* macromolecular monomers (Appendix C). This trend indicates that the increased presence of distilled water during the synthesis decreased crosslink density of the hydrogels (p79, Section 3.1.1.8). Thus, with the distilled water acting as a spacer between the polymer chains, the elastic response and thus strength of the gels decrease, which is reflected by the reduction in the G' value as illustrated in Figure 3.9.

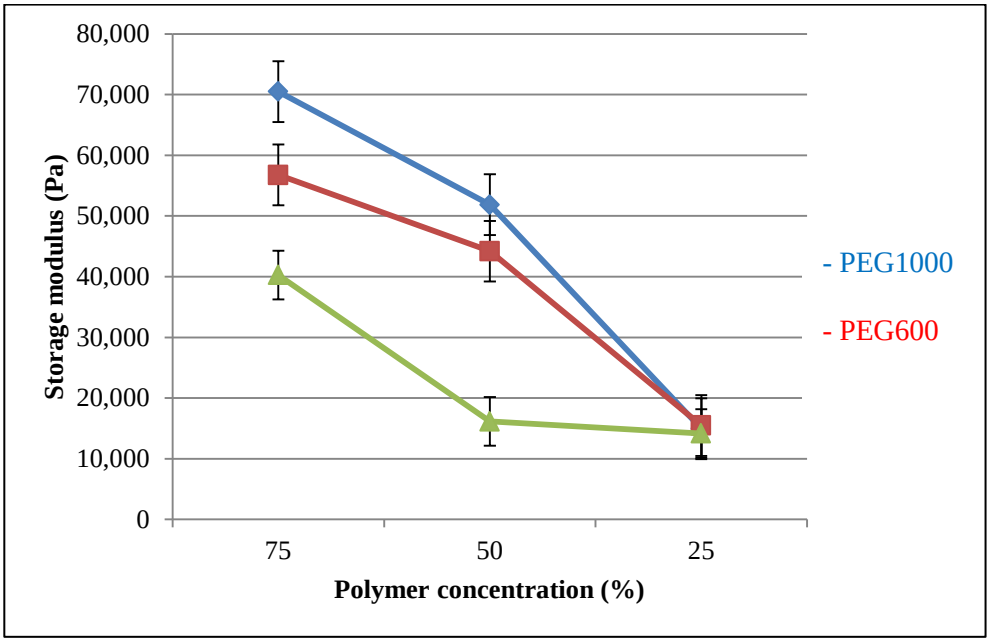

Figure 3.9 *Storage modulus for hydrogels of various molecular weights and associated macromolecular monomer concentration*

Additionally, when comparing hydrogels synthesised using various molecular weights of PEGDMA, significant changes in G' were observed. The gel strength values in this study are favourable in comparison to other studies. Huang *et al.* (2011) used a chitosan/nHAP/collagen gel for potential use in bone tissue engineering and it obtained a gel strength of approximately 10,000Pa which is 6 times inferior than the hydrogels in this study.

3.1.1.10 Uniaxial tensile testing

It has been known for some time that a scaffold must possess adequate mechanical properties to match the intended site of implantation and handling (Hutmacher 2001). The mechanical properties of bone regeneration scaffolds have become even more relevant in recent times as studies have shown that cell migration, spreading, growth and differentiation are all influenced by the substrate's mechanics (Brandl *et al.* 2007). Despite this, the mechanical performance of such scaffolds for bone regeneration are still seen as a secondary requirement and are oftentimes overlooked in favour of more biologically based analysis.

The Young's modulus, tensile strength and percentage elongation of the samples was investigated to determine what influence distilled water incorporation had on the mechanical properties of the hydrogels (Table 3.3). Based on the stress-strain measurements of the hydrogels it was found that hydrogel PEG600A had a significantly higher tensile strength than that of hydrogels PEG600B-D ($p \leq 0.001$ for all comparisons). Similarly, hydrogel PEG600 B had a significantly higher tensile strength than that of PEG600C-D ($p \leq 0.001$ for both comparisons). Modulus results showed that by decreasing polymer concentration, it significantly lowered Young's modulus values between all hydrogels ($p \leq 0.05$). Elongation results showed that PEG600A had a significantly lower elongation than that of hydrogels PEG600C-D ($p \leq 0.5$). Similarly, PEG600B had a significant higher elongation than that of PEG600C-D hydrogels, and PEG600C had significantly higher elongation than PEG600D ($p \leq 0.001$). Young's modulus values varied from 1.96-26.38MPa. These values are significant higher than that reported for other PEG/silicate hydrogels

(1.1kPa) which have been proposed for potential bone regeneration applications (Gaharwar *et al.* 2011b).

Table 3.3 *Mean tensile results for PEGDMA 600*

Sample Reference	Young's modulus (MPa)	Tensile strength (MPa)	Percentage elongation (%)
PEG600A	26.38±4.483	6.22±0.727	43.77±7.289
PEG600B	15.79±0.9565	4.49±0.703	46.21±6.902
PEG600C	5.62±0.778	2.55±0.422	58.55±10.778
PEG600D	1.96±0.289	2.16±0.276	135.61±10.15

3.1.1.11 Cytocompatibility studies

Biocompatibility is an essential property of any material being implanted into the body. Prior to any *in vivo* preclinical testing on animals, the materials must exhibit good biocompatibility. The evaluation of biocompatibility and cytoxicity of hydrogels is therefore a critical step in the development of a material for tissue engineering applications. In order to examine the cytocompatibility of the hydrogels, the cytotoxicity to surrounding cells was investigated. Since any unreacted residues and by-products (unreacted monomers and initiators) from the radical polymerisation reaction can be critical to cell viability, the cytotoxicity of any substance leached from the crosslinked hydrogels was determined.

Even though polyethylene glycol is biocompatible and FDA approved, toxicological assessment is still essential to ensure that the formulation and photopolymerisation process does not alter the properties of the material. The purpose of the MTT assay system is to obtain knowledge concerning the cytotoxic potential of the polymers (p65, Section 2.4.15). This test detects the level of toxicity the sample exerts by assessing mitochondrial activity.

3.1.1.12 The 3-(4, 5-dimethylthiazol-2yl)-2, 5-diphenyl-2 tetrazoliumbromid (MTT Assay)

Many hydrogels are biocompatible in nature, resulting in minimal inflammatory responses and tissue damage (Graham 1998a). Previous work in our laboratory has involved the synthesis of a variety of hydrogels from monomeric precursors (Devine *et al.* 2006; Geever *et al.* 2006; Kennedy and Higginbotham 2011). Toxicological analysis however has shown that such hydrogels require a number of time consuming washing steps to ensure cytocompatibility. This is mainly a result of the high photoinitiator concentration and the presence of minute levels of unreacted monomer following the photopolymerisation process (Geever *et al.* 2008).

In this study, chemically crosslinked hydrogel samples were suitable for elution testing according to the methodology outlined in ISO 10993-5 (2009) due to their insoluble nature. The ability of the mitochondria to convert yellow tetrazolium salt (MTT) to a blue formazan product (Mosmann, 1983) can only occur in viable cells. Based on this testing, the cell viability results for selected hydrogels are shown in Figure 3.10. These hydrogels showed minimal adverse effects on the NIH/3T3 cells. Cell viability was greater than 86% for the hydrogels tested at the different extraction concentrations. It can be concluded that these hydrogels are good candidates for use in implantation.

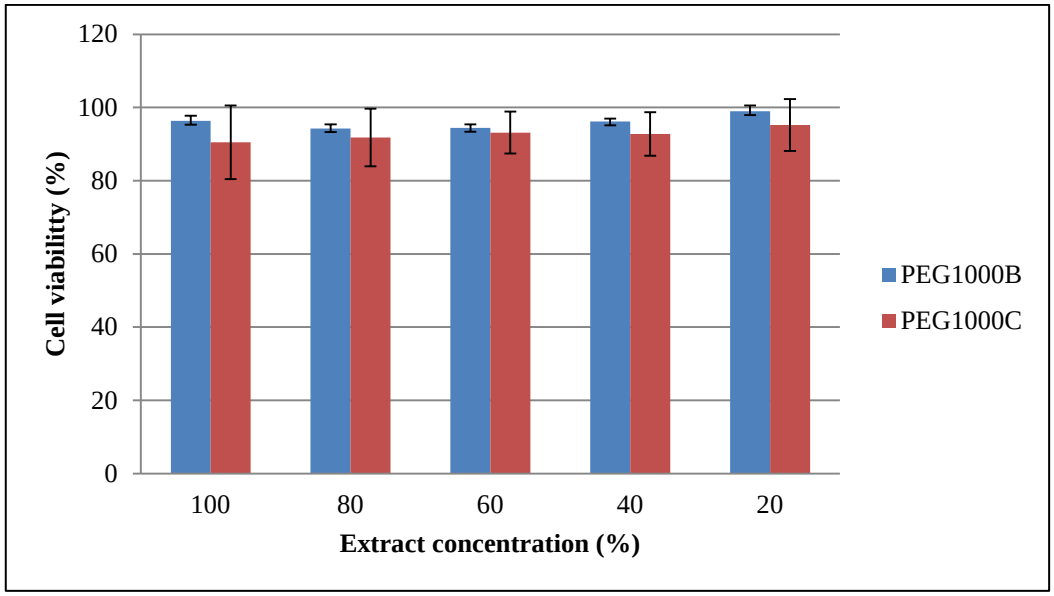

Figure 3.10 *Cell viability of* NIH/3T3 *cells after 24hr exposure at 37°C to various concentrations of PEGDMA hydrogels aqueous solutions as assessed by direct contact testing with the MTT endpoint where n=9±SEM*

3.1.1.13 Summary

The mechanical performance of any biomedical device is of utmost importance. This is particularly the case for materials that will be exploited for bone regeneration applications, where scaffolds are subjected to various loading conditions *in vivo*. The mechanical properties of the PEGDMA hydrogels were controlled by varying the macromolecular monomer concentrations and molecular weights prior to photopolymerisation where tensile strength ranged from 2.16 to 6.20MPa (Table 3.3). These results are lower than those reported for cancellous bone which is typically 40-60MPa (Murugan and Ramakrishna 2005). This would imply that the hydrogel alone would not be sufficient for use in load bearing applications. However, if these hydrogels were used in conjunction with fixation devices, they could be beneficial as bone void filling materials. Alternatively, these materials could be used in other areas of orthopaedic regeneration, for example in guided bone regeneration in the cranomaxcilla facial area (Von Arx *et al*. 2005). In this area, a barrier membrane is used to prevent soft tissue ingrowth into defects typically created in the

alveolar bone following tooth abstraction. In doing so, bone is permitted to grow uninterrupted into the defect space. The MTT assay of selected hydrogels at different extraction concentrations detected no adverse effects due to unreacted species after photopolymerisation, therefore rendering the materials cytocompatible (cell viability >86% for all samples). In light of the lack of mechanical strength of this set of hydrogels, further work was required and involved the selection of a second hydrophobic macromolecular monomer (polypropylene glycol) to further improve the mechanical strength.

3.1.2 Incorporation of PPGDMA into PEGDMA precursor: Investigation of the mechanical properties and thermal behaviour of the hydrogel blends

3.1.2.1 Preface

Due to the ever-increasing number of such cases, bone regeneration has recently come to the forefront of the field of tissue engineering. Bone has the natural ability to heal through the action of osteoblasts, osteoclasts and osteocyte cells, which play vital roles in bone formation and resorption. However in some select circumstances, bone remodelling and repair of large injuries will not occur naturally, e.g. bone resection site following the removal of tumours (Andronescu *et al.* 2010; Wu *et al.* 2011a), bone loss after skeletal trauma (Robert P 1991), spinal arthrodesis (Hsu and Wang 2006) and trabecular voids (Jones and Hench 2003). In such cases biological and synthetic grafts are used to assist the regeneration of bone.

Hydrogels are well suited for tissue engineering applications because their polymeric chains can be varied considerably to meet the desired properties of the host tissue. Photopolymerised hydrogels in particular have been investigated for a number of biomedical applications including prevention of thrombosis (Hill-West *et al.* 1994), wound dressing (Chinanat 2011), controlled release from coatings (Devine and Higginbotham 2005), cartilage (Bryant and Anseth 2003) and bone tissue engineering (Yang *et al.* 2010).

The selection of polypropylene glycol was to improve mechanical strength by reducing the percentage swelling. These scaffolds must offer

adequate initial mechanical strength to replace the mechanical function of the damaged tissue (Hutmacher *et al.* 2008). In this study, the properties of novel crosslinked hydrogels were investigated using polyethylene glycol dimethacrylate (PEGDMA) crosslinked with polypropylene glycol dimethacrylate (PPGDMA). The variation of these two macromolecular monomers at different ratios is reported and the possible molecular weight dependence of various parameters such as mechanical properties (compression strength and gel strength), glass transition temperatures, swelling studies and the ability of these hydrogels to form a 3D network was investigated.

3.1.2.2 Preparation of samples

The hydrogels investigated were chemically crosslinked via photopolymerisation (p46, Section 2.2.1). Similar to the PEGDMA samples described previously (p46, Section 2.2.1), a biocompatible photoinitiator Irgacure 2929 was selected based on the potential tissue engineering application of these hydrogels (Studer *et al.* 2003a; Studer *et al.* 2003b; Karaca *et al.* 2010). Prior to photopolymerisation, an attempt was made to incorporate distilled water into the prepolymerisation mixture which had high concentrations of PPGDMA content, i.e. PPG/PEG400C and PPG/PEG600C. However, this was unsuccessful; the precursor did not form a homogenous mixture thus a hydrogel could not be formed. Similar behaviour had been previously reported for PPG based systems (Bajpai *et al.* 2009; Bajpai *et al.* 2011).

Preliminary studies were carried out (Appendix C) using three different polypropylene glycols (PPGDMA, PPGDA and PPGA) with the addition of distilled water at different concentrations. However, due to the hydrophobic nature of PPG, the solutions were immiscible, therefore, preventing a homogenous mixture for photopolymerisation. After analysis of 100% concentration for the three PPG's, polypropylene glycol dimethacrylate was selected based on obtaining the highest gel strength.

3.1.2.3 Gel fraction measurement

The changes in gel fraction for the PEG/PPG hydrogels are reported in Table 3.4. It was found that the incorporation of increased levels of PEG400 into the system (PPG/PEG400A-C) led to a significantly lower gel fraction ($p<0.05$). This observation was also consistent for PEG600 where sample PPG/PEG600A had a significantly lower gel fraction compared with PPG/PEG600C ($p<0.05$). This variation in gel fraction was associated with the PPG having a higher gel fraction than PEG600 (99.36±0.14% and 96.02±1.05%, respectively).

When comparing gel fraction between similar composition ratios (PPG/PEG400A and PPG/PEG600A) it was significantly higher ($p<0.001$) for the higher molecular weight composition, i.e. PEG600. This increase in gel fraction is linked to the increase in molecular weight of PEGDMA. Single polymer hydrogels of PEGDMA 600 have a higher gel fraction than those of PEGDMA 400 as shown in Section 3.1.1.3. Since gel fraction determines the efficiency of network formation, analysis on batch to batch variation was carried out using hydrogel PPG/PEG400A. Gel fraction was conducted on four separate batches that were synthesised independently. No significant difference was observed between these four batches ($p>0.05$).

Table 3.4 *Gel fraction, glass transition and swelling study results for crosslinked hydrogels*

Hydrogel code*	Gel fraction (%)	Glass transition (°C)	Swelling (%)
PPG	99.36±0.14	-39.22	1.21±0.18
PPG/PEG400A	94.5±1.3	-18.4	12.2±2.2
PPG/PEG400B	95.6±1.2	-31.8	8.1±1.9
PPG/PEG400C	96.4±0.8	-37.3	3.6±1.4
PPG/PEG600A	96.2±1.5	-31.4	36.4±2.0
PPG/PEG600B	98.0±1.8	-33.7	21.0±1.5
PPG/PEG600C	99.8±0.7	-35.5	7.7±0.9

See Table 2.2*

3.1.2.4 Fourier transform infrared spectroscopy

Fourier transform infrared spectroscopy (FTIR) analysis of the hydrogels was carried out and validation of the photopolymerisation reaction was observed through the disappearance of appropriate peaks. A comparison between the precursor solution and photopolymerised hydrogel PPG/PEG400B is shown in Figure 3.11. Similar to PEG hydrogels, the spectra indicate polymerisation occurred with the disappearance of bonds C-H (815cm^{-1}), and C-O (1167cm^{-1}) which is in accordance with the literature (Lin *et al.* 2006; Kalakkunnath *et al.* 2007; Ma *et al.* 2010). The spectra for the other photopolymerised hydrogels demonstrate a similar trend (Appendix A).

The chemical structures of PEG and PPG are very similar, apart from an additional methyl group present in poly(propylene glycol). This difference is evident in Figure 3.11; PPGDMA has two bands, one at 2871cm^{-1} and the second in 2973cm^{-1} corresponding with an alkane dissymmetric stretch. PEGDMA exhibits just one bond at 2869cm^{-1} corresponding with the C-H for an alkane with symmetric stretch.

After photopolymerisation, the surface of the hydrogels again contained small amounts of low molecular weight solution that was not connected to the network. FTIR confirmed that the surface solution was low molecular weight polymer. Previous studies have reported similar behaviour for other acrylates (Lin-Gibson *et al.* 2004; Sagle *et al.* 2009; Smith *et al.* 2009).

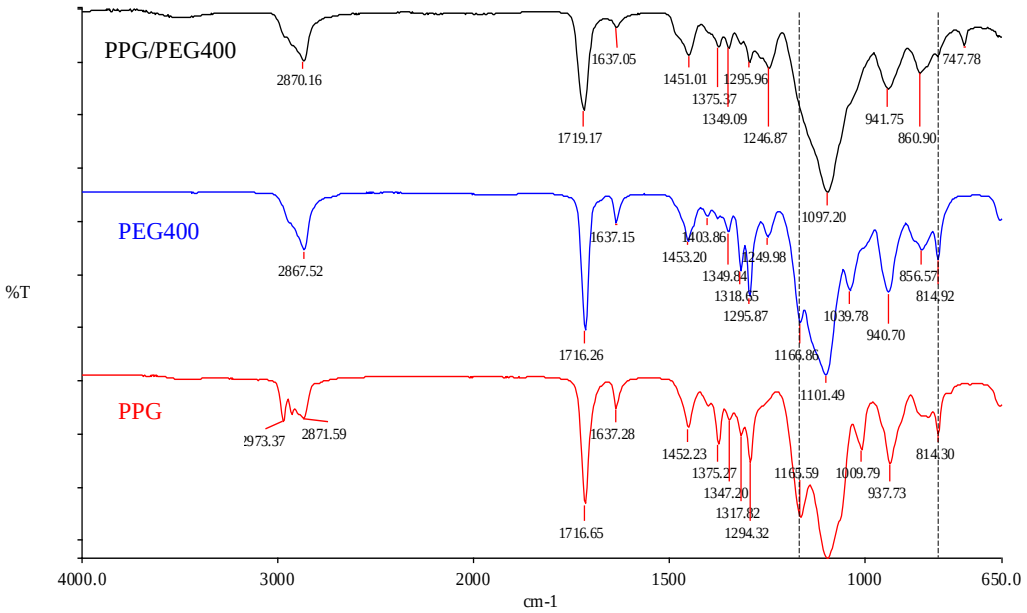

Figure 3.11 *FTIR spectra of macromolecular monomers PEGDMA and PPGDMA and photopolymerised PPG/PEG400 hydrogel*

3.1.2.5 Differential scanning calorimetry

For each xerogel tested, a single glass transition temperature (T_g) was detected (Table 3.4). Subsequently, no melting transition was observed, suggesting a lack of crystalline phases thus preventing the xerogel from melting. When incorporating PPG into the hydrogel the T_g value decreased as shown in Figure 3.12. This trend was consistent for both the PEG400 and PEG600 hydrogels. Therefore, the addition of the PPGDMA with its additional methyl group lowers the overall glass transition temperature of the material, indicating an increase in the mobility of the backbone chain.

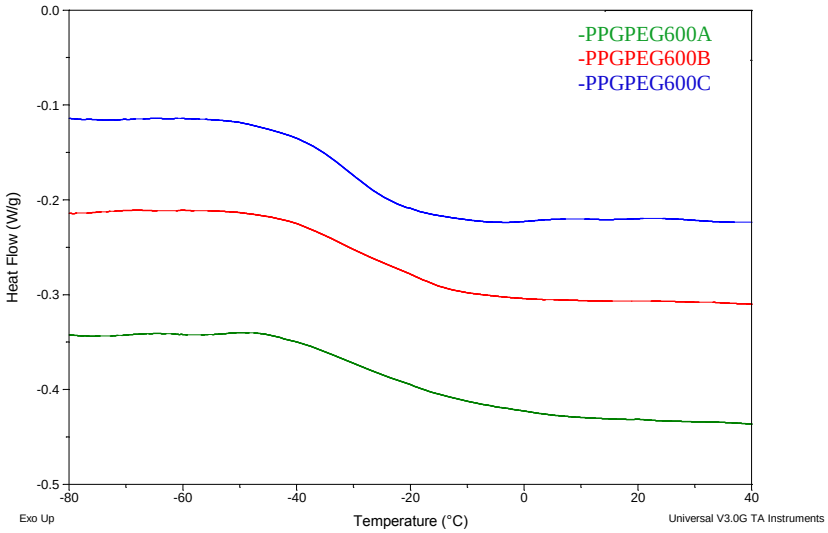

Figure 3.12 *DSC thermographs of PPG/PEG600A-C hydrogels*

3.1.2.6 Swelling studies

Hydrogels are a group of materials that have been recently used to produce scaffolds with potential for bone regeneration applications (Ratanavaraporn *et al.* 2011). Hydrogels are 3-D networks formed from hydrophilic polymers which are crosslinked to form insoluble polymer matrices (Slaughter *et al.* 2009). Their unique structure allows hydrogels to maintain large quantities of water. Many papers in this research area have developed PEG based hydrogels which are biocompatible, but also have relatively high water content. This research endeavours to develop hydrogels that mimic bone to a great extent in terms of water content, hence the use of the more hydrophobic PPG material.

Figure 3.13 shows the swelling study results for hydrogels PPG/PEG600A-C. It was found that the percentage swelling could be controlled by modulating the composition ratio of PEG and PPG. Hydrogel PPG/PEG600A had a significantly higher percentage swelling than that of PPG/PEG600B-C ($p<0.001$), and hydrogel PPG/PEG600B had a significantly higher swelling percentage than that of PPG/PEG600C ($p<0.001$). This series of results correlate with results for hydrogels PPG/PEG400A-C, where PPG/PEG400A had a significantly higher percentage swelling than that of PPG/PEG600C ($p<0.001$), where the percentage swelling varied from 12.2±2.2% to 3.6±1.4% respectively, which is in line with values for native human bone which has a water content of

approximately 10% (Murugan and Ramakrishna 2005). This reduction in percentage swelling is due to the hydrophobic nature of PPG which repels water out of the hydrogel structure. A previous study on PPG based system reported similar findings (Bajpai *et al.* 2011). In designing bone substitute materials, researchers must consider the percentage swelling in terms of the mechanical strength of the bone substitute material (i.e. increases in percentage swelling negatively affects the mechanical properties of hydrogels (Devine and Higginbotham 2005) and also the distance between polymer chains which influences cell migration and neovascularisation). Also, variation in molecular weight had an effect on the swelling properties of the hydrogels (Table 3.4). PPG/PEG400A had a significantly lower swelling percentage than that of PPG/PEG600A ($p<0.001$), PPG/PEG400B had a significantly lower percentage swelling than that of PPG/PEG600B ($p<0.001$), and PPG/PEG400C had a significantly lower percentage swelling than that of PPG/PEG600C ($p<0.001$). This decrease in percentage swelling with variation in molecular weight was due to the shortening in distance between crosslinks for the lower molecular weight PEGDMA 400; causing the hydrogel to imbibe less aqueous solution. These findings are in agreement with those of Devine *et al.* (2005) who observed similar outcomes when using PEGDMA as a crosslinking agent for polyvinylpyrrolidinone/polyacrylic acid systems, where hydrogels containing higher molecular weight crosslinker exhibited higher water contents in the equilibrium swollen state.

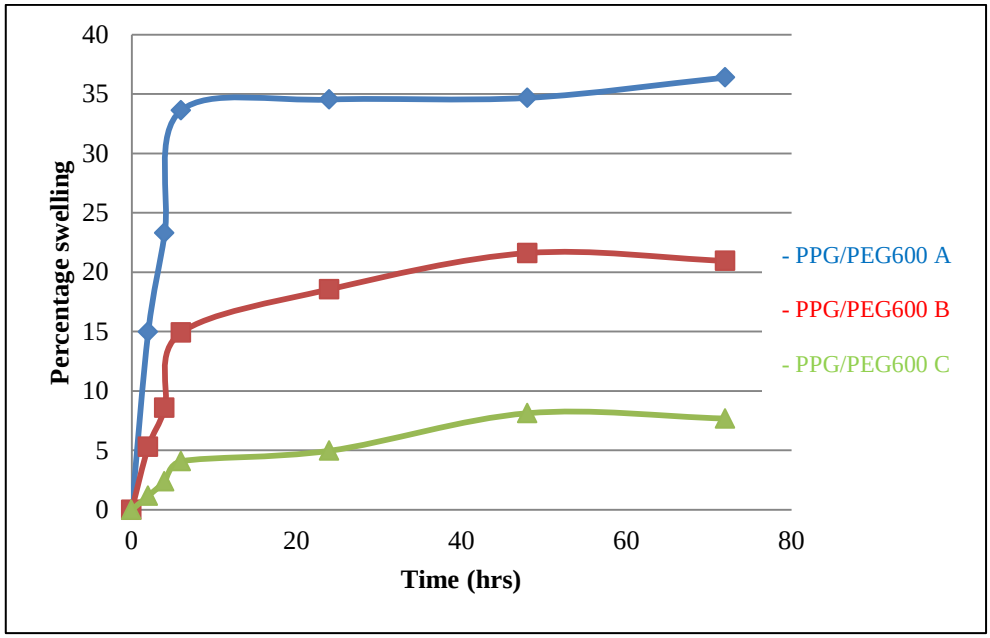

Figure 3.13 *Swelling studies for PPG/PEG600A-C hydrogels*

3.1.2.7 Rheological measurement

3.1.2.7.1 Strain sweep

Strain sweep tests were carried out to determine the variation in shear storage modulus (G') of the hydrogels and also to ascertain the region of linear viscoelasticity for frequency sweep tests. For all samples tested, storage modulus (G') was much greater than that of shear loss modulus (G") where G' for all samples are reported in Table 3.5. The reason for this phenomenon is that the elastic response dominates over the viscous response, which is typical for hydrogels and solid like materials. Initial studies were carried out using the three polypropylene glycols (polypropylene glycol dimethacrylate, polypropylene glycol diacrylate and polypropylene glycol acrylate). After subsequent testing, PPGDMA exhibited the highest gel strength (Appendix C); therefore, further studies were based on the PPGDMA and PEGDMA blends.

Based on the strain measurement (Figure 3.14) it was found that hydrogel PPG/PEG400A had a significantly higher G' value than hydrogel PPG/PEG400C ($p<0.001$). This decrease in G' can be related to PPGDMA having greater flexibility than the PEGDMAs, which is evident for the glass transition temperatures of the material as shown in Section 3.1.2.5, where

hydrogels with higher concentrations of PPG exhibited a reduction in glass transition temperatures. Furthermore, strain sweep measurements were conducted on four separate batches that were synthesised independently. No significant difference was observed between these four batches ($p>0.05$).

Table 3.5 *Mean ± SD values for mechanical testing for crosslinked hydrogels*

	Strain sweep test	Unconfined compression test	Cyclic test	
Hydrogel code*	**Storage modulus (G')**	**Young's modulus (MPa)**	**First cycle load (N)**	**Last cycle load (N)**
PPG	1,571±356	2.8±1.6	142±23.8	109±16.3
PPG/PEG400A	39,721±15,997	4.1±0.8	326.7±116.5	236.9±56.2
PPG/PEG400B	27,709±7,218	3.7±0.1	268.8±47.6	194.2±62.4
PPG/PEG400C	14,996±4,290	3.2±0.3	187.6±18.5	141.6±18.9

See Table 2.2 *

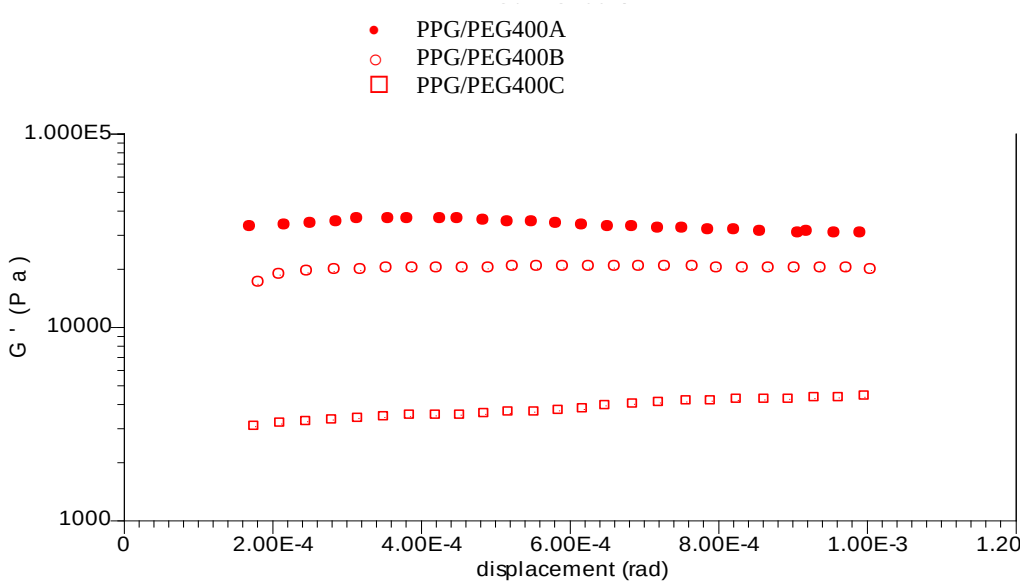

Figure 3.14 *Typical strain sweep plots for PPG/PEG400A-C hydrogels*

3.1.2.7.2 Frequency sweep

Figure 3.15 plots frequency vs. storage modulus (G') for PPG/PEG600A-C hydrogels. The graph illustrates a slight increase in G' with increasing frequency. This indicates that the material is elastic with a small dissipation in energy. There was no experimental evidence for G' being constant (reaching a plateau). This trend is comparable for hydrogels PPG/PEG400A-C. These results also correlate with the strain sweep tests, with increasing PEG content in the composition ratio resulting in a shift upwards in G'.

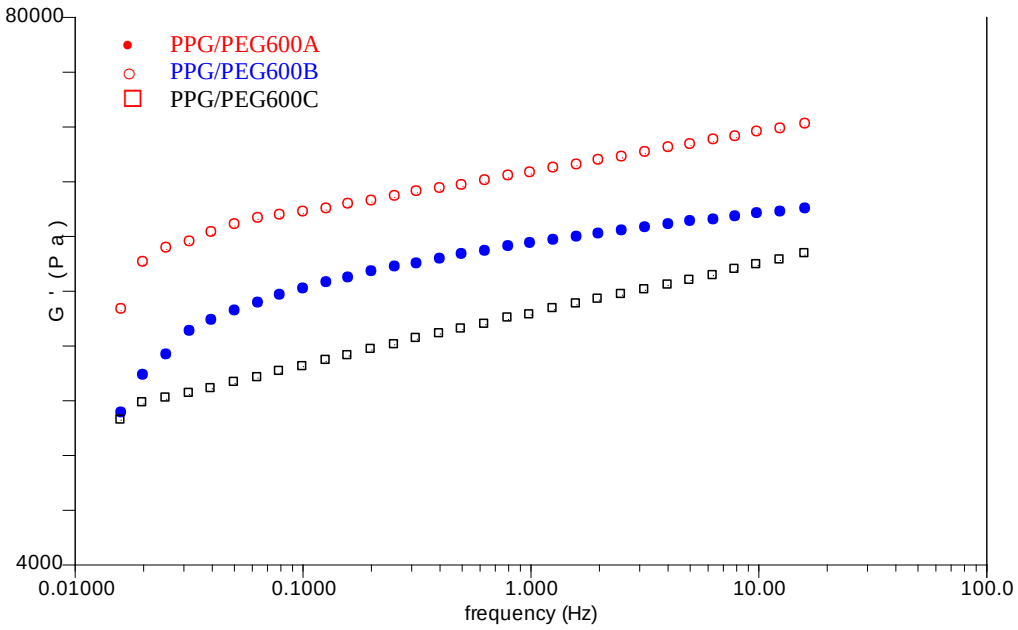

Figure 3.15 *Frequency sweep results for hydrogels PPG/PEG600A-C*

3.1.2.8 Compression testing

Mechanical properties can be used to regulate gene expression of cells in hydrogels (Nicodemus and Bryant 2010). The strength and stiffness of scaffolds *in vivo* are important for the integration with surrounding tissue (Kim and Mooney 1998). Therefore, it is vitally important to ascertain the mechanical properties of any potential tissue engineering scaffold. Results for unconfined compression tests and cyclic tests are summarised in Table 3.5. Unconfined compression tests revealed that the incorporation of PPG into the hydrogel caused a reduction in Young's modulus; values for hydrogel PPG/PEG400A was

significantly higher than for hydrogel PPG/PEG400C ($p<0.05$) as shown in Figure 3.16. These results compare favourable to values reported in the literature for cancellous bone (Murugan and Ramakrishna 2005). This would indicate that the current scaffolds could provide the required mechanical stability for use as a bone substitute material. It can be argued of course that the properties are not sufficient for use in cortical bone which has a compressive strength of 170-193MPa (Murugan and Ramakrishna 2005). Nevertheless, in autologous bone grafting procedures cortio-cancellous bone harvested from the ilium is routinely used.

When testing new tissue engineering scaffolds for bone tissue regeneration, it is important to keep the natural biological reaction to bone remodelling in mind. Bone itself is a dynamic environment which is constantly under remodelling. This remodelling is induced through loading of the bone as occurs for example when walking. It is therefore important to determine the effect of several 'steps' (cyclic loading) on the scaffold. Therefore, in this study a loading rate of 0.5mm/min was selected which would equate to a person slowly loading the limb. It may be argued that 10 loading cycles is insufficient to determine the failure rate of the hydrogel as normal locomotive motion would imply a much greater number of loading cycles. However, in this study 10 cycles were selected to replicate the motion of a patient shortly following injury where motion is restricted and ambulation is normally with assistance. Cyclic test results showed that with the incorporation of higher levels of PEGDMA, the initial cycle load value increased. For example, hydrogel PPG/PEG400A had a significantly higher first cycle load compared to hydrogel PPG/PEG400C ($p<0.05$). This trend remained consistent for the last cycle load ($p<0.05$). When comparing the first cycle load and last cycle load, even though a drop in value was observed, no significant difference was found for hydrogel PPG/PEG400A ($p>0.05$), which would indicate that the structure of the hydrogel was not significantly deformed.

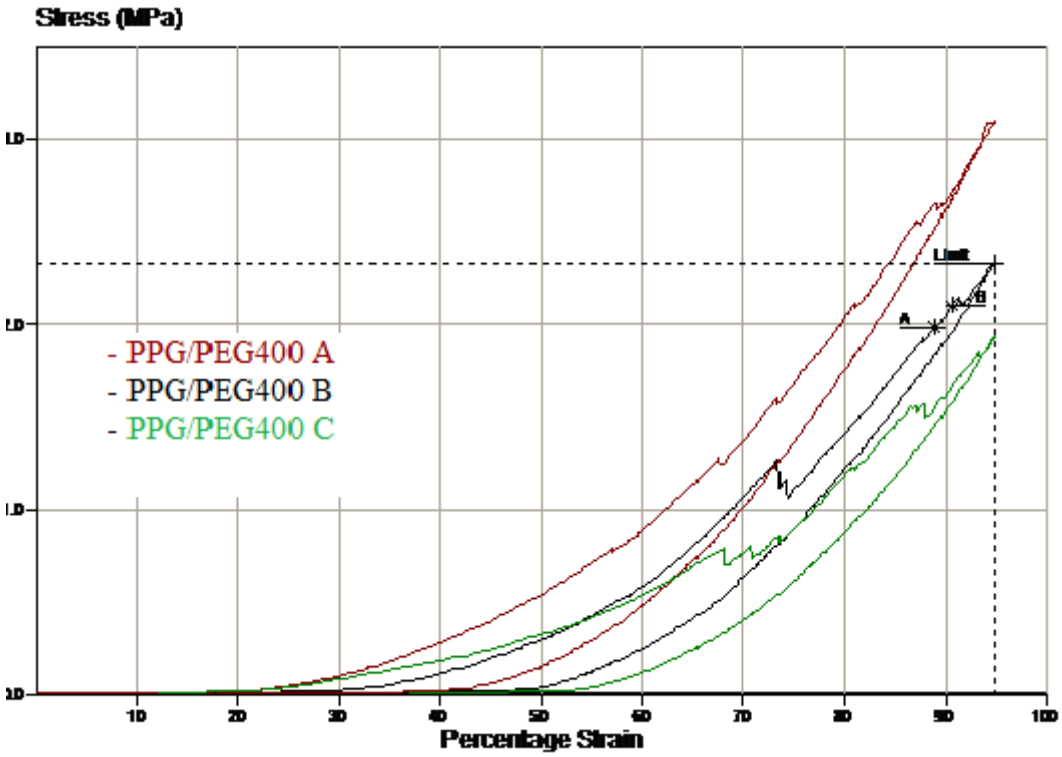

Figure 3.16 *A typical plot for unconfined compression testing for PPG/PEG400A-C hydrogels*

3.1.2.9 Cytocompatibility studies

The MTT assay was carried out under the same guidelines as PEG hydrogels (p84, Section 3.1.1.11). Initial studies were carried out using the polypropylene glycol hydrogels and results are shown in Figure 3.17. In comparing the three different hydrogels, PPGDMA had a slightly higher cell viability percentage. One possible explanation for the increase in toxicity of the PPGDMA hydrogel compared to PEGDMA hydrogels was the incomplete disappearance of the C=C peak at 1640cm^{-1} in IR spectrum for PPG based hydrogels (Figure 3.11) compared to complete disappearance of this peak for PEGDMA based hydrogels (Figure 3.1).

The cell viability values were significantly lower compared to PEG hydrogels (p84, Section 3.1.1.11). According to standards, cell viability requires greater than 70% cell survival for *in vivo* applications. These materials would therefore not be suitable for implantation directly after photopolymerisation. To

overcome the toxic nature of the PPGDMA hydrogels, the samples may require several washing steps.

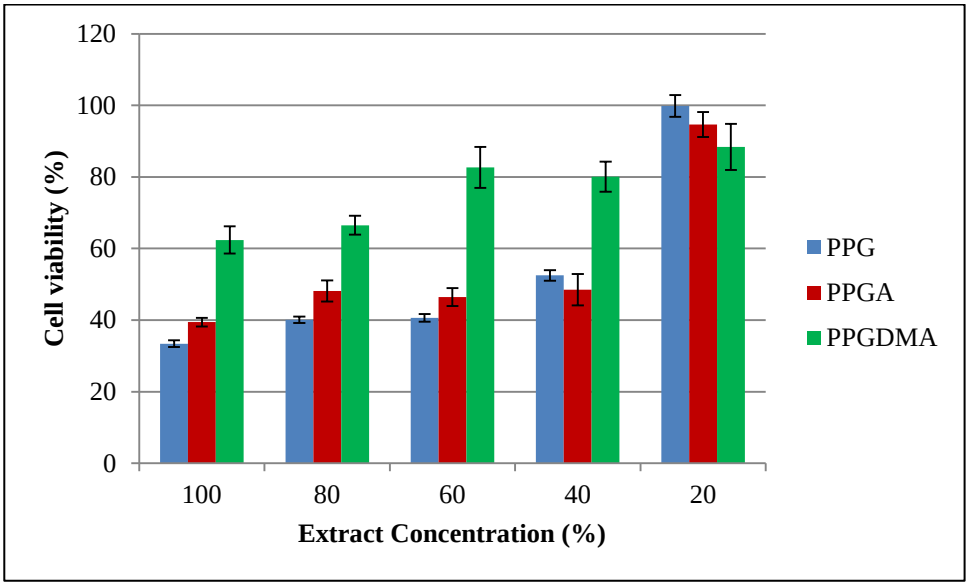

Figure 3.17 *Cell viability of NIH/3T3 cells after 24hr exposure at 37°C to various concentrations of PPG hydrogel aqueous solutions as assessed by direct contact testing with the MTT endpoint where n=9±SEM*

3.1.2.10 Summary

In this body of work, a novel series of crosslinked PEG/PPG hydrogels were prepared via photopolymerisation. The mechanical properties for these hydrogels were controlled by varying the molecular weights of PEG and macromolecular monomer concentrations prior to photopolymerisation. This work illustrates that the addition of PPG into PEG hydrogels negatively affects the mechanical properties of the hydrogels. Unconfined and cyclic compression tests were carried out in order to evaluate potential application as scaffolds for bone tissue regeneration. Results revealed that the incorporation of PPG into the system reduced the compressive strength of the hydrogels. These results are consistent with rheological studies carried out using both strain and frequency sweep tests.

Furthermore, based on the toxicity results, this group of hydrogels are not suitable for implantation unless numerous time-consuming washing steps are performed. It was decided that the addition of polypropylene glycol into the system was not advantageous; therefore, new photopolymerisable hydrogels were selected for further analysis and testing. A literature review of photopolymerisable polymers revealed that polymers such as chitosan derivates, PEG derivatives, hyaluronic acid derivatives and dextran derivatives have been extensively studied, however, little attention has been given to photopolymerised polyvinyl alcohol (PVA). The next body of work therefore, focuses on the synthesis and characterisation of novel maleic PVA for bone tissue engineering.

3.2 Synthesis and photopolymerisation of maleic polyvinyl alcohol based hydrogels

3.2.1 Preface

Polymers and in particular hydrogels, are attractive materials for use in tissue engineering (TE) based on their ability to mimic the chemical composition and water content of the extracellular matrix. Hydrogels can provide a base onto which cells may adhere, proliferate, and differentiate (Fedorovich *et al.* 2009). Studies have shown that hydrogels can be synthesised using either natural or synthetic materials, or a combination of both (Martínez-Ruvalcaba *et al.* 2007; Alina 2011; Wu *et al.* 2011b). Natural hydrogels are generally very weak in terms of mechanical strength because of their limited ability to bond and crosslink. On the other hand synthetic hydrogels are appealing because their chemical properties can be controlled and reproduced. These tailored properties in turn influence the mechanical strength of the material through variation in formation dynamics and crosslinking density (Drury and Mooney 2003). Polyvinyl alcohol (PVA) is a hydrophilic synthetic polymer that has been widely used in different areas of the biomedical field. Recently, PVA hydrogels have become especially attractive in tissue engineering for repairing and regenerating tissues and organs, ophthalmic materials (Kobayashi *et al.* 2004), tendon repair (Kobayashi *et al.* 2001), drug delivery (Yang *et al.* 2007), heart values (Jiang *et al.* 2004), wound healing (Smith *et al.* 2009) and cartilage repair materials (Ma *et al.* 2009). PVA hydrogels can be physically crosslinked using a freeze-thaw fabrication technique. From a mechanical and thermal perspective however, physical crosslinks are not as strong or stable when compared to chemical crosslinks. This fact has led researchers to focus on chemically crosslinked hydrogels for tissue engineering applications that require high mechanical strength, i.e. bone graft substitutes.

PVA was selected for use in this study because of its promising material properties for tissue engineering and also the lack of previous research via photopolymerisation. In addition, using PVA as the base polymer for hydrogel formation was particularly advantageous due to its known biocompatibility and favourable mechanical properties.

3.2.2 Synthesis of maleic PVA

One of the advantages of chemically crosslinked PVA is that it is easy to crosslink due to the abundance of hydroxyl pendent groups on the PVA chains. These hydroxyl groups can be easily substituted with various functional groups. The different methods of fabricating chemically crosslinked PVA hydrogels have included the addition of methacrylate and acrylate pendent groups onto the PVA macromer (Mühlebach *et al.* 1997; Martens *et al.* 2002; Nilasaroya *et al.* 2008). Specifically, acrylic and methacrylic acid (Muhlebach *et al*. 1997), glycidyl acrylate (Martens *et al*. 2002), glycidyl methacrylate and 2-isocyanatoethyl methacrylate (Bryant *et al*. 2003) have all been used to functionalise the PVA backbone. PVA can also be chemically crosslinked without solvents via gamma radiation (Peppas and Merrill 1976; Panda *et al.* 2000). Unfortunately, such crosslinking processes create an inhospitable environment that is not compatible with cells and tissues. One method of crosslinking PVA hydrogels which has received limited attention is via photopolymerisation. The photopolymerisation process is particularly advantageous over the aforementioned chemically crosslinked PVA fabrication techniques because the reaction conditions are mild: gelation occurs within minutes at physiological temperature and pH with temporal and spatial control. These conditions are suitable for preparing a cell carrier system.

A water soluble precursor, maleic PVA, was prepared based on a one-step chemical reaction between maleic anhydride and PVA in toluene sulfonic acid/formamide mixed solvent (p48, Section 2.2.2.1). The present work on the maleic derivate of PVA was undertaken by introducing a free carboxyl to PVA. This process was executed by reacting a monocarboxyl of maleic anhydride with the hydroxyl groups of PVA to increase the density of the negative charge. Yield of the final product was as high as 90% using this one step process. The mixed solvent provided homogeneous mild reaction conditions which minimised the risk of degradation of the maleic component. This particular maleic derivate has a rapid cure rate compared to other chemically crosslinking fabrication techniques. For example, a study by Yu *et al*. (2007) reported that a

methacrylamide chitosan required a two hour gelation time compared to 10min in this study.

Specific chemical characterisation of the maleic PVA structure using both nuclear magnetic resonance (NMR) and Fourier transform infrared spectroscopy (FTIR) is discussed below. A schematic drawing of maleic PVA can be seen in Figure 3.18.

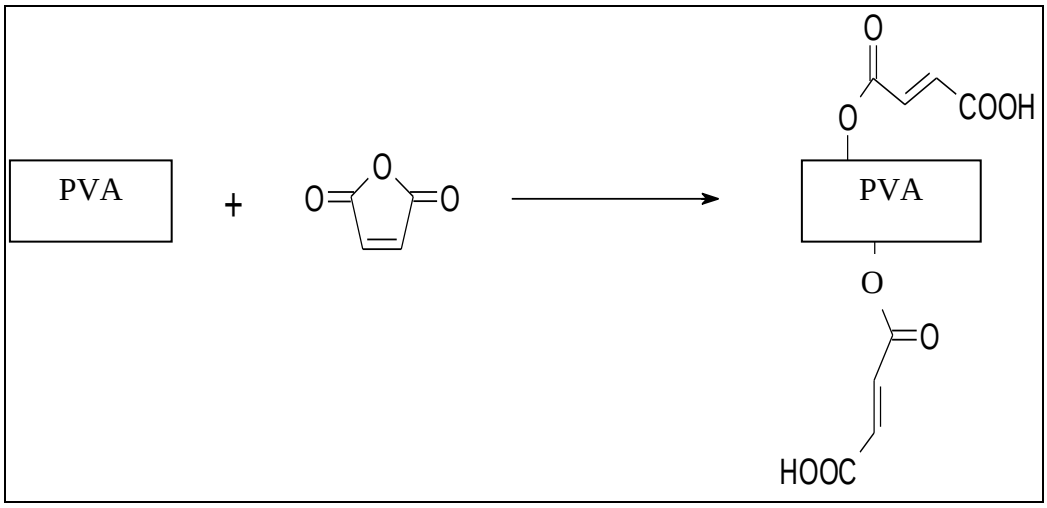

Figure 3.18 *Schematic representation of maleic PVA*

Representative ^{1}H NMR and ^{13}C NMR spectra for maleic PVA are shown in Figures 3.19 and 3.20. The incorporation of double bonds into the PVA backbone was confirmed by ^{1}H NMR, as indicated by the appearance of a proton signal from =C-H at δ_H 5.65 and 6.68ppm (Figure 3.19). A 6.25% integration of the hydroxyl groups of PVA illustrate that it contains the fumaric group. The maleic group isomerises to the fumaric group during synthesis (Zhong *et al*. 2010). One out of every 16 OH groups were acylated by maleic anyhydride. Integration of the peak at 1.48ppm was compared to the integration of the peak at 5.65ppm to determine the percentage of acylation.

Additionally, the formation of new peaks at δ 118 and 142ppm in ^{13}C NMR spectrum was attributed to C signals from the C=C bonds, while the peaks around δ 162 and 175ppm in ^{13}C NMR could be attributed to C signals from the C=O of the acid and ester groups (Figure 3.20) (Zhong *et al*. 2010).

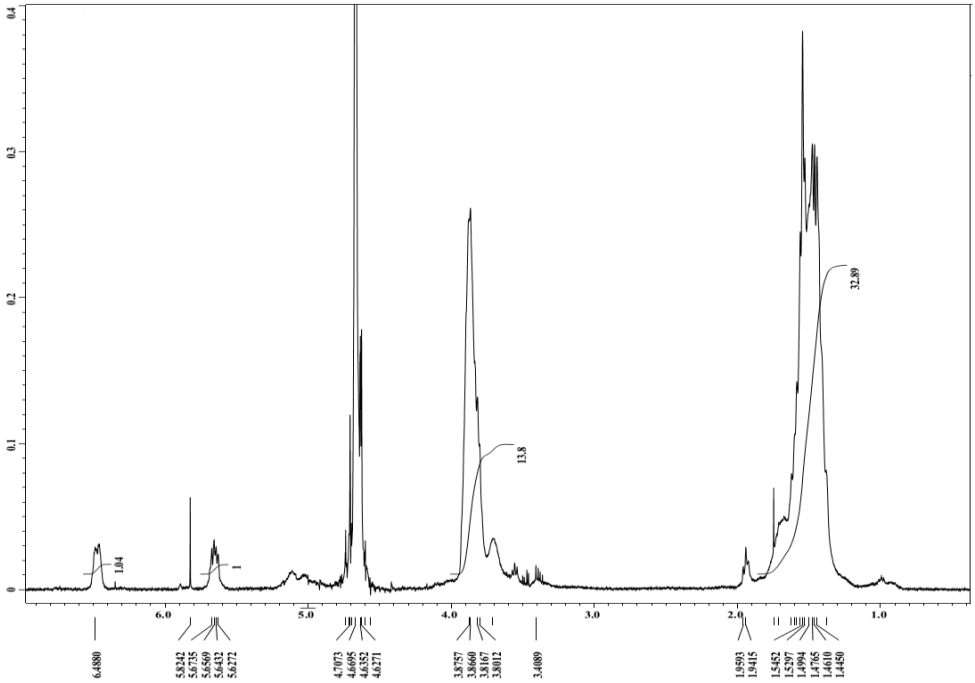

Figure 3.19 *^{1}H NMR spectrum of maleic polyvinyl alcohol*

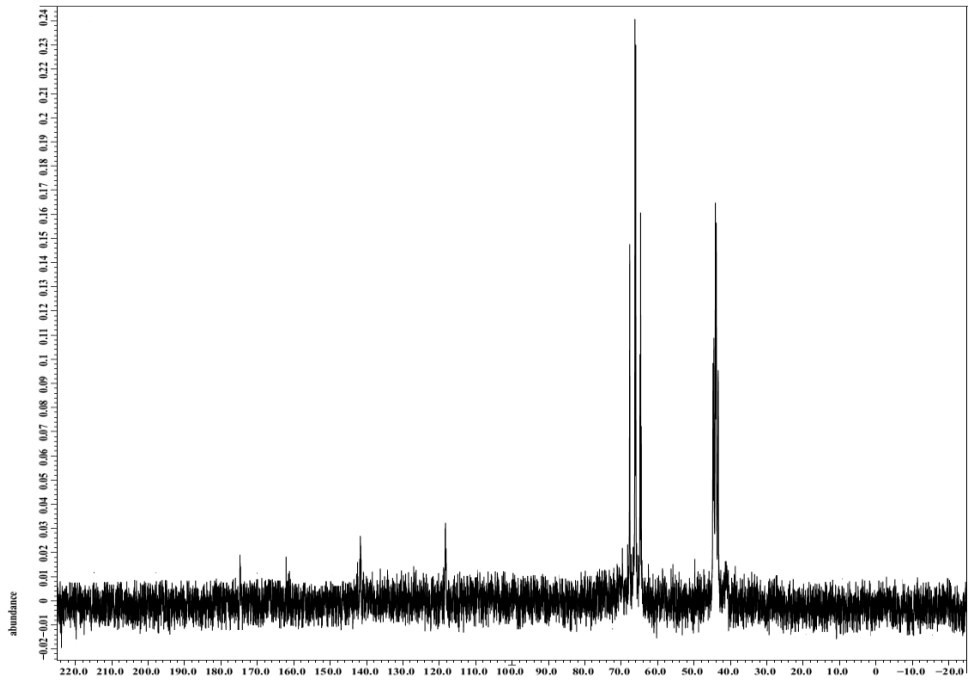

Figure 3.20 *^{13}C NMR spectrum of maleic polyvinyl alcohol*

FTIR analysis was also carried out to confirm the synthesis of maleic PVA. Figure 3.21 shows the FTIR spectrum of PVA before and after the reaction with maleic anhydride. Observations of the region at 1706, 1641, 1577

and 1420cm^{-1} indicates the portion of maleic component which is similar for other maleic derived materials, i.e. carrageenan (Jiang and Guo 2005). These peaks were attributed to asymmetrical stretching vibration and systemetrical stretching vibration of (C=O), (C=C) and –COO of carboxylate.

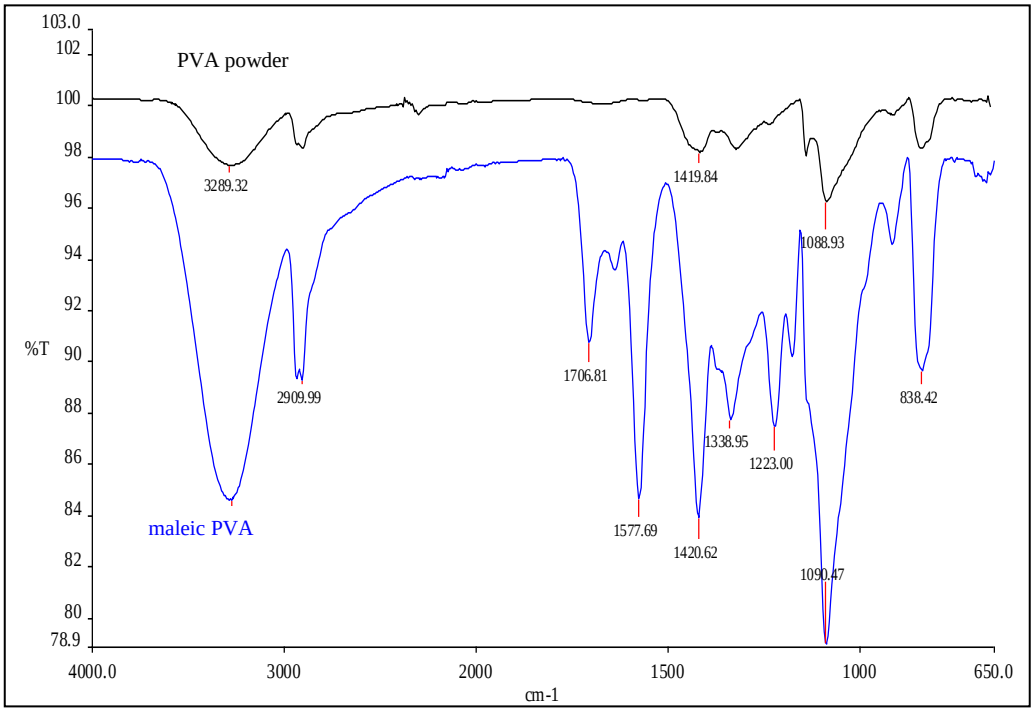

Figure 3.21 *FTIR spectra of PVA before and after the reaction with maleic anhydride*

3.2.3 Freeze drying

After synthesis of maleic PVA, it was required that the polymer be extracted out of solution prior to photopolymerisation. Initial studies were carried out using methanol to separate the water from the polymer, however this technique was unsuccessful. In this case, the maleic bonds broke and converted the synthesised material back into PVA. In order to overcome this drawback, freeze drying was employed. In this process, moisture can be extracted through sublimation which prevents damage to the polymer structure, thereby protecting the integrity of the product (Abdelwahed *et al.* 2006). This process takes a solid (maleic PVA solution frozen at -40°C) and converts the ice to a gas, by-passing

the liquid phase and leaving the polymer product behind. Figure 3.22 shows the final product after sublimation.

Figure 3.22 *Maleic PVA product after freeze drying*

3.2.4 Fabrication of maleic PVA/PEG hydrogels

Initial studies were carried out on photopolymerising maleic PVA alone (p49, Section 2.2.2.2). At low concentrations (1-2wt%), maleic PVA was unable to crosslink due to the increase in inter-chain distance. This increase was caused by water prohibiting polymerisation between the double bonds in the carboxyl end groups (Zhong *et al.* 2010). At higher concentrations, i.e. 5%, a hydrogel was formed however it was very weak and dissolved readily in buffer solution. As the concentration of maleic PVA increased (>10%), the material became insoluble. Therefore, in order to improve the mechanical properties of the hydrogel, PEG 600 and 1000 at different ratios were added into the system in order to obtain material properties of both materials.

3.2.5 Fourier transform infrared spectroscopy

Fourier transform infrared spectroscopy (FTIR) analysis was performed to ascertain the success of photocrosslinking between maleic PVA and PEG hydrogels. The FTIR spectra of the hydrogel samples were compared with those of the corresponding precursors. As shown in Figure 3.23, the main characteristic peaks for maleic PVA were present. These included band 3289cm^{-1}

(characteristic of O–H stretching), and peaks 2909cm^{-1} and 1420cm^{-1} (characteristic of C-H bending and stretching respectively). The main peaks and associated functional groups in the FTIR spectrum for PEGDMA (p73, Section 3.1.1.4) were 2867cm^{-1} (stretching of CH group), 1638cm^{-1} and 1724cm^{-1} (indicating bending of C=C group), 1452cm^{-1} (indicating scissoring band of CCH_2 group), 1349cm^{-1} (indicating C-H vibrations of CH_3 group), and finally 1140cm^{-1} (indicating symmetric and antisymmetric stretching of the O-R group) (Dobić *et al.* 2012). The FTIR spectra of all PVA/PEG hydrogels were similar, although they differed slightly due to the varying feed ratios of the two base materials used. The shift of the C=O peak at 1723cm^{-1} (ester groups of PEGDMA due to conjugation before reaction) and 1719cm^{-1} (ester groups of maleic PVA due to conjugation of C=O before reaction) was due to an overlapping normal ester group at 1736cm^{-1} indicated successful crosslinking of both materials.

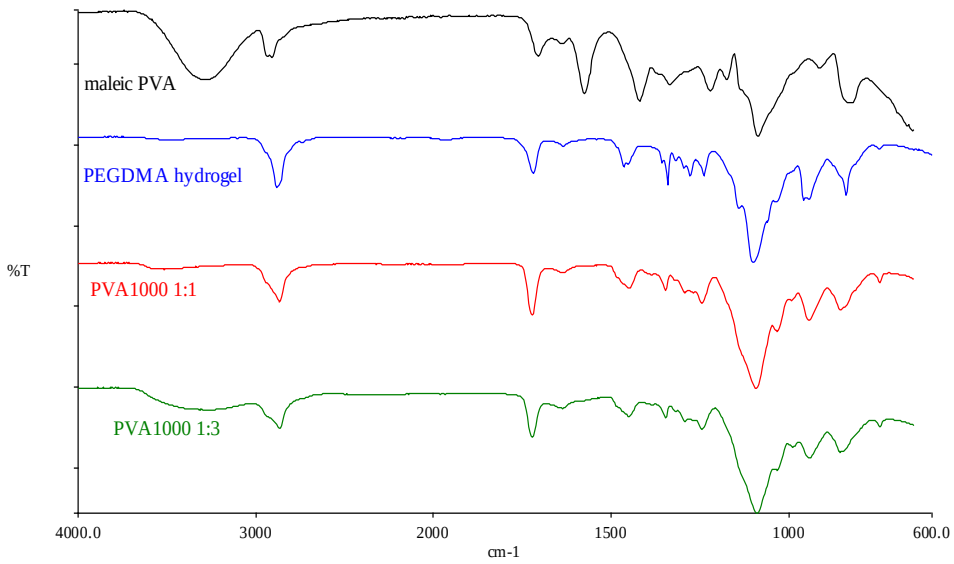

Figure 3.23 *FTIR spectra of maleic PVA, PEGDMA hydrogel, PVA1000 1:1 hydrogel and PVA1000 1:3 hydrogel*

3.2.6 Swelling studies

Figure 3.24 shows the equilibrium percentage swelling for PVA/PEG hydrogels. For all samples tested, hydrogels reached equilibrium swelling within

three days and exhibited high swelling rates during the initial six hours. In this study, PVA/PEG hydrogels exhibited swelling percentages ranging from 41.56±2.81% to 87.76±2.31% as the PEG and maleic PVA ratios varied.

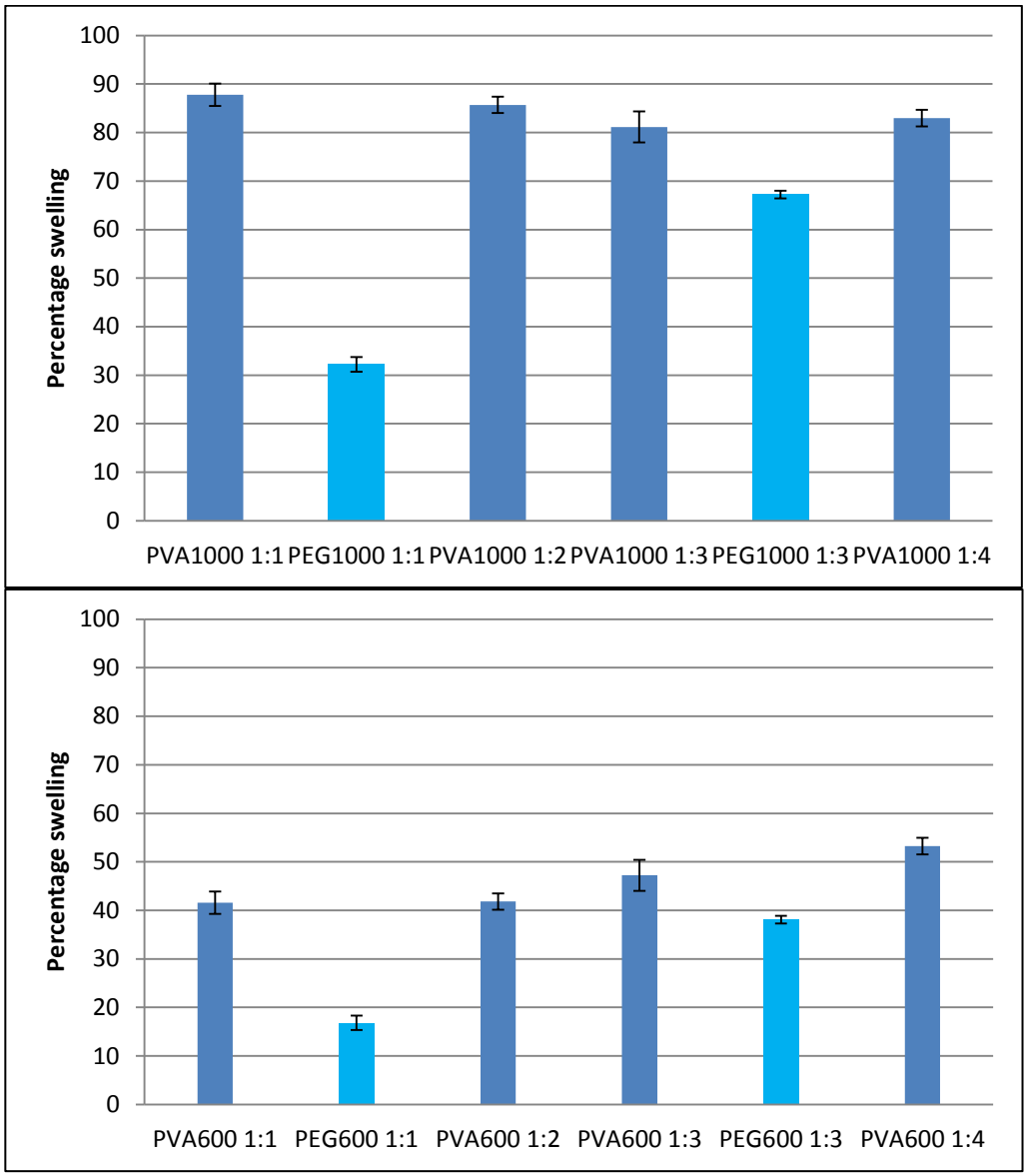

Figure 3.24 *Equilibrium swelling percentage for PVA1000 hydrogels* ***(top)*** *and PVA600 hydrogels* ***(bottom)***

As expected, higher PEG molecular weights created large chain lengths, which provided a larger contact surface between the hydrogel and the buffer solution which resulted in a higher degree of swelling. These results are in

agreement with previous work using PEGDMA hydrogels (p78, Section 3.1.1.7). When comparing the maleic PVA based hydrogels and PEGDMA hydrogels at identical molecular weight and polymer concentrations (Figure 3.24), one can clearly see that PVA based hydrogels had a higher degree of swelling. This increase is associated with the hydrophilic groups of PVA.

3.2.7 Compression testing

As previously stated for the PEG and PPG hydrogels, mechanical strength is a fundamental requirement in tissue engineering, especially for bone regeneration in load bearing applications. Based on the results for PEG and PPG hydrogels in Section 3.1, the aim of this body of work was to chemically crosslink a photopolymerisable polymer blend to further increase the scaffolds mechanical properties. Results for PVA/PEG blends containing different ratios of PEG are collectively shown in Table 3.6. Most of the samples exhibited a linear stress-strain region up to 30%. The compressive modulus for each was calculated within this linear region. Results demonstrated that with the addition of maleic PVA at different ratios, the stress at limit values ranged between 1.04±0.28MPa and 2.08±0.56MPa. Similarly, Young's modulus values ranged from 4.36±0.68MPa to 7.59±0.39MPa. When comparing PEGDMA samples and PVA/PEGDMA hydrogels, the latter had a slight increase in compressive strength. For example, when investigating hydrogels with and without maleic PVA concentration (PEG1000C and PVA1000 1:1, which have the same molecular weight and polymer concentration of PEGDMA), Young's modulus for PEG1000C was 4.36MPa compared to 5.56MPa for PVA1000 1:1. Similarly, this was the case for stress at limit values for the hydrogels. This increase in strength can be attributed to additional crosslinking in the system with the introduction of maleic PVA. This increase in compressive strength could be further improved by controlling the degree of swelling since hydrogels would typically reduce in mechanical strength with an increase in water content. However, in statistical comparison between batches, the increase in strength was not significant ($p>0.05$).

Table 3.6 *Mechanical properties for PVA/PEGDMA hydrogels*

Hydrogel Code	Stress at limit (MPa)	Young's modulus (MPa)	Strain sweep (G')
PVA1000 1:1	1.42±0.24	5.00±0.09	23,221±4,218
PVA1000 1:2	1.48±0.46	5.69±0.60	31,461±5,994
PVA1000 1:3	1.69±0.23	6.18±0.60	48,002±17,646
PVA1000 1:4	2.08±0.56	7.59±0.39	51,752±8,160
PVA600 1:1	1.04±0.28	4.36±0.68	19,619±9,483
PVA600 1:2	1.38±0.11	4.69±0.74	26,947±8,244
PVA600 1:3	1.51±0.35	5.36±0.71	39,641±13,418
PVA600 1:4	1.74±0.25	5.89±0.35	41,243±6,434

3.2.8 Rheological studies

Biomaterials are inherently structured and often exhibit nonlinear mechanical properties. The *in vivo* physiological conditions commonly produce mechanical loading which evokes a nonlinear rheological response. In some instances this is essential for biological functioning, i.e. strain-stiffening of arterial walls (Doyle *et al.* 2012). A material mechanical response may be associated with either deformation (elastic properties) or the rate of deformation (viscous properties). In the case of a purely elastic material, the stress response is only a function of the imposed strain. On the other hand, a purely viscous material can be measured by imposing a constant rate of simple shear deformation and measuring the resulting shear stress. Polymers and particular hydrogels behave mostly as viscoelastic materials, where the stress response is a function of both strain and strain-rate. Rheological studies were carried out in oscillatory mode where both viscous and elastic properties can be simultaneously tested by subjecting a material to oscillatory deformation. Studies were carried out using a strain sweep to first verify the strength and secondly to determine the hydrogels linear viscoelastic region (LVR) for subsequent frequency sweep tests.

For strain sweep results, a representative strain sweep plot for PVA/PEGDMA hydrogels is shown in Figure 3.25. Similar to hydrogels in

Section 3.1.2.7, the elastic response (storage modulus, G') was much greater than the viscous response, i.e. loss modulus (G"). Initial attempts were made to carry out strain sweep tests on hydrogels containing only maleic PVA, however due to the ease of dislocation in buffer solution, neither G' or G" was recorded. Storage modulus (G') values for PVA/PEG hydrogels are shown in Table 3.6. In the case of both PVA1000 and PVA600 hydrogels, an increase in G' was observed with the increase in PEG ratio for all samples. This increase was associated with the addition in crosslinking in the system with the PEG component.

Further rheological studies were carried out on PVA based hydrogels by subjecting them to a frequency sweep. From strain sweep tests, the linear viscoelastic region (LVR) for all samples was within 0.1% strain. The LVR parameter is an important factor as the material function is interrelated within this region for frequency sweep tests. Outside this region, the viscoelastic response for materials measured is not always consistent. Figure 3.26 illustrates the increase of the storage modulus with the increase in frequency. Similar to the hydrogels in Section 3.1.2.7.2, this phenomenon was due to the differences in the intertwined polymer chains between crosslinks. At low frequencies, the polymeric chains had the ability to relax and return to their original position. When the hydrogel is placed under a higher frequency, the recovery of the chains was not instantaneous due of the restriction of the chains. This resulted in a higher storage modulus (G') (Gaharwar et al. 2011b).

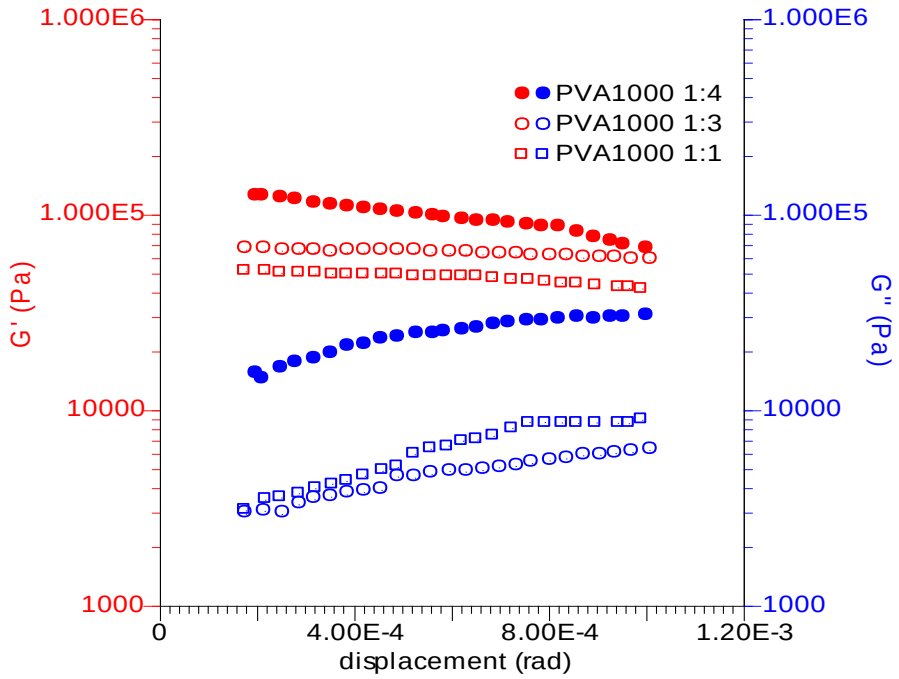

Figure 3.25 *Strain sweep results for PVA/PEG blends*

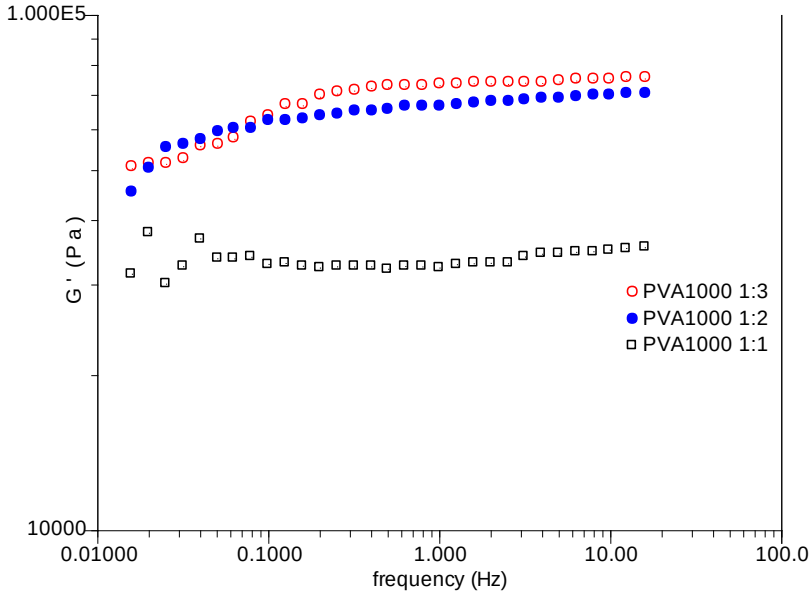

Figure 3.26 *Frequency sweep results for PVA/PEG blends*

3.2.9 Drug release

Bone is the storage house for blood cells, fat, mineral and growth factors, however it has very poor perfusion properties due to its compact nature (Baro *et*

al. 2002). In this study selected hydrogels were tested to determine the release profile using dexamethasone (Figure 2.5). Hydrogels are ideal candidates for drug delivery because they have unique tunable properties that are controlled by their chemical structure, molecular weight, interaction between the polymer and the drug, and drug molecule size (Hoare and Kohane 2008).

In this study the initial dexamethasone content of the hydrogel composites was 6.25wt% and the drug release was measured as a function of *in vitro* immersion time. Figure 3.27 shows that each hydrogel had an initial burst release followed by a delay and continuous release of dexamethasone. Initial burst release within 24hr was due to rapid swelling of hydrogel composites and drug located on the surface of the hydrogel. The variation in drug release profiles between PVA600 1:1 and PVA600 1:4 hydrogels was associated with the change in pore size which was controlled by PEGDMA content. The higher the water concentration in the sample prior to photopolymerisation resulted in an increase of the pore size within the sample. This trend was observed for the PEGDMA hydrogels in Section 3.1.1.8. On the creation of larger pores, this allows the drug molecule to release more quickly out of the hydrogel composite.

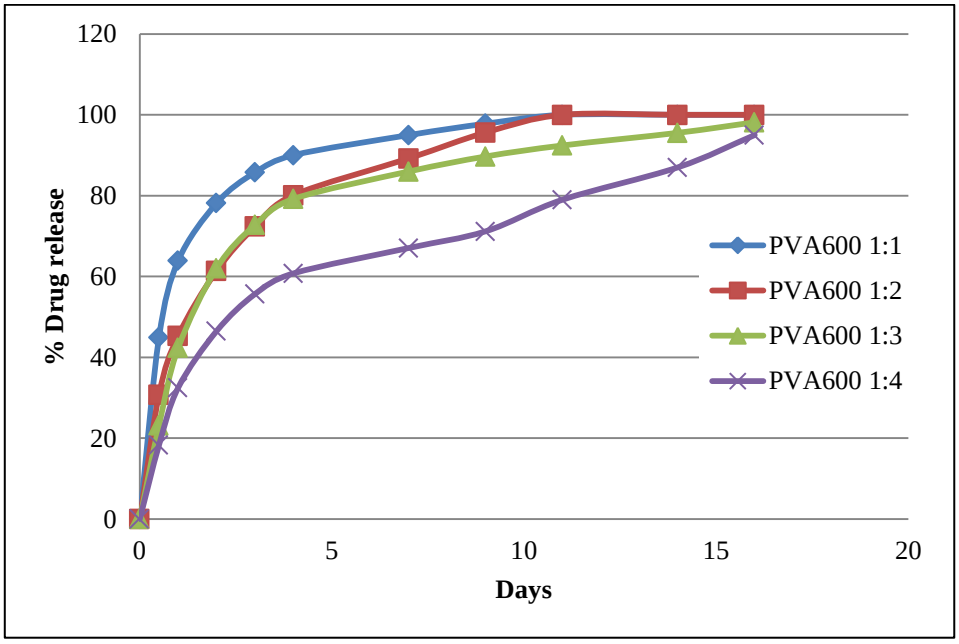

Figure 3.27 *Drug release studies for PEG600 maleic PVA samples*

3.2.10 Cytocompatibility testing

The cytotoxicity of PVA/PEG hydrogels was evaluated using the MTT assay (Figure 3.28). After subsequent mechanical characterisation, the PVA1000 1:3 hydrogel was selected for MTT assay analysis because of its compressive strength. Photopolymerisation of these hydrogels was in compliance with cytocompatible initiating conditions (Bryant *et al.* 2000). The results of the MTT assay indicated no adverse effects on the NIH/3T3 cells. For samples run using the blank control, more than 88% of cells treated were viable at all concentrations tested. Therefore, it can be concluded that successful polymerisation occurred between polymer blends. This indicates that these hydrogels have good potential as candidates for the use in implantation devices since no toxic by-products (such as unreacted monomers, maleic PVA and PEGDMA) or photoinitiator leached out of the hydrogel.

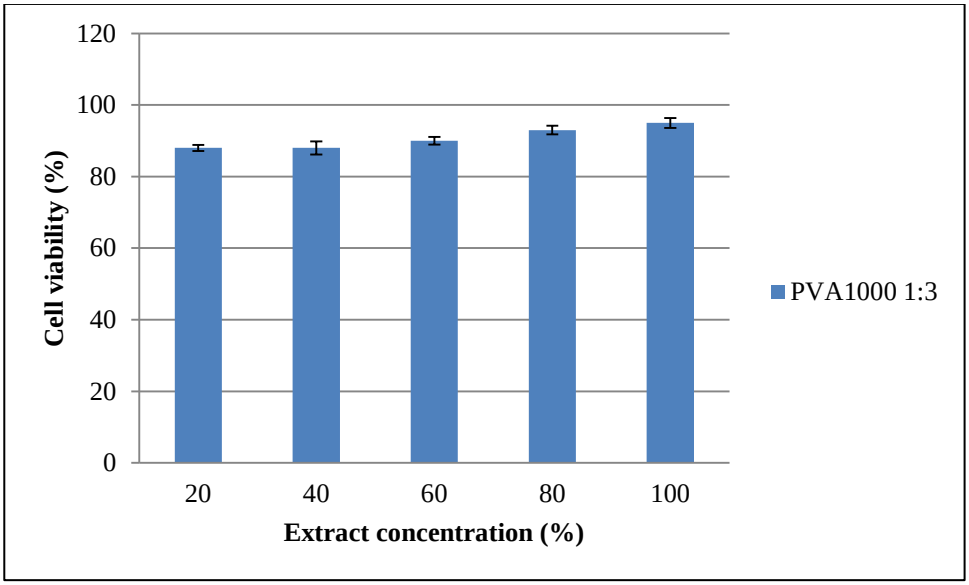

Figure 3.28 *Cell viability of NIH/3T3 cells after 24hr exposure at 37°C to various concentrations of PVA1000 1:3 hydrogel aqueous solutions as assessed by direct contact testing with the MTT endpoint where n=9±SEM*

3.2.11 Summary

The novel synthesis of photopolymerisable maleic PVA was conducted through a one step reaction between maleic anhydride and PVA in toluene sulfonic acid/formamide mixed solvent. Synthesis was confirmed using NMR by the 6.25% integration of the hydroxyl groups of PVA contained in the fumaric group (the maleic group isomerises to the fumaric group during the synthesis), namely 1 out of every 16 OH groups were acylated by maleic anhydride. FTIR further confirmed successful synthesis by the peaks and their corresponding groups of the maleic component: 1706cm^{-1} (associated with C=O), 1641cm^{-1} (corresponding to C=C), 1590 and 1420cm^{-1} (related to -COO). Photopolymerisation of maleic PVA hydrogels resulted in a weak material which was caused by water prohibiting polymerisation between the double bonds in the carboxyl end groups. As a result PEG was incorporated into the system to improve the material's mechanical strength. In comparing hydrogels with and without maleic PVA incorporated, compression tests showed an increase in Young's modulus and stress at limit values for PVA based hydrogels. MTT assay results illustrated that the hydrogels were biocompatible making them a viable potential scaffold for bone tissue engineering. Even with these improvements in compressive properties, the hydrogels were still limited in terms of mechanical strength compared to actual bone. In addition, polymers are known to have limited bioactive properties. Therefore, the next step in this study was to incorporate different bioceramics to improve mechanical strength and bioactivity of the hydrogels.

3.3 Photopolymerisation and mechanical testing of hydrogel based composites

Since the first bone graft substitute was carried out in 1889, the goal in bone tissue engineering has been to repair and restore damaged bone to its original function (Williams 1987). From 2009 the European market for bone grafts and bone cements is expected to almost double by 2016 (Sullivan 2011). Due to the anticipated increase in the market size and the current issues with biological grafts, synthetic bone graft substitutes are expected to play a vital role in bone regeneration.

Polymers are frequently used; however, they are limited in terms of mechanical strength (mechanical properties to replicate *in vivo* conditions for load bearing systems) which has been demonstrated by the hydrogels photopolymerised in Sections 3.1-3.2. Similarly, bioceramics are often used; but they have issues in terms of particle migration, settling, handleability, flexibility, fatigue strength and are brittle in nature and therefore, are not suitable or reliable as load bearing bone graft substitutes (Wu and Xiao 2009). To overcome these drawbacks, polymer composites are coming to the forefront as synthetic materials used in bone regeneration (Murugan and Ramakrishna 2005; Yunos et al. 2008; Hajiali et al. 2010; Puértolas et al. 2011; Vivanco et al. 2012). The mechanical properties of these composites can be modified to produce a synthetic bone graft substitute that exhibits toughness and plasticity from the polymeric phase and the compressive strength and bioactivity properties typical of the bioceramics.

This section focuses on the incorporation of three different bioceramics (bioactive glass, beta tricalcium phosphate and hydroxyapatite) into the PEGDMA precursor to improve the mechanical performance of the scaffolds. The main objective of the work presented in this section was to determine the optimum bioceramic in terms of mechanical properties by varying the formulations using different bioceramic and polymer concentrations.

3.3.1 Bioactive glass based composites

3.3.1.1 Photopolymerisation of BG composites

The synthesised bioactive glass (BG) utilised in these studies was obtained from Dr. Daniel Boyd at the Department of Applied Oral Sciences, Dalhousie University (<45µm particle size). The glass composition was the result of optimisation of bone graft performance from preceding studies (Murphy *et al.* 2009; Murphy *et al.* 2010). Prior to photopolymerisation, to ensure the bioactive glass was evenly dispersed in the precursor, a combination of thorough stirring for 1hr followed by sonication for 30min was experimentally selected. A schematic representation of the fabrication process is presented in Figure 3.29. Gel fraction was carried out on each of the hydrogel based composites to determine the efficiency of the network formation upon incorporation of bioactive glass into the system. Gel fraction for all batches ranged ±1% for hydrogel based composites at different loadings compared to the control hydrogel; therefore, the incorporation of bioactive glass into the prepolymerised mixture was found not to disrupt the network connectivity.

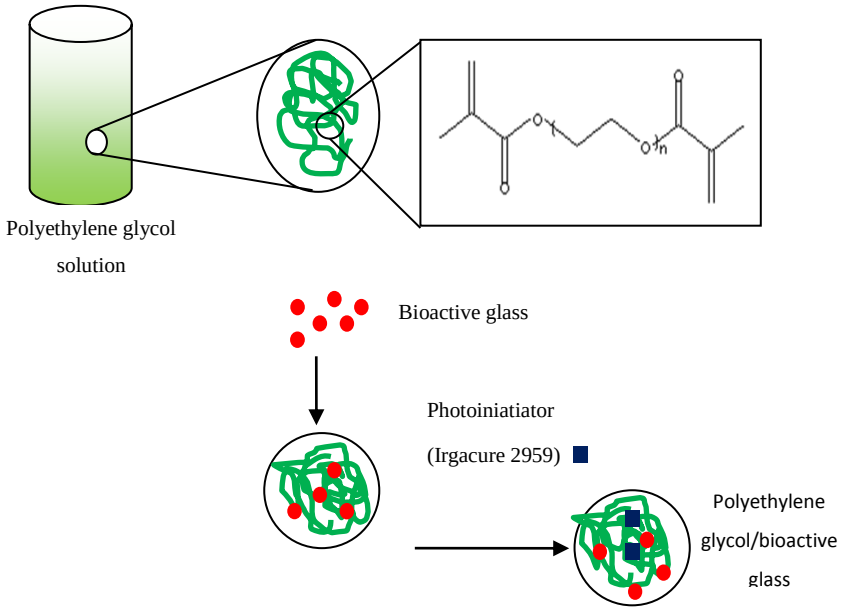

Figure 3.29 *Schematic representation of the process used to fabricate the hydrogel based composites*

3.3.1.2 Thermogravimetric analysis of BG composites

The percentage of the bioactive glass component present in the hydrogel based composite was determined by thermal decomposition of the polymer component. On completion of each test, residual mass confirms the bioactive glass loading of PEG1000A G5, in which 94.70wt% had degraded, and PEG1000A G20, in which 78.87wt% had degraded. The degradation temperature (T_d) of the polymeric phase was chosen at the onset of weight loss. The T_d of the control hydrogel was approximately 250°C, whereas T_d of the hydrogel based composites with 5wt% loading was approximately 430°C (Figure 3.30). From these results it can clearly be concluded that the composite hydrogels display better thermal stability than the control hydrogel. This phenomenon may be explained by the entrapment of the bioactive glass within the PEGDMA.

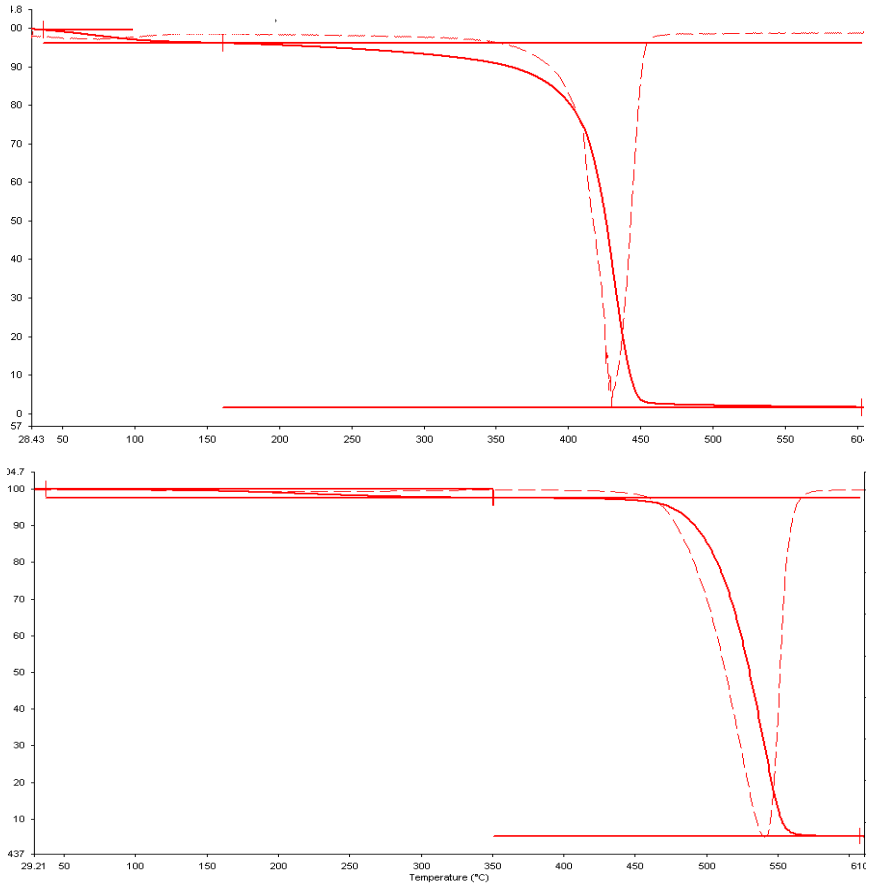

Figure 3.30 *TGA's for **(top)** control hydrogel and **(bottom)** 5wt% bioactive glass loading*

3.3.1.3 X-ray diffraction of BG composites

Figure 3.31 displays the XRD results for the control hydrogel (a), the hydrogel based composite with 20wt% loading (b), and the bioactive glass powder (c). The XRD pattern for the bioactive glass powder indicates the material is generally in amorphous state with negligible crystalline diffraction peaks apart from a broad band between 26° and 39° (2θ). On the other hand, the covalently crosslinked network of the control hydrogel indicates a partially crystalline material with a broad band between 10° and 27° (2θ). In relation to the hydrogel based composite, two distinct broad bands are present. These peaks are representative of both materials. Of particular importance in Figure 3.31 is the band associated with PEGDMA; it notably decreased in intensity for the composite sample compared to the control hydrogel. This can be attributed to the entrapment of bioactive glass particles where the incorporation of glass powder reduces the crystalline properties (Raucci *et al.* 2010).

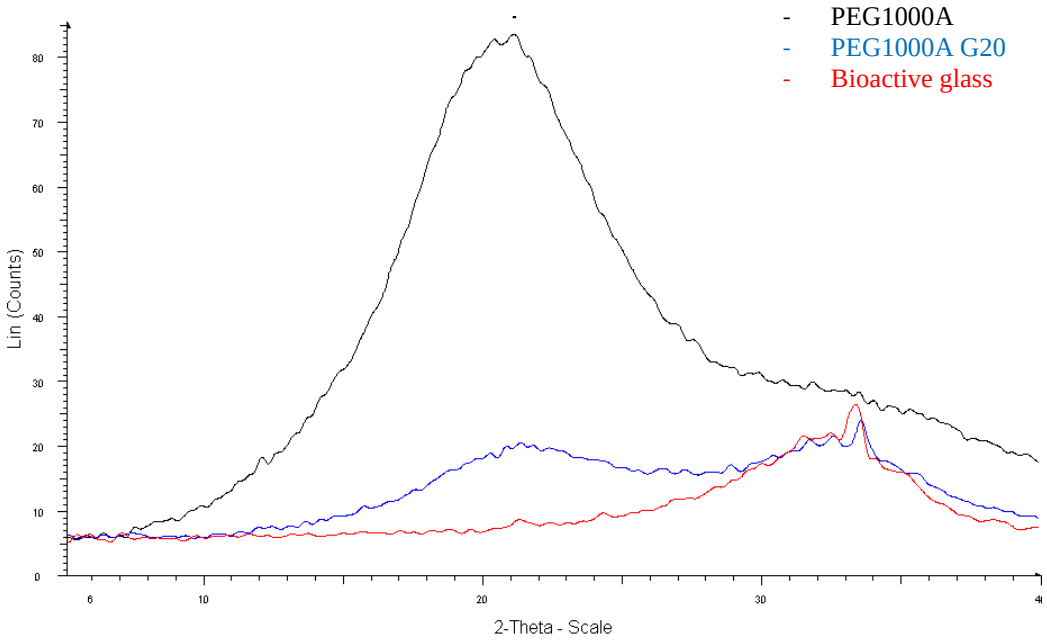

Figure 3.31 *X-ray diffraction of control hydrogel PEG1000A, hydrogel based composite PEG1000A G20 and bioactive glass powder*

3.3.1.4 Differential scanning calorimetry of BG composites

For each hydrogel composite tested, a single glass transition temperature (T_g) was detected. A slight decrease in glass transition was observed with the incorporation of bioactive glass into the hydrogel based composites. This slight reduction in glass transition indicates a weak interaction between PEG and the bioactive glass (Table 3.7). A greater effect on glass transition temperature was observed by altering the molecular weight ratios of the polymer component of the hydrogel based composites (PEG1000A G5: -50.07°C; PEG600A G5: -36.86°C). As expected, the samples became less flexible with the decrease in the length of the polymer chain. Similar to DSC results in Section 3.1.1.5, PEGDMA had no melting peaks and thus did not hinder the crosslinking to the extent of the polymer melt capacity.

3.3.1.5 Fourier transform infrared spectroscopy of BG composites

FTIR spectra of bioactive glass powder, hydrogel based composites and control hydrogel are shown in Figure 3.32. The FTIR spectrum for the control hydrogel exhibited various bands between 1638 and 1140cm^{-1} that are characteristic of the ethylene glycol groups. Their peaks and corresponding groups for PEGDMA hydrogels are in agreement with the literature (Dobić *et al.* 2012) which has been previously explained in Section 3.1.1.4.

Bioactive glass powder exhibits two characteristic bands at 850 and 913cm^{-1}. These peaks are assigned to the stretching vibrations of Si-O bonds in each SiO_4 group (Costa *et al.* 2012). The combined characteristic peaks for the bioactive glass and control hydrogel are present in the hydrogel based composite. However in comparing the hydrogel based composite to the control hydrogel, the peaks at 2867 and 1725cm^{-1} are smaller based on the reduction in polymer content within the sample. Overlapping occurs between 700 and 1000cm^{-1}, which is more intense than the bioactive glass powder and control hydrogel. This increased intensity is due to the combination of the bioactive glass (Si-O and SiO_4 bonds) and PEGDMA (O-R group). Additionally, no physical crosslinking was observed between the bioactive glass and PEGDMA since there was no shift in peaks.

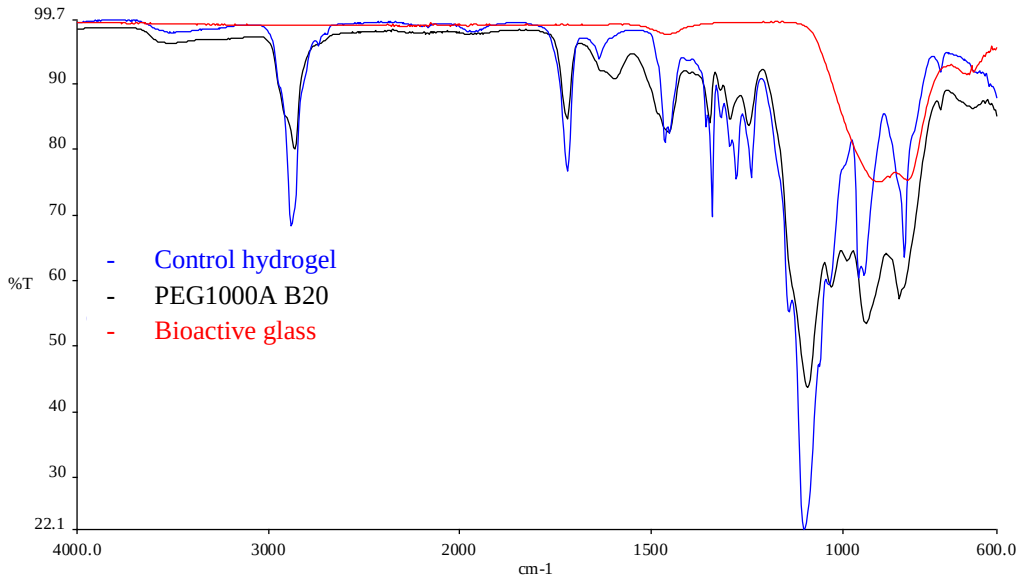

Figure 3.32 *FTIR spectra for bioactive glass powder, hydrogel composite and control hydrogel*

3.3.1.6 Swelling studies of BG composites

When a hydrogel based composite begins to swell, it inhabits the free volume within the sample. The sample continues to absorb the solvent until it reaches a state of equilibrium. Equilibrium is accomplished when the osmotic pressure from the swelling and the elasticity of the polymer network are equal (Neffe *et al.* 2011). Whilst synthesising bone graft substitutes, scientists and engineers must take into account the swelling properties of the scaffolds as this can influence cell migration and neovascularisation (Seeherman and Wozney 2005). The degree and type of crosslinking present controls the swelling properties in hydrogels and can alter the mechanical properties of hydrogel composites. An increase in percentage swelling can negatively affect both the mechanical properties of hydrogels (Devine and Higginbotham 2005; Lin *et al.* 2007) and also the distance between polymer chains, which subsequently influences cell migration and neovascularisation.

For hydrogel based composites, changes in the bioactive glass loading, polymer concentration and molecular weight altered the percentage swelling as shown in Table 3.7. Results illustrate that the incorporation of bioactive glass into the precursor caused a reduction in percentage swelling in all samples. For

example the control hydrogel PEG1000A had a significantly higher percentage swelling than that of the hydrogel based composites PEG1000A G5 and PEG1000A G20 ($p<0.05$). This reduction in percentage swelling may be due to the bioactive glass occupying the empty voids within the polymeric scaffold which induces greater strength in the overall hydrogel based composites (Roberts *et al.* 2011). These results are congruent with compression testing and rheological studies. Controlled swelling is required for tissue engineering especially where mechanical properties play a critical role (Marguerite 2006; Liu *et al.* 2008).

Table 3.7 *Gel fraction, glass transition and swelling percentage for hydrogels and hydrogel based composites*

Hydrogel Code	Gel fraction (%)	Glass transition (°C)	Swelling (%)
PEG1000A	95.63±2.91	-49.25	67.22±0.8
PEG1000A G5	96.75±0.56	-50.09	62.65±2.24
PEG1000A G20	96.10±0.63	-50.01	58.47±0.89
PEG1000B	95.95±1.03	-49.41	32.23±1.51
PEG1000A G5	94.72±1.14	-51.62	30.30±1.37
PEG1000A G20	94.08±0.85	-49.52	28.99±0.57
PEG600A	93.37±0.67	-37.12	38.07±1.45
PEG600A G5	92.63±0.74	-38.87	33.69±0.77
PEG600A G20	91.74±0.87	-38.26	27.88±0.61

3.3.1.7 Compression testing of BG composites

3.3.1.7.1 Unconfined compressive loading

Ideally, bone graft substitutes should have sufficient mechanical strength to endure *in vivo* conditions while simultaneously promoting the formation of new bone growth. At the very least, a scaffold should exhibit the mechanical integrity to promote the formation of new bone (Elisseeff *et al.* 2005). The mechanical performance of scaffolds is therefore a fundamental requirement in designing bone graft substitutes. Replicating cortical bone is

extremely difficult due to its impressive mechanical properties (Young's modulus 11GPa and ultimate strength 106MPa) (Duchemin *et al.* 2008). Bone grafts with sufficient mechanical strength are able to withstand the load at the interface of the scaffold, therefore providing an environment for adequate regeneration of the damaged tissue.

In this study, unconfined compression tests were carried out on hydrogel based composites with different organic and inorganic contents to determine their compressive stress (Figure 3.33) and Young's modulus (Figure 3.34). This analysis revealed that the incorporation of bioactive glass resulted in hydrogel based composites exhibiting an increase in compressive stress and Young's modulus values. For example, control hydrogel PEG1000A, had significantly lower compressive stress and Young's modulus values than those of hydrogel based composite PEG1000A G20 ($p<0.05$). This improvement in mechanical properties may be attributed to the reduction in the degree of swelling and the bioceramic absorbing the load.

These PEGDMA/bioactive glass composites compare favourably to other organic/inorganic hydrogel composites proposed for orthopaedic applications. The PEGDMA/bioactive glass composites in this study have vastly superior compressive strength and Young's modulus compared to studies based on PEG and nanohydroxyapatite (nHAP) hydrogel composites (Gaharwar *et al.* 2011a) and silicate nanoparticles (Gaharwar et al. 2011b) used for potential bone regeneration applications. For example, under identical testing conditions the compressive stress of the PEG/nHAP composites ranged between 0.05-0.066MPa in comparison to values of 1.20-2.55MPa in this study. The compressive strength of these hydrogel based composites are comparable with that reported for cancellous bone, 0.145-13.535MPa (Schoenfeld *et al.* 1974). Therefore, these hydrogel based composites could be used in cancellous bone defects, or low load bearing orthopaedic applications such as a bone defect filler or as a coating-agent onto metallic bioimplants.

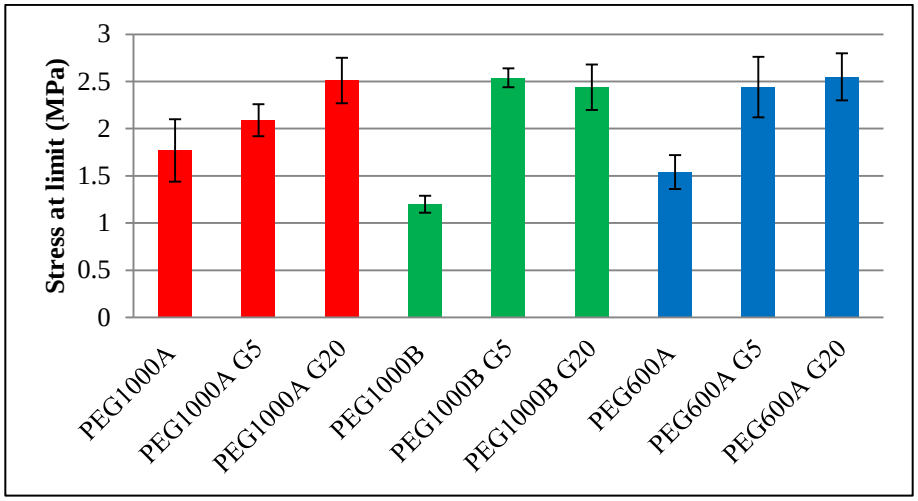

Figure 3.33 *Stress at limit results for bioactive glass hydrogel based composites*

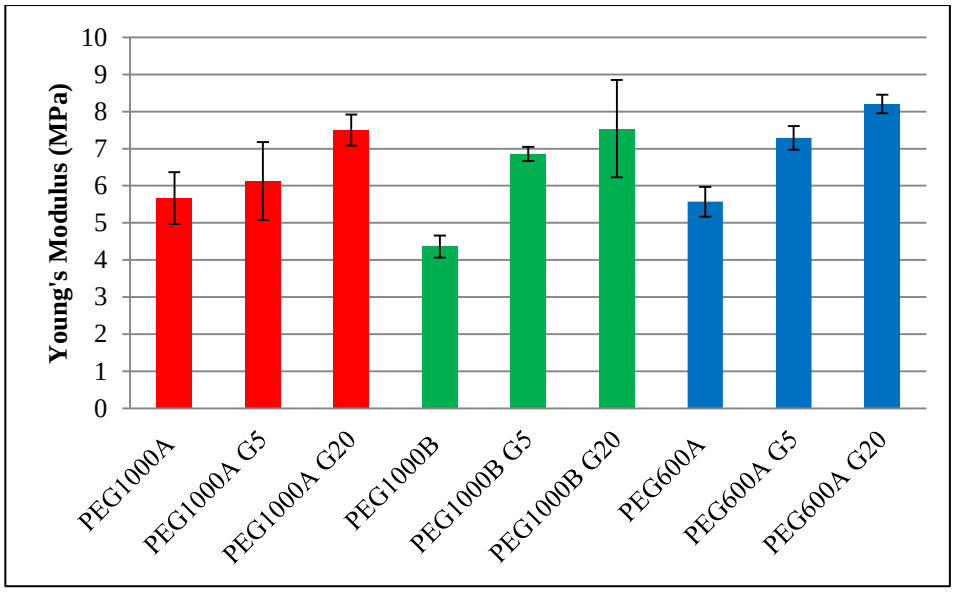

Figure 3.34 *Young's modulus results for bioactive glass hydrogel based composites*

3.3.1.7.2 Cyclic compressive loading

Each sample tested was subjected to cyclic testing to determine the behaviour of hydrogel based composites under repetitive loading scenario. Observations herein are made between the first and last cycle (Figure 3.35). A slight reduction in load values was observed between first and last cycle load.

However in carrying out statistical analysis using a paired t-test, no significant difference was observed for all samples tested ($p>0.05$).

Similar to unconfined compression tests, in comparison between the first cycle load of samples tested, the incorporation of bioactive glass resulted in an increased load value (N). For example, hydrogel PEG1000A had a significantly higher first cycle load when compared to hydrogel based composites PEG1000A G5 ($p<0.05$).

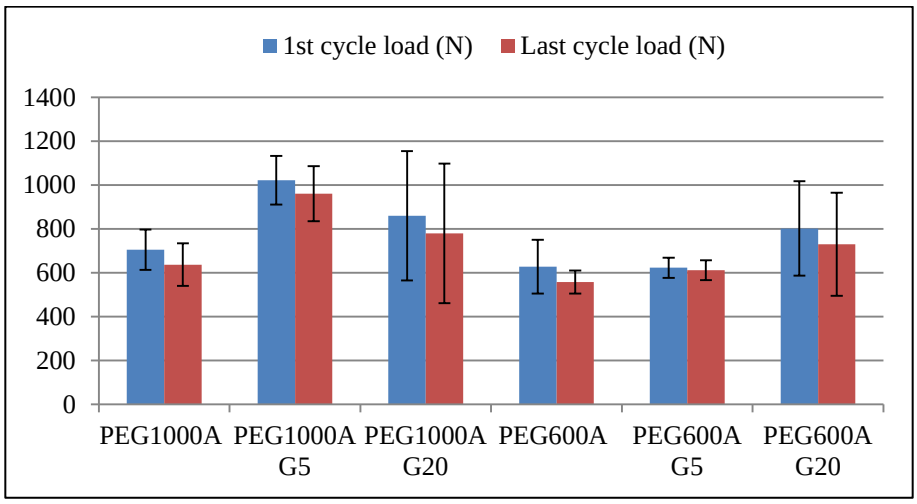

Figure 3.35 *Cyclic testing for selected bioactive glass hydrogel composites*

3.3.1.8 Rheological measurement of BG composites

The mechanical properties and viscoelastic behaviour of the hydrogel based composites were further examined using rheological measurement to assess their physical strength (Figure 3.36). Prior to carrying out frequency sweep tests, a strain sweep test was conducted to ascertain the linear viscoelastic region. Additionally, to ensure batch to batch variation did not affect results, strain sweep tests were conducted on four separate batches that were synthesised independently. Analysis of this data showed that no statistical difference occurred between batches ($p>0.05$).

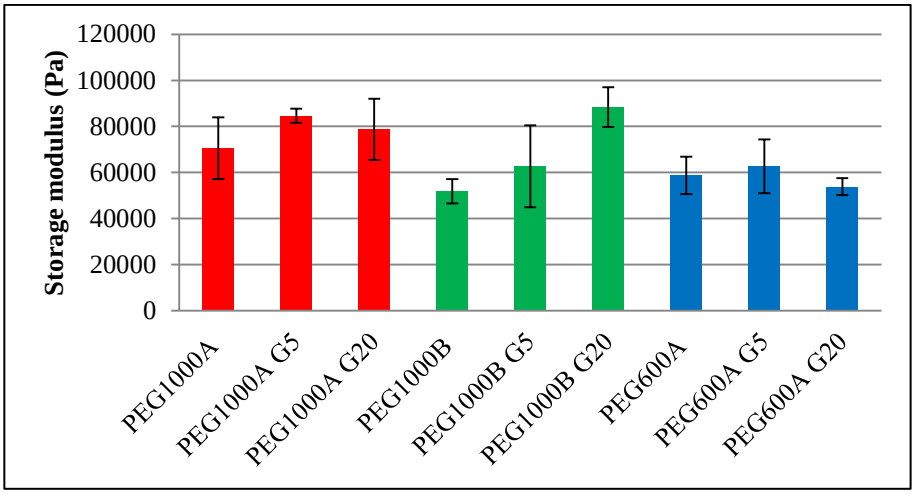

Figure 3.36 *Storage modulus results for bioactive glass hydrogel based composites*

As Figure 3.37 illustrates, the storage modulus increased with the increase in frequency for all samples tested. This was due to the intertwined polymer chains between crosslinks. Similar to maleic PVA samples, when the hydrogel based composites were stressed at low frequencies, the polymeric chains had the ability to relax and return to their original position. However, when the hydrogel based composite were placed under high frequency, recovery was not instant due to the restriction of the chains (Gaharwar et al. 2011b). This constraint in the polymeric chains resulted in a higher storage modulus (G').

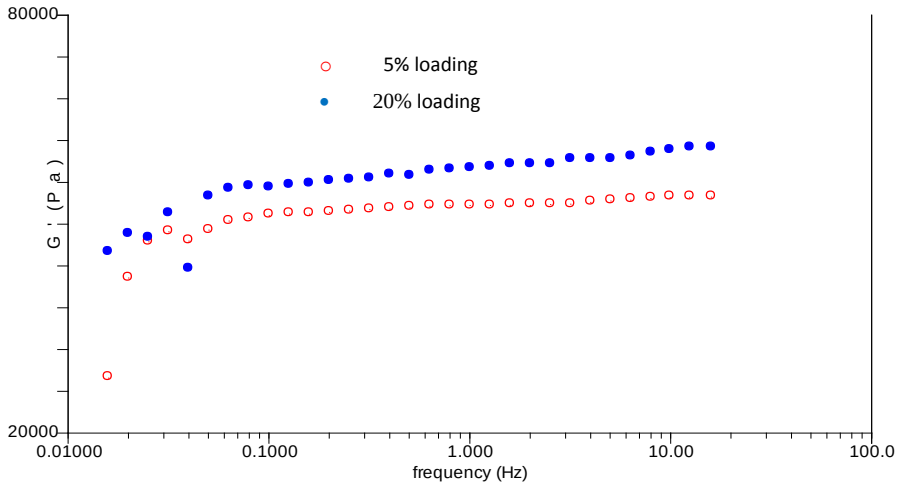

Figure 3.37 *Frequency sweep results for bioactive glass hydrogel based composites*

Stress sweep results are congruent with both strain sweep and frequency sweep tests. A shift upwards in G' was detected with incorporation of bioactive glass into the precursor (Figure 3.38). The stress sweep storage modulus values of the hydrogel based composites in this study are much higher than other hydrogel based composites proposed in the literature for orthopaedic applications. The stress sweep values in this study ranged from 60,000-80,000Pa. Other PEG hydrogel based composites exhibit significantly lower values, ranging between 8,000-14,000Pa (Gaharwar *et al*. 2011a).

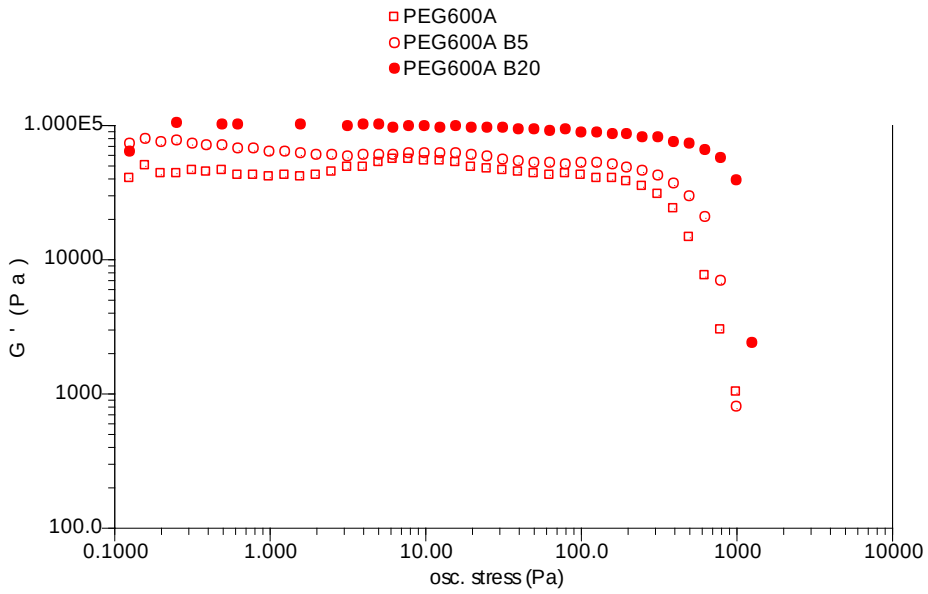

Figure 3.38 *Stress sweep results for bioactive glass hydrogel based composites*

Considering the significant improvement in mechanical properties via the addition of bioactive glass without any physical crosslinking present between both components (p120, Section 3.3.1.5), it was deemed necessary to investigate the use of other bioceramic filler, i.e. beta tricalcium phosphate, to attempt to further improve the mechanical properties of the tissue engineering scaffolds.

3.3.2 Beta-tricalcium phosphate based composite

3.3.2.1 Sample preparation of β-TCP composites

Bone is composite in nature and has an inorganic to organic ratio of approximately 2:1 (Kang *et al.* 2007). Initial studies were carried out to replicate this ratio. The addition of inorganic beta-tricalcium phosphate (β-TCP) into the system at such levels however did not form a homogenous mixture due to the low viscosity of the PEGDMA solution. The maximum amount of β-TCP which could be incorporated into the precursor was 20wt%. It was found that increasing the wt% β-TCP in solution beyond this limit resulted in the bioceramic precipitating out of solution. This was due to the low viscosity of the solution (polymer and distilled water), and precipitation became more pronounced for higher bioceramic loadings. Additionally, bioceramics could not be incorporated into hydrogels synthesised using high concentrations of distilled water which further reduced the overall viscosity of the solutions. FTIR analysis was carried out on hydrogel based composites with low viscosity precursors. Figure 3.39 shows the results of unevenly distributed β-TCP within a hydrogel based composite where the bottom of the sample had higher β-TCP peak intensities compared to the top of the sample which had higher PEGDMA peak intensities. In order to overcome this occurrence, high viscosity solution samples were selected (75% and 50% polymer concentration), and after thorough mixing, samples were immediately placed in moulds and photopolymerised for subsequent testing.

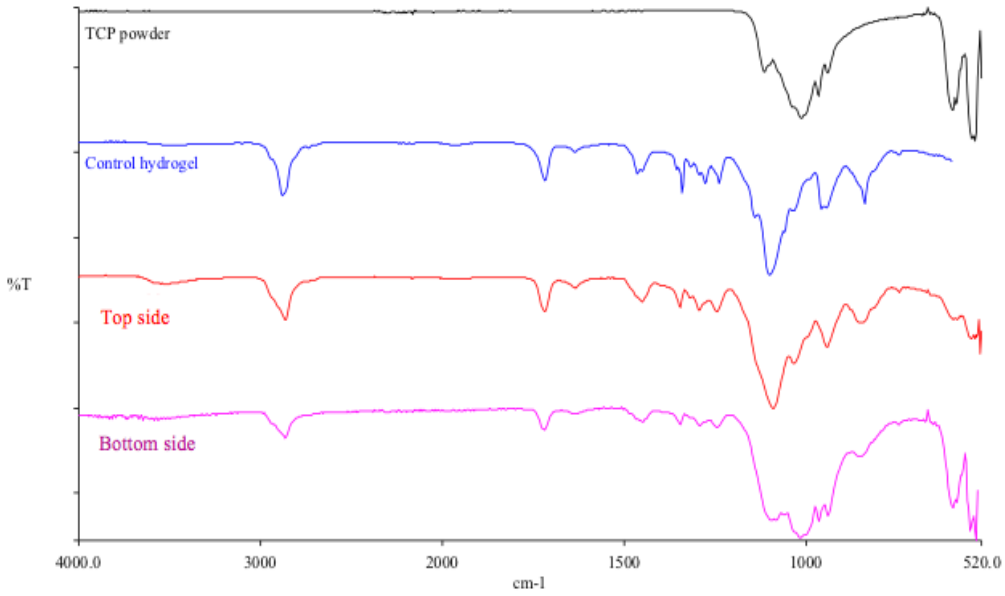

Figure 3.39 *FTIR spectra of unevenly distributed bioceramic within hydrogel based composite*

3.3.2.2 Thermal property analysis of β-TCP composites

The thermal properties of the hydrogel based composites, such as glass transition (T_g) and melting temperature (T_m), were measured via DSC. For all batches tested (see Table 3.10), a distinct glass transition temperature (T_g) was observed for each sample. Figure 3.40 shows no significant changes were observed in the glass transition temperature between the control hydrogel and hydrogel based composites containing 5wt% and 20wt% (±2°C). Similar to the bioactive glass samples, no melt temperature (T_m) value was recorded which was due to the high degree of crosslinking of the PEGDMA component.

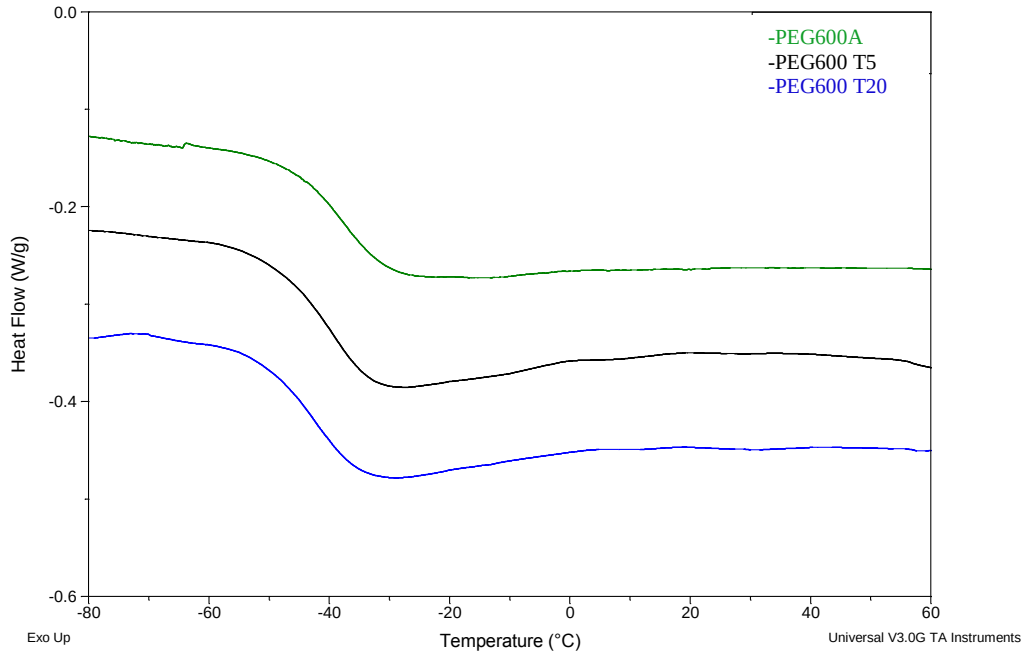

Figure 3.40 *DSC thermographs of the variation in β-TCP loadings*

TGA was used to measure the quantitative composition of β-TCP within the hydrogel based composites. PEG1000A T5 and PEG1000A T20 were selected as representative samples for the purpose of this discussion. As expected, the organic component (PEGDMA) burnt off almost completely with a weight loss of 99.39wt% recorded. For the hydrogel based composites PEG1000A T5 and PEG1000A T20, the total weight loss was 94.44wt% and 84.68wt% respectively. In comparing TGA to theoretical values, only a slight difference occurred as shown in Table 3.8. This slight variation was due to partial sedimentation of the bioceramic in the precursor prior to photopolymerisation.

Table 3.8 *TGA analysis for β-TCP hydrogel based composites*

Scaffold code	Total wt loss (wt%)	TGA β-TCP content (wt%)	Theoretical β-TCP content (wt%)
PEG1000A	99.39	-	0
PEG1000A T5	94.44	4.95	4.76
PEG1000A T20	84.68	14.71	16.67

3.3.2.3 FTIR and XRD analysis of β-TCP composites

FTIR was used to confirm the presence of specific chemical groups and the interaction between the organic and inorganic components. As shown in Figure 3.41a, the FTIR spectrum of β-TCP powder has 5 primary vibrational peaks which can be seen at 1170, 1016, 969, 603 and 538cm^{-1} which correspond to the findings of Coelho *et al.* (2009). The associated side groups for these peaks can be seen in Table 3.9. In comparison, the FTIR spectra for the control hydrogel in Figure 3.41b has 7 primary vibrational peaks (Table 3.9) which are comparable with the values in the literature and in Section 3.1.1.4.

The FTIR spectra for hydrogel based composites at 5wt% and 20wt% loadings are shown in Figure 3.41c and d respectively. The characteristic bands of both β-TCP and PEGDMA are present in the hydrogel based composite and variation of the absorption intensity was dependent on the relative content of each individual component. A shift in particular peaks for the hydrogel based composites was observed when compared to the control hydrogel spectrum. For example, with the 5wt% hydrogel based composite, the group CH stretching at 2882cm^{-1} shifted to 2867cm^{-1}, CCH_2 bending at 1466cm^{-1} shifted to 1453cm^{-1} and C-H vibrations of CH_3 group at 1342cm^{-1} shifted to 1348cm^{-1}. The shift in these peaks indicate physical crosslinking between organic and inorganic components.

Figure 3.42 shows XRD patterns of the control hydrogel and the hydrogel based composites at different loadings. In the control hydrogel, a region of low crystallinity was observed between 15-28^o (2θ). New peaks were observed with the addition of β-TCP powder into the hydrogel matrix and the intensity of these β-TCP characteristic peaks varied (28, 31 and 34^o (2θ)) with the content of β-TCP within each sample. Similar observation occurred for bioactive glass samples, most notably the decrease in height of the polymer peaks. This reduction in peak height was a result of the interaction between β-TCP and PEGDMA matrix which led to a decrease in crystallinity of the polymer phase (Shen *et al.* 2010).

Table 3.9 *Band assignments for β-TCP powder and PEGDMA*

β-TCP powder		PEGDMA	
Band assignment	**Frequency (cm^{-1})**	**Band assignment**	**Frequency (cm^{-1})**
PO_4^{3-}, v_3 stretching	1117	OH stretching	3569
	1016		
PO_4^{3-}, v_1 stretching	969	CH stretching	2867
PO_4^{3-}, v bending	603	CO bending	1724
	538		1638
		CCH_2 bending	1452
		CH vibrations of CH_3 group	1349
		OR stretching	1140

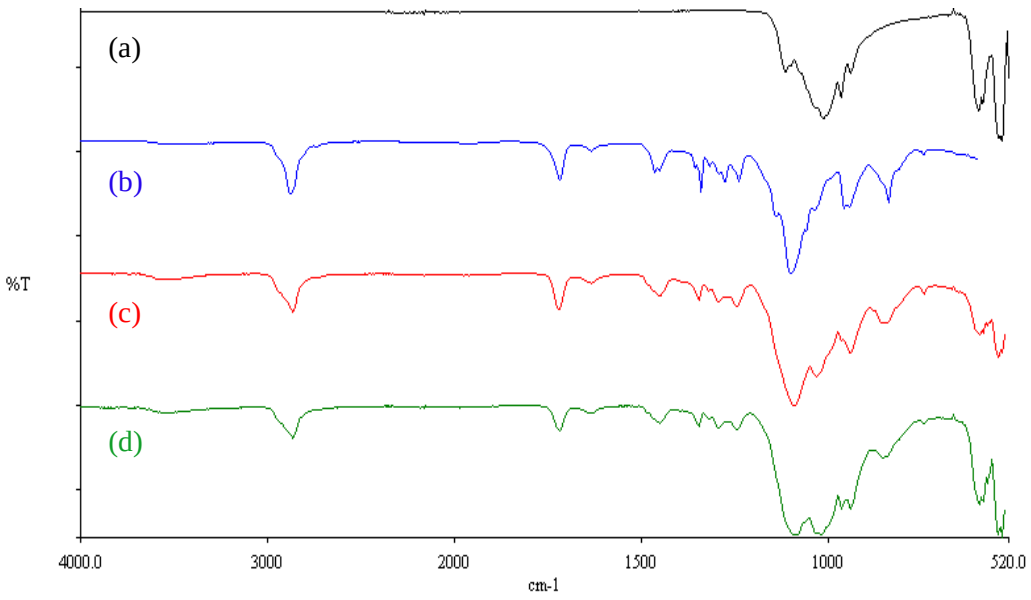

Figure 3.41 *FTIR spectra for β-TCP powder (a), control hydrogel (b), hydrogel composites at 5wt% (c), and 20wt% loadings (d)*

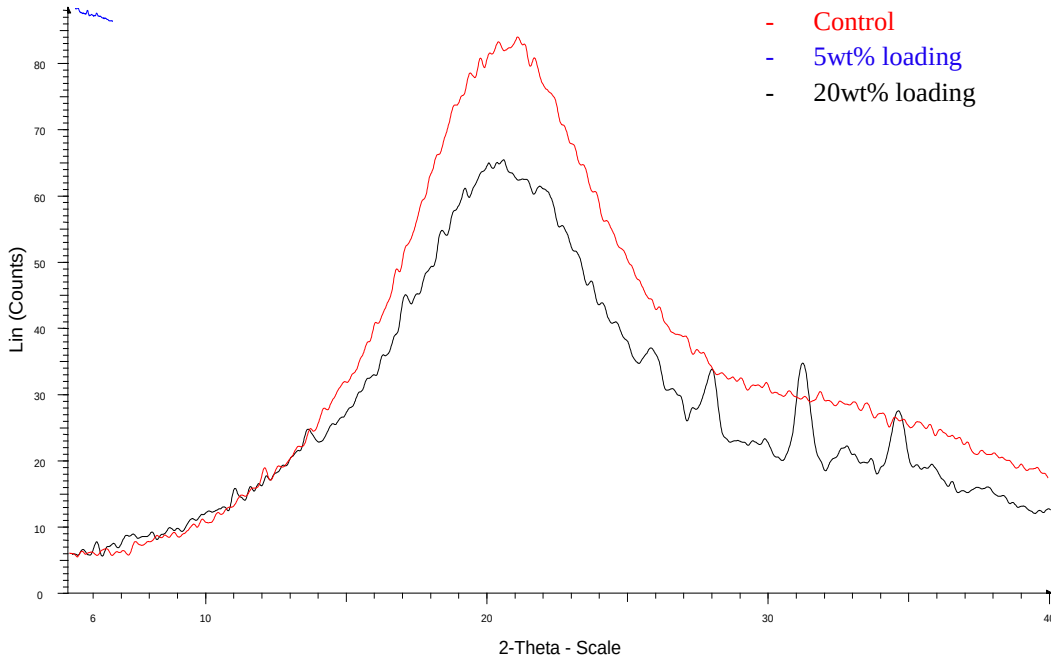

Figure 3.42 *X-ray diffraction of control hydrogel and hydrogel based composites at different loadings*

3.3.2.4 Swelling studies of β-TCP composites

One of the leading attributes to the biocompatibility of synthetic hydrogels is the ability of them to absorb aqueous solutions, which bestows unique physiochemical properties to the scaffolds (Kamaraj *et al.* 2008). This promotes the scaffold to be physiologically stable, permeable to biomolecules and have low interfacial tension. For these reasons the degree of swelling was investigated as discussed below.

The percentage swelling graphs for hydrogel based composites are displayed in Figures 3.43 and 3.44 respectively. The equilibrium percentages swelling for all samples ranged from 25.90 to 67.22% as displayed in Table 3.10. A reduction in percentage swelling as a function of β-TCP loading was observed for all samples tested which were similar to other hydrogel composites reported in the literature (Rezwan *et al.* 2006; Mohamad Yunos *et al.* 2008; Deplaine *et al.* 2010). For example, as the feed ratio of β-TCP increased in the hydrogel based composites, PEG1000A had a significantly higher percentage swelling than both PEG1000A T5 and PEG1000A T20 ($p<0.05$). Following the same trend, PEG1000A T5 had a significantly higher percentage swelling than

PEG1000A T20 ($p<0.05$). Similar to the bioactive glass hydrogel based composites, this behaviour occurs because β-TCP occupies the free space in the pores of the hydrogel composite which would otherwise be taken up by the buffer solution (Zhou *et al.* 2009). A further reduction in percentage swelling was observed for β-TCP based composites compared to bioactive glasses composites which was associated with additional physical bonding between the polymeric component and β-TCP (p131, Section 3.3.2.3).

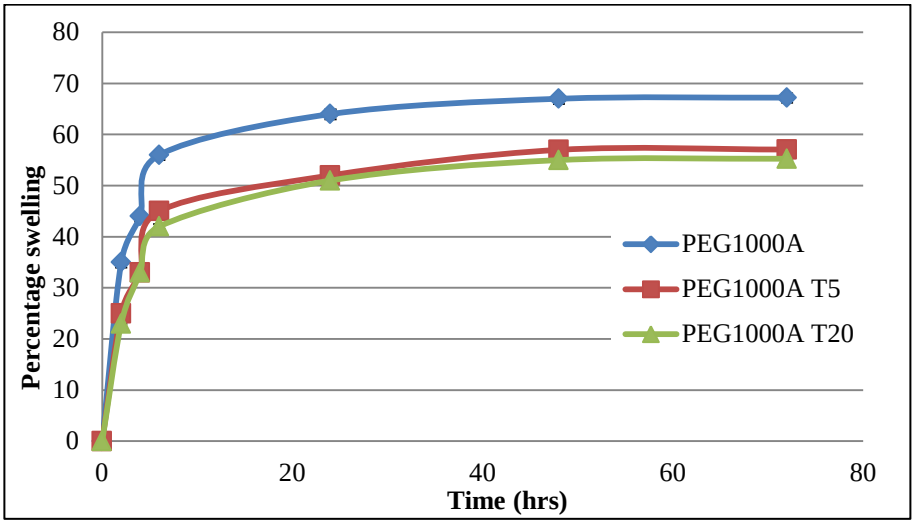

Figure 3.43 *Swelling studies data for β-TCP PEG1000A hydrogel based composites*

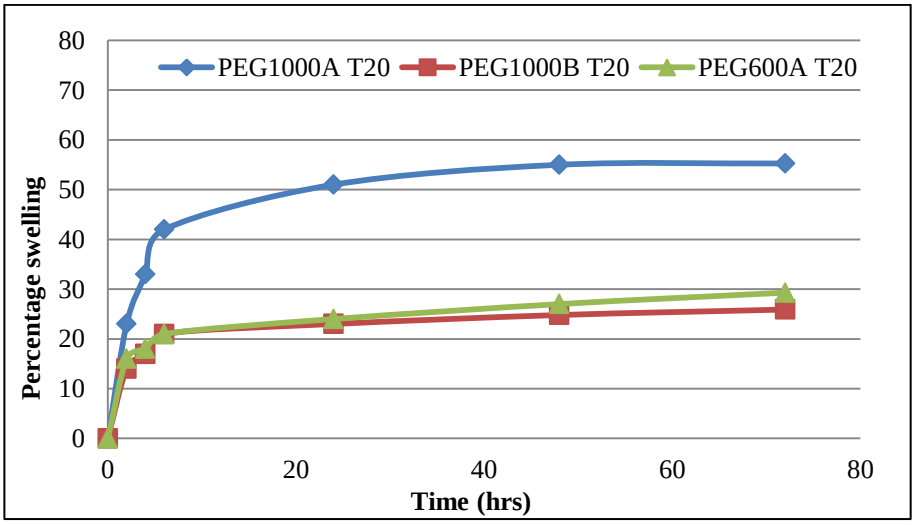

Figure 3.44 *Swelling studies data for hydrogel based composites at β-TCP 20wt% loading*

Table 3.10 *Mean ± SD data for percentage swelling and glass transition temperature for β-TCP hydrogel based composites*

Hydrogel Code	Swelling (%)	Glass transition (°C)
PEG1000A	67.22±0.80	-49.25
PEG1000A T5	57.06±0.52	-50.12
PEG1000A T20	55.26±0.23	-49.68
PEG1000B	32.23±1.51	-49.41
PEG1000B T5	30.08±1.21	-48.39
PEG1000B T20	25.90±0.59	-19.03
PEG600A	38.07±1.45	-37.12
PEG600A T20	34.04±2.19	-37.91
PEG1000A T20	29.60±0.58	-37.68

3.3.2.5 Compression testing of β-TCP composites

Calcium phosphate compounds are widely used as bone substitutes in the fields of dentistry, orthopaedics and reconstructive surgery. One of the most commonly used bioceramics in this area is beta tricalcium phosphate (β-TCP). This material is a commercially available synthetic bone graft substitute and is commonly used in surgery for alveolar ridge augmentation and sinus reconstruction (Miyai *et al.* 2008; Kang *et al.* 2009; Lin *et al.* 2011; Sowmya *et al.* 2011).

The mechanical properties of implants for bone tissue engineering are essential parameters due to the forces experienced from the surrounding tissues when the material is placed *in vivo*. Studies have shown that mechanical stiffness can play a vital role in regulating gene expression of cells (Liu et al. 2010). This study investigated the influence of molecular weight, polymer concentration and β-TCP loading on the scaffolds mechanical properties (Figures 3.45 and 3.46). The compressive strength of hydrogel based composites ranged from 4.36-8.70MPa in terms of Young's modulus and 1.20-3.10MPa for stress at limit. It is clear that the incorporation of β-TCP into the polymeric system resulted in an increase in both Young's modulus and stress at limit. This increase in compressive strength can be attributed to two factors. Firstly, as illustrated in

Section 3.3.2.4, incorporation of β-TCP into the matrix causes a reduction in the percentage swelling for the composites. Secondly, the physical bonding present between both components causes an increase in compressive strength, as mentioned in Section 3.3.2.3.

However, there was a limit to the improvement in mechanical properties with the addition of β-TCP. For example, no significant difference in Young's modulus was recorded between hydrogel based composites PEG1000B T5 and PEG1000B T20 ($p>0.05$). Moreover, a reduction in compressive strength was observed between PEG600A T5 and PEG600A T20. This reduction in hydrogel material properties was due to the limited degree of crosslinking because these samples had the lowest molecular weight and polymer concentration. It can be concluded that the incorporation of β-TCP particles into the hydrogel composites can improve mechanical properties, however higher loadings of β-TCP can interrupt the crosslinking and negatively affect mechanical performance. In comparison between, bioactive glass and β-TCP hydrogel based composites, β-TCP samples exhibited better compressive properties. This was attributed to the physical crosslinking between β-TCP and polymer which further reduced the degree of swelling.

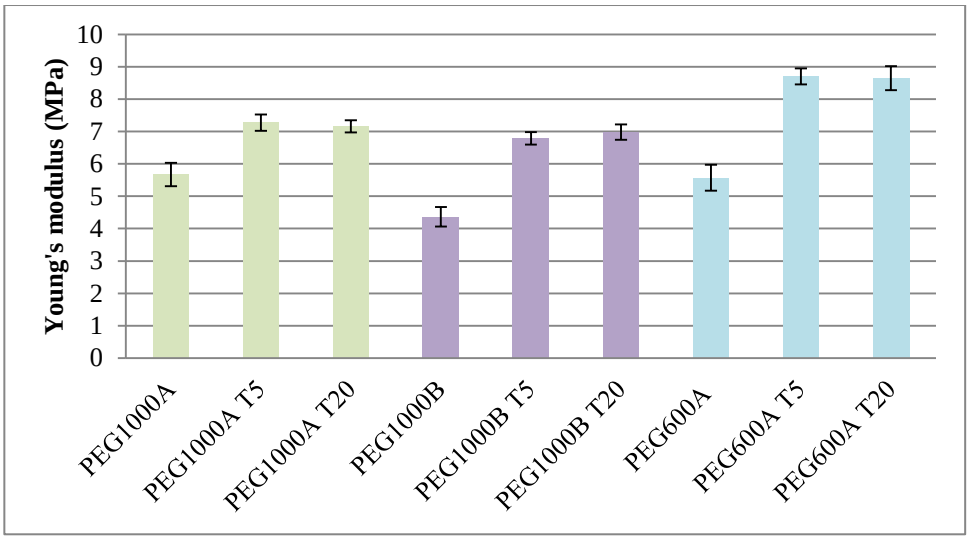

Figure 3.45 *Young's modulus results for β-TCP based hydrogels*

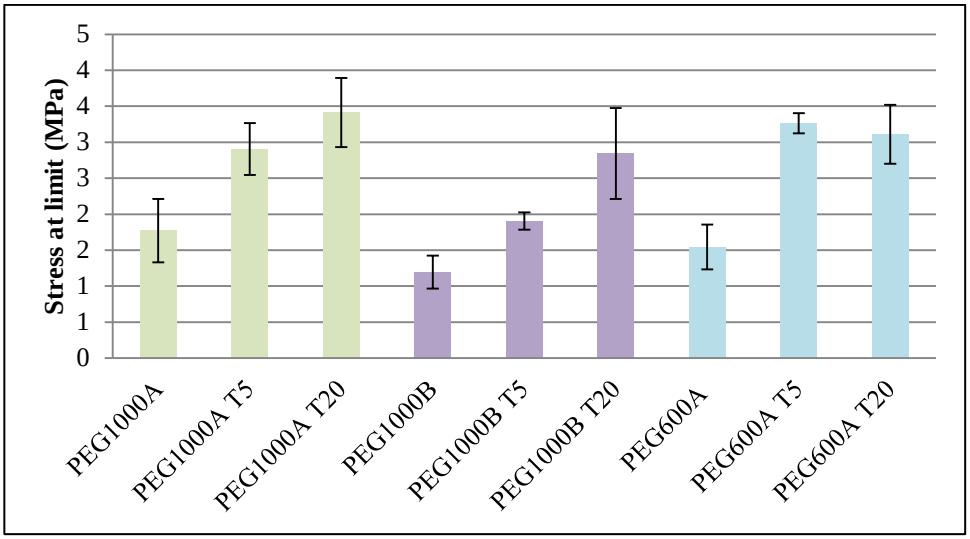

Figure 3.46 *Stress at limit results for β-TCP based hydrogels*

3.3.2.6 Rheological studies of β-TCP composites

The viscoelastic properties and mechanical strength of the hydrogels were additionally tested using an Advanced Rheometer to assess their retention behaviour and physical integrity for potential *in vivo* applications. The scaffolds viscoelastic properties were investigated based on the concept that hydrogels with good mechanical strength are expected to maintain their integrity under different loading conditions. A strain sweep test was performed on control hydrogel and hydrogel based composites at different loadings in order to establish the regime of linear viscoelasticity (LVE) and determine if the elasticity of the formulations differed. For all samples, G′ was over an order of magnitude higher than G″, suggesting that the hydrogel based composites were more elastic than viscous within the frequency range tested. This trend was similar for previous hydrogels (see Sections 3.1 & 3.2) which suggest that incorporation of β-TCP did not affect the elastic/viscous components of the samples. Furthermore, the loss tangent (tan δ) was calculated **(**G″/ G′). Figure 3.49 shows that values for tan δ were very low, which is indicative of an elastic material (Abdurrahmanoglu *et al.* 2009).

In conclusion, a significant improvement in the mechanical properties was identified with the addition of β-TCP. Likewise, a significant improvement in mechanical properties was also observed for β-TCP samples compared to

bioactive glasses samples. This increase in strength was associated with the physical crosslinking present between both components for β-TCP based samples.

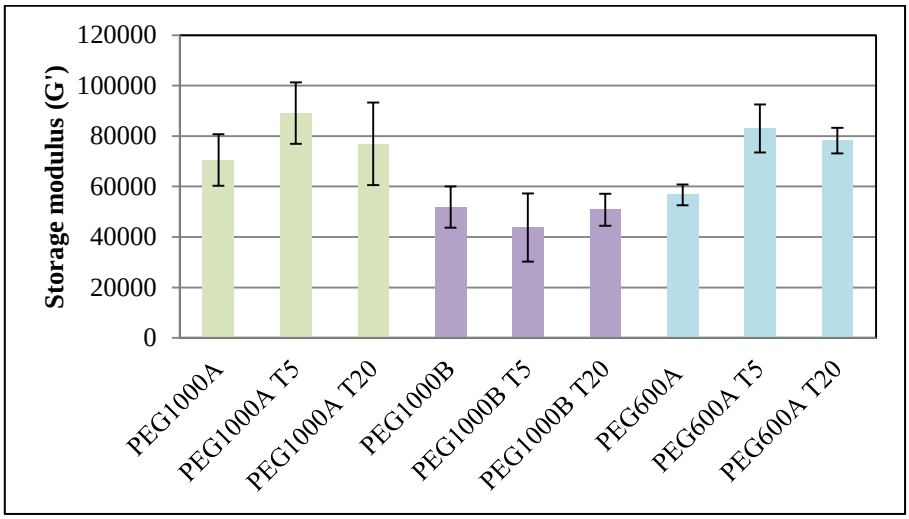

Figure 3.47 *Storage modulus results for β-TCP based hydrogels in strain sweep mode*

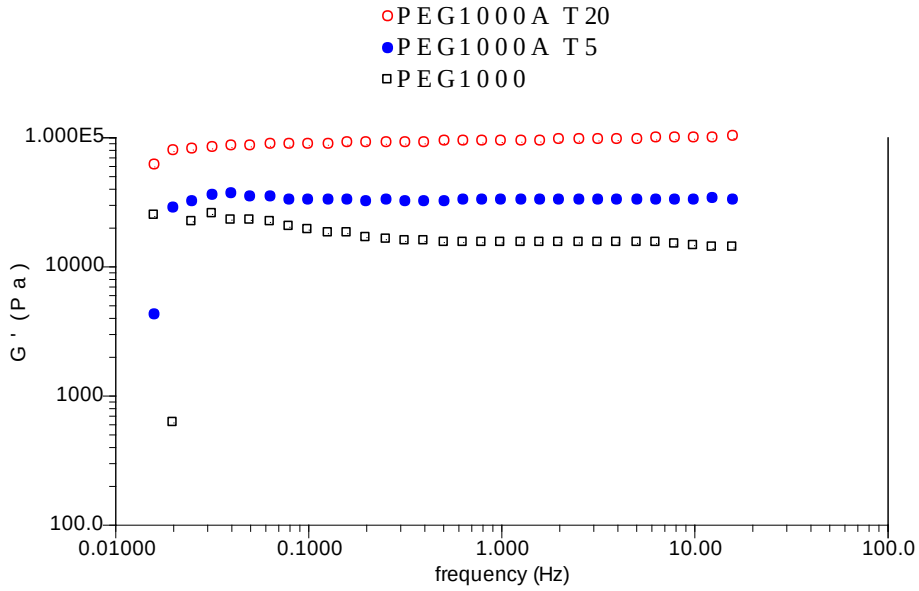

Figure 3.48 *Storage modulus results β-TCP hydrogel based composites in frequency sweep mode*

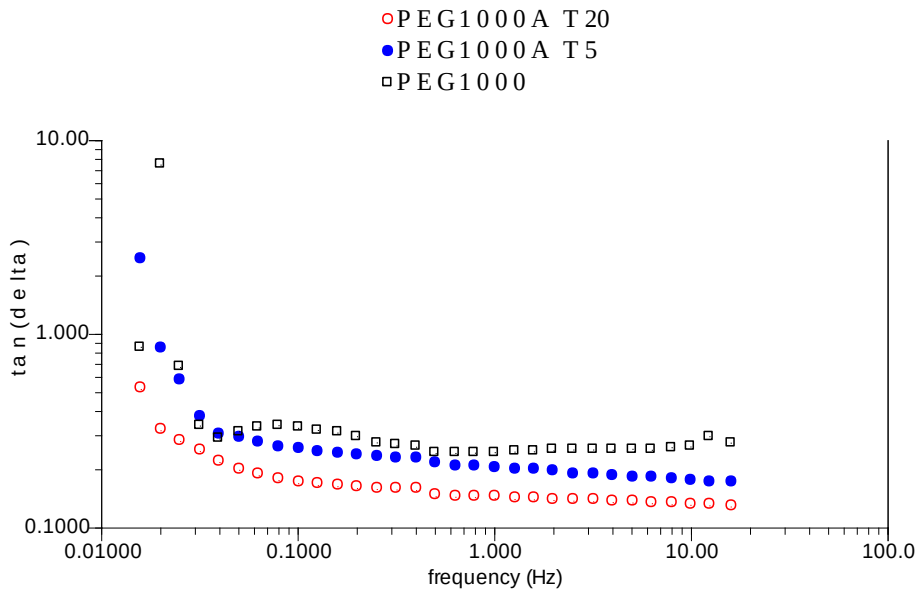

Figure 3.49 *Tan delta results β-TCP hydrogel based composites in frequency sweep mode*

3.3.3 Hydroxyapatite based composites

3.3.3.1 Thermal analysis of HAP composites

DSC results show that no noteworthy change in glass transition was observed with the incorporation of hydroxyapatite (HAP) into the system where values ranged ±3°C compared to the neat hydrogels (Table 3.11). In addition, no melt peak was observed for these hydrogel composites which were similar for bioactive glass and β-TCP hydrogel based composites (p120, Section 3.3.1.4 and p129, 3.3.2.2).

Figure 3.50 depicts the burn-off percentage of the polymer component within the samples PEG1000A H5 (94.44wt%) and PEG1000A H20 (87.11wt%). These values compare favourably to theoretical values of PEG1000A H5 (95.24wt%) and PEG1000A H20 (83.33wt%). The minor discrepancy between the actual and theoretical values is due to the precipitation of HAP out of the precursor prior to photopolymerisation.

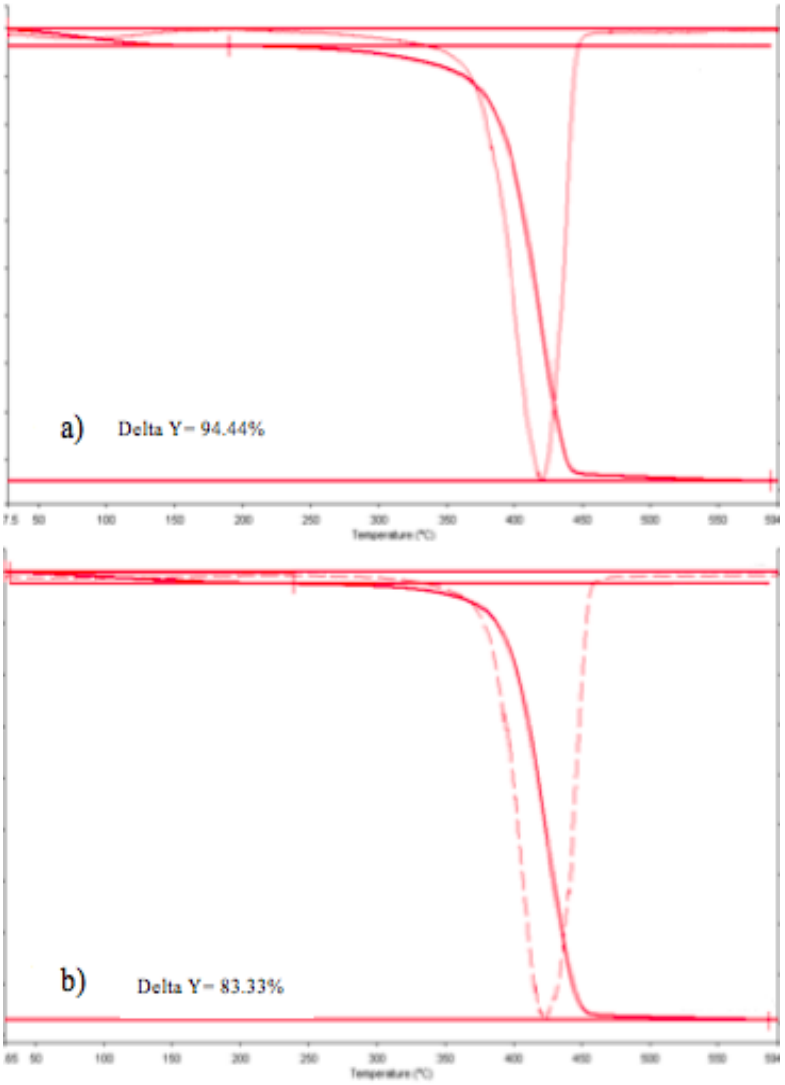

Figure 3.50 *TGA analysis of hydroxyapatite hydrogel composites at 5wt% (a) and 20wt% (b) loadings*

Table 3.11 *Mean ± SD data for percentage swelling and glass transition temperatures for hydroxyapatite hydrogel based composite*

Code	Swelling (%)	T_g (°C)
PEG1000A	67.22±0.80	-49.25
PEG1000A H5	63.24±0.94	-49.92
PEG1000A H20	59.84±0.32	-53.74
PEG1000A	32.23±1.51	-49.41
PEG1000B H5	30.46±0.58	-49.49
PEG1000B H20	27.76±0.33	-52.70
PEG600A	38.07±1.45	-37.12
PEG600A H5	32.36±0.54	-37.79
PEG600 H20	27.90±0.75	-38.42

3.3.3.2 Fourier transform infrared spectroscopy of HAP composites

FTIR spectra of synthesised HAP and hydrogel composites are shown in Figure 3.51(a-d). The characteristic phosphate group peaks of synthesised hydroxyapatite were observed where the most notable peaks were at 1023cm^{-1} (corresponding to PO_4^{3-} $_{V3}$ stretching), 962cm^{-1} (associated with PO_4^{3-}, $_{V1}$ stretching) and 600, 560 and 524cm^{-1} (related to PO_4^{3-}, $_{V}$ bending) (Jongwattanapisan *et al.* 2011). Synthesis of pure hydroxyapatite and the complete reaction of constituents were confirmed by the absence of any calcium carbonate groups between 1400-1500cm^{-1}. The main characteristic peaks of the control hydrogel are shown in Figure 3.51b and associated peaks have been previously explained in Section 3.1.1.4. Figure 3.51c and d are the FTIR spectra of PEG/HAP hybrids and their associated peaks were present due to the amalgamation between both components. The intensity of each peak in the hydrogel composites varied with the relative content of each individual component. Furthermore, physical crosslinking occurred between both components, illustrated by a shift in the peaks. In particular the CH stretch at 2864cm^{-1} shifted to 2867cm^{-1} and C=C bending shifted from 1724 to 1718cm^{-1}.

Physical crosslinking was further confirmed by an increase in compressive properties.

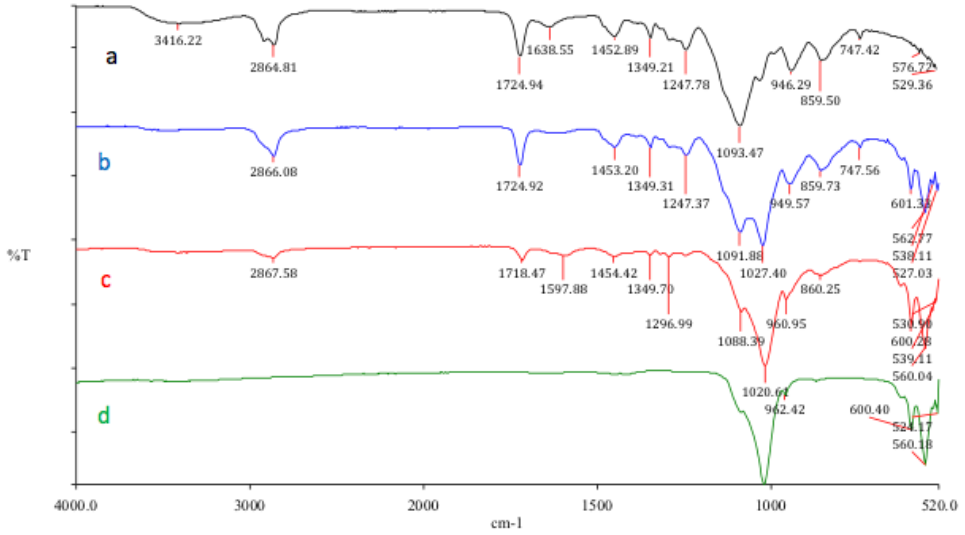

Figure 3.51 *FTIR spectra for control hydrogel (a), 5wt% hydrogel composite (b), 20wt% hydrogel composite (c), and HAP powder (d)*

3.3.3.3 X-ray diffraction of HAP composites

Hydroxyapatite $Ca_{10}(OH)_2(PO_4)_6$ is one of the most biocompatible bioceramics because of its unique chemical structure and resemblance to the mineral constituents of human bone and teeth. Hydroxyapatite is the most stable calcium phosphate ceramic compound and is closest to the pH and composition of real physiological fluid. Due to the chemical similarities between hydroxyapatite and mineralised bone (60% hydroxyapatite crystals) and the material's ability to exhibit a strong affinity to host hard tissues *in vivo*, synthetic hydroxyapatite is the most commonly used bioceramic in bone regeneration (Chu *et al.* 2002; Murugan and Ramakrishna 2004; Xianmiao *et al.* 2009; Zhou *et al.* 2009; Andronescu *et al.* 2010; Gaharwar *et al.* 2011a).

In this study the crystallographic structure of hydroxyapatite powder and hydrogel composites were verified using X-ray diffraction (XRD). The XRD pattern of synthesised HAP in Figure 3.52c exhibits all the characteristic peaks of the apatite phase at 26°, 29° and 32° (2θ) (Murugan and Ramakrishna 2004; Rapacz-Kmita *et al.* 2005). The broad apatite peaks indicate that the synthesised

HAP was low in crystallinity. This is a favourable characteristic for bone tissue engineering applications since natural bone too is also low in crystallinity (Murugan and Ramakrishna 2004). The XRD patterns in Figure 3.52b-c display the distinctive peaks of HAP within the hydrogel composites and the intensity of the apatite phase was based on the content of HAP in the precursor.

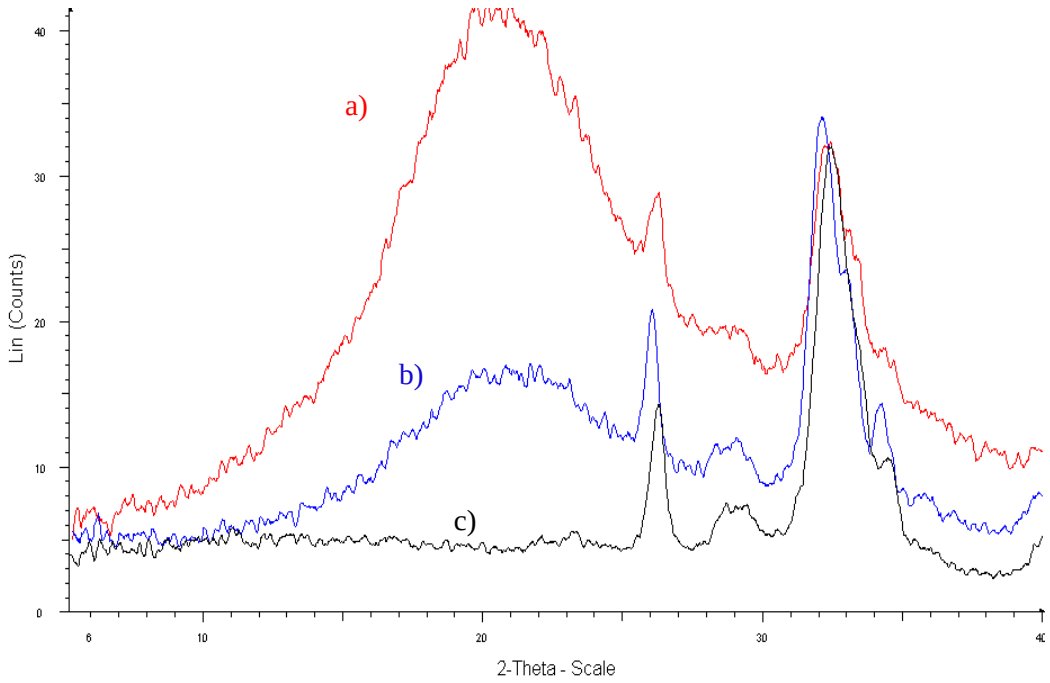

Figure 3.52 *XRD patterns of hydrogel composites at 5wt% (a), 20wt% (b) and HAP powder (c)*

3.3.3.4 Swelling studies of HAP composites

In this study it was found that the percentage swelling could be controlled by altering the HAP content. Similar to both bioactive glass and β-TCP hydrogel bases composites, a decrease in percentage swelling was observed with the addition of hydroxyapatite. This reduction was caused by physical crosslinking between both components (p 141, Section 3.3.3.2) and the HAP occupying the free space between the pores. This phenomenon was observed for other hydrogel based composites (Gaharwar et al. 2011b). In comparison of percentage swelling between the three different bioceramics, hydroxyapatite and bioactive glasses obtained similar values. In the case of β-TCP samples, a slight reduction in

percentage swelling was observed for these hydrogel based composites. The variation between samples was associated with the extent of physical interaction since individual bioceramics do not have the capabilities to absorb moisture.

3.3.3.5 Compression testing of HAP composites

In this study, both Young's modulus and compressive stress were shown to be dependent on HAP content (Figures 3.53 and 3.54). The unconfined compression test found that the control hydrogel PEG1000A had a significantly lower Young's modulus than that of PEG1000A H5 and PEG1000A H20 hydrogel composites ($p \leq 0.001$ for all comparisons). Similarly, hydrogel composite PEG1000A H5 had a significantly lower Young's modulus than that of PEG1000A H20 ($p \leq 0.001$). Likewise, the stress at limit results demonstrated that the control hydrogel PEG1000B (1.20±0.09MPa) was significantly lower ($p \leq 0.05$) than that of hydrogel composites PEG1000B H5 (1.91±0.18MPa) and PEG1000B H20 (2.84±0.15MPa). This twofold increase in compressive strength was related to three factors: strong physical crosslinking between PEGDMA and HAP (p141, Section 3.3.3.2), the decrease in the percentage swelling (p143, Section 3.3.3.4) and hydroxyapatite absorbing the compressive load. These values compare favourably to other PEG/HAP hydrogels. Zhou *et al*. (2009) fabricated injectable polyethylene glycol and polyvinylpolypyrrolidone along with hydroxyapatite and reported compressive strength and Young's modulus of 0.15 and 0.6MPa which were tested under similar test conditions. The hydrogel composites in this study exhibit a twentyfold increase in compressive strength compare to such samples. This increase in mechanical performance was associated with sample preparation via photopolymerisation (high degree of crosslinking) and a superior interaction between PEG and HAP.

Similarly to bioactive glass and β-TCP samples, the hydroxyapatite hydrogel based composites with the highest compressive properties were PEG1000A H20 and PEG600A H20. HAP composites values are favourable compared to BG and β-TCP composites (p122, Section 3.3.1.7 and p135, Section 3.3.2.5). For example Young's modulus for PEG1000A B20 (7.5±0.42MPa) was significantly lower ($p<0.05$) than that of PEG1000A H20 (12.73±1.24MPa). The

contributing factor to the significant variation in compressive properties was associated with the absence of physical crosslinking between bioactive glass and PEGDMA.

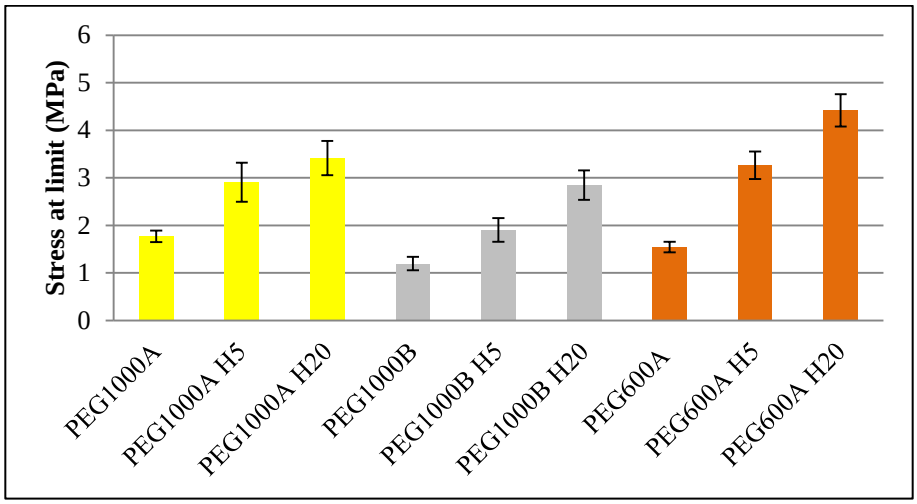

Figure 3.53 *Stress at limit results for HAP based hydrogels*

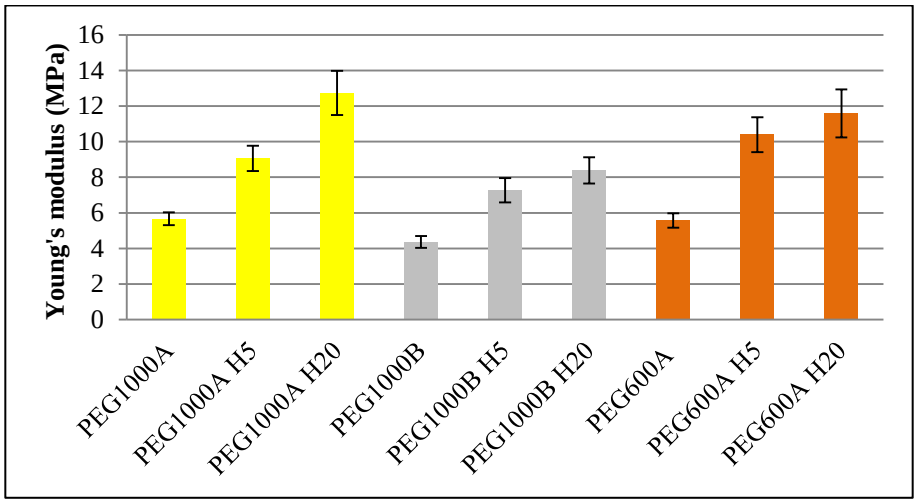

Figure 3.54 *Young's modulus results for HAP based hydrogels*

Figure 3.55 shows a reduction of load (N) between 1st cycle and 10th cycle for all samples tested. Statistical analysis using a paired t-test showed however that the reduction in load (N) was not significantly different for any samples tested ($p>0.05$) which was likewise observed for bioactive glass composites.

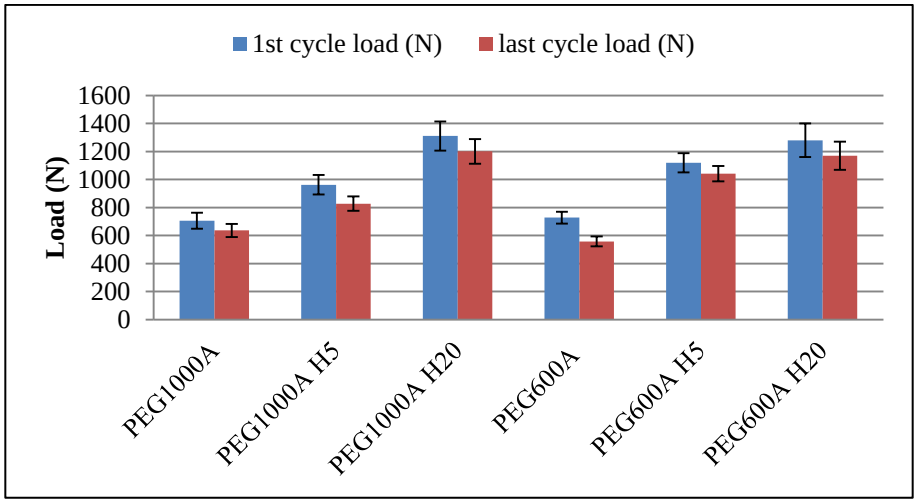

Figure 3.55 *Cyclic testing results for HAP based hydrogels*

3.3.4 Summary of hydrogel based composites

A series of hydrogel based composites (bioactive glass, beta-tricalcium phosphate and hydroxyapatite) were prepared via photopolymerisation. Gel fraction results showed that the incorporation of bioceramics into the prepolymerised mixture did not disrupt the network connectivity of the hydrogel based composites. Only a slight variation in glass transition temperature was observed between control hydrogel and hydrogel based composites (±2°C). For TGA analysis, only a minute difference was observed between actual and theoretical content values which were due to partial sedimentation of the bioceramics. FTIR analysis confirmed the presence of specific chemical groups and interaction between polymer and bioceramic. The variation of the absorption intensity was dependent on the relative content of each individual component. A shift in peaks for both β-TCP and HAP composites was observed which suggests that physical crosslinking was observed for these samples. In terms of percentage swelling, changes in the bioceramic loading, polymer concentration and molecular weight altered the swelling capabilities of hydrogel based composites. This reduction in percentage swelling with the addition of bioceramics was due to the bioceramic occupying the empty voids within the polymeric scaffold and/or the retractive forces of the hydrogel based composites, i.e. physical crosslinking.

The compressive results indicate that the incorporation of bioceramics improves the mechanical strength of the scaffolds which was based on three factors 1) bioceramics absorbing the initial compressive load and the polymeric matrix distributing the load between the reinforcement, 2) increase in the interaction between bioceramic and polymer, and 3) reduction in percentage swelling. Young's modulus values for hydrogel based composites ranged from 4.36±0.34 to 11.59±1.35MPa. Of the three bioceramics, bioactive glasses had the smallest increase in compressive strength which was associated with the absence of physical crosslinking present in the composites. On the other hand, hydroxyapatite hydrogel based composites obtained the most significant increase in terms of compressive and rheological studies. This was associated with the physical crosslinking in the system and the lowest degree of swelling.

3.4 Bioactive, antimicrobial and drug release properties of hydrogel based composites

Optimised samples for each bioceramic/PEG hydrogel composite were selected for further analysis based on the material characterisation of numerous formulations as discussed in Sections 3.3.1 to 3.3.3. As previously described, the key requirements for any synthetic material designed for implantation in the body are biocompatibility and mechanical properties. Other crucial requirements for synthetic materials which are often overlooked in tissue engineering are bioactive, antimicrobial and drug release properties.

- *Bioactivity*: This characteristic plays an important role in the integration of the implant with the surrounding tissue. If a synthetic material is biocompatible, the body can still reject it by encapsulating the scaffold in a fibrous tissue and thus rendering it ineffective. This process occurs unless the material has sufficient bioactive properties (Kokubo and Takadama 2006).
- *Controlled drug release*: Bone is renowned to have poor perfuse properties and consequently treatment with antibiotics requires extensive high doses (Baro *et al.* 2002). This increases this risk of morbidity, repeated operations and lengthy treatment (Chidambaram Soundrapandia *et al.* 2009). Drugs can be incorporated within the system to promote the formation of new bone through the differentiation of adult stem cells into osteoblasts. Scaffolds that exhibit controlled drug delivery results in significantly lower doses being required compared with systemic administration, i.e. intravenously.
- *Antimicrobial properties*: Bone infection is one of the most serious complications for bone grafts after implantation. In biological bone grafts, allografting can result in infection rates of 16% (Mankin *et al.* 1983; Bullens *et al.* 2009; Ketonis *et al.* 2011). On account of this high infection rate, surgeons recommend patients be treated with antibiotics post-surgery intravenously.

3.4.1 *In vitro* biomineralisation study

It is critical that any potential synthetic scaffold used in bone tissue engineering has bioactive properties, as this plays a major role in cellular interactions such as adhesion, infiltration, differentiation and proliferation (Labbaf *et al.* 2011). *In vitro* biomineralisation studies can determine a material's *in vivo* osteoinductive properties by placing samples in simulated body fluid (SBF). In this study, the bioactive properties of the hydrogel based composites were studied *in vitro* by analysing the ability of the scaffold to form an apatite layer. An acellular protein free SBF, with ion concentration, pH and temperature similar to those of the human blood plasma, was employed as the medium for apatite nucleation. The formation of an apatite layer is essential in assisting a synthetic biomaterial, i.e. foreign material, to bond with the surrounding bone tissue *in vivo*.

Polymers, in particular polyethylene glycol, have very limited if any bioactive surface properties due to their low protein absorption (Chen *et al.* 2008). Therefore to overcome this, three separate bioceramics were selected to determine which hydrogel based composite obtained the highest level of bioactivity.

3.4.1.1 Bioactive glasses

Bioactive glasses can be defined as a material that produce specific biological responses. These materials offer an approach to achieve interfacial attachment without using expensive peptides. Previous studies have shown the formation of apatite on the surface of various bioglasses (Balamurugan *et al.* 2007; Balamurugan *et al.* 2008; Ravarian *et al.* 2010), and polymer composites (Peter *et al.* 2010; Wu *et al.* 2010a; Xia and Chang 2010); however, limited attention has been paid to the incorporation of bioactive glasses into polyethylene based hydrogels via photopolymerisation. In the study samples were soaked in simulated body fluid (SBF) for 3 weeks prior to surface analysis of the hydrogel based composites using SEM, EDX and FTIR. The surface of the control hydrogel (0% bioactive glass loading) when soaked in SBF was smooth and the elements associated with the hydrogel were confirmed by EDX (C and

O), which is typical for polyethylene glycol. Minute levels of sodium and chlorine were also detected in the EDX scan. This was attributed to the method of drying the sample; it was soaked in SBF solution causing the precipitation of these particular salts. Confirmation of the lack of bioactivity for the control hydrogel was proven due to the absence of Ca and P from the EDX analysis, it can be concluded that the control hydrogel did not form an apatite layer on its surface. In the case of the bioactive glass powder (Figure 3.56a) the following elements at various concentrations were present in the EDX spectrum: C, O, Na, Si, Ca, Zn and Sr which correspond to the original elements of bioactive glass (p50, Section 2.2.3.1).

When comparing the samples soaked in SBF, new elements were formed following the former treatment, namely Mg, P and Cl. In addition, the amount of Ca increased from ≈1%wt when soaked in distilled water compared to ≈11wt% when soaked in SBF (Figure 3.56b-c). These finding confirm the formation of apatite on the surface of the hydrogel based composite *in vitro*. Further confirmation can be seen in the SEM image in Figure 3.56c, which demonstrates the formation of dense globular crystals tightly packed to the surface of the hydrogel based composite. The formation of apatite in SBF was also verified using FTIR (Figure 3.57). When comparing before vs. after samples soaked in SBF, the former exhibited an increase in intensity at peak 560cm^{-1}. This peak corresponds to the stretching and vibration of the P-O bond in calcium phosphate which further confirms the deposition of an apatite layer on the surface of the hydrogel based composite soaked in SBF which is in agreement with Saboori *et al*. (2009).

The changes to the bioactive glass hydrogel composite in terms of apatite deposition was caused by two mechanisms: (1) preferential diffusion-controlled extraction of Na^+ and/or Ca^{2+} ions out of the glass by exchange with protons from the solution, and (2) hydration and dissolution of the silica network itself, which is rather slow at physiological pH (Vallés Lluch *et al.* 2009). The degradation of the silica network of the bioactive glass results in the formation of ≡Si-OH groups at the surface of the hydrogel based composite and release of soluble $Si(OH)_4$ into the SBF solution. The Si-OH groups provide favourable

locations for nucleation of the apatite, i.e. formation of apatite layer.

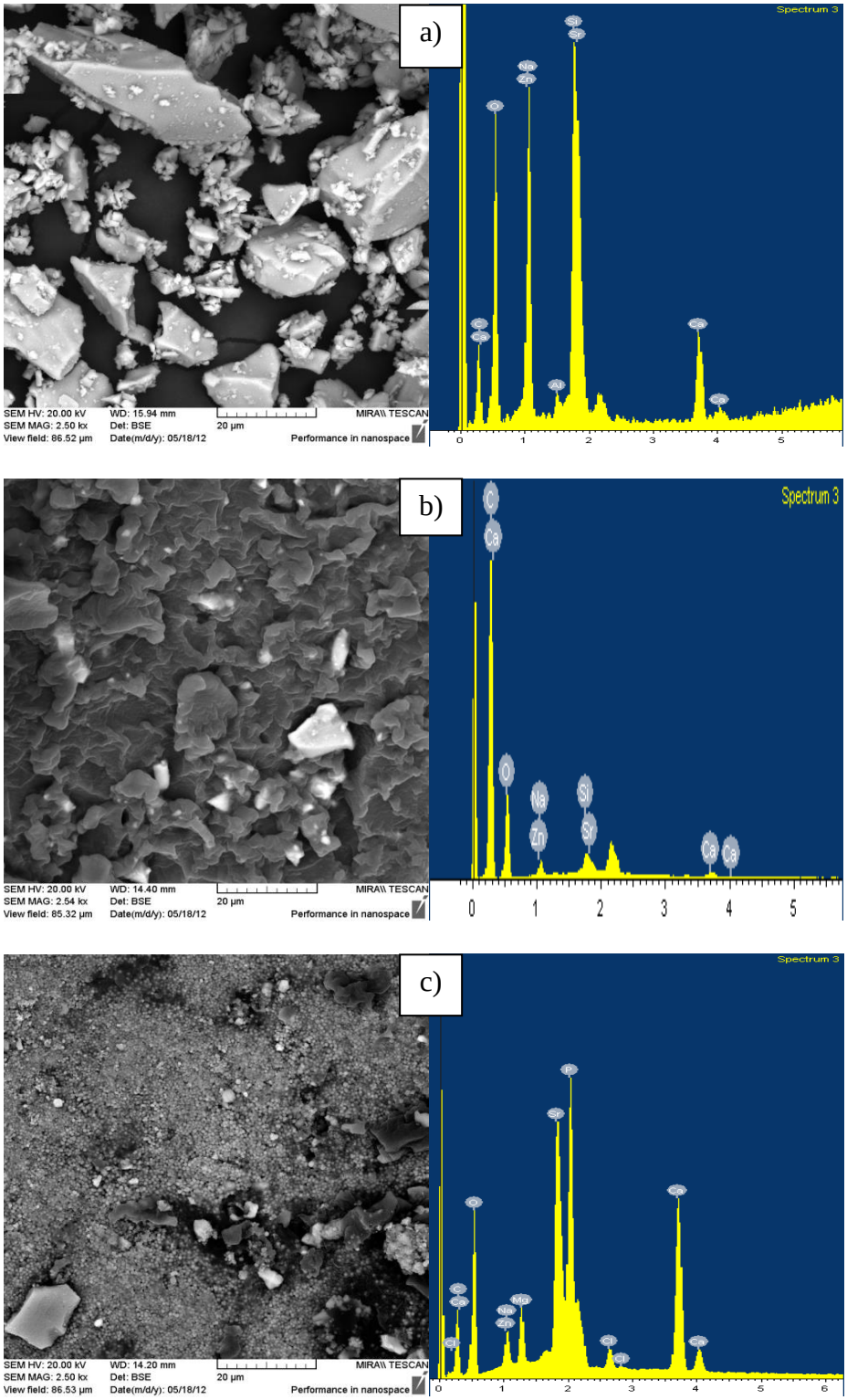

Figure 3.56 *SEM image and EDX spectra of bioactive glass powder (a), hydrogel based composite PEG600A G20 before (b) and after (c) being soaked in SBF*

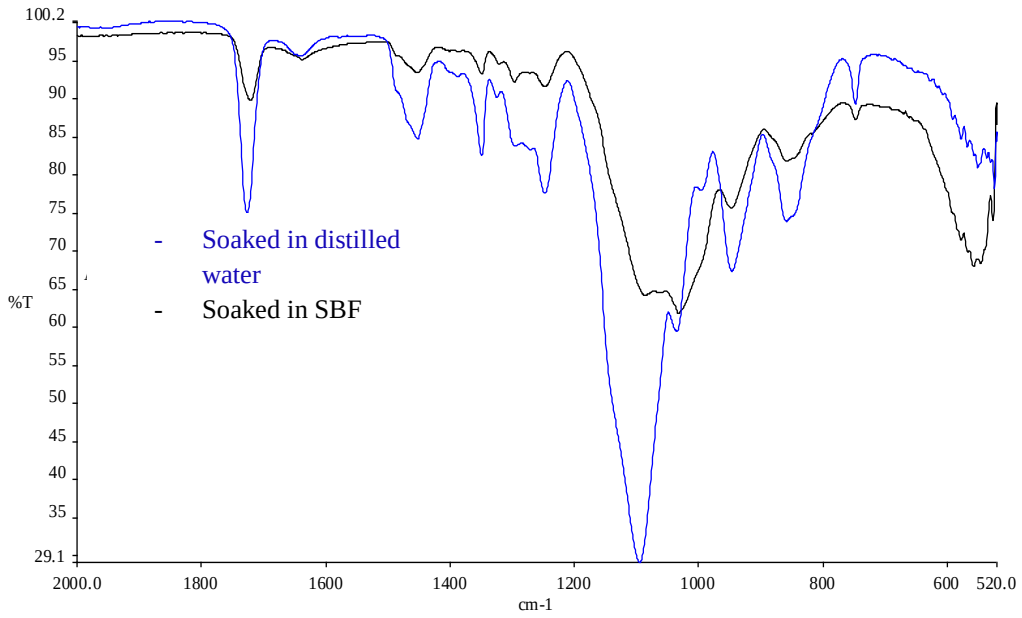

Figure 3.57 *FTIR spectra for hydrogel based composite PEG600A G20 before and after being soaked in simulated body fluid*

3.4.1.2 β-TCP hydrogel based composites

Similarly, a study was carried out to determine the bioactivity properties of PEGDMA hydrogel composite with the incorporation of β-TCP. Subsequent to placing hydrogel based composite PEG600A T20 into SBF for three weeks a bioactive surface was successfully obtained. This was verified by analysis of the surface via SEM and XRD. SEM images (Figure 3.58b-c) of the hydrogel composite before and after immersion in SBF show the formation of globular crystals with a typical cauliflower shape and an average diameter of 2μm for the samples soaked in SBF. The formation of the apatite layer was also confirmed by XRD analysis. Figure 3.59a-b show the polymer peak ($2\theta=20^{o}$) has almost disappeared and new carbonated hydroxyapatite peaks have formed at 29 and 31^{o} for the samples soaked in SBF.

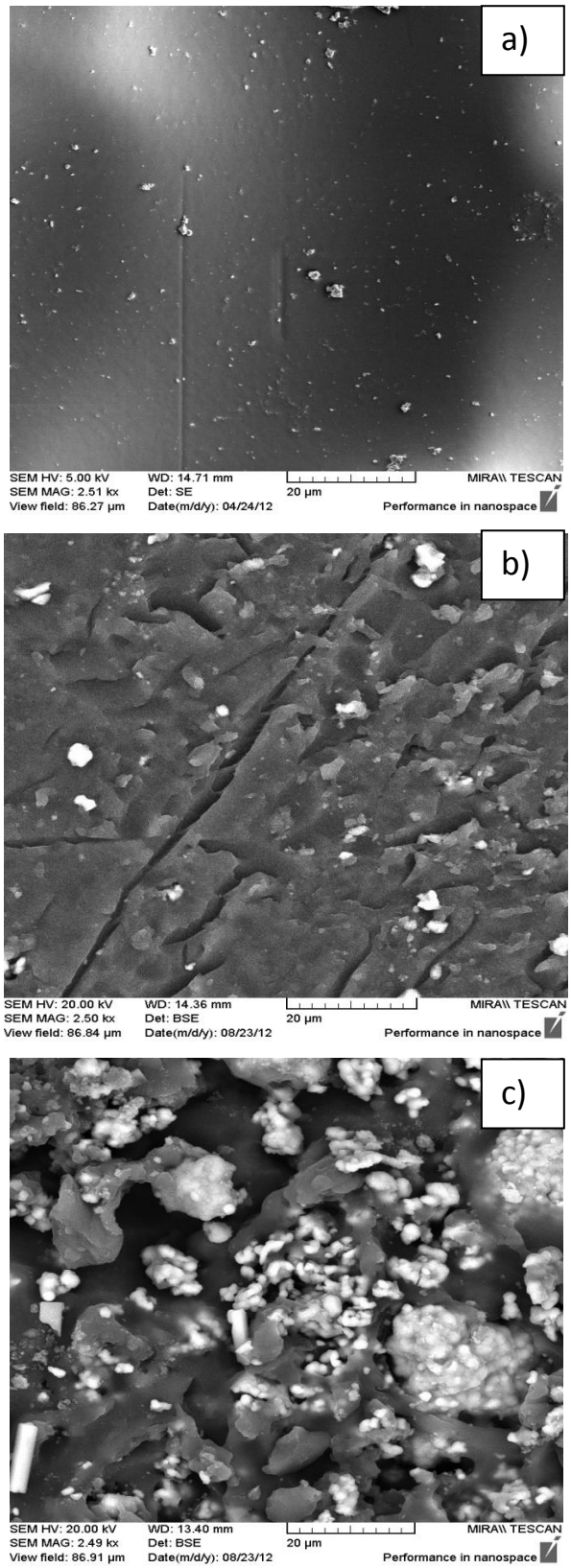

Figure 3.58 *SEM micrographs of control hydrogel (a), hydrogel based composite PEG600A T20 before (b) and after (c) soaking in SBF*

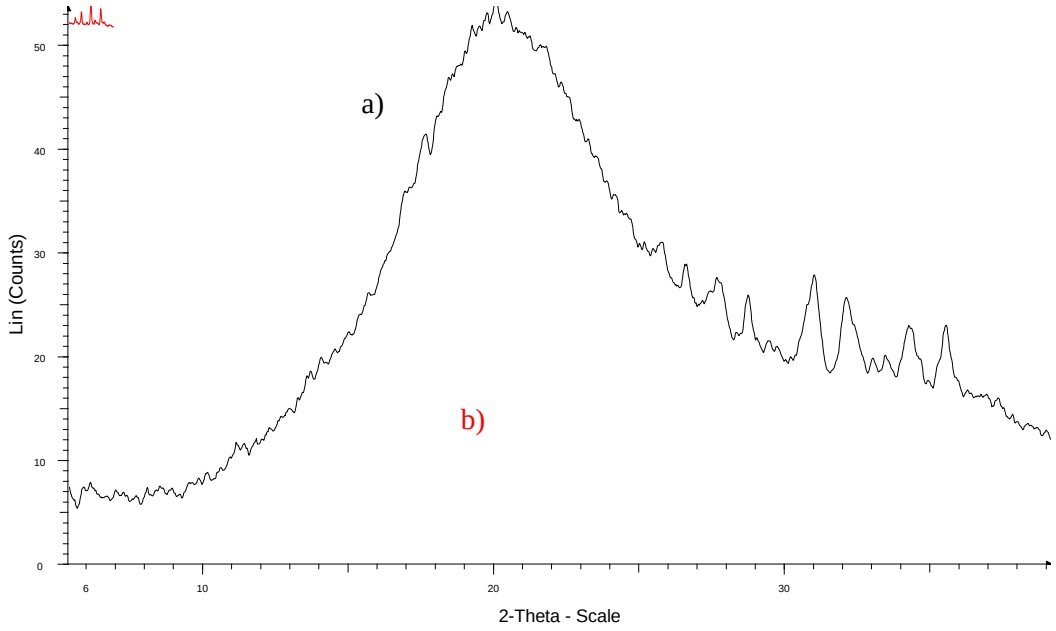

Figure 3.59 *X-ray diffraction of hydrogel based composite PEG600A T20 before (a) and after (b) immersion in SBF*

3.4.1.3 Hydroxyapatite hydrogel based composites

In this study the hydrogel composite with the highest compressive strength was examined in terms of potential bioactive properties by X-ray diffraction. Formation of apatite was confirmed by comparing hydrogel composite PEG1000A H20 before and after immersion in SBF (Figure 3.60b-c), where the polymer phase at 20^{o} almost completely disappears and new apatite peaks form at 28, 31 and 35^{o} (2θ) (Jongwattanapisan *et al.* 2011). The formation of apatite layer takes place through a number of steps involving Ca^{2+}, PO^{3-}_{4} and OH^{-} groups of hydroxyapatite. Initially, PO^{3-}_{4} and OH^{-} groups are responsible for negative charge on the hydroxyapatite surface and Ca^{2+} group form the positive charge. The amount of apatite formation is dependent on negative groups, which in turn depends on the large number of negative groups on the scaffold surface. After immersion in SBF the Ca^{2+} ions from the solution are attracted by the PO^{3-}_{4} and OH^{-} ions present on the hydroxyapatite surface. This results in the hydroxyapatite surface acquiring a positive charge from the solution which in turn attracts additional negatively charged from PO^{3-}_{4} and OH^{-} ions with the

SBF. This continued process results in the formation of the apatite layer *(Chavan et al.* 2010).

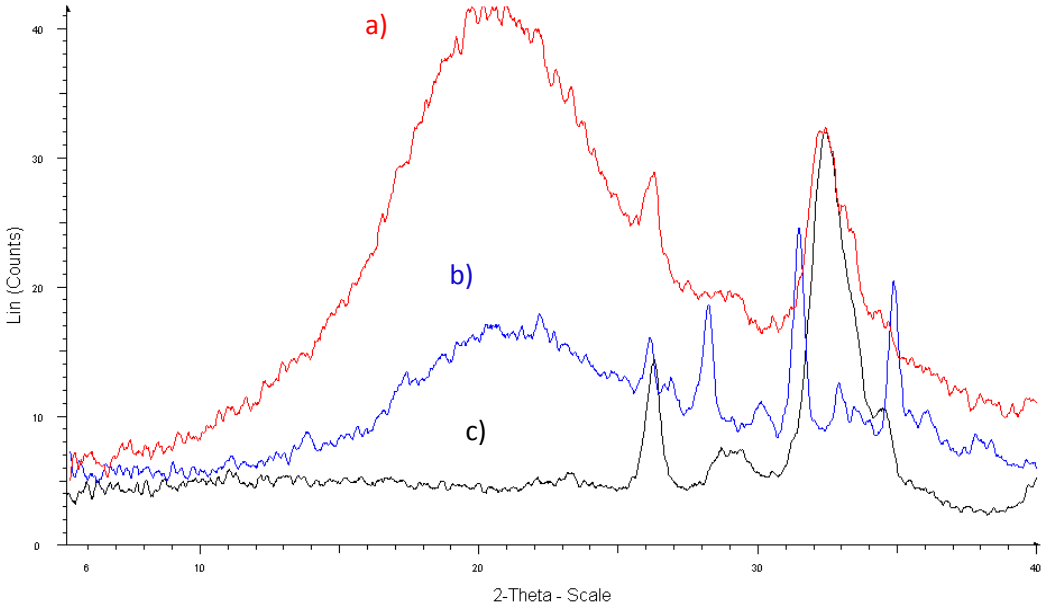

Figure 3.60 *X-ray pattern of hydrogel composite PEG1000A H20 before (a) and after (b) immersion in SBF and HAP powder (c)*

3.4.2 Drug dissolution

In the event of a patient having osteomyelitis, drugs are normally administered intravenously in high doses for prolonged periods of time. This can result in side effects including immunity to antibiotics, increased hospitalisation duration and increased medical expenses (Chidambaram Soundrapandia *et al.* 2009). To overcome these drawbacks, localised drug delivery is becoming more attractive. A scaffold allows for a lower dose of drugs which in turn reduces the risk of side effects. Hydrogels are ideal candidates for drug delivery as they have unique tunable properties that are controlled by their chemical structure, molecular weight, interaction between the polymer and the drug, and drug molecule size. In this study, the release profiles of selected hydrogel based composites were investigated using water-soluble drugs dexamethasone and vancomycin. Dexamethasone was selected because it is a cost-effective alternative to growth factors, which act as osteogenic inducers for stem cells to form new bone

tissue. Vancomycin was chosen based on its antimicrobial properties and its potential to minimise the risk of infection post surgery.

3.4.2.1 β-TCP hydrogel based composites

Photopolymerisation is a suitable technique for drug encapsulation. It has received significant research attention of late, given that hydrogels can control drug release by alternating the crosslink density, pore size, molecular weight, gel composition and filler content (Banerjee *et al.* 2012; Bertz *et al.* 2013). Drug release profiles from both dexamethasone and vancomycin loaded hydrogel based composites are illustrated in Figures 3.61 and 3.62. In this study, the initial dexamethasone content of the hydrogel composites was 6.25wt% and drug release was measured as a function of *in vitro* immersion time. For dexamethasone samples, the variation in the burst affect and controlled drug release duration was dependent on β-TCP loading. The first region (burst effect) was a result of the release of drug molecules at the surface and in close proximity to the surface of the hydrogel based composite. Sustained release was observed in the second region which was due to the diffusion and swelling mechanism with the expansion of pores allowing the drug molecules to escape freely out of the hydrogel based composite. The advantage of designing a burst release system for antimicrobial drugs is that the initial burst release over the first day would sterilise the infected site, which is followed by sustained release which would prevent any surviving bacteria from reappearing on the surface of the scaffold (Moskowitz *et al.* 2010).

For dexamethasone loaded hydrogel based composites, PEG600A T20 had the greatest "burst affect" with full release after 11 days, while hydrogel based composite PEG600A T5 had slightly less burst affect but obtained full release after the same duration (Figure 3.61). Control hydrogel PEG600A had the slowest sustained drug release profile with controlled drug release lasting for 16 days. The decrease in duration of drug release was due to the abruption of crosslinking by the β-TCP particles within the hydrogel based composite, allowing the drug molecules to freely diffuse out of the material. A similar pattern was observed for hydrogel based composites loaded with vancomycin.

Hydrogel based composite with the highest loading of β-TCP, PEG600A T20, released the quickest, (16 days), compared to PEG600A hydrogel which released after 18 days (Figure 3.62).

In comparing the drug release of vancomycin and dexamethasone for all samples tested, dexamethasone samples released the quickest. For example, in the case of hydrogel based composite PEG600A T20 dexamethasone released after 11 days compared to 16 days for vancomycin. The disparity in release time was due to the molecular weights of the drugs; dexamethasone and vancomycin have a molecular weight of 392 and 1500 respectively. It can be concluded that the rate of drug release can be controlled by the amount of crosslinking present between the polymeric components and by the molecular weight of the drug molecule. In the case of both dexamethasone and vancomycin, drug release was observed to be both diffusion and swelled-controlled (p34, Section 1.9.1.1).

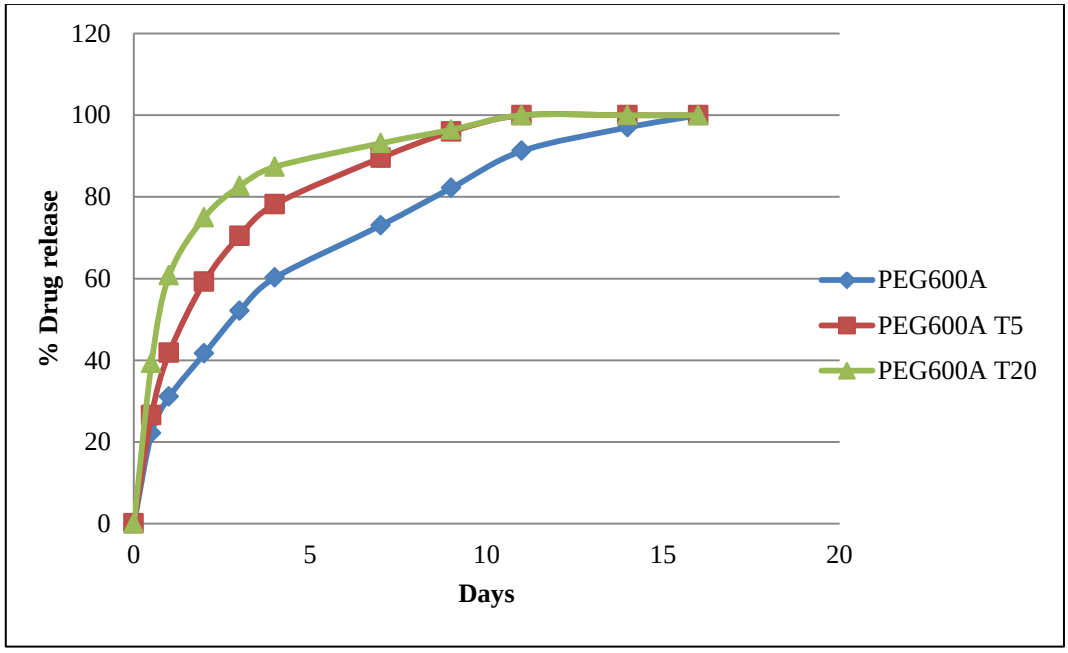

Figure 3.61 *Effect of β-TCP loadings on the release of dexamethasone from hydrogel based composites*

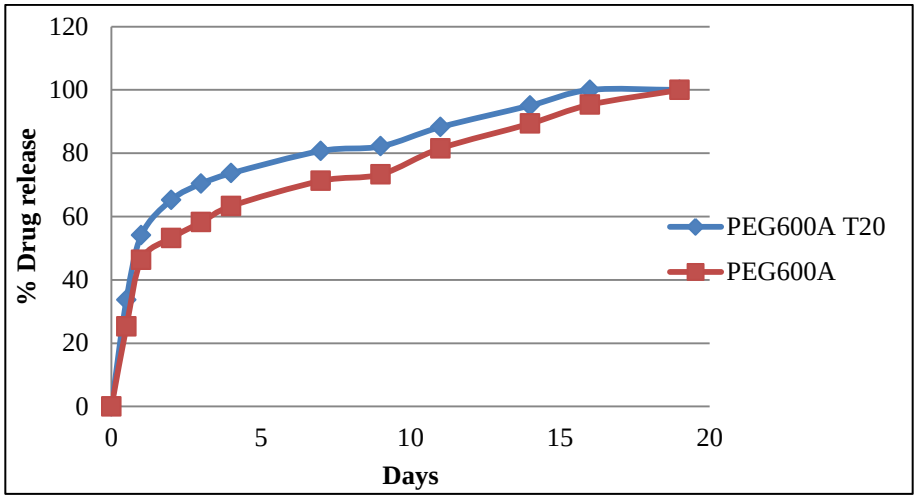

Figure 3.62 *Release of vancomycin from hydrogel based composites with different β-TCP loadings*

3.4.2.2 Hydroxyapatite hydrogel based composites

Figure 3.63 shows that each hydrogel composite had an initial burst release followed by a delay and continuous release of dexamethasone which was similar to β-TCP hydrogel based composites. In the study of the effect of variation in molecular weight of polymer was investigated where PEG1000A H20 had an initial burst of 65% (325±20μm/ml) compared to 52% (260±35μm/ml) for hydrogel composite PEG600A H20 after 24hr. The variation in drug release was associated with the change in pore size between the two materials. Higher molecular weight increases the pore size, allowing the drug molecules to release more quickly out of the hydrogel composite.

Figure 3.64 shows the *in vitro* drug release of vancomycin loaded samples by varying HAP content. Similar to dexamethasone release profiles, an initial burst release was observed and this was followed by a slow sustained release. For example hydrogel composite PEG600A H20 had an initial burst release of 40%, compared to 27% (108±38μm/ml) for the control hydrogel. Furthermore, the hydrogel composite obtained full release faster than the control hydrogel (16 and 19 days, respectively). The variation in the drug release profiles was associated with the introduction of partial physical crosslinking with the addition of HAP content into the already highly chemically crosslinked system. In comparison between drug release for both β-TCP and HAP hydrogel

based composites, no statistical difference was observed (pair t-test) for vancomycin loaded samples ($p>0.05$). Therefore, this suggests that the type of bioceramic does not alter the drug release profile for the hydrogel composites.

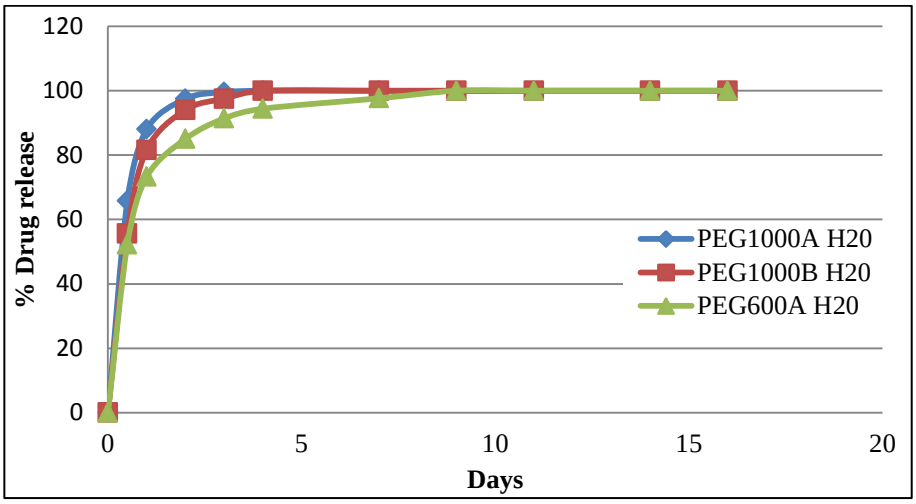

Figure 3.63 *Dexamethasone release profile for hydroxyapatite based hydrogels*

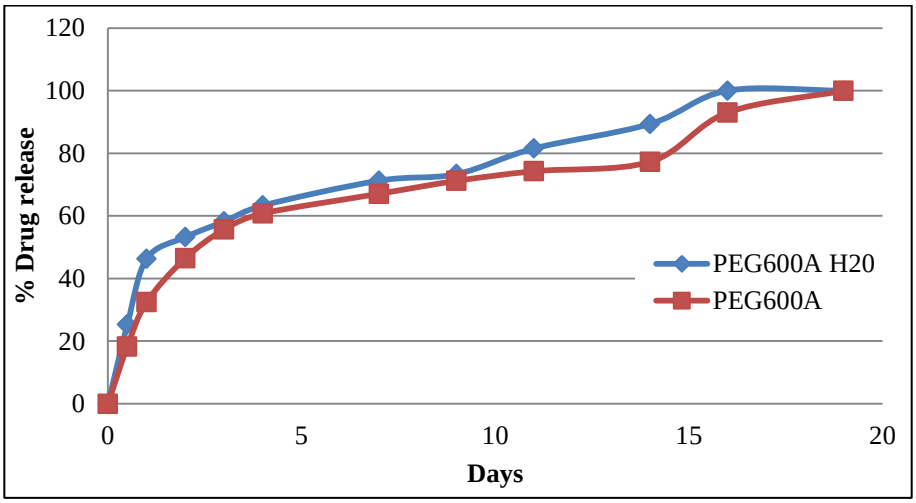

Figure 3.64 *Vancomycin release profile for hydroxyapatite based hydrogels*

3.4.3 Antimicrobial analysis

Despite constant advancements in surgical and antimicrobial treatments, bone infections remain a constant and serious challenge. The local delivery of antibiotics using polymeric materials is a promising treatment and offers several benefits over present therapies. This work evaluated the efficacy of a

vancomycin hydrogel based composites for the treatment of *Staphylococcus aureus in vitro*. *Staphylococcal aureus* is the most widespread pathogen and results in over one third of all acute cases, as well as half of all vertebral infections (McNally and Nagarajah 2010).

The function of this test was to observe the effectiveness of the released antibiotics in terms of the inhibition of bacterial growth (a zone of inhibition) using vancomycin. Vancomycin is a tricyclic glycopeptides antibiotic and has been used clinically for over 50 years. It is an effective treatment of many gram positive bacteria's such as MRSA (Lee *et al.* 2004b). Vancomycin limits the effects of pathogens on osteoblasts and other bone cells *in vitro* (Antoci *et al.* 2007), and does not negatively affect bone growth in fractures *in vivo* (Li *et al.* 2010). These properties are unique compared to other antibiotics used for the treatment of osteomyelitis.

3.4.3.1 β-TCP hydrogel based composites

Successful photopolymerisation occurred with the incorporation of vancomycin into the scaffolds. UV irradiation did not have an effect on vancomycin activity as an antimicrobial agent. FTIR were able to prove this as scans of vancomycin before and after photopolymerisation were identical which suggests the UV light did not denature the drug. Vancomycin was incorporated into the hydrogel based composite prior to photopolymerisation which embedded the drug within the crosslinked network. Antimicrobial activity is controlled by the initial concentration of drug available. In agar diffusion plate method, drug can be released onto the plates by two avenues. Firstly, the drug on the surface of the hydrogel based composite is released directly. Secondly, the drug is released onto the plates through swelling controlled-release mechanism. The hydrogel based composites absorbs moisture to relax the polymer chain and creating larger pores diffusing the drug out of the system.

Unsurprisingly, the hydrogel based composite without vancomycin incorporated did not form a zone of inhibition (Figure 3.65a). Therefore in the absence of vancomycin, the hydrogel based composite exhibited no antimicrobial behaviour. When vancomycin was loaded into the hydrogel based

composite (3.2mg/hydrogel) a zone of inhibition was found (25.29±0.54mm) as shown in Figure 3.65b-d. Hence it can be concluded that the drug loading for this hydrogel based composite is above the minimum inhibitory concentration (MIC) and would be suitable for the treatment of localised infections *in vivo*. This study therefore indicates that photopolymerisation is a useful fabrication technique for development of drug eluting scaffolds for potential bone regeneration applications.

Antimicrobial studies were carried out against a second bacterial strain, *Escherichia coli* (e-coli). However after agar diffusion tests, no zone of inhibition was observed. Therefore it can be concluded that vancomycin loaded hydrogel composites do exhibit any antimicrobial behaviour against e-coli.

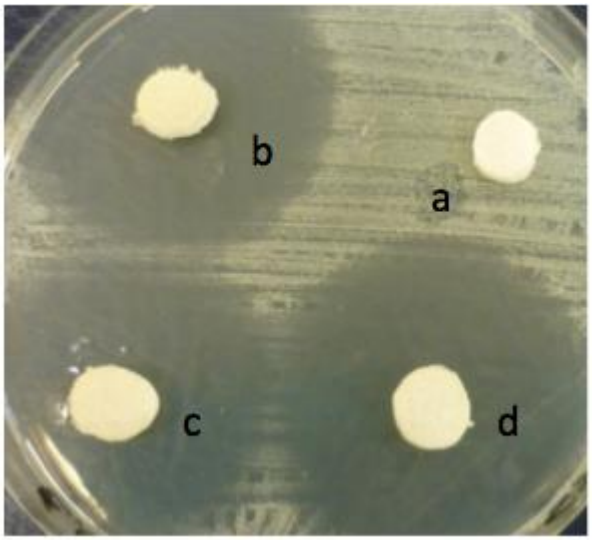

Figure 3.65 *Antimicrobial studies of hydrogel composite PEG600A T20 in the absence (a) and loaded with vancomycin (b-d)*

3.4.3.2 Hydroxyapatite based composites

This study evaluated the antimicrobial properties of hydrogel based composite PEG1000A H20 with vancomycin for the treatment of *Staphylococcus aureus*. In the case of vancomycin-loaded samples, shown in Figure 3.66b-d, a zone of inhibition of 25.62±0.66mm was reported. No statistical difference was observed in running a pair t-test for the zones of inhibition between both HAP and β-TCP hydrogel based composites ($p>0.05$). Therefore, this suggests that the

type of bioceramic does not have an adverse affect on the antimicrobial activity for the hydrogel composites.

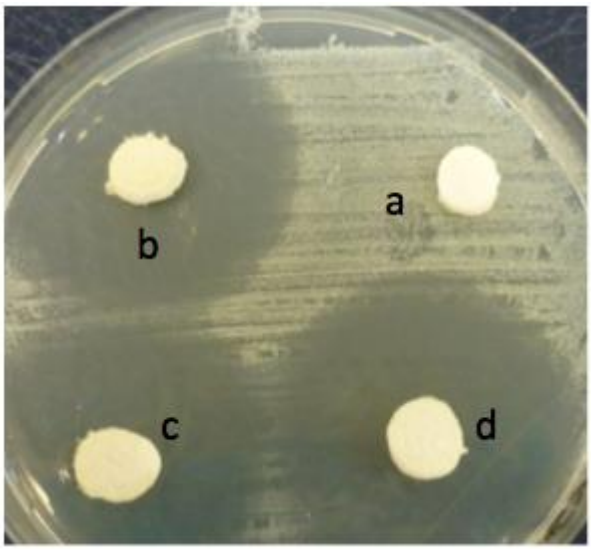

Figure 3.66 *Antimicrobial studies of hydrogel composite PEG600A H20 in the absence (a) and loaded with vancomycin (b-d)*

3.4.4 Summary

The work in this section describes the bioactivity, antimicrobial properties and drug release studies for hydrogel based composites. In the absence of any bioceramic, the hydrogel obtained no bioactive properties. With the incorporation of the bioceramics into the matrix, an apatite layer was formed on the surface of each hydrogel based composite when placed in simulated body fluid. Bioactive glass hydrogel based composites confirmed formation of an apatite layer through the formation of globular crystals on the surface of the hydrogel composite. This apatite layer took place through the degradation of the silica network of the bioactive glass results in the formation of ≡Si-OH groups at the surface of the hydrogel based composite and release of soluble $Si(OH)_4$ into the SBF solution. Similarly, an apatite layer was formed for both HAP and β-TCP which was confirmed through XRD with the almost completely disappearance of polymer peak and the formation of new apatite peaks.

All samples tested for drug release profiles was diffusion and swelled-controlled of a matrix system (p33, Section 1.9.1). The variation in molecular

weight of PEGDMA altered the release profile of the drug which was correlated with the change in pore size between the two materials. For both HAP and β-TCP hydrogel based composites, drug dissolution studies showed that the incorporation of bioceramics into the polymer matrix results in an accelerated drug release profile. This was associated with the abruption of the crosslinking between the macromolecular chains with the bioceramics. However, the type of bioceramic used was not significant ($p>0.05$).

Hydrogel based composites did not exhibit antimicrobial behaviour for samples in the absence of vancomycin. However, with the introduction of an antimicrobial drug, a zone of inhibition was observed, suggesting these hydrogels would be suitable candidates for preventing bone infection *in vivo*. No significant difference was observed between different bioceramic which suggests the type of bioceramic does not alter its antimicrobial properties.

Chapter 4

Conclusion

4. Conclusions

Bone has the ability to repair itself, as humans replace approximately 10-15% of their bone annually through the process of bone absorption and deposition of osteoclasts and osteoblast cells. However, in the case of a critical size defect, the process of bone regeneration is unable to repair the defected bone. These defects may be as a result of fractures, spinal disorders and tumours. The current biological treatments for bone grafts include autografts, allografts and xenografts, where each type has its own limitations. This has led to researchers to focus towards synthetic alternatives such as bioceramics (hydroxyapatite, tricalcium phosphate and bioactive glasses), polymers (collagen, chitosan and polycaprolactone), polymer composites, growth factors and stem cells. Currently, there are over 2.2 million bone graft procedures performed annually and according to the market reports, it is expected to double in the next five years. Therefore, with the limitations in the current treatments and the market size doubling, a demand in new synthetic alternatives is of growing interest to researchers.

The current fabrication techniques employed in the manufacture of synthetic alternatives include solvent casting, gas foaming, electrospinning and melt moulding. Limited research has been conducted using photopolymerisation in the area of bone regeneration. The advantages of photopolymerisation over the aforementioned techniques include ease of fabrication, spatial control, absence of inorganic/organic solvents, low processing temperatures and the potential to incorporate cells into the system prior to polymerisation.

The mechanical performance of any biomedical device is of utmost importance. This is particularly the case for materials that will be utilised for bone regeneration application, where scaffolds are subjected to various loading conditions *in vivo*. With this in mind, the aim of this study was to synthesise a range of hydrogels and hydrogel based composites with the intention of fabricating a scaffold with potential for use in bone regeneration. Initially, a series of hydrogels comprised of PEGDMA were photopolymerised at different monomeric feed ratios. FTIR tests confirmed successful photopolymerisation of the PEGDMA hydrogels had taken place through the disappearance of the

dimethacrylate groups (C-H, C=C and C-O). The hydrogel properties were shown to vary consistently by changing the macromolecular monomer concentrations and molecular weights prior to photopolymerisation. This variation in properties of the hydrogels was related to the mesh size, which was influenced by the degree of swelling. Mesh size expanded with the increase in molecular weight and water concentration (37 to 491 Angstrom units). Rheological and tensile test results showed that both of these factors could be used as a means of manipulating the strength and flexibility of the hydrogels. An MTT assay of selected hydrogels at different extraction concentrations detected no unreacted species after photopolymerisation, therefore rendering the materials biocompatible (cell viability >86% for all samples). DSC thermograms on all examined networks revealed no melting transitions, demonstrating an absence of crystalline PEG phases and illustrating that crosslinking had hindered the polymer's capacity to melt. A single distinctive glass transition was observed and it varied for each sample. This was due to two factors: the first was water acting as a plasticiser in the polymer and second was the variation in the length of polymer chain (molecular weight). An increase in gel fraction was shown for hydrogels with higher molecular weights and polymer concentrations. Overall, the mechanical values recorded for the scaffolds fall short of those typically reported for long bones (femur and tibia). As a consequence, the focus of the project was shifted towards polymer blends to further improve the scaffolds mechanical performance.

Polypropylene glycol was chosen mainly due to its hydrophobic nature. Preliminary studies were carried out using three different polypropylene glycols (PPGDMA, PPGDA and PPGA). After analysis of the three PPG's, polypropylene glycol dimethacrylate was selected based on its superior mechanical strength. Unfortunately, the work illustrated that the addition of PPGDMA into PEGDMA hydrogels negatively affected the mechanical properties of the resultant composites. It was shown that the incorporation of PPGDMA into the system decreased compressive strength. These results are consistent with rheological studies carried out using both strain and frequency sweep tests. Similarly, toxicological results showed that these hydrogel blends

are not suitable for implantation unless numerous time consuming washing steps are to be performed. These hydrogels were therefore not suitable in the field of bone tissue engineering; therefore, the next body of work involved the synthesis and characterisation of novel biocompatible photopolymerisable PVA.

The synthesis of photopolymerisable maleic PVA was conducted through a one step reaction between maleic anhydride and PVA in toluene sulfonic acid/formamide mixed solvent. Synthesis was confirmed by NMR and FTIR. NMR results showed the hydroxyl groups of PVA were acylated by maleic anhydride. Photopolymerisation of subsequent maleic PVA hydrogels resulted in a weak hydrogel. As a result, PEGDMA was incorporated into the system to improve the material's strength. A slight improvement in mechanical properties was observed with the addition of maleic PVA in terms of Young's modulus and stress at limit, however these values are still low compared to those of actual bone. An MTT assay illustrated that the hydrogels have high levels of biocompatibility, making them a viable potential scaffold for bone tissue engineering. To further improve the properties of these polymer blends, fillers (in particular bioceramics) were selected for incorporation with PEGDMA. It was hoped this alteration would help further improve the strength and bioactivity of the scaffolds.

Bioactive glass, beta tricalcium phosphate and hydroxyapatite were chosen as reinforcing fillers with PEGDMA. Collectively, the mechanical properties for the three bioceramic composites indicate that the incorporation of filler improves the mechanical strength of the hydrogel composite materials. The improvement in compressive properties was due to two factors. Firstly, the bioceramics occupied the free space between pores, reducing the ability of the hydrogel based composite to swell. Secondly, the compressive properties improved because of the physical bonding interaction between both components, detected by a shift in the peaks of FTIR analysis. In comparison between the three hydrogel based composites, bioactive glass had the smallest improvement in terms of Young's modulus, increasing approximately 30% in strength. This relatively small increase was due to the lack of physical crosslinking observed for the bioactive glass composites. In comparison, both β-TCP and HAP showed

a significant increase in Young's modulus (100%) which was due to physical crosslinking and the reduction in percentage swelling. Thermal gravimetric analysis indicated that theoretical values were very similar to burn-off weights, which suggests only minute amounts of bioceramic precipitated out of the precursor prior to photopolymerisation. Gel fraction showed that the network connectivity was not disrupted by the introduction of bioceramics. Similarly, glass transition temperature did not significantly change with the introduction of each bioceramic.

Finally, the bioactivity, antimicrobial and drug release profiles were determined for optimised bioceramic hydrogel based composites. In the case of synthetic implants, bioactivity behaviour (formation of an apatite layer) is essential in assisting in the integration of the scaffold *in vivo* with surrounding tissue. In the case of the control hydrogel, an apatite layer was not formed when placed in simulated body fluid. This was due to the low protein absorption of polyethylene glycol which would lead to the scaffold being encapsulated by a fibrous tissue if it were to be implanted *in vivo*. However, each bioceramic formed an apatite layer *in vitro* when placed in simulated body fluid. These findings were confirmed through various techniques: EDX, SEM, FTIR and XRD.

Hydrogels based composites exhibited no antimicrobial properties in the absence of vancomycin. Vancomycin loaded hydrogel based composites inhibited the growth of *S. aureus*, hence confirming that the efficacy of the antibiotic was not compromised during photopolymerisation. The formation of a zone of inhibition suggested that these hydrogels would be suitable candidates for preventing bone infection *in vivo*.

Drug release profiles for both vancomycin and dexamethasone hydrogels were controlled by varying the concentration of the bioceramic and the molecular weight of the polymer. High concentrations of the bioceramic resulted in an accelerated drug release profile. Similarly, the higher the polymer molecular weight, the faster the drug release. This alteration in drug release was related to the pore size of the material. The larger molecular weight and higher bioceramic loadings resulted in larger pore size, allowing the drug to escape

more freely. Molecular weight of the drug was also dependent on the release profile of the drug. For both drugs, the release was found to be diffusion controlled, swelling controlled and affected by the nature of the polymer matrix.

Considering the improvements in this study in terms of mechanical properties and bioactivity of these hydrogels with the introduction of three different bioceramics, some of the things that could further enhance the findings of this study are summarised:

- Confirm the formation of apatite layer is osteoconductive.
- Carry out a comparison study between micro and nano particle bioceramics.
- Incorporate bone cells in the precursor prior to photopolymerisation.
- Carry out *in vivo* studies on hydrogel composites with the incorporation of dexamethasone.

References

Abdelwahed, W., Degobert, G. & Fessi, H. (2006) Freeze-drying of nanocapsules: Impact of annealing on the drying process. *International Journal of Pharmaceutics*, 324 (1) pp. 74-82.

Abdurrahmanoglu, S., Can, V. & Okay, O. (2009) Design of high-toughness polyacrylamide hydrogels by hydrophobic modification. *Polymer*, 50 (23) pp. 5449-5455.

Albrektsson T & C., J. (2001) Osteoinduction, osteoconduction and osseointegration. *Eur Spine J*, pp. 96-101.

Alcântara, M.T.S., Brant, A.J.C., Giannini, D.R., Pessoa, J.O.C.P., Andrade, A.B., Riella, H.G. & Lugão, A.B. (2012) Influence of dissolution processing of PVA blends on the characteristics of their hydrogels synthesized by radiation—Part I: Gel fraction, swelling, and mechanical properties. *Radiation Physics and Chemistry*, 81 (9) pp. 1465-1470.

Aldrich, S. (2012a) Dexamethasone. [Online]. Available [Accessed: 12/09/2012].

Aldrich, S. (2012b) Vancomycin. [Online]. Available [Accessed 13/09/2012].

Alina, S. (2011) Current research on the blends of natural and synthetic polymers as new biomaterials: Review. *Progress in Polymer Science*, 36 (9) pp. 1254-1276.

Alves, A., Duarte, A.R.C., Mano, J.F., Sousa, R.A. & Reis, R.L. (2012) PDLLA enriched with ulvan particles as a novel 3D porous scaffold targeted for bone engineering. *The Journal of Supercritical Fluids* 65 (1) pp. 32-38.

Amirfeyz, R. & Bannister, G. (2009) The effect of bone porosity on the shear strength of the bone–cement interface. *Int Orthop*, 33 (3) pp. 843–846.

Andronescu, E., Ficai, M., Voicu, G., Ficai, D., Maganu, M. & Ficai, A. (2010) Synthesis and characterization of collagen/hydroxyapatite: Magnetite composite material for bone cancer treatment. *Journal of Materials Science: Materials in Medicine*, 21 (7) pp. 2237-2242.

Antoci, J., Adams, C., Hickok, N., Shapiro, I. & Parvizi, J. (2007) Antibiotics for local delivery systems cause skeletal cell toxicity in vitro. *Clin Orthop Relat Res*., 462 pp. 200-206.

Azab, A.K., Kleinstern, J., Doviner, V., Orkin, B., Srebnik, M., Nissan, A. & Rubinstein, A. (2007) Prevention of tumor recurrence and distant metastasis formation in a breast cancer mouse model by biodegradable implant of 131I-norcholesterol. *Journal of Controlled Release*, 123 (2) pp. 116-122.

Bajpai, S., Rai, J.S.P. & Nigam, I. (2009) Swelling behavior of poly(MMA-co-BA-co-PPGDA) polymers. *Journal of Applied Polymer Science*, 112 (4) pp. 2374-2382.

Bajpai, S., Rai, J.S.P. & Nigam, I. (2011) Synthesis and characterization of poly[methyl methacrylate-co-2-ethylhexyl acrylate-co-poly(propylene glycol diacrylate)] latices. *Journal of Applied Polymer Science*, 122 (1) pp. 676-684.

Balamurugan, A., Balossier, G., Kannan, S., Michel, J., Rebelo, A.H.S. & Ferreira, J.M.F. (2007) Development and in vitro characterization of sol–gel derived CaO–P2O5–SiO2–ZnO bioglass. *Acta Biomaterialia*, 3 (2) pp. 255-262.

Balamurugan, A., Balossier, G., Laurent-Maquin, D., Pina, S., Rebelo, A.H.S., Faure, J. & Ferreira, J.M.F. (2008) An in vitro biological and anti-

bacterial study on a sol–gel derived silver-incorporated bioglass system. *Dental Materials*, 24 (10) pp. 1343-1351.

Banerjee, S., Siddiqui, L., Bhattacharya, S.S., Kaity, S., Ghosh, A., Chattopadhyay, P., Pandey, A. & Singh, L. (2012) Interpenetrating polymer network (IPN) hydrogel microspheres for oral controlled release application. *International Journal of Biological Macromolecules*, 50 (1) pp. 198-206.

Baro, M., Sánchez, E., Delgado, A., Perera, A. & Évora, C. (2002) In vitro–in vivo characterization of gentamicin bone implants. *Journal of Controlled Release*, 83 (3) pp. 353-364.

Barone, D.T.J., Raquez, J.M. & Dubois, P. (2011) Bone-guided regeneration: from inert biomaterials to bioactive polymer (nano)composites. *Polymers for Advanced Technologies*, 22 (5) pp. 463-475.

Bauer, T.W. & Muschler, G.F. (2000) Bone graft materials. An overview of the basic science. *Clinical Orthopaedics and Related Research*, 371 pp. 10-27.

Bertram, J.A. & Swartz, S. (1991) The "Law of bone transformation": A case of crying Wolff? *Biological Reviews of the Cambridge Philosophical Society*, 22 (3) pp. 245-273.

Bertz, A., Wöhl-Bruhn, S., Miethe, S., Tiersch, B., Koetz, J., Hust, M., Bunjes, H. & Menzel, H. Encapsulation of proteins in hydrogel carrier systems for controlled drug delivery: *Influence of network structure and drug size on release rate. Journal of Biotechnology*, In press.

Best, S.M., Porter, A.E., Thian, E.S. & Huang, J. (2008) Bioceramics: Past, present and for the future. *Journal of the European Ceramic Society*, 28 (7) pp. 1319-1327.

Bhattarai, N., Gunn, J. & Zhang, M. (2010) Chitosan-based hydrogels for controlled, localized drug delivery. *Advanced Drug Delivery Reviews*, 62 (1) pp. 83-99.

Black, J. (1981) Biomaterials Science and Engineering (Vol. 1). New York: Plenum Press, pp 97-184.

Bodugoz-Senturk, H., Macias, C.E., Kung, J.H. & Muratoglu, O.K. (2009) Poly(vinyl alcohol)–acrylamide hydrogels as load-bearing cartilage substitute. *Biomaterials*, 30 (4) pp. 589-596.

Bose, S. & Tarafder, S. (2012) Calcium phosphate ceramic systems in growth factor and drug delivery for bone tissue engineering: A review. *Acta Biomaterialia*, 8 (4) pp. 1401-1421.

Boyan, B.D., Lohmann, C.H., Romero, J. & Schwartz, Z. (1999) Bone and cartilage tissue engineering. *Clinics in Plastic Surgery*, 26 (4) pp. 629-645.

Boyd, D., Carroll, G., Towler, M., Freeman, C., Farthing, P. & Brook, I. (2009) Preliminary investigation of novel bone graft substitutes based on strontium–calcium–zinc–silicate glasses. *Journal of Materials Science: Materials in Medicine*, 20 (1) pp. 413-420.

Brandl, F., Sommer, F. & Goepferich, A. (2007) Rational design of hydrogels for tissue engineering: Impact of physical factors on cell behaviour. *Biomaterials*, 28 (2) pp. 134-146.

Brin, Y.S., Golenser, J., Mizrahi, B., Maoz, G., Domb, A.J., Peddada, S., Tuvia, S., Nyska, A. & Nyska, M. (2008) Treatment of osteomyelitis in rats by injection of degradable polymer releasing gentamicin. *Journal of Controlled Release*, 131 (2) pp. 121-127.

Bryant, S., Nuttelman, C. & Anseth, K. (2000) Cytocompatibility of UV and visible light photoinitiating systems on cultured NIH/3T3 fibroblasts in vitro. *J Biomater Sci Polym Ed*., 11 (5) pp. 439-457.

Bryant, S.J. & Anseth, K.S. (2003) Controlling the Spatial Distribution of ECM Components in Degradable PEG Hydrogels for Tissue Engineering Cartilage. *Journal of Biomedical Materials Research*, 64A pp. 70-79.

Bullens, P., Minderhoud, N., De Waal Malefijt, M., Veth, R., Buma, P. & Schreuder, H. (2009) Survival of massive allografts in segmental oncological bone defect reconstructions. *International Orthopaedics*, 33 (3) pp. 757-760.

Calori, G.M., Albisetti, W., Agus, A., Iori, S. & Tagliabue, L. (2007) Risk factors contributing to fracture non-unions. *Injury*, 38, Supplement 2 (0) pp. S11-S18.

Calori, G.M., Mazza, E., Colombo, M. & Ripamonti, C. (2011) The use of bone-graft substitutes in large bone defects: Any specific needs? *Injury*, 42, Supplement 2 (0) pp. S56-S63.

Cannillo, V., Chiellini, F., Fabbri, P. & Sola, A. (2010) Production of Bioglass® 45S5 – Polycaprolactone composite scaffolds via salt-leaching. *Composite Structures*, 92 (8) pp. 1823-1832.

Chatterjee, K., Gibson, S.L., Wallace, W.E., Parekh, S.H., Lee, Y.J., Cicerone, M.T.,, Young, M.F., Simon, C.J. (2010) The effect of 3D hydrogel scaffold modulus on osteoblast differentiation and mineralization revealed by combinatorial screening, *Biomaterials*, vol.31, pp.5051-5062.

Chavan, P.N., Bahir, M.M., Mene, R.U., Mahabole, M.P. & Khairnar, R.S. (2010) Study of nanobiomaterial hydroxyapatite in simulated body fluid:

Formation and growth of apatite. *Materials Science and Engineering: B*, 168 (1–3) pp. 224-230.

Chen, H., Yuan, L., Song, W., Wu, Z. & Li, D. (2008) Biocompatible polymer materials: Role of protein-surface interactions. *Progress in Polymer Science*, 33 (11) pp. 1059-1087.

Cheng, L., Ye, F., Yang, R., Lu, X., Shi, Y., Li, L., Fan, H. & Bu, H. (2010) Osteoinduction of hydroxyapatite/β-tricalcium phosphate bioceramics in mice with a fractured fibula. *Acta Biomaterialia*, 6 (4) pp. 1569-1574.

Chidambaram Soundrapandia, Biswanath Sa & Datta, S. (2009) Organic–Inorganic Composites for Bone Drug Delivery. *AAPS PharmSciTech*, 10 (4) pp. 10(14): 1158–1171.

Chinanat, W. (2011) Design and Preparation of Synthetic Hydrogels Via Photopolymerisation for Biomedical Use as Wound Dressings. *Procedia Engineering*, 8 (0) pp. 286-291.

Cho, S.B., Nakanishi, K., Kokubo, T., Soga, N., Ohtsuki, C., Nakamura, T., Kitsugi, T. & Yamamuro, T. (1995) Dependence of apatite formation on silica gel on its structure: effect of heat treatment. *Journal of the American Ceramic Society*, 78 (7) pp. 1769-1774.

Chu, T.M.G., Orton, D.G., Hollister, S.J., Feinberg, S.E. & Halloran, J.W. (2002) Mechanical and in vivo performance of hydroxyapatite implants with controlled architectures. *Biomaterials*, 23 (5) pp. 1283-1293.

Chung, E.H., Gilbert, M., Virdi, A.S., Sena, K., Sumner, D.R., Healy, K.E. (2006) Biomimetic artificial ECMs stimulate bone regeneration, *J Biomed Mater Res* A, vol.15, pp. 815-826.

Chwalek, K., Levental, K.R., Tsurkan, M.V., Zieris, A., Freudenberg, U. & Werner, C. (2011) Two-tier hydrogel degradation to boost endothelial cell morphogenesis. *Biomaterials,* 32 (36) pp. 9649-9657.

Coelho, P.G., Coimbra, M.E., Ribeiro, C., Fancio, E., Higa, O., Suzuki, M. & Marincola, M. (2009) Physico/chemical characterization and preliminary human histology assessment of a β-TCP particulate material for bone augmentation. *Materials Science and Engineering: C*, 29 (7) pp. 2085-2091.

Colthup, N.B., Daly, L.H. & Wiberely, S.E. (1975) Introduction to Infrared and Raman Spectroscopy. New York: Academic Press

Cook, E.A. & Cook, J.J. (2009) Bone Graft Substitutes and Allografts for Reconstruction of the Foot and Ankle. *Clinics in Podiatric Medicine and Surgery*, 26 (4) pp. 589-605.

Costa, H., Mansur, A., Pereira, M. & Mansur, H. (2012) Engineered Hybrid Scaffolds of Poly(vinyl alcohol)/Bioactive Glass for Potential Bone Engineering Applications: Synthesis, Characterization, Cytocompatibility, and Degradation. *Journal of Nanomaterials*, 718470.

Couto, D.S., Hong, Z. & Mano, J.F. (2009) Development of bioactive and biodegradable chitosan-based injectable systems containing bioactive glass nanoparticles. *Acta Biomaterialia*, 5 (1) pp. 115-123.

Coxon, J., Oades, G., Colston, K. & Kirby, R. (2004) Advances in the use of bisphosphonates in the prostate cancer setting. *Prostate Cancer Prostatic Dis*, 7 (2) pp. 99-104.

Crescenzi, V., Francescangeli, A., Capitani, D., Mannina, L., Renier, D. & Bellini, D. (2003) Hyaluronan networking via Ugi's condensation using lysine as cross-linker diamine. *Carbohydrate Polymers*, 53 (3) pp. 311-316.

Csucs, G., Michel, R., Lussi, J.W., Textor, M. & Danuser, G. (2003) Microcontact printing of novel co-polymers in combination with proteins for cell-biological applications. *Biomaterials*, 24 (10) pp. 1713-1720.

Cypher, T.J. & Grossman, J.P. (1996) Biological principles of bone graft healing. *The Journal of Foot and Ankle Surgery*, 35 (5) pp. 413-417.

Damien, C.J. & Parsons, J.R. (1991) Bone graft and bone substitutes: a review of current technology and applications. *J. Appl. Biomater*, pp. 187-208.

Danesin, R., Brun, P., Roso, M., Delaunay, F., Samouillan, V., Brunelli, K., Iucci, G., Ghezzo, F., Modesti, M., Castagliuolo, I. & Dettin, M. (2012) Self-assembling peptide-enriched electrospun polycaprolactone scaffolds promote the h-osteoblast adhesion and modulate differentiation-associated gene expression. *Bone*, 51 (5) pp. 851-859.

Datta, P., Dhara, S. & Chatterjee, J. (2012) Hydrogels and electrospun nanofibrous scaffolds of N-methylene phosphonic chitosan as bioinspired osteoconductive materials for bone grafting. *Carbohydrate Polymers*, 87 (2) pp. 1354-1362.

Decker, C. & Moussa, K. (1987) Photopolymerization of multifunctional monomers in condensed phase. *Journal of Applied Polymer Science*, 34 pp. 1603-1618.

Demirkiran, H., Mohandas, A., Dohi, M., Fuentes, A., Nguyen, K. & Aswath, P. (2010) Bioactivity and mineralization of hydroxyapatite with bioglass as sintering aid and bioceramics with $Na_3Ca_6(PO_4)_5$ and $Ca_5(PO_4)_2SiO_4$ in a silicate matrix. *Materials Science and Engineering: C*, 30 (2) pp. 263-272.

Deplaine, H., Ribelles, J.L.G. & Ferrer, G.G. (2010) Effect of the content of hydroxyapatite nanoparticles on the properties and bioactivity of poly(l-lactide) – Hybrid membranes. *Composites Science and Technology*, 70 (13) pp. 1805-1812.

Devine, D.M., Devery, S.M., Lyons, J.G., Geever, L.M., Kennedy, J.E. & Higginbotham, C.L. (2006) Multifunctional polyvinylpyrrolidinone-polyacrylic acid copolymer hydrogels for biomedical applications. *International Journal of Pharmaceutics*, 326 (1-2) pp. 50-59.

Devine, D.M. & Higginbotham, C.L. (2005) Synthesis and characterisation of chemically crosslinked N-vinyl pyrrolidinone (NVP) based hydrogels. *European Polymer Journal*, 41 (6) pp. 1272-1279.

Di Martino, A., Sittinger, M. & Risbud, M.V. (2005) Chitosan: A versatile biopolymer for orthopaedic tissue-engineering. *Biomaterials*, 26 (30) pp. 5983-5990.

Dietmar W.H. (2000) Scaffolds in tissue engineering bone and cartilage. *Biomaterials*, 21 (24) pp. 2529-2543.

Dobić, S.N., Filipović, J.M. & Tomić, S.L. (2012) Synthesis and characterization of poly(2-hydroxyethyl methacrylate/itaconic acid/poly(ethylene glycol) dimethacrylate) hydrogels. *Chemical Engineering Journal*, 179 (0) pp. 372-380.

Dorozhkin, S.V. (2010) Bioceramics of calcium orthophosphates. *Biomaterials*, 31 (7) pp. 1465-1485.

Doyle, B.J., Killion, J. & Callanan, A. (2012) Use of the photoelastic method and finite element analysis in the assessment of wall strain in abdominal aortic aneurysm models. *Journal of Biomechanics*, 45 (10) pp. 1759-1768.

Drumheller, P.D., Elber, D.L. & Hubbell, J.A. (1994) Multifunctional poly(ethylene glycol) semiinterpenetrating polymer networks as highly selective adhesive substrate for bioadhesive peptide grafting. *Biotech. Bioeng*, 43 pp. 772-780.

Drury, J.L. & Mooney, D.J. (2003) Hydrogels for tissue engineering: scaffold design variables and applications. *Biomaterials*, 24 (24) pp. 4337-4351.

Duchemin, L., Bousson, V., Raossanaly, C., Bergot, C., Laredo, J.D., Skalli, W. & Mitton, D. (2008) Prediction of mechanical properties of cortical bone by quantitative computed tomography. *Medical Engineering and Physics*, 30 (3) pp. 321-328.

Elisseeff, J., Anseth, K., Sims, D., Mcintosh, W., Randoloph, M. & Langer, R. (1999) Transdermal photopolymerization for minimally invasive implantation. *Medical Science*, 96 pp. 3104-3107.

Elisseeff, J., Mcintosh, W., Anseth, K., Riley, S., Ragan, P. & Langer, R. (2000) Photoencapsulation of chondrocytes in poly(ethylene oxide)-based semi-interpenetrating networks. *Journal of Biomedical Materials Research*, 51 (2) pp. 164-171.

Elisseeff, J., Puleo, C., Yang, F. & Sharma, B. (2005) Advances in skeletal tissue engineering with hydrogels. *Orthodontics & Craniofacial Research*, 8 (3) pp. 150-161.

Am Ende, M.T. & Brannon Peppas, L.P.N.A. (1997) Transport of ionizable drugs and proteins in crosslinked poly (acrylic acid) and poly (acrylic acid-co-2-hydroxyethyl methacrylate) hydrogels. II. Diffusion and release studies. *Journal of Controlled Release*, 48 (1) pp. 47-56.

Fedorovich, N.E., Oudshoorn, M.H., Van Geemen, D., Hennink, W.E., Alblas, J. & Dhert, W.J.A. (2009) The effect of photopolymerization on stem cells embedded in hydrogels. *Biomaterials*, 30 (3) pp. 344-353.

Fitzgerald, R.H., Kaufer, H. & Malkani, A.L. (2002) Orthopaedics. 1st ed. Vol. 1: Mosby, pp 61-88.

Flory, P. & Rehner, J. (1943) Statistical Mechanics of Cross-Linked Polymer Networks II. Swelling. *Journal of Chemical Physics*, 11 pp. 521-526.

Folkman, J. & Long, D.M. (1964) The use of silicone rubber as a carrier for prolonged drug therapy. *Journal of Surgical Research*, 4 (3) pp. 139-142.

Fouassier, J. & Rabek, J. (1995) Photoinitiation, photopolymerization and photocuring. Munich: Hanser

Fr, M. (2012) Bone Physiology. [Online]. Available [Accessed: 02/12/2012].

Frohbergh, M.E., Katsman, A., Botta, G.P., Lazarovici, P., Schauer, C.L., Wegst, U.G.K. & Lelkes, P.I. (2012) Electrospun hydroxyapatite-containing chitosan nanofibers crosslinked with genipin for bone tissue engineering. *Biomaterials*, 33 (36) pp. 9167-9178.

Frost, R., Sullivan, F.A. (2011) European Orthopaedic Devices Market Outlook.

Fu, X.J., Cao, S.Q., Wang, N.X., Zhang, S.Z., Wang, H. & Yang, Y.J. (2007) Effect of hydrogen bonding and hydrophobic interaction on the formation of supramolecular hydrogels formed by l-phenylalanine derivative hydrogelator. *Chinese Chemical Letters*, 18 (8) pp. 1001-1004.

Förster, S. & Antonietti, M. (1998) Amphiphilic Block Copolymers in Structure-Controlled Nanomaterial Hybrids. *Advanced Materials*, 10 (3) pp. 195-217.

Gaharwar, A.K., Dammu, S.A., Canter, J.M., Wu, C.-J. & Schmidt, G. (2011a) Highly Extensible, Tough, and Elastomeric Nanocomposite Hydrogels from Poly(ethylene glycol) and Hydroxyapatite Nanoparticles. *Biomacromolecules*, 12 (5) pp. 1641-1650.

Gaharwar, A.K., Rivera, C.P., Wu, C.-J. & Schmidt, G. (2011b) Transparent, elastomeric and tough hydrogels from poly(ethylene glycol) and silicate nanoparticles. *Acta Biomaterialia*, 7 (12) pp. 4139-4148.

Geever, L.M., Cooney, C.C., Lyons, J.G., Kennedy, J.E., Nugent, M.J.D., Devery, S. & Higginbotham, C.L. (2008) Characterisation and controlled drug release from novel drug-loaded hydrogels. *European Journal of Pharmaceutics and Biopharmaceutics*, 69 (3) pp. 1147-1159.

Geever, L.M., Devine, D.M., Nugent, M.J.D., Kennedy, J.E., Lyons, J.G., Hanley, A. & Higginbotham, C.L. (2006) Lower critical solution temperature control and swelling behaviour of physically crosslinked thermosensitive copolymers based on N-isopropylacrylamide. *European Polymer Journal*, 42 (10) pp. 2540-2548.

Giannoudis, P.V., Dinopoulos, H. & Tsiridis, E. (2005) Bone substitutes: An update. *Injury*, 36 (3, Supplement) pp. S20-S27.

Goldberg, V.M. & Stevenson, S. (1987) Natural history of autografts and allografts. *Clin Orthop Relat Res*, 225 pp. 7-16.

Graham, N.B. (1987) Poly(ethylene oxide) and related hydrogels. Vol. II. Boca Raton: CRC Press

Graham, N.B. (1998a) Hydrogels: their future, Part I. *Medical Device Technology*, pp. 18-22.

Graham, N.B. (1998b) Hydrogels: their future, Part II. *Medical Device Technology*, 9 pp. 22-25.

Grimm, M.J. (2004). Othopedic Biomaterials. Standard Handbook of Biomedical Engineering and Design, McGraw-Hill, pp 6-29.

Guillerminet, F., Beaupied, H., Fabien-Soulé, V., Tomé, D., Benhamou, C.-L., Roux, C. & Blais, A. (2010) Hydrolyzed collagen improves bone metabolism and biomechanical parameters in ovariectomized mice: An in vitro and in vivo study. *Bone*, 46 (3) pp. 827-834.

Hajiali, H., Karbasi, S., Hosseinalipour, M. & Rezaie, H. (2010) Preparation of a novel biodegradable nanocomposite scaffold based on poly (3-hydroxybutyrate)/bioglass nanoparticles for bone tissue engineering. *Journal of Materials Science: Materials in Medicine*, 21 (7) pp. 2125-2132.

Hamidi, M., Azadi, A. & Rafiei, P. (2008) Hydrogel nanoparticles in drug delivery. *Advanced Drug Delivery Reviews*, 60 (15) pp. 1638-1649.

Helms, J.A., Amasha, R.R. & Leucht, P. (2007) Bone voyage: An expedition into the molecular and cellular parameters affecting bone graft fate. *Bone*, 41 (4) pp. 479-485.

Hench, L. (1998) Bioceramics. *J. Am. Ceram. Soc*, 81 (7) pp. 1705-1728.

Hench, L. & Wilson, J. (1993) An Introduction to Bioceramics. Singapore: World Scienctific

Hench, L.L. & Polak, J.M. (2002) Third-Generation Biomedical Materials. *Science*, 295 (5557) pp. 1014-1017.

Hench, L.L. & West, J.K. (2006) Biological applications of bioactive glasses. *Life Chemistry Reports*, 13 pp. 187-241.

Hill-West, J.L., Chowdhury, S.M., Slepian, M.J. & Hubbell, J.A. (1994) Inhibition of thrombosis and intimal thickening by in situ photopolymerization of thin hydrogel barriers. *Proceedings of the National Academy of Sciences of the United States of America*, 91 (13) pp. 5967-5971.

Hillery, A., Lloyd, A. & Swarbrick, J. (2001) Drug Delivery and Targeting for Pharmacists and Pharmaceutical Scientists. Florida: Taylor & Francis Group, pp. 7-49.

Hing, K.A. (2005) Bioceramic Bone Graft Substitutes: Influence of Porosity and Chemistry. International *Journal of Applied Ceramic Technology*, 2 (3) pp. 184-199.

Hoare, T.R. & Kohane, D.S. (2008) Hydrogels in drug delivery: Progress and challenges. *Polymer*, 49 (8) pp. 1993-2007.

Hoffman, A.S. (2002) Hydrogels for biomedical applications. *Advanced Drug Delivery Reviews*, 64, Supplement (0) pp. 18-23.

Hollister, S.J. (2009) Scaffold Design and Manufacturing: From Concept to Clinic. *Advanced Materials*, 21 (32-33) pp. 3330-3342.

Hong, Y., Chirila, M., Cuypers, M. & Constable, I. (1996) Polymers of 1-vinyl-2-pyrrolidinone as potential vitreous substitutes: physical selection. *Journal of Biomaterials Application*, 11 pp. 135–181.

Horan, R.L., Antle, K., Collette, A.L., Wang, Y., Huang, J., Moreau, J.E., Volloch, V., Kaplan, D.L. & Altman, G.H. (2005) In vitro degradation of silk fibroin. *Biomaterials*, 26 (17) pp. 3385-3393.

Hsu, W.K. & Wang, J.C. (2006) Demineralized Bone Matrix for Spinal Arthrodesis. *Seminars in Spine Surgery*, 18 (1) pp. 22-25.

Hu, D.S.-G. & Chou, K.J.-N. (1996) Kinetics of water swelling and development of porous structure in ionic poly(acrylonitrile-acrylamide-acrylic acid) hydrogels. *Polymer*, 37 (6) pp. 1019-1025.

Hu, H.-T., Shin, T.-C., Lee, S.-Y., Chen, C.-C. & Yang, J.-C. (2011) Influence of hydrolytic degradation on the surface properties of poly-5d/95l-lactide resorbable bone plates. *Polymer Degradation and Stability*, 96 (8) pp. 1522-1529.

Huang, Z., Yu, B., Feng, Q., Li, S., Chen, Y. & Luo, L. (2011) In situ-forming chitosan/nano-hydroxyapatite/collagen gel for the delivery of bone marrow mesenchymal stem cells. *Carbohydrate Polymers*, 85 (1) pp. 261-267.

Hutmacher (2001) Polymeric Scaffolds in Tissue Engineering Bone and Cartilage. *Biomaterials*, 12 pp. 107-124.

Hutmacher, D., Woodfield, T., Dalton, P. & Lewis, J. (2008). Chapter 14 - Scaffold design and fabrication. In B. Clemens van, T. Peter, L. Anders, H. Jeffrey, F.W. David, C. Ranieri, P.T.A.L.J.H.D.F.W.R.C.J.D.d.B. Joost D. de Bruijn and Jérôme SohierA2 - Clemens van Blitterswijk & S. Jérôme (Eds.), *Tissue Engineering* (pp. 403-454). Burlington: Academic Press.

Ikada, Y. (2006) Tissue engineering: fundamentals and applications. UK: Elsevier Ltd

Jayaswal, G., Dange, S. & Khalikar, A. (2010) Bioceramic in dental implants: A review. *The Journal of Indian Prosthodontic Society*, 10 (1) pp. 8-12.

Jiang, H., Campbell, G., Boughner, D., Wan, W.-K. & Quantz, M. (2004) Design and manufacture of a polyvinyl alcohol (PVA) cryogel tri-leaflet heart valve prosthesis. *Medical Engineering and Physics*, 26 (4) pp. 269-277.

Jiang, Y.-P. & Guo, X.-K. (2005) O-maleoyl derivative of low-molecular-weight κ-carrageenan: Synthesis and characterization. *Carbohydrate Polymers*, 61 (4) pp. 441-445.

Jin, R., Moreira Teixeira, L.S., Dijkstra, P.J., Karperien, M., Van Blitterswijk, C.A., Zhong, Z.Y. & Feijen, J. (2009) Injectable chitosan-based hydrogels for cartilage tissue engineering. *Biomaterials*, 30 (13) pp. 2544-2551.

Jing, R., Yanqun, Z., Jiuqiang, L. & Hongfei, H. (2001) Radiation synthesis and characteristic of IPN hydrogels composed of poly(diallyldimethylammonium chloride) and Kappa-Carrageenan. *Radiation Physics and Chemistry*, 62 (2-3) pp. 277-281.

Jones, J.I. (1973) Polyvinyl alcohol. Properties and applications. Edited by C. A. Finch. John Wiley, Chichester. 1973. *British Polymer Journal*, 5 (6) pp. 493-494.

Jones, J.R. & Hench, L.L. (2003) Regeneration of trabecular bone using porous ceramics. *Current Opinion in Solid State and Materials Science*, 7 (4-5) pp. 301-307.

Jongwattanapisan, P., Charoenphandhu, N., Krishnamra, N., Thongbunchoo, J., Tang, I.M., Hoonsawat, R., Smith, S.M. & Pon-on, W. (2011)

In vitro study of the SBF and osteoblast-like cells on hydroxyapatite/chitosan–silica nanocomposite. *Materials Science and Engineering: C*, 31 (2) pp. 290-299.

Ju, H., McCloskey, B.D., Sagle, A.C., Kusuma, V.A. & Freeman, B.D. (2009) Preparation and characterization of crosslinked poly(ethylene glycol) diacrylate hydrogels as fouling-resistant membrane coating materials. *Journal of Membrane Science*, 330 (1-2) pp. 180-188.

Kahn, S.N., Cammisa, F.P., Sandhu, H.S., Diwan, A.D., Girardi, F.P. & Lane, J.M. (2005) The biology of bone grafting. *J AM Acad Orthop Surg*, 13 (1) pp. 77-86.

Kalakkunnath, S., Kalika, D.S., Lin, H., Raharjo, R.D. & Freeman, B.D. (2007) Molecular relaxation in cross-linked poly(ethylene glycol) and poly(propylene glycol) diacrylate networks by dielectric spectroscopy. *Polymer*, 48 (2) pp. 579-589.

Kamaraj, J., Swaminathan, E. & Dharmalingam, S. (2008) Development and characterization of polymer ceramic composites for orthopedic applications. *Trends in Biomaterials and Artificial Organs*, 22 (3) pp. 169-178.

Kandile, N.G., Mohamed, M.I., Zaky, H.T., Nasr, A.S. & Abdel-Bary, E.M. (2009) Synthesis and properties of chitosan hydrogels modified with heterocycles. *Carbohydrate Polymers*, 75 (4) pp. 580-585.

Kaneko, Y., Sakai, K., & Okane, T,. 1998, 'Temperature-Responsive Hydrogels as Intelligent Materials', in T. Okano (Ed), Biorelated polymer and gels, controlled release and applications in biomedical engineering, Academic Press, New York, pp. 29-69.

Kang, G., Cao, Y., Zhao, H. & Yuan, Q. (2008) Preparation and characterization of crosslinked poly(ethylene glycol) diacrylate membranes with

excellent antifouling and solvent-resistant properties. *Journal of Membrane Science*, 318 (1-2) pp. 227-232.

Kang, Y., Xu, X., Yin, G., Chen, A., Liao, L., Yao, Y., Huang, Z. & Liao, X. (2007) A comparative study of the in vitro degradation of poly(l-lactic acid)/β-tricalcium phosphate scaffold in static and dynamic simulated body fluid. *European Polymer Journal*, 43 (5) pp. 1768-1778.

Kang, Y., Yao, Y., Yin, G., Huang, Z., Liao, X., Xu, X. & Zhao, G. (2009) A study on the in vitro degradation properties of poly(l-lactic acid)/β-tricalcuim phosphate(PLLA/β-TCP) scaffold under dynamic loading. *Medical Engineering and Physics*, 31 (5) pp. 589-594.

Karaca, N., Temel, G., Karaca Balta, D., Aydin, M. & Arsu, N. (2010) Preparation of hydrogels by photopolymerization of acrylates in the presence of Type I and one-component Type II photoinitiators. *Journal of Photochemistry and Photobiology A: Chemistry*, 209 (1) pp. 1-6.

Karmaker, A., Dibenedetto, A. & Goldberg, A. (1997) Extent of conversion and its effect on the mechanical performance of BIS-GMA/PEGDMA-based resins and their composites with continuous glass fibers. *J. Mater. Sci. Mater. Med.*, 8 pp. 333–401.

Kellomäki, M., Niiranen, H., Puumanen, K., Ashammakhi, N., Waris, T. & Törmälä, P. (2000) Bioabsorbable scaffolds for guided bone regeneration and generation. *Biomaterials*, 21 (24) pp. 2495-2505.

Kennedy, J.E. & Higginbotham, C.L. (2011) Synthesis and characterisation of styrene butadiene styrene-g-N-vinyl-2-pyrrolidinone for use in biomedical applications. *Materials Science and Engineering: C*, 31 (2) pp. 246-251.

Ketonis, C., Barr, S., Shapiro, I.M., Parvizi, J., Adams, C.S. & Hickok, N.J. (2011) Antibacterial activity of bone allografts: Comparison of a new vancomycin-tethered allograft with allograft loaded with adsorbed vancomycin. *Bone*, 48 (3) pp. 631-638.

Kim, B.S. & Mooney, D.J. (1998) Development of biocompatible synthetic extracellular matrices for tissue engineering. *Trends in Biotechnology*, 16 (5) pp. 224-229.

Kim, H.-M., Himeno, T., Kokubo, T. & Nakamura, T. (2005) Process and kinetics of bonelike apatite formation on sintered hydroxyapatite in a simulated body fluid. *Biomaterials*, 26 (21) pp. 4366-4373.

Kim, J., Kim, I.S., Cho, T.H., Lee, K.B., Hwang, S.J., Tae, G., Noh, I., Lee, S.H., Park, Y. & Sun, K. (2007) Bone regeneration using hyaluronic acid-based hydrogel with bone morphogenic protein-2 and human mesenchymal stem cells. *Biomaterials*, 28 (10) pp. 1830-1837.

Kobayashi, H., Kato, M., Taguchi, T., Ikoma, T., Miyashita, H., Shimmura, S., Tsubota, K. & Tanaka, J. (2004) Collagen immobilized PVA hydrogel-hydroxyapatite composites prepared by kneading methods as a material for peripheral cuff of artificial cornea. *Materials Science and Engineering: C*, 24 (6–8) pp. 729-735.

Kobayashi, M., Toguchida, J. & Oka, M. (2001) Development of Alcohol-Hydrogel (PVA-H) Shields with a High Water Content for Tendon Injury repair. *The Journal of Hand Surgery: British & European Volume*, 26 (5) pp. 436-440.

Kokubo, T., Ito, S., Huang, Z.T., Hayashi, T., Sakka, S., Kitsugi, T. & Yamamuro, T. (1990a) Ca, P-rich layer formed on high-strength bioactive glass-ceramic A-W. *Journal of Biomedical Materials Research*, 24 (3) pp. 331-343.

Kokubo, T., Kushitani, H., Sakka, S., Kitsugi, T. & Yamamuro, T. (1990b) Solutions able to reproduce in vivo surface-structure changes in bioactive glass-ceramic A-W3. *Journal of Biomedical Materials Research*, 24 (6) pp. 721-734.

Kokubo, T. & Takadama, H. (2006) How useful is SBF in predicting in vivo bone bioactivity? *Biomaterials*, 27 (15) pp. 2907-2915.

Kraehenbuehl, T.P., Zammaretti, P., Van der viles, A.J., Schoenmakers, R.G., Lutolf, M.P., Jaconi, M.E., Hubbell, J.A. (2008) Three dimensional extracellular matrix directed cardioprogenitor differentiation: Systematic modulation of a synthetic cell-responsive PEG hydrogel, *Biomaterials* , vol.29, pp.2757-2766.

Kusuma, V.A., Matteucci, S., Freeman, B.D., Danquah, M.K. & Kalika, D.S. (2009) Influence of phenoxy-terminated short-chain pendant groups on gas transport properties of cross-linked poly(ethylene oxide) copolymers. *Journal of Membrane Science*, 341 (1-2) pp. 84-95.

Labbaf, S., Tsigkou, O., Müller, K.H., Stevens, M.M., Porter, A.E. & Jones, J.R. (2011) Spherical bioactive glass particles and their interaction with human mesenchymal stem cells in vitro. *Biomaterials*, 32 (4) pp. 1010-1018.

Langer, R. & Vacanti, J. (1993) Tussue Engineering. *Science*, 260 pp. 920-926.

Lauzon, M.-A., Bergeron, É., Marcos, B. & Faucheux, N. (2012) Bone repair: New developments in growth factor delivery systems and their mathematical modeling. Journal of Controlled Release, 162 (3) pp. 502-520.

Lee, C.H., Singla, A. & Lee, Y. (2001) Biomedical applications of collagen. *International Journal of Pharmaceutics*, 221 (1–2) pp. 1-22.

Lee, K.-W.D., Chan, P.K. & Feng, X. (2004a) Morphology development and characterization of the phase-separated structure resulting from the thermal-induced phase separation phenomenon in polymer solutions under a temperature gradient. *Chemical Engineering Science*, 59 (7) pp. 1491-1504.

Lee, S.H., Lee, J.E., Baek, W.Y. & Lim, J.O. (2004b) Regional delivery of vancomycin using pluronic F-127 to inhibit methicillin resistant Staphylococcus aureus (MRSA) growth in chronic otitis media in vitro and in vivo. *Journal of Controlled Release*, 96 (1) pp. 1-7.

Lee, T.Y., Guymon, C.A., Jönsson, E.S. & Hoyle, C.E. (2004c) The effect of monomer structure on oxygen inhibition of (meth)acrylates photopolymerization. Polymer, 45 (18) pp. 6155-6162.

Lee, F. & Kurisawa, M. (2013) Formation and stability of interpenetrating polymer network hydrogels consisting of fibrin and hyaluronic acid for tissue engineering. *Acta Biomaterialia*, 9 (2) pp. 5143-5152.

Lewandrowski, K.-U., D. Gresser, J., Wise, D.L. & Trantolo, D.J. (2000) Bioresorbable bone graft substitutes of different osteoconductivities: a histologic evaluation of osteointegration of poly(propylene glycol-co-fumaric acid)-based cement implants in rats. *Biomaterials*, 21 (8) pp. 757-764.

Li, B., Brown, K.V., Wenke, J.C. & Guelcher, S.A. (2010) Sustained release of vancomycin from polyurethane scaffolds inhibits infection of bone wounds in a rat femoral segmental defect model. *Journal of Controlled Release*, 145 (3) pp. 221-230.

Lin, C.-C. & Anseth, K. (2009) PEG Hydrogels for the Controlled Release of Biomolecules in Regenerative Medicine. *Pharmaceutical Research*, 26 (3) pp. 631-643.

Lin, H., Wagner, E.V., Swinnea, J.S., Freeman, B.D., Pas, S.J., Hill, A.J., Kalakkunnath, S. & Kalika, D.S. (2006) Transport and structural characteristics of crosslinked poly(ethylene oxide) rubbers. *Journal of Membrane Science*, 276 (1-2) pp. 145-161.

Lin, K., Chen, L., Qu, H., Lu, J. & Chang, J. (2011) Improvement of mechanical properties of macroporous β-tricalcium phosphate bioceramic scaffolds with uniform and interconnected pore structures. *Ceramics International*, 37 (7) pp. 2397-2403.

Lin, Z., Wu, W., Wang, J. & Jin, X. (2007) Studies on swelling behaviors, mechanical properties, network parameters and thermodynamic interaction of water sorption of 2-hydroxyethyl methacrylate/novolac epoxy vinyl ester resin copolymeric hydrogels. *Reactive and Functional Polymers*, 67 (9) pp. 789-797.

Lin-Gibson, S., Bencherif, S., Cooper, J.A., Wetzel, S.J., Antonucci, J.M., Vogel, B.M., Horkay, F. & Washburn, N.R. (2004) Synthesis and Characterization of PEG Dimethacrylates and Their Hydrogels. *Biomacromolecules*, 5 (4) pp. 1280-1287.

Liu, A., Hong, Z., Zhuang, X., Chen, X., Cui, Y., Liu, Y. & Jing, X. (2008) Surface modification of bioactive glass nanoparticles and the mechanical and biological properties of poly(l-lactide) composites. *Acta Biomaterialia*, 4 (4) pp. 1005-1015.

Liu, B., Kim, T.-J. & Wang, Y. (2010) Live cell imaging of mechanotransduction. *Journal of The Royal Society Interface*, 7 (Suppl 3) pp. S365-S375.

Liu, C., Xia, Z. & Czernuszka, J.T. (2007) Design and Development of Three-Dimensional Scaffolds for Tissue Engineering. *Chemical Engineering Research and Design*, 85 (7) pp. 1051-1064.

Lu, G., Kong, L., Sheng, B., Wang, G., Gong, Y. & Zhang, X. (2007) Degradation of covalently cross-linked carboxymethyl chitosan and its potential application for peripheral nerve regeneration. *European Polymer Journal*, 43 (9) pp. 3807-3818.

Ma, G., Yang, D., Li, Q., Wang, K., Chen, B., Kennedy, J.F. & Nie, J. (2010) Injectable hydrogels based on chitosan derivative/polyethylene glycol dimethacrylate/N,N-dimethylacrylamide as bone tissue engineering matrix. *Carbohydrate Polymers*, 79 (3) pp. 620-627.

Ma, R., Xiong, D., Miao, F., Zhang, J. & Peng, Y. (2009) Novel PVP/PVA hydrogels for articular cartilage replacement. *Materials Science and Engineering: C*, 29 (6) pp. 1979-1983.

Mankin, H.J., Doppelt, S. & Tomford, W. (1983) Clinical Experience with Allograft Implantation The First Ten Years. *Clinical Orthopaedics and Related Research*, 174.

Marguerite, R. (2006) Chitin and chitosan: Properties and applications. Progress in Polymer Science, 31 (7) pp. 603-632.

Martens, P., Holland, T. & Anseth, K.S. (2002) Synthesis and characterization of degradable hydrogels formed from acrylate modified poly(vinyl alcohol) macromers. *Polymer*, 43 (23) pp. 6093-6100.

Martínez-Ruvalcaba, A., Chornet, E. & Rodrigue, D. (2007) Viscoelastic properties of dispersed chitosan/xanthan hydrogels. *Carbohydrate Polymers*, 67 (4) pp. 586-595.

Martínez-Sanz, E., Ossipov, D.A., Hilborn, J., Larsson, S., Jonsson, K.B. & Varghese, O.P. (2011) Bone reservoir: Injectable hyaluronic acid hydrogel for minimal invasive bone augmentation. *Journal of Controlled Release*, 152 (2) pp. 232-240.

Mastrogiacomo, M., Papadimitropoulos, A., Cedola, A., Peyrin, F., Giannoni, P., Pearce, S.G., Alini, M., Giannini, C., Guagliardi, A. & Cancedda, R. (2007) Engineering of bone using bone marrow stromal cells and a silicon-stabilized tricalcium phosphate bioceramic: Evidence for a coupling between bone formation and scaffold resorption. *Biomaterials*, 28 (7) pp. 1376-1384.

Mc Gann, M.J., Higginbotham, C.L., Geever, L.M. & Nugent, M.J.D. (2009) The synthesis of novel pH-sensitive poly(vinyl alcohol) composite hydrogels using a freeze/thaw process for biomedical applications. *International Journal of Pharmaceutics*, 372 (1–2) pp. 154-161.

McGuire, D.A. & Hendricks, S.D. (2007) Allografts in Sports Medicine. *Operative Techniques in Sports Medicine*, 15 (2) pp. 46-52.

McNally, M. & Nagarajah, K. (2010) (iv) Osteomyelitis. *Orthopaedics and Trauma*, 24 (6) pp. 416-429.

Merrill, E.W., Dennison, K.A. & Sung, C. (1993) Partitioning and diffusion of solutes in hydrogels of poly(ethylene oxide). *Biomaterials*, 14 (15) pp. 1117-1126.

Mikos, A.G., Sarakinos, G., Lyman, M.D., Ingber, D.E., Vacanti, J.P. & Langer, R. (1993) Prevascularization of porous biodegradable polymers. *Biotechnology and Bioengineering*, 42 (6) pp. 716-723.

Mikos, A.G., Thorsen, A.J., Czerwonka, L.A., Bao, Y., Langer, R., Winslow, D.N. & Vacanti, J.P. (1994) Preparation and characterization of poly(l-lactic acid) foams. *Polymer*, 35 (5) pp. 1068-1077.

Miyai, T., Ito, A., Tamazawa, G., Matsuno, T., Sogo, Y., Nakamura, C., Yamazaki, A. & Satoh, T. (2008) Antibiotic-loaded poly-ε-caprolactone and porous β-tricalcium phosphate composite for treating osteomyelitis. *Biomaterials*, 29 (3) pp. 350-358.

Moon, J., Shul, Y., Han, H.S., Hong, S., Choi, Y. & Kim, H. (2005) A study on UV-curable adhesives for optical pick-up: I. Photo-initiator effects. *International Journal of Adhesion and Adhesives*, 25 pp. 301-312.

Morgan, S.M., Tilley, S., Perera, S., Ellis, M.J., Kanczler, J., Chaudhuri, J.B. & Oreffo, R.O.C. (2007) Expansion of human bone marrow stromal cells on poly-(dl-lactide-co-glycolide) (PDLLGA) hollow fibres designed for use in skeletal tissue engineering. *Biomaterials*, 28 (35) pp. 5332-5343.

Moskowitz, J.S., Blaisse, M.R., Samuel, R.E., Hsu, H.-P., Harris, M.B., Martin, S.D., Lee, J.C., Spector, M. & Hammond, P.T. (2010) The effectiveness of the controlled release of gentamicin from polyelectrolyte multilayers in the treatment of Staphylococcus aureus infection in a rabbit bone model. *Biomaterials*, 31 (23) pp. 6019-6030.

Mosmann, T. (1983) Rapid colorimetric assay for cellular growth and survival: Application to proliferation and cytotoxicity assays. *Journal of Immunological Methods*, 65 (1–2) pp. 55-63.

Mühlebach, A., Müller, B., Pharisa, C., Hofmann, M., Seiferling, B. & Guerry, D. (1997) New water-soluble photo crosslinkable polymers based on modified poly(vinyl alcohol). Journal of Polymer Science Part A: *Polymer Chemistry*, 35 (16) pp. 3603-3611.

Muramatsu, K., Ihara, K., Doi, K., Shigetomi, M., Hashimoto, T. & Taguchi, T. (2006) Reconstruction of massive femur defect with free vascularized fibula graft follwoing tumor resection. *Anticancer Res*, 26 (5B) pp. 3679-3683.

Murphy, C.M., Haugh, M.G. & O'Brien, F.J. (2010a) The effect of mean pore size on cell attachment, proliferation and migration in collagen–glycosaminoglycan scaffolds for bone tissue engineering. *Biomaterials*, 31 (3) pp. 461-466.

Murphy, S., Boyd, D., Moane, S. & Bennett, M. (2009) The effect of composition on ion release from Ca–Sr–Na–Zn–Si glass bone grafts. Journal of Materials Science: *Materials in Medicine*, 20 (11) pp. 2207-2214.

Murphy, S., Wren, A., Towler, M. & Boyd, D. (2010) The effect of ionic dissolution products of Ca–Sr–Na–Zn–Si bioactive glass on in vitro cytocompatibility. *Journal of Materials Science: Materials in Medicine*, 21 (10) pp. 2827-2834.

Murray, K.A., Kennedy, J.E., McEvoy, B., Vrain, O., Ryan, D., Cowman, R. & Higginbotham, C.L. (2013) Effects of gamma ray and electron beam irradiation on the mechanical, thermal, structural and physicochemical properties of poly (ether-block-amide) thermoplastic elastomers. *Journal of the Mechanical Behavior of Biomedical Materials*, 17 (0) pp. 252-268.

Murugan, R. & Ramakrishna, S. (2004) Bioresorbable composite bone paste using polysaccharide based nano hydroxyapatite. *Biomaterials*, 25 (17) pp. 3829-3835.

Murugan, R. & Ramakrishna, S. (2005) Development of nanocomposites for bone grafting. *Composites Science and Technology*, 65 (15-16) pp. 2385-2406.

Muschler, G.F. & Lane, J.M. (1992) Bone grafts and bone substitutes. *Orthopaedic Surgery*, pp. 375-407.

Neffe, A.T., Loebus, A., Zaupa, A., Stoetzel, C., Müller, F.A. & Lendlein, A. (2011) Gelatin functionalization with tyrosine derived moieties to increase the interaction with hydroxyapatite fillers. *Acta Biomaterialia*, 7 (4) pp. 1693-1701.

Nicodemus, G.D. & Bryant, S.J. (2010) Mechanical loading regimes affect the anabolic and catabolic activities by chondrocytes encapsulated in PEG hydrogels. *Osteoarthritis and Cartilage*, 18 (1) pp. 126-137.

Nilasaroya, A., Poole-Warren, L.A., Whitelock, J.M. & Jo Martens, P. (2008) Structural and functional characterisation of poly(vinyl alcohol) and heparin hydrogels. *Biomaterials*, 29 (35) pp. 4658-4664.

O'Brien, F. (2011) Biomaterials & scaffolds for tissue engineering. *Materials Today*, 14 (3) pp. 88-95.

O'Hara, R.M., Dunne, N.J., Orr, J.F., Buchanan, F.J., Wilcox, R.K. & Barton, D.C. (2010) Optimisation of the mechanical and handling properties of an injectable calcium phosphate cement. *Journal of materials science. Materials in medicine*, 21 (8) pp. 2299-2305.

O'Hara, R.M., Orr, J.F., Buchanan, F.J., Wilcox, R.K., Barton, D.C. & Dunne, N.J. (2012) Development of a bovine collagen-apatitic calcium phosphate cement for potential fracture treatment through vertebroplasty. *Acta Biomaterialia*, 8 (11) pp. 4043-52.

Obara, K., Ishihara, M., Ishizuka, T., Fujita, M., Ozeki, Y., Maehara, T., Saito, Y., Yura, H., Matsui, T., Hattori, H., Kikuchi, M. & Kurita, A. (2003) Photocrosslinkable chitosan hydrogel containing fibroblast growth factor-2 stimulates wound healing in healing-impaired db/db mice. *Biomaterials*, 24 (20) pp. 3437-3444.

Oh, S.H., Kang, S.G., Kim, E.S., Cho, S.H. & Lee, J.H. (2003) Fabrication and characterization of hydrophilic poly(lactic-co-glycolic acid)/poly(vinyl alcohol) blend cell scaffolds by melt-molding particulate-leaching method. *Biomaterials*, 24 (22) pp. 4011-4021.

Oyen, M.L. (2008) The materials science of bone: lessons from nature for biomimetic materials synthesis. MRS Bulletin (Materials Research Society), 33 (1) pp. 49-55.

Panda, A., Manohar, S.B., Sabharwal, S., Bhardwaj, Y.K. & Majali, A.B. (2000) Synthesis and swelling characteristics of poly (N-isopropylacrylamide) temperature sensitive hydrogels crosslinked by electron beam irradiation. *Radiation Physics and Chemistry*, 58 (1) pp. 101-110.

Park, J.B. (2009) The use of hydrogels in bone tissue engineering. *Biomaterials and Bioengineering in Dentistry*, vol.16, pp. 115-118.

Paul, M., Park, H.B., Freeman, B.D., Roy, A., Mcgrath, J.E. & Riffle, J.S. (2008) Synthesis and crosslinking of partially disulfonated poly(arylene

ether sulfone) random copolymers as candidates for chlorine resistant reverse osmosis membranes. *Polymer*, 49 (9) pp. 2243-2252.

Peppas, N.A. & Khare, A.R. (1993) Preparation, structure and diffusional behavior of hydrogels in controlled release. *Advanced Drug Delivery Reviews*, 11 (1-2) pp. 1-35.

Peppas, N.A. & Merrill, E.W. (1976) Poly(vinyl alcohol) hydrogels: Reinforcement of radiation-crosslinked networks by crystallization. Journal of Polymer Science: *Polymer Chemistry Edition*, 14 (2) pp. 441-457.

Perrie, Y., Badhan, R.K.S., Kirby, D.J., Lowry, D., Mohammed, A.R. & Ouyang, D. (2012) The impact of ageing on the barriers to drug delivery. *Journal of Controlled Release*, 161 (2) pp. 389-398.

Peter, M., Binulal, N.S., Soumya, S., Nair, S.V., Furuike, T., Tamura, H. & Jayakumar, R. (2010) Nanocomposite scaffolds of bioactive glass ceramic nanoparticles disseminated chitosan matrix for tissue engineering applications. *Carbohydrate Polymers*, 79 (2) pp. 284-289.

Place, E.S., George, J.H., Williams, C.K. & Stevens, M.M. (2009) Synthetic polymer scaffolds for tissue engineering. Chemical Society Reviews, 38 (4) pp. 1139-1151.

Puppi, D., Chiellini, F., Piras, A.M. & Chiellini, E. (2010) Polymeric materials for bone and cartilage repair. *Progress in Polymer Science*, 35 (4) pp. 403-440.

Puértolas, J.A., Vadillo, J.L., Sánchez-Salcedo, S., Nieto, A., Gómez-Barrena, E. & Vallet-Regí, M. (2011) Compression behaviour of biphasic calcium phosphate and biphasic calcium phosphate–agarose scaffolds for bone regeneration. *Acta Biomaterialia*, 7 (2) pp. 841-847.

Rahaman, M.N., Day, D.E., Sonny Bal, B., Fu, Q., Jung, S.B., Bonewald, L.F. & Tomsia, A.P. (2011) Bioactive glass in tissue engineering. *Acta Biomaterialia*, 7 (6) pp. 2355-2373.

Rapacz-Kmita, A., Paluszkiewicz, C., Ślósarczyk, A. & Paszkiewicz, Z. (2005) FTIR and XRD investigations on the thermal stability of hydroxyapatite during hot pressing and pressureless sintering processes. *Journal of Molecular Structure*, 744–747 (0) pp. 653-656.

Ratanavaraporn, J., Furuya, H., Kohara, H. & Tabata, Y. (2011) Synergistic effects of the dual release of stromal cell-derived factor-1 and bone morphogenetic protein-2 from hydrogels on bone regeneration. *Biomaterials*, 32 (11) pp. 2797-2811.

Ratner, B.D., Hoffman, A.S., Schoen, F.J. & Lemons, J.E. (2002) Biomaterials Science - An Introduction to Materials in Medicine (2nd Edition): Elsevier.

Raucci, M.G., Guarino, V. & Ambrosio, L. (2010) Hybrid composite scaffolds prepared by sol–gel method for bone regeneration. *Composites Science and Technology*, 70 (13) pp. 1861-1868.

Ravarian, R., Moztarzadeh, F., Hashjin, M.S., Rabiee, S.M., Khoshakhlagh, P. & Tahriri, M. (2010) Synthesis, characterization and bioactivity investigation of bioglass/hydroxyapatite composite. *Ceramics International*, 36 (1) pp. 291-297.

Rezwan, K., Chen, Q.Z., Blaker, J.J. & Boccaccini, A.R. (2006) Biodegradable and bioactive porous polymer/inorganic composite scaffolds for bone tissue engineering. *Biomaterials*, 27 (18) pp. 3413-3431.

Robert P, H. (1991) Effect of calcium on skeletal development, bone loss, and risk of fractures. *The American Journal of Medicine*, 91 (5, Supplement 2) pp. S23-S28.

Roberts, J.J., Earnshaw, A., Ferguson, V.L. & Bryant, S.J. (2011) Comparative study of the viscoelastic mechanical behavior of agarose and poly(ethylene glycol) hydrogels. *Journal of Biomedical Materials Research Part B: Applied Biomaterials*, 99B (1) pp. 158-169.

Saboori, A., Rabiee, M., Moztarzadeh, F., Sheikhi, M., Tahriri, M. & Karimi, M. (2009) Synthesis, characterization and in vitro bioactivity of sol-gel-derived SiO_2–CaO–P_2O_5–MgO bioglass. *Materials Science and Engineering: C*, 29 (1) pp. 335-340.

Sagle, A.C., Ju, H., Freeman, B.D. & Sharma, M.M. (2009) PEG-based hydrogel membrane coatings. *Polymer*, 50 (3) pp. 756-766.

Sahoo, S., Sasmal, A., Nanda, R., Phani, A.R. & Nayak, P.L. (2010) Synthesis of chitosan-polycaprolactone blend for control delivery of ofloxacin drug. *Carbohydrate Polymers*, 79 (1) pp. 106-113.

Salerno, A., Zeppetelli, S., Di Maio, E., Iannace, S. & Netti, P.A. (2012) Architecture and properties of bi-modal porous scaffolds for bone regeneration prepared via supercritical CO_2 foaming and porogen leaching combined process. *The Journal of Supercritical Fluids*, 67 (0) pp. 114-122.

Salerno, A., Zeppetelli, S., Maio, E.D., Iannace, S. & Netti, P.A. (2010) Novel 3D porous multi-phase composite scaffolds based on PCL, thermoplastic zein and ha prepared via supercritical CO_2 foaming for bone regeneration. *Composites Science and Technology*, 70 (13) pp. 1838-1846.

Santos, M.I., Fuchs, S., Gomes, M.E., Unger, R.E., Reis, R.L. & Kirkpatrick, C.J. (2007) Response of micro- and macrovascular endothelial cells to starch-based fiber meshes for bone tissue engineering. *Biomaterials*, 28 (2) pp. 240-248.

Schmitz, J.P. & Hollinger, J.O. (1986) The crictical size defect as an experimental model for craniomandibulofacial nonunions. *Clin Orthop*, 205 pp. 299-308.

Schoenfeld, C., Lautenschlager, E. & Meyer, P. (1974) Mechanical properties of human cancellous bone in the femoral head. *Medical and Biological Engineering and Computing*, 12 (3) pp. 313-317.

Seeherman, H. & Wozney, J.M. (2005) Delivery of bone morphogenetic proteins for orthopedic tissue regeneration. *Cytokine and Growth Factor Reviews*, 16 (3) pp. 329-345.

Shen, J., Li, Y., Zuo, Y., Zou, Q., Cheng, L., Zhang, L., Gong, M. & Gao, S. (2010) Characterization and cytocompatibility of biphasic calcium phosphate/polyamide 6 scaffolds for bone regeneration. *Journal of Biomedical Materials Research Part B: Applied Biomaterials*, 95B (2) pp. 330-338.

Silva, G.A., Coutinho, O.P., Ducheyne, P., Shapiro, I.M. & Reis, R.L. (2007) The effect of starch and starch-bioactive glass composite microparticles on the adhesion and expression of the osteoblastic phenotype of a bone cell line. *Biomaterials*, 28 (2) pp. 326-334.

Slaughter, B.V., Khurshid, S.S., Fisher, O.Z., Khademhosseini, A. & Peppas, N.A. (2009) Hydrogels in Regenerative Medicine. *Advanced Materials*, 21 (32-33) pp. 3307-3329.

Smith, T.J., Kennedy, J.E. & Higginbotham, C.L. (2009) The rheological and thermal characteristics of freeze-thawed hydrogels containing hydrogen peroxide for potential wound healing applications. *Journal of the Mechanical Behavior of Biomedical Materials*, 2 (3) pp. 264-271.

Sowmya, S., Sudheesh Kumar, P.T., Chennazhi, K.P., Nair, S.V., Tamura, H. & Rangasamy, J. (2011) Biocompatible β-chitin Hydrogel/Nanobioactive Glass Ceramic Nanocomposite Scaffolds for Periodontal Bone Regeneration. *Trends in Biomaterials and Artificial Organs*, 25 pp. 1-11.

Studer, K., Decker, C., Beck, E. & Schwalm, R. (2003a) Overcoming oxygen inhibition in UV-curing of acrylate coatings by carbon dioxide inerting, Part I. *Progress in Organic Coatings*, 48 (1) pp. 92-100.

Studer, K., Decker, C., Beck, E. & Schwalm, R. (2003b) Overcoming oxygen inhibition in UV-curing of acrylate coatings by carbon dioxide inerting: Part II. *Progress in Organic Coatings*, 48 (1) pp. 101-111.

Subia, B., Kundu, J. & Kundu, S. (2010). Biomaterial Scaffold Fabrication Techniques for Potential Tissue Engineering Applications. In D. Eberli (Ed.), *Tissue Engineering*.

Sullivan, F.A. (2011) European Orthopaedic Devices Market Outlook.

Sun, F., Zhou, H. & Lee, J. (2011) Various preparation methods of highly porous hydroxyapatite/polymer nanoscale biocomposites for bone regeneration. *Acta Biomaterialia*, 7 (11) pp. 3813-3828.

Tierney, E.G., Duffy, G.P., Hibbitts, A.J., Cryan, S.-A. & O'Brien, F.J. (2012) The development of non-viral gene-activated matrices for bone

regeneration using polyethyleneimine (PEI) and collagen-based scaffolds. *Journal of Controlled Release*, 158 (2) pp. 304-311.

Tomić, S.L.J., Mićić, M.M., Filipović, J.M. & Suljovrujić, E.H. (2010) Synthesis, characterization and controlled release of cephalexin drug from smart poly(2-hydroxyethyl methacrylate/poly(alkylene glycol)(meth)acrylates hydrogels. *Chemical Engineering Journal*, 160 (2) pp. 801-809.

Tzioupis, C. & Giannoudis, P.V. (2007) Prevalence of long-bone non-unions. *Injury*, 38, Supplement 2 (0) pp. S3-S9.

Ulici, V., Hoenselaar, K.D., Agoston, H., Mcerlain, D.D., Umoh, J., Chakrabarti, S., Holdsworth, D.W. & Beier, F. (2009) The role of Akt1 in terminal stages of endochondral bone formation: Angiogenesis and ossification. *Bone*, 45 (6) pp. 1133-1145.

Vacanti, J.P., Morse, M.A., Saltzman, W.M., Domb, A.J., Perez-Atayde, A. & Langer, R. (1988) Selective cell transplantation using bioabsorbable artificial polymers as matrices. *Journal of Pediatric Surgery*, 23 (1) pp. 3-9.

Vallet-Regí, M., Balas, F., Colilla, M. & Manzano, M. (2008) Bone-regenerative bioceramic implants with drug and protein controlled delivery capability. *Progress in Solid State Chemistry*, 36 (3) pp. 163-191.

Vallés Lluch, A., Gallego Ferrer, G. & Monleón Pradas, M. (2009) Biomimetic apatite coating on P(EMA-co-HEA)/SiO2 hybrid nanocomposites. *Polymer*, 50 (13) pp. 2874-2884.

Vaz, C.M., Van Tuijl, S., Bouten, C.V.C. & Baaijens, F.P.T. (2005) Design of scaffolds for blood vessel tissue engineering using a multi-layering electrospinning technique. *Acta Biomaterialia*, 1 (5) pp. 575-582.

Veríssimo, D.M., Leitão, R.F.C., Ribeiro, R.A., Figueiró, S.D., Sombra, A.S.B., Góes, J.C. & Brito, G.A.C. (2010) Polyanionic collagen membranes for guided tissue regeneration: Effect of progressive glutaraldehyde cross-linking on biocompatibility and degradation. *Acta Biomaterialia*, 6 (10) pp. 4011-4018.

Vivanco, J., Aiyangar, A., Araneda, A. & Ploeg, H.-L. (2012) Mechanical characterization of injection-molded macro porous bioceramic bone scaffolds. *Journal of the Mechanical Behavior of Biomedical Materials*, 9 (0) pp. 137-152.

Vo, T.N., Kasper, F.K. & Mikos, A.G. (2012) Strategies for controlled delivery of growth factors and cells for bone regeneration. *Advanced Drug Delivery Reviews*, 64 (12) pp. 1292-1309.

Von Arx, T., Broggini, N., Jensen, S., Bornstein, M., Schenk, R. & Buser, D. (2005) Membrane Durability abd Tissue Response of different Bioresorable Barrier Membranes: A Histologic Study in the Rabbit Calvarium. *International Journal of Oral and Maxillofacial Implants*, 20 (6) pp. 843-853.

Wang, C., Xue, Y., Lin, K., Lu, J., Chang, J. & Sun, J. (2012) The enhancement of bone regeneration by a combination of osteoconductivity and osteostimulation using β-CaSiO3/β-Ca3(PO4)2 composite bioceramics. *Acta Biomaterialia*, 8 (1) pp. 350-360.

Wang, L. & Stegemann, J.P. (2010) Thermogelling chitosan and collagen composite hydrogels initiated with β-glycerophosphate for bone tissue engineering. *Biomaterials*, 31 (14) pp. 3976-3985.

Wichterle, O. & Lim, D. (1960) Hydrophilic Gels for Biological Use. *Nature*, 185 (4706) pp. 117-118.

Williams, D.F. (1987) Definitions in biomaterials. Amsterdam: Elsevier

Williams, J.M., Adewunmi, A., Schek, R.M., Flanagan, C.L., Krebsbach, P.H., Feinberg, S.E., Hollister, S.J. & Das, S. (2005) Bone tissue engineering using polycaprolactone scaffolds fabricated via selective laser sintering. *Biomaterials*, 26 (23) pp. 4817-4827.

Wu, C., Fan, W., Zhu, Y., Gelinsky, M., Chang, J., Cuniberti, G., Albrecht, V., Friis, T. & Xiao, Y. (2011a) Multifunctional magnetic mesoporous bioactive glass scaffolds with a hierarchical pore structure. *Acta Biomaterialia*, 7 (10) pp. 3563-3572.

Wu, C. & Xiao, Y. (2009) Evaluation of the In Vitro Bioactivity of Bioceramics. *Bone and Tissue Regeneration Insights*, 2 pp. 25-29.

Wu, C., Zhu, Y., Chang, J., Zhang, Y. & Xiao, Y. (2010a) Bioactive inorganic-materials/alginate composite microspheres with controllable drug-delivery ability. *Journal of Biomedical Materials Research Part B: Applied Biomaterials*, 94B (1) pp. 32-43.

Wu, W., Liu, J., Cao, S., Tan, H., Li, J., Xu, F. & Zhang, X. (2011b) Drug release behaviors of a pH sensitive semi-interpenetrating polymer network hydrogel composed of poly(vinyl alcohol) and star poly[2-(dimethylamino)ethyl methacrylate]. *International Journal of Pharmaceutics*, 416 (1) pp. 104-109.

Wu, X. (1996) Controlled drug delivery systems. Pa: Technomic Publishing

Wu, X., Liu, Y., Li, X., Wen, P., Zhang, Y., Long, Y., Wang, X., Guo, Y., Xing, F. & Gao, J. (2010b) Preparation of aligned porous gelatin scaffolds by unidirectional freeze-drying method. *Acta Biomaterialia*, 6 (3) pp. 1167-1177.

Wu, Y.-H., Park, H.B., Kai, T., Freeman, B.D. & Kalika, D.S. (2010c) Water uptake, transport and structure characterization in poly(ethylene glycol) diacrylate hydrogels. *Journal of Membrane Science*, 347 (1-2) pp. 197-208.

Xia, W. & Chang, J. (2010) Bioactive glass scaffold with similar structure and mechanical properties of cancellous bone. *Journal of Biomedical Materials Research Part B: Applied Biomaterials*, 95B (2) pp. 449-455.

Xianmiao, C., Yubao, L., Yi, Z., Li, Z., Jidong, L. & Huanan, W. (2009) Properties and in vitro biological evaluation of nano-hydroxyapatite/chitosan membranes for bone guided regeneration. *Materials Science and Engineering: C*, 29 (1) pp. 29-35.

Xu, C.Y., Inai, R., Kotaki, M. & Ramakrishna, S. (2004) Aligned biodegradable nanofibrous structure: a potential scaffold for blood vessel engineering. *Biomaterials*, 25 (5) pp. 877-886.

Yang, D., Li, Y. & Nie, J. (2007) Preparation of gelatin/PVA nanofibers and their potential application in controlled release of drugs. *Carbohydrate Polymers*, 69 (3) pp. 538-543.

Yang, X., Yang, K., Wu, S., Chen, X., Yu, F., Li, J., Ma, M. & Zhu, Z. (2010) Cytotoxicity and wound healing properties of PVA/ws-chitosan/glycerol hydrogels made by irradiation followed by freeze–thawing. *Radiation Physics and Chemistry*, 79 (5) pp. 606-611.

Yasmin, M., Gupta, M. & Shukla, J.P. (2011) Molecular interactions and structural effects on mixing pentanol in polyethylene glycol diacrylate and polyethylene glycol dimethacrylate. *Journal of Molecular Liquids*, 164 (3) pp. 212-217.

Yoshikawa, T., Noshi, T., Mitsuno, H., Hattori, K., Ichijima, K., Takakura, Y. (2001) Bone and soft tissue regeneration by bone marrow mesenchymal cells, *Materials science and engineering*, vol.17, pp.19-26

Yu, L.M.Y., Kazazian, K. & Shoichet, M.S. (2007) Peptide surface modification of methacrylamide chitosan for neural tissue engineering applications. *Journal of Biomedical Materials Research Part A*, 82A (1) pp. 243-255.

Yuan, J., Cui, L., Zhang, W.J., Liu, W. & Cao, Y. (2007) Repair of canine mandibular bone defects with bone marrow stromal cells and porous β-tricalcium phosphate. *Biomaterials*, 28 (6) pp. 1005-1013.

Yunos, M., Bretcanu, D., & Boccaccini, A. (2008) Polymer-bioceramic composites for tissue engineering scaffolds. *Journal of Materials Science*, 43 (13) pp. 4433-4442.

Zanchetta, P., Lagarde, N., Uguen, A. & Marcorelles, P. (2012) Mixture of hyaluronic acid, chondroitin-6-sulphate and dermatan sulphate used to completely regenerate bone in rat critical size defect model. *Journal of Cranio-Maxillofacial Surgery*, 40 (8) pp. 783-787.

Zeng, R., Tu, M., Liu, H., Zhao, J., Zha, Z. & Zhou, C. (2009) Preparation, structure, drug release and bioinspired mineralization of chitosan-based nanocomplexes for bone tissue engineering. *Carbohydrate Polymers*, 78 (1) pp. 107-111.

Zhai, W., Lu, H., Chen, L., Lin, X., Huang, Y., Dai, K., Naoki, K., Chen, G. & Chang, J. (2012) Silicate bioceramics induce angiogenesis during bone regeneration. *Acta Biomaterialia*, 8 (1) pp. 341-349.

Zhang, K., Simon, C.J., Washburn, N., Antonucci, J. & Lin-Gibson, S. (2005) In situ formation of blends by photopolymerization of poly(ethylene glycol) dimethacrylate and polylactide. *Biomacromolecules*, 6 pp. 1615-1622.

Zhang, L.F., Sun, R., Xu, L., Du, J., Xiong, Z.C., Chen, H.C. & Xiong, C.D. (2008) Hydrophilic poly (ethylene glycol) coating on PDLLA/BCP bone scaffold for drug delivery and cell culture. *Materials Science and Engineering: C*, 28 (1) pp. 141-149.

Zhang, W., Zhang, Z. & Wang, X. (2009) Investigation on surface molecular conformations and pervaporation performance of the poly(vinyl alcohol) (PVA) membrane. *Journal of Colloid and Interface Science*, 333 (1) pp. 346-353.

Zhao, L., Mitomo, H., Zhai, M., Yoshii, F., Nagasawa, N. & Kume, T. (2003) Synthesis of antibacterial PVA/CM-chitosan blend hydrogels with electron beam irradiation. *Carbohydrate Polymers*, 53 (4) pp. 439-446.

Zhong, C., Wu, J., Reinhart-King, C.A. & Chu, C.C. (2010) Synthesis, characterization and cytotoxicity of photo-crosslinked maleic chitosan–polyethylene glycol diacrylate hybrid hydrogels. *Acta Biomaterialia*, 6 (10) pp. 3908-3918.

Zhou, Z., Yang, D., Nie, J., Ren, Y. & Cui, F. (2009) Injectable Poly(ethylene glycol) Dimethacrylate-based Hydrogels with Hydroxyapatite. *Journal of Bioactive and Compatible Polymers*, 24 (5) pp. 405-423.

Zhu, J. (2010) Bioactive modification of poly(ethylene glycol) hydrogels for tissue engineering. *Biomaterials*, 31 (17) pp. 4639-4656.

Appendices

Appendix A

ATR-FTIR of hydrogels and hydrogel based composites

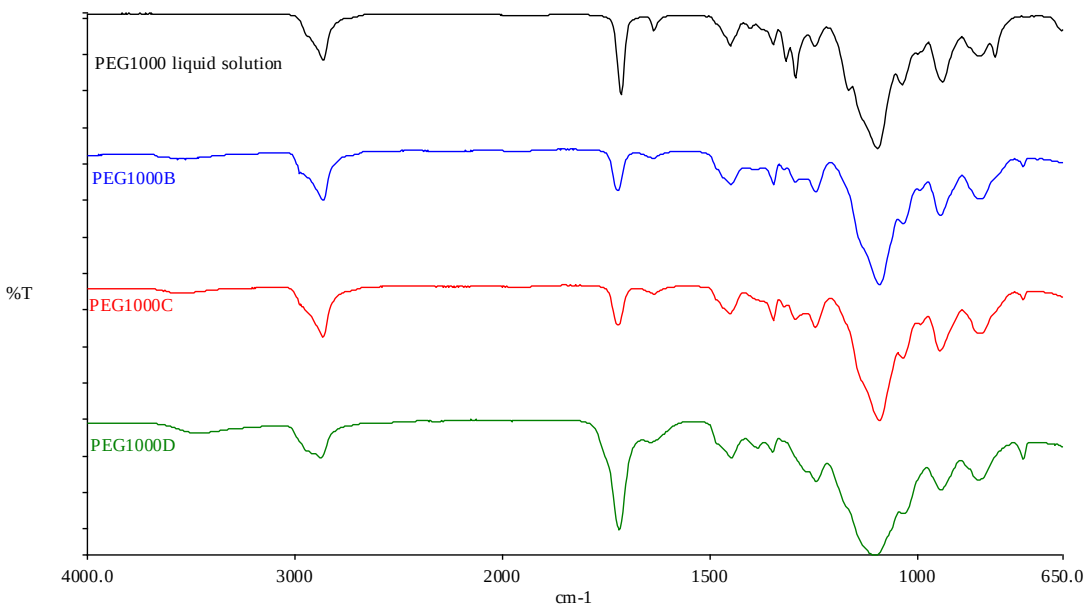

FTIR spectrum of PEG1000 hydrogels

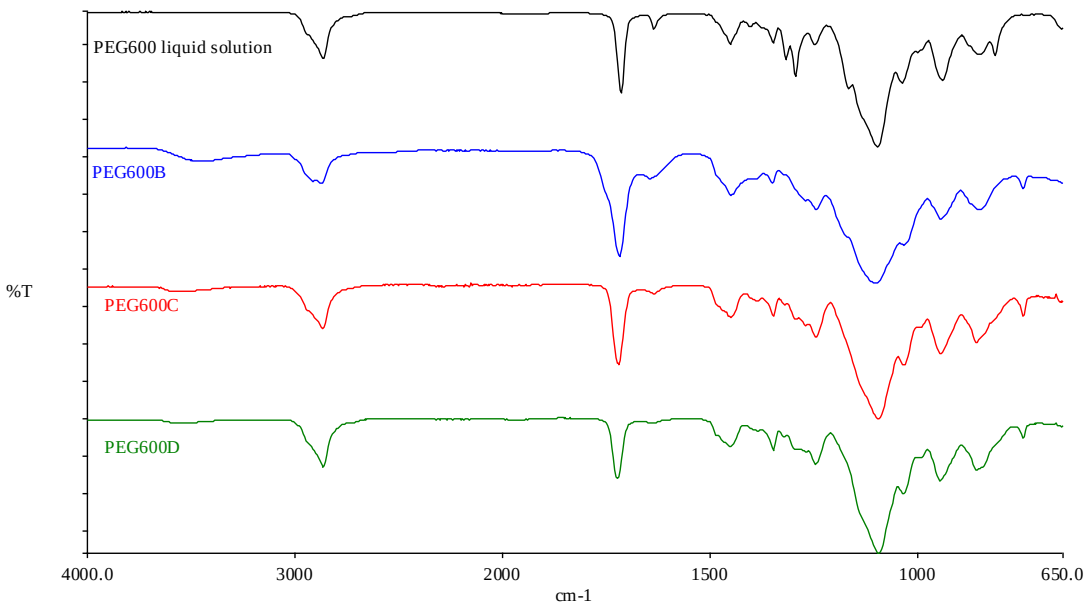

FTIR spectrum of PEG600 hydrogels

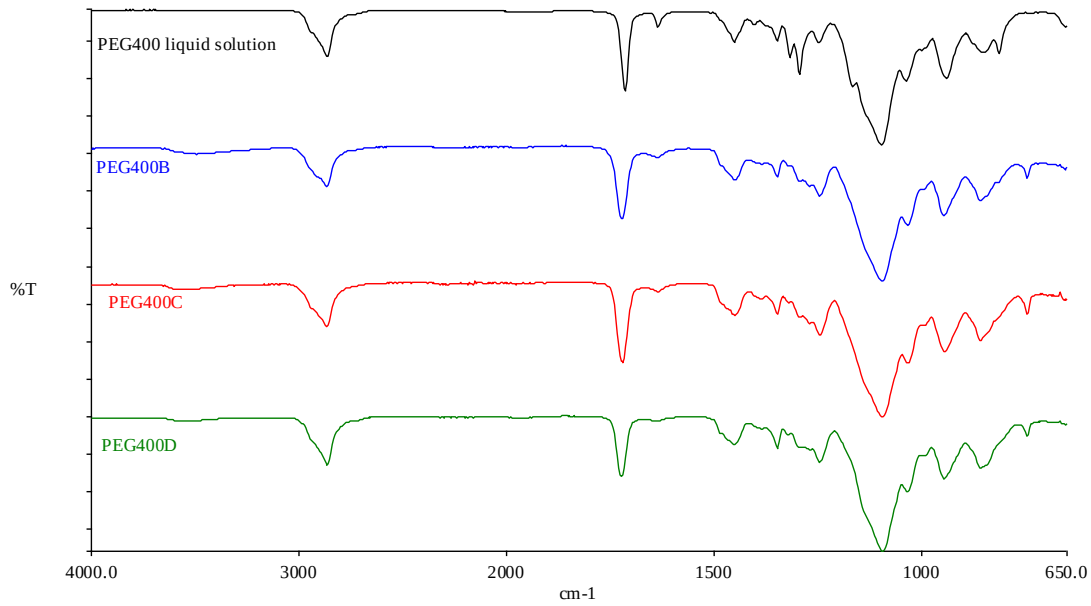

FTIR spectrum of PEG400 hydrogels

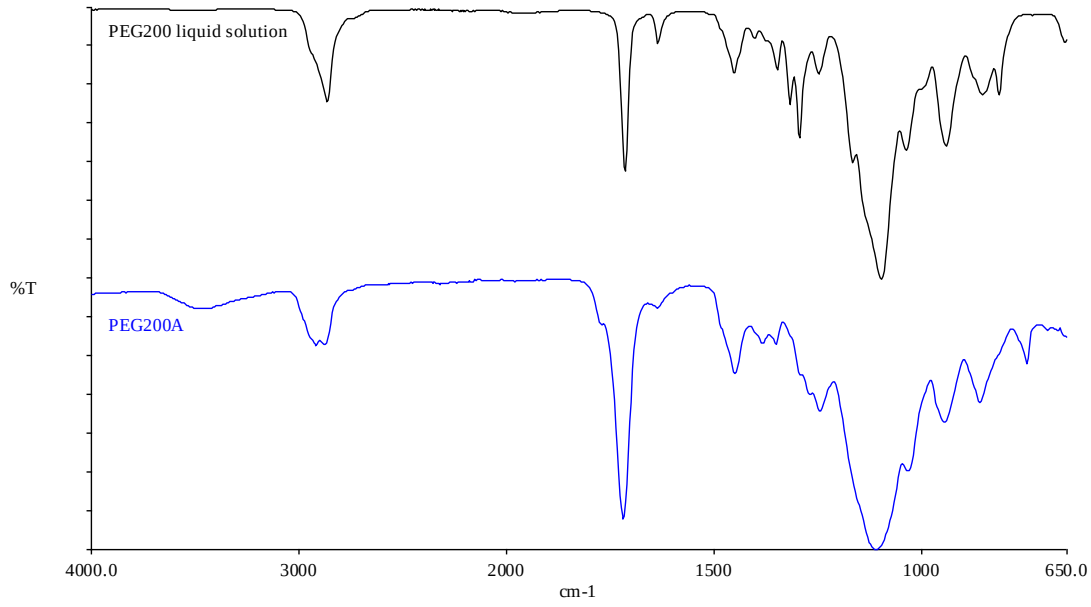

FTIR spectrum of PEG200 hydrogels

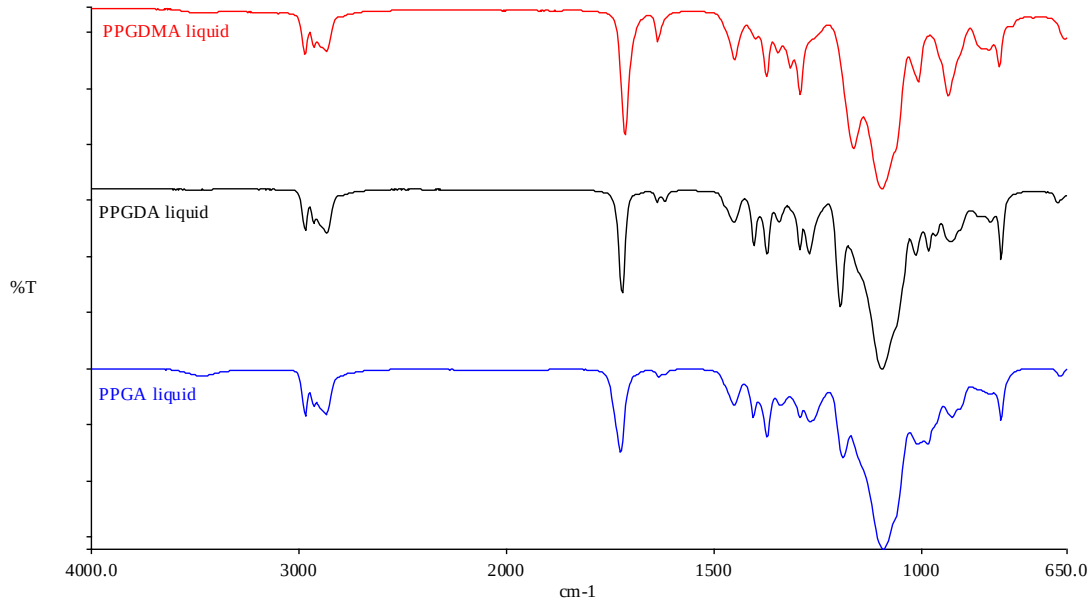

FTIR spectrum of polypropylene glycol DMA, DA and A liquid solutions

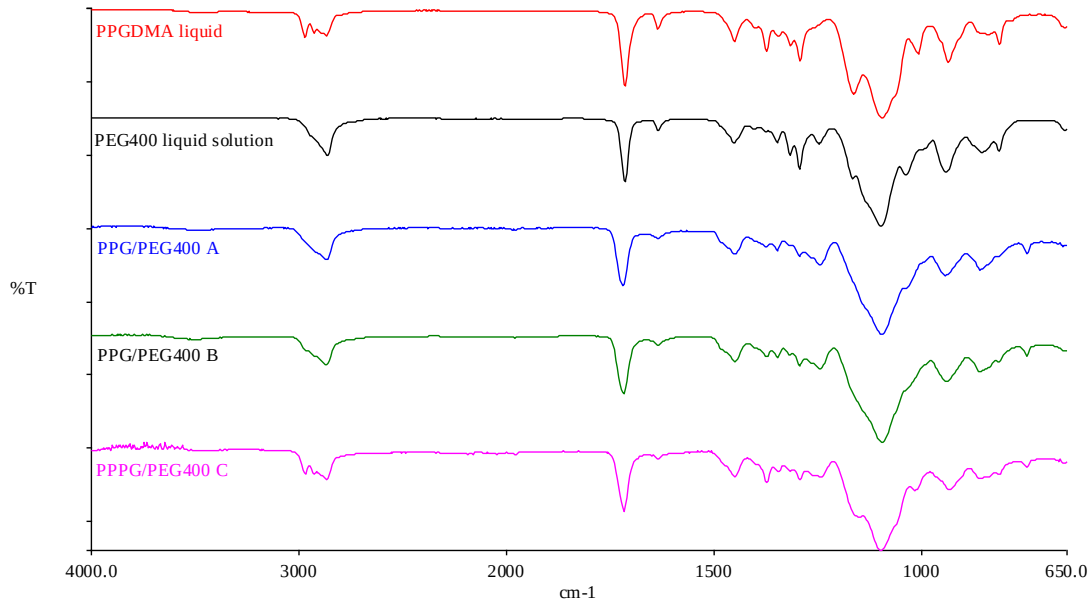

FTIR spectrum of polypropylene glycol and polyethylene glycol 400 based hydrogels

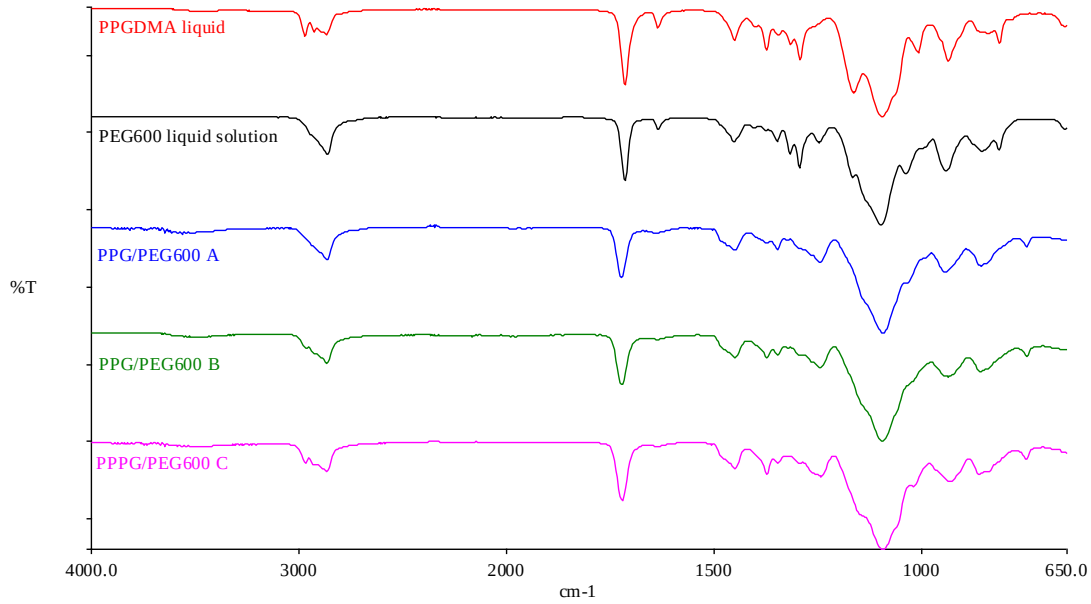

FTIR spectrum of polypropylene glycol and polyethylene glycol 600 based hydrogels

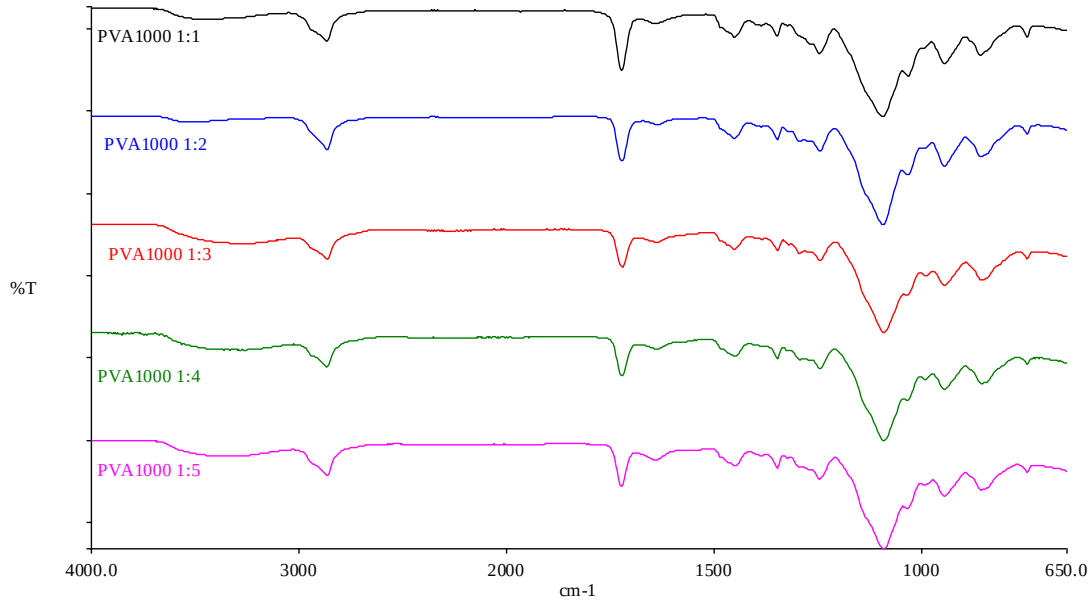

FTIR spectrum of PEG1000 maleic PVA based hydrogels

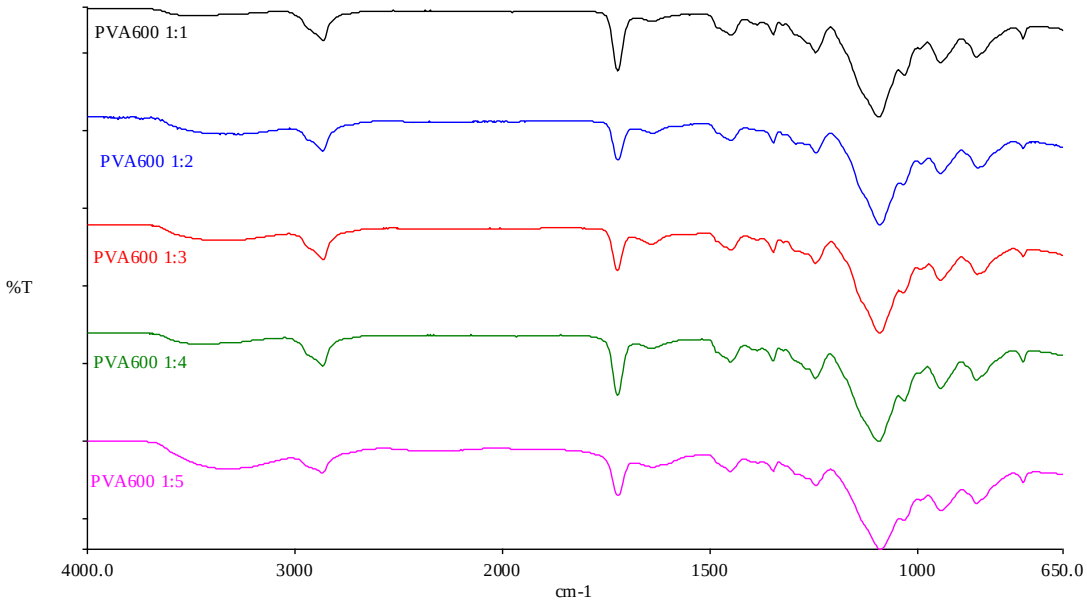

FTIR spectrum of PEG600 maleic PVA based hydrogels

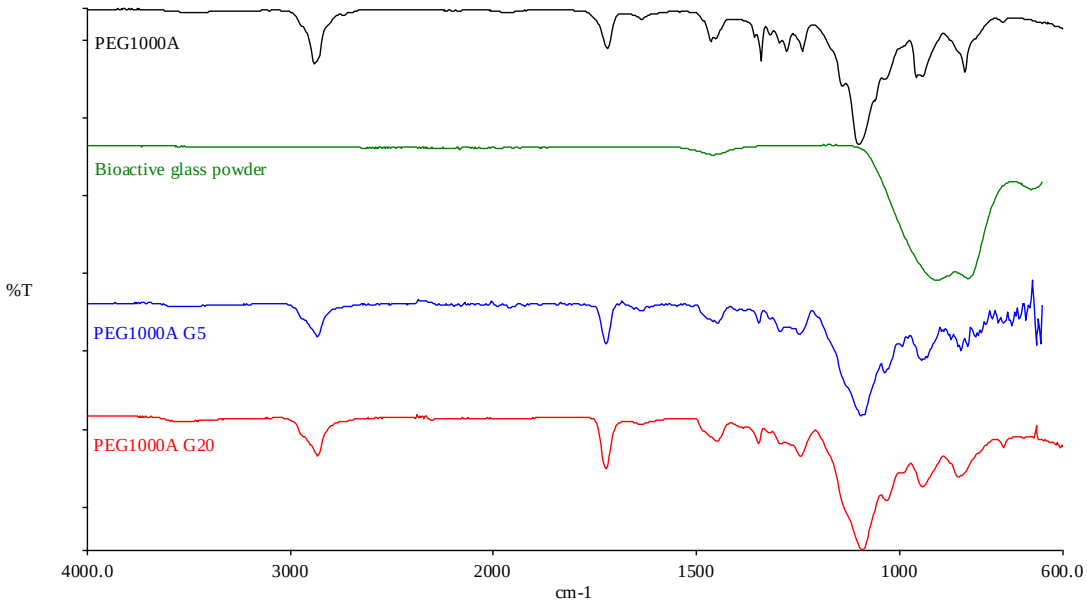

FTIR spectrum of PEG1000A bioactive glass hydrogel based composites

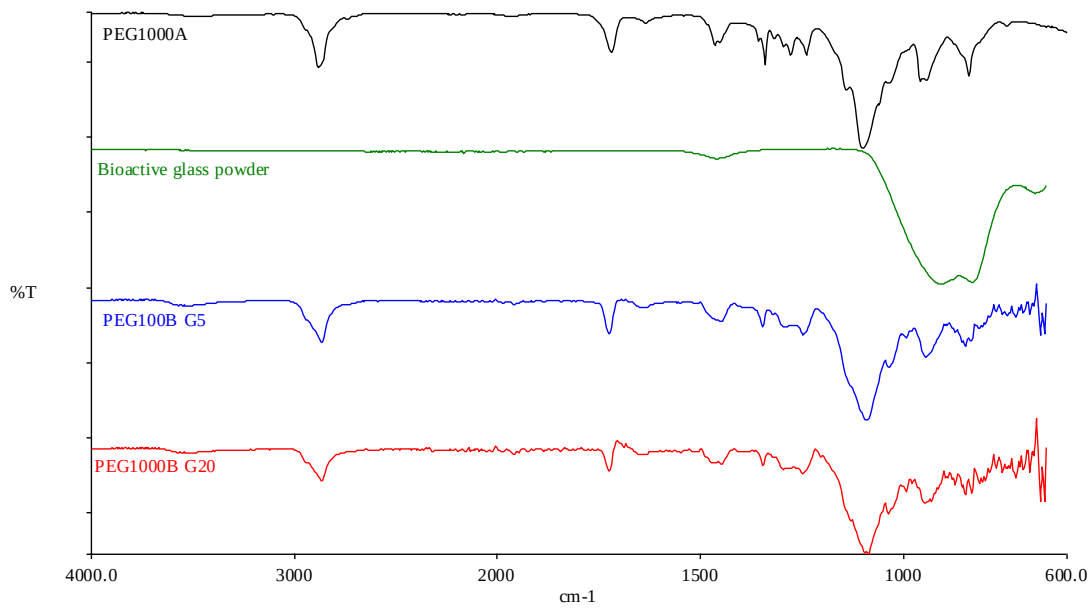

FTIR spectrum of PEG1000B bioactive glass hydrogel based composites

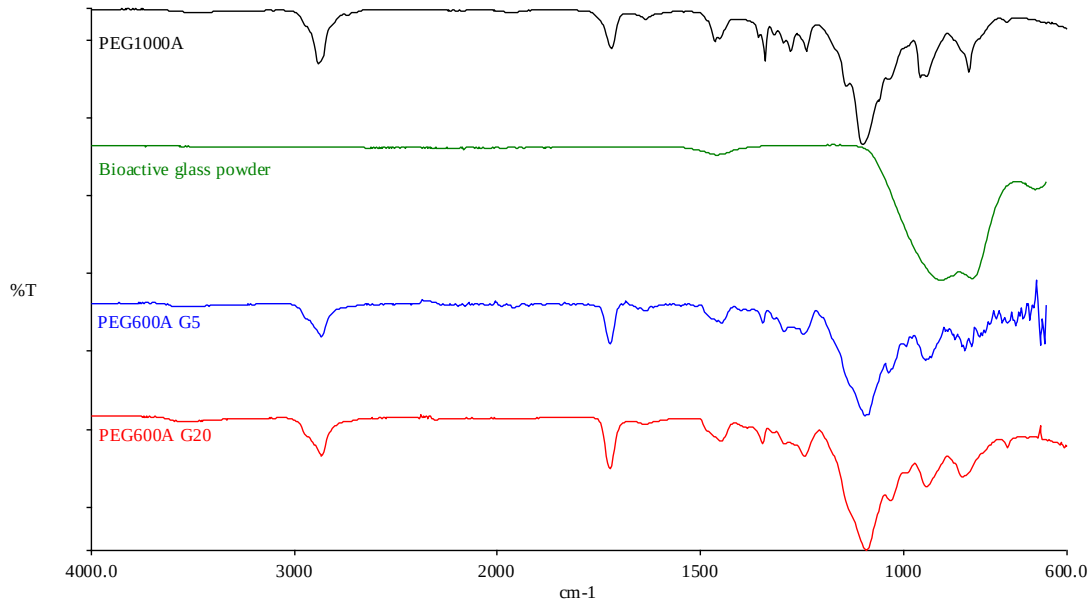

FTIR spectrum of PEG600A bioactive glass hydrogel based composites

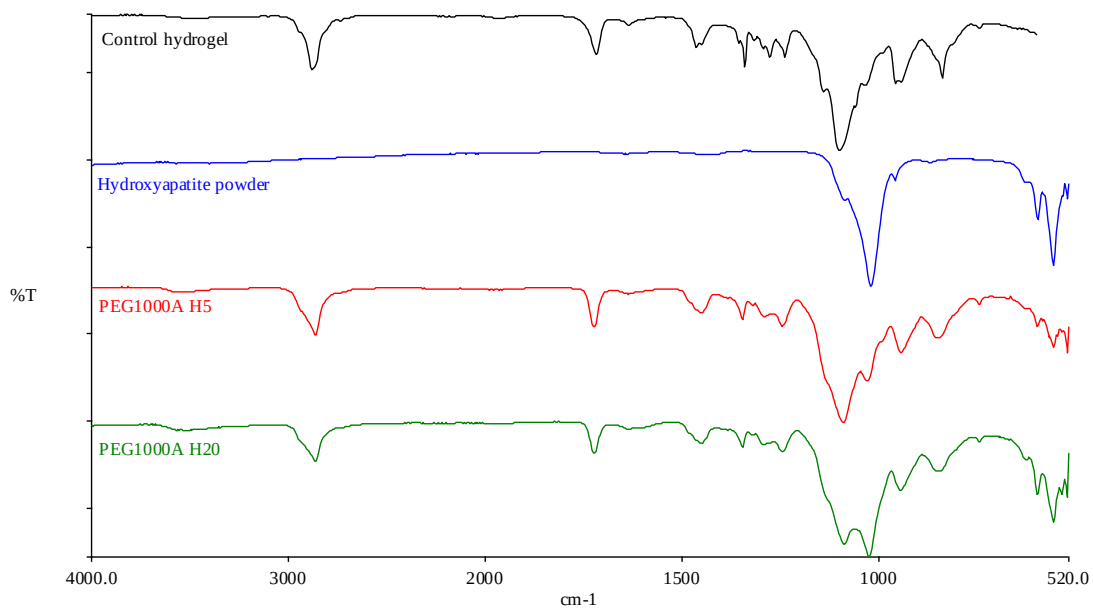

FTIR spectrum of PEG1000A hydroxyapatite hydrogel based composites

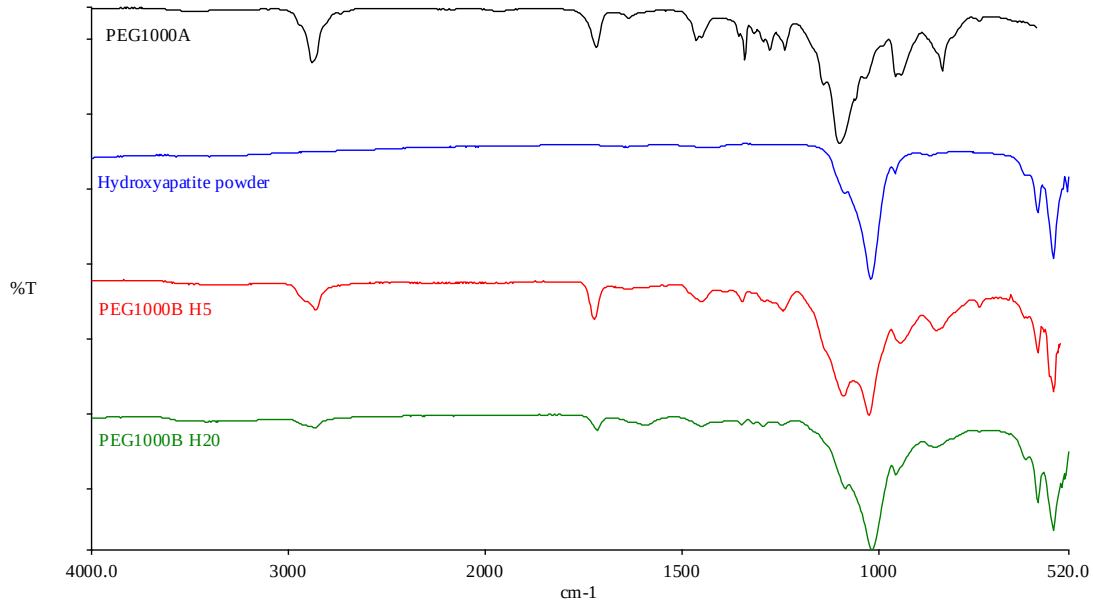

FTIR spectrum of PEG1000B hydroxyapatite hydrogel based composites

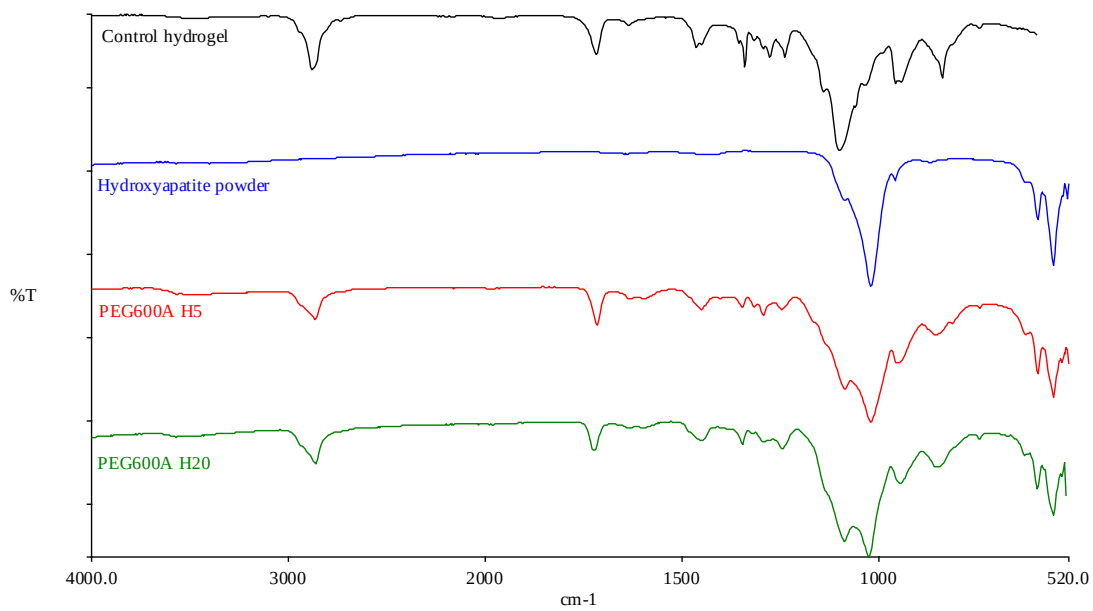

FTIR spectrum of PEG600A hydroxyapatite hydrogel based composites

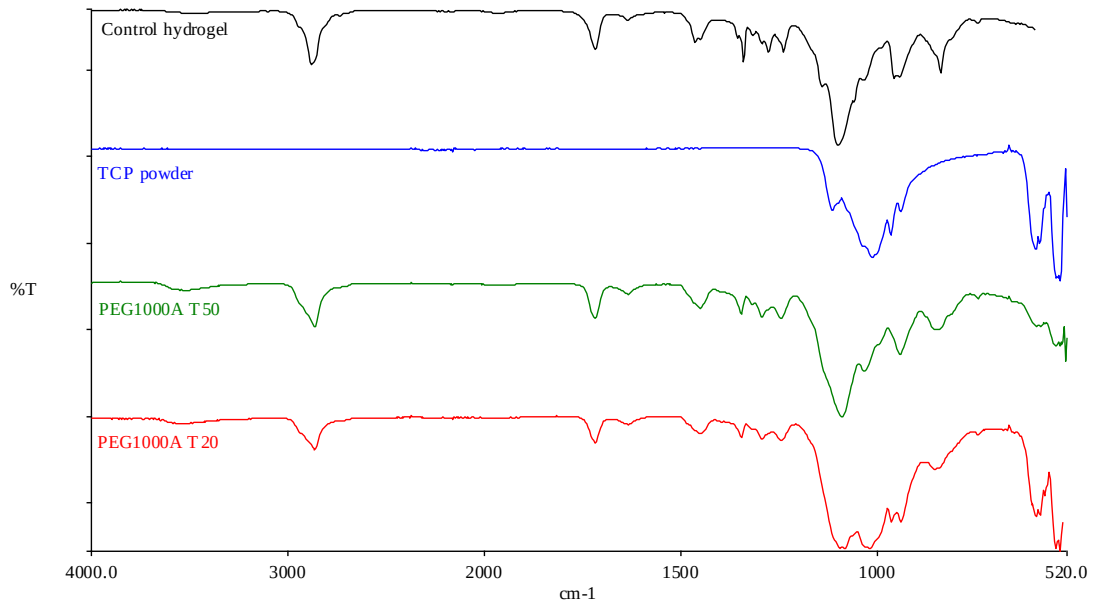

FTIR spectrum of PEG1000A tricalcium phosphate hydrogel based composites

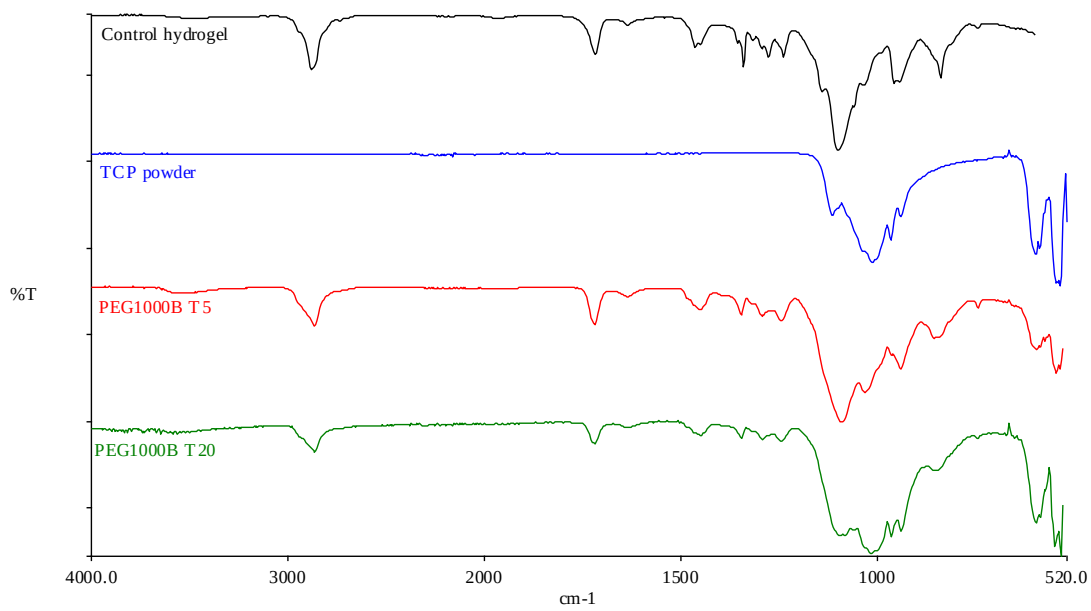

FTIR spectrum of PEG100BA tricalcium phosphate hydrogel based composites

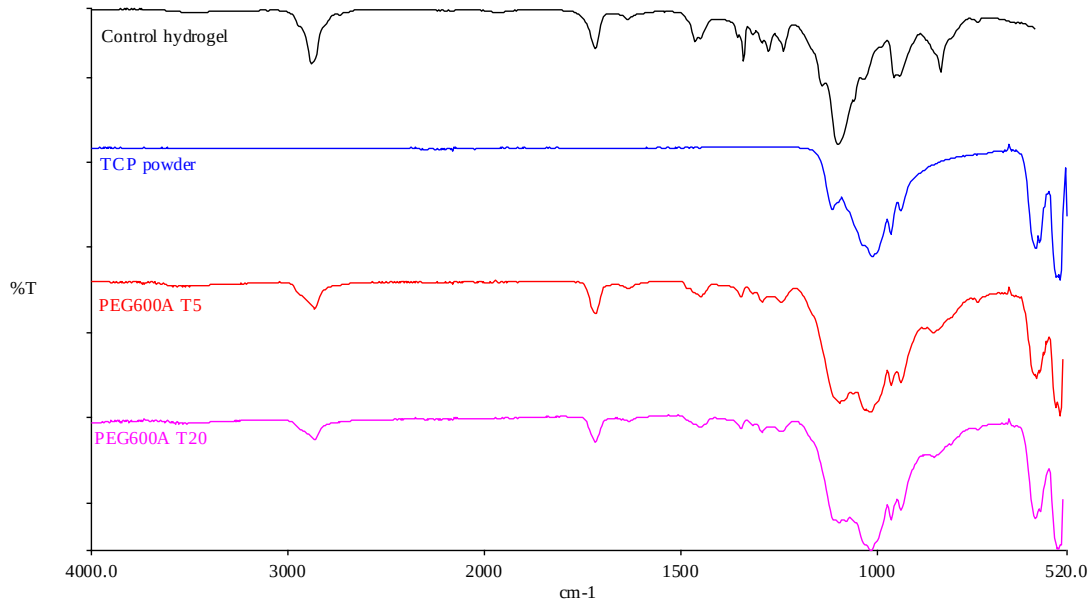

FTIR spectrum of PEG600A tricalcium phosphate hydrogel based composites

Appendix B

Swelling studies data for hydrogels and hydrogel based composites

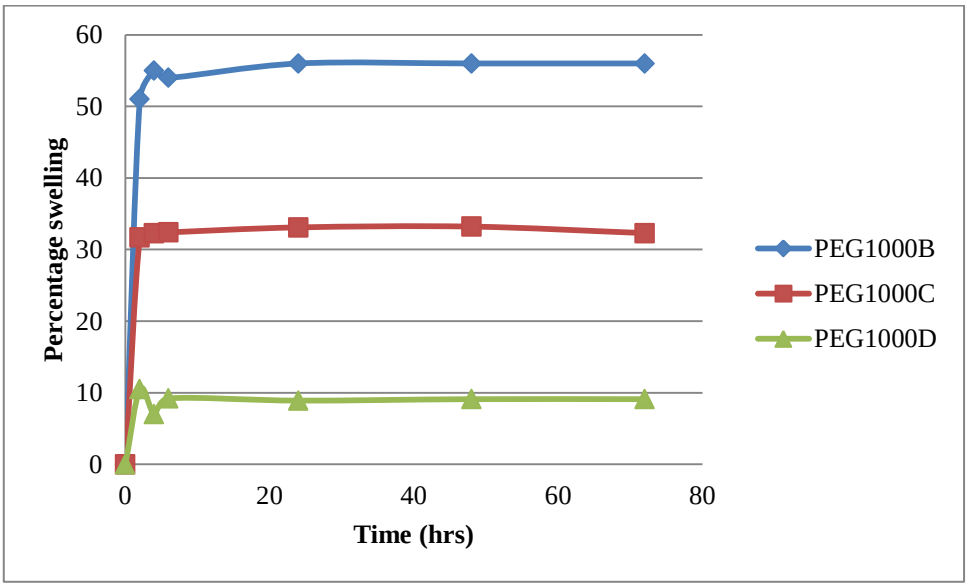

Swelling studies data for PEG1000 hydrogels

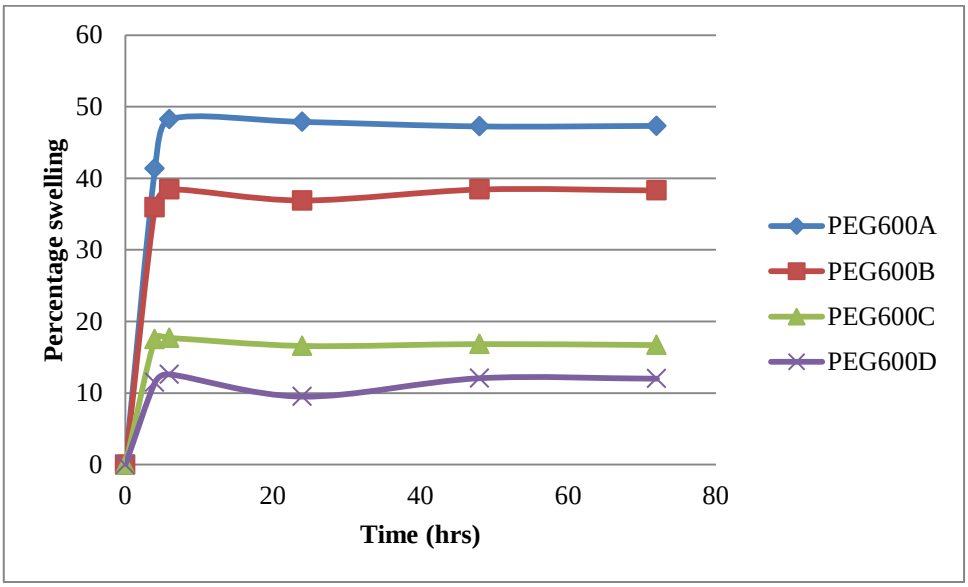

Swelling studies data for PEG600 hydrogels

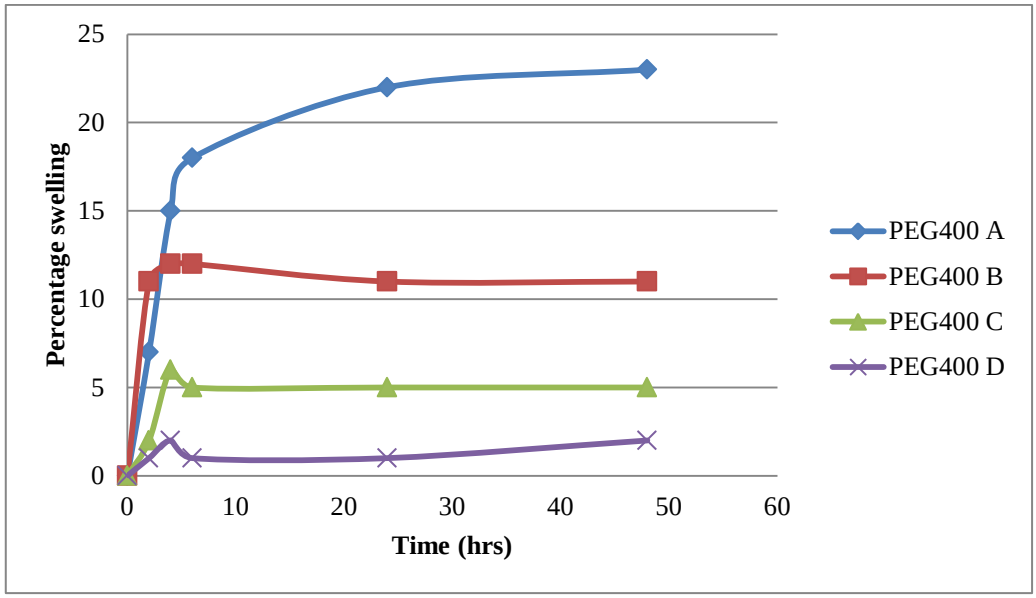

Swelling studies data for PEG400 hydrogels

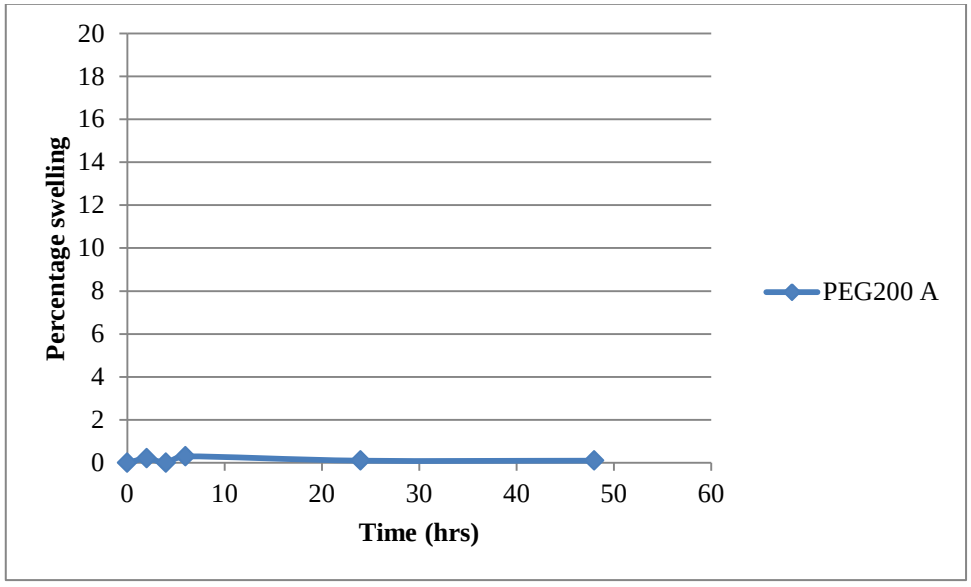

Swelling studies data for PEG200 hydrogel

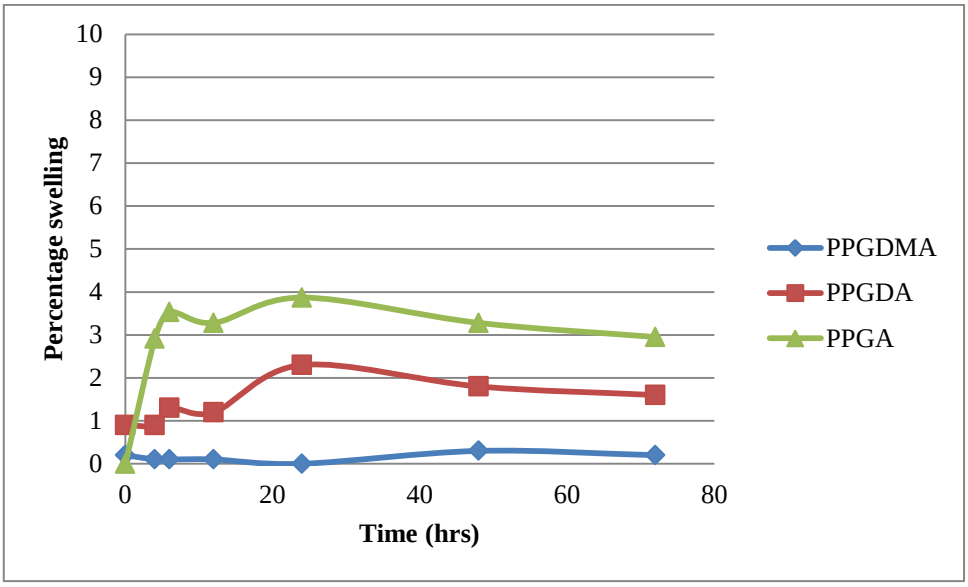

Swelling studies data for PPGDMA, PPGDA and PPGA hydrogels

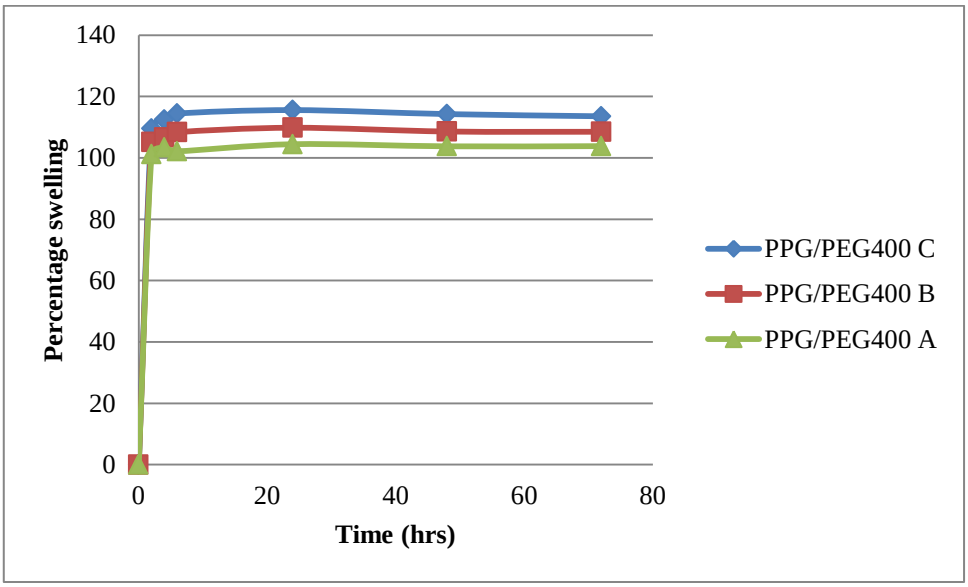

Swelling studies data for PPG/PEG400 hydrogels

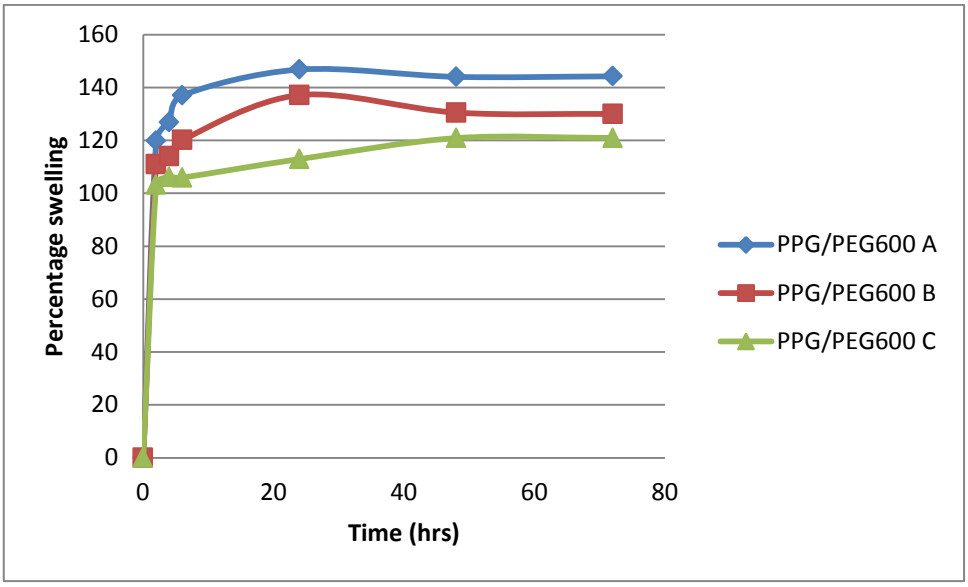

Swelling studies data for PPG/PEG600 hydrogels

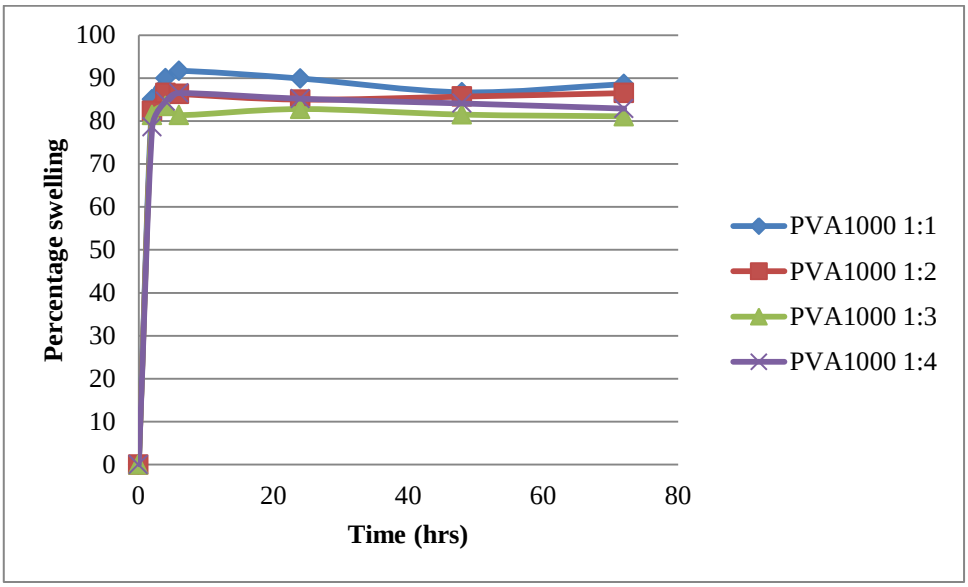

Swelling studies data for maleic PVA/PEG1000 hydrogel

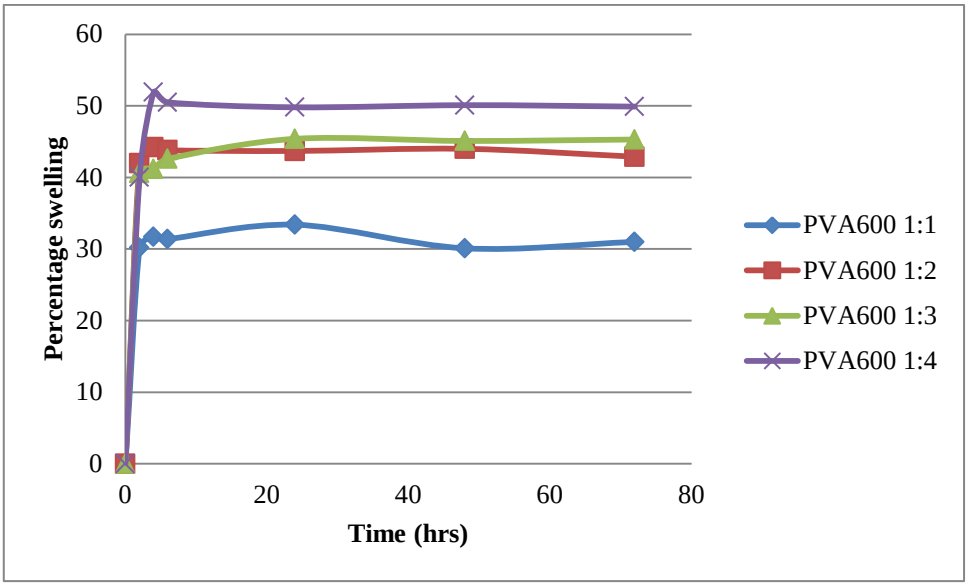

Swelling studies data for maleic PVA/PEG600 hydrogel

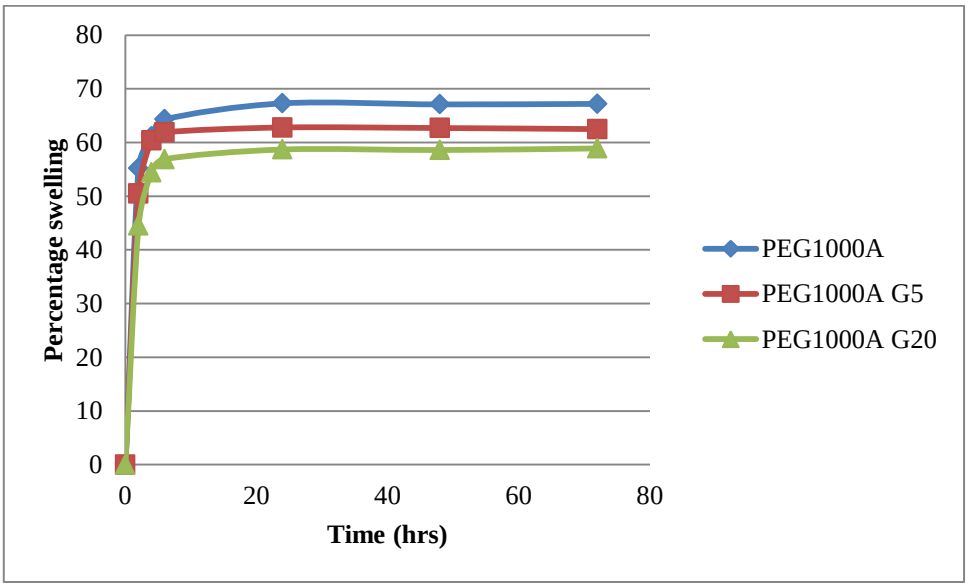

Swelling studies data for PEG1000A bioactive glass hydrogel based composites

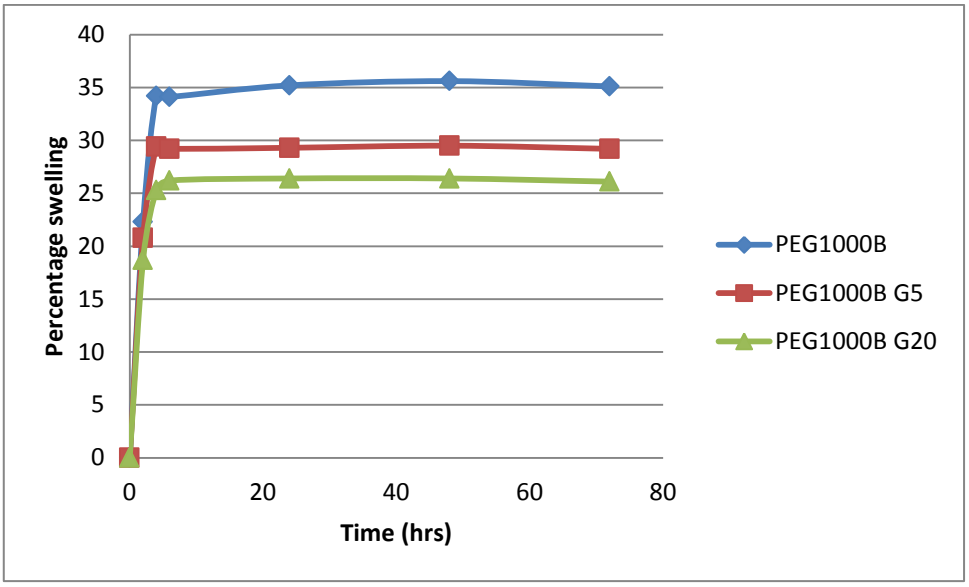

Swelling studies data for PEG1000B bioactive glass hydrogel based composites

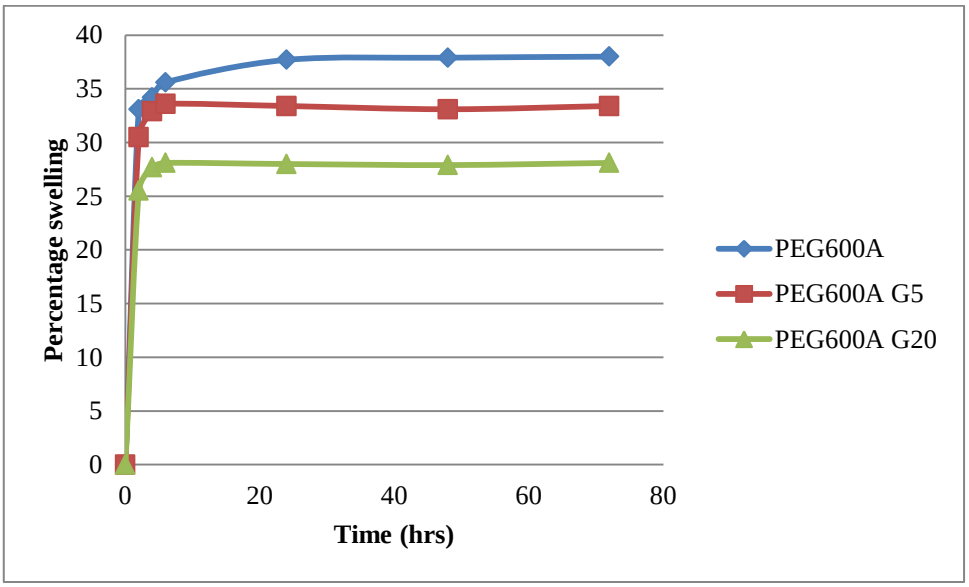

Swelling studies data for PEG600A bioactive glass hydrogel based composites

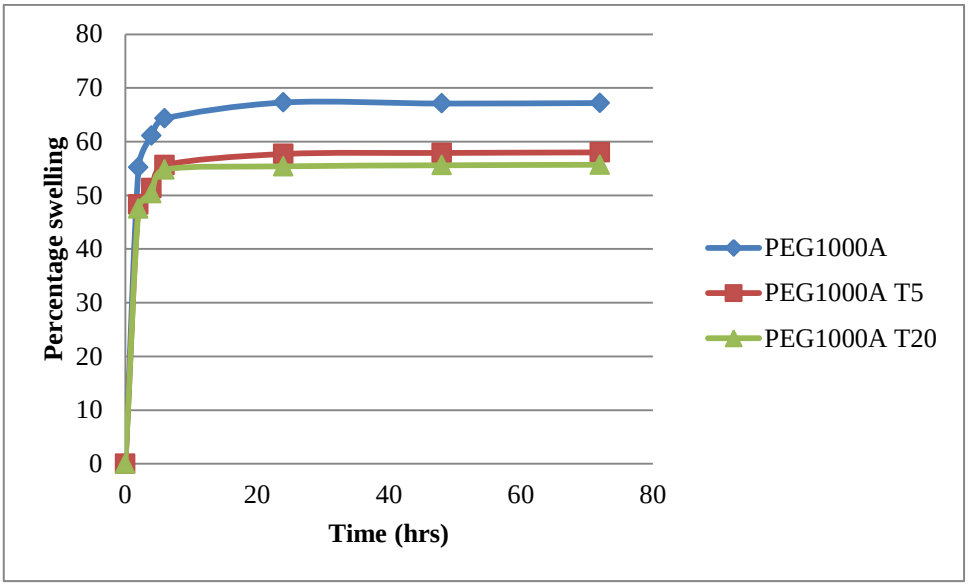

Swelling studies data for PEG1000A tricalcium phosphate hydrogel based composites

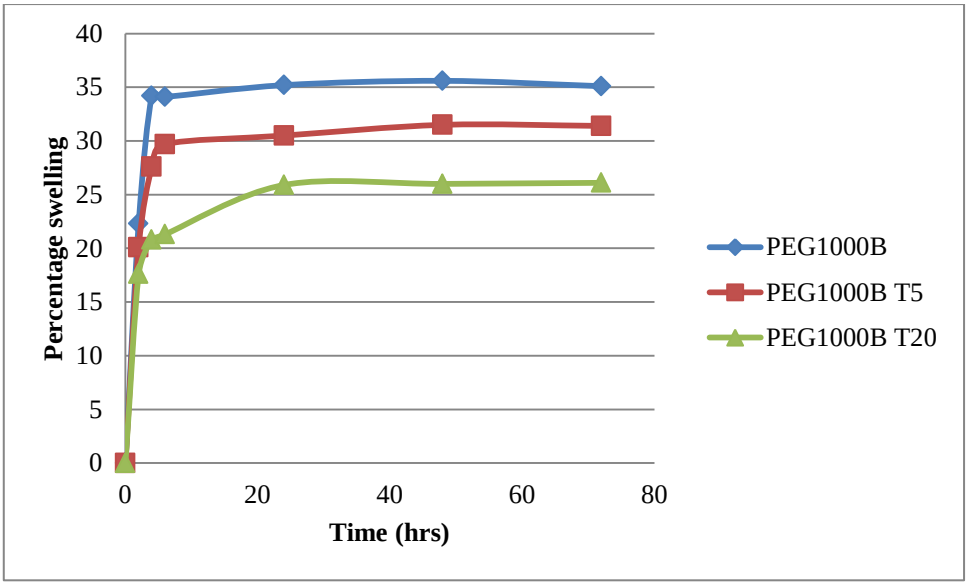

Swelling studies data for PEG1000B tricalcium phosphate hydrogel based composites

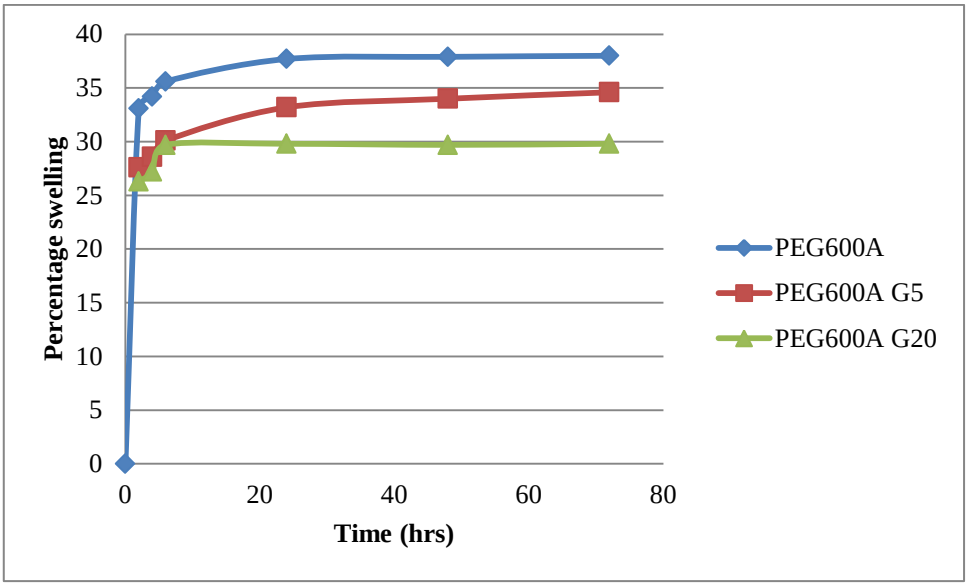

Swelling studies data for PEG600A tricalcium phosphate hydrogel based composites

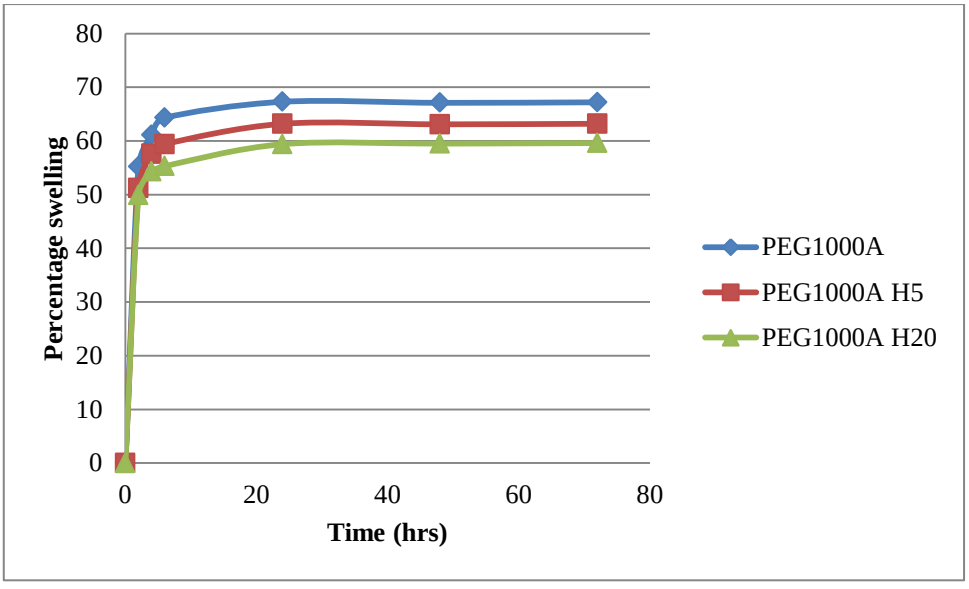

Swelling studies data for PEG1000A hydroxyapatite hydrogel based composites

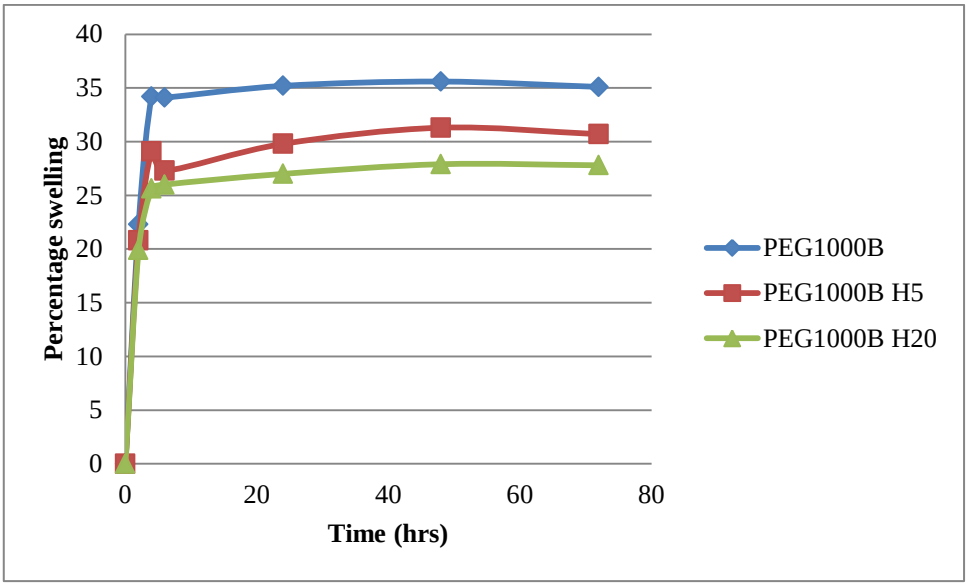

Swelling studies data for PEG1000b hydroxyapatite hydrogel based composites

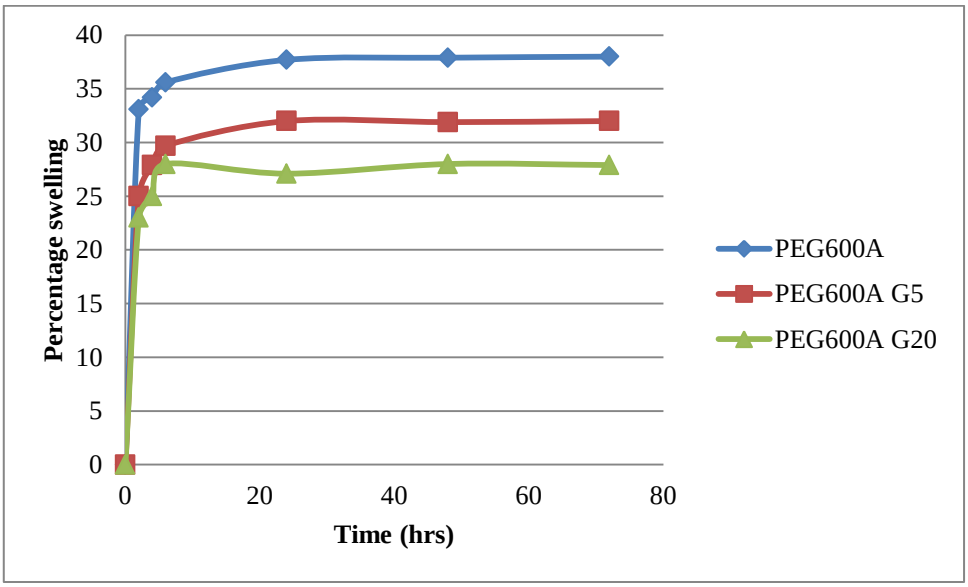

Swelling studies data for PEG600A hydroxyapatite hydrogel based composites

Appendix C

Strain sweep data for hydrogels and hydrogel based composites

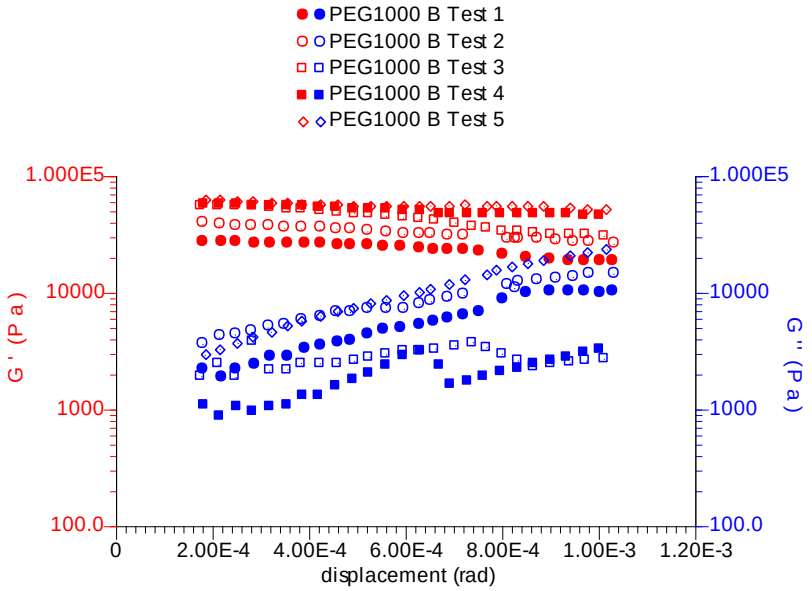

Strain sweep plot for PEG1000 B hydrogels

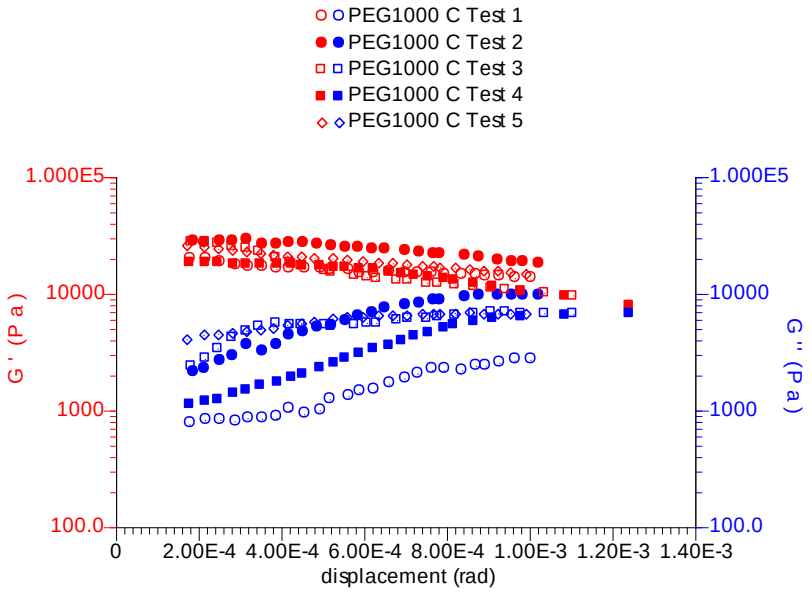

Strain sweep plot for PEG1000 C hydrogels

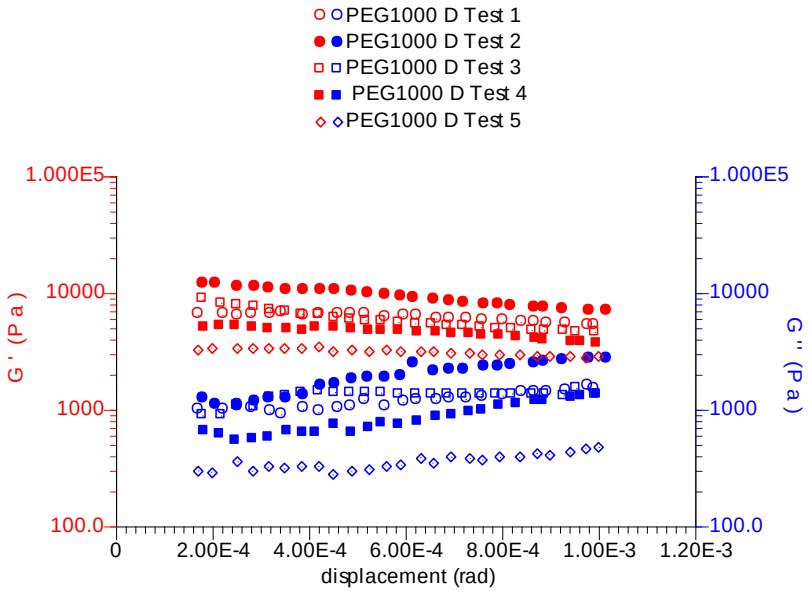

Strain sweep plot for PEG1000 D hydrogels

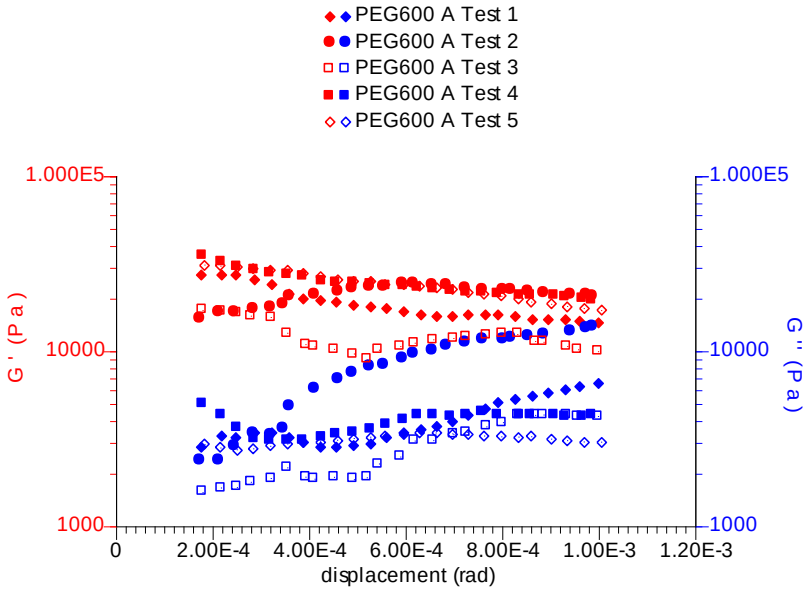

Strain sweep plot for PEG600 A hydrogels

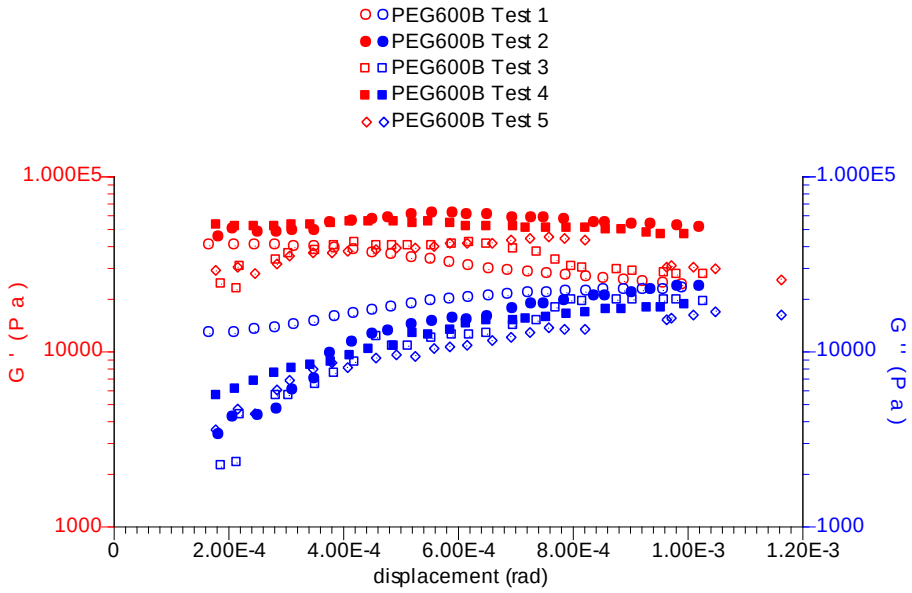

Strain sweep plot for PEG600 B hydrogels

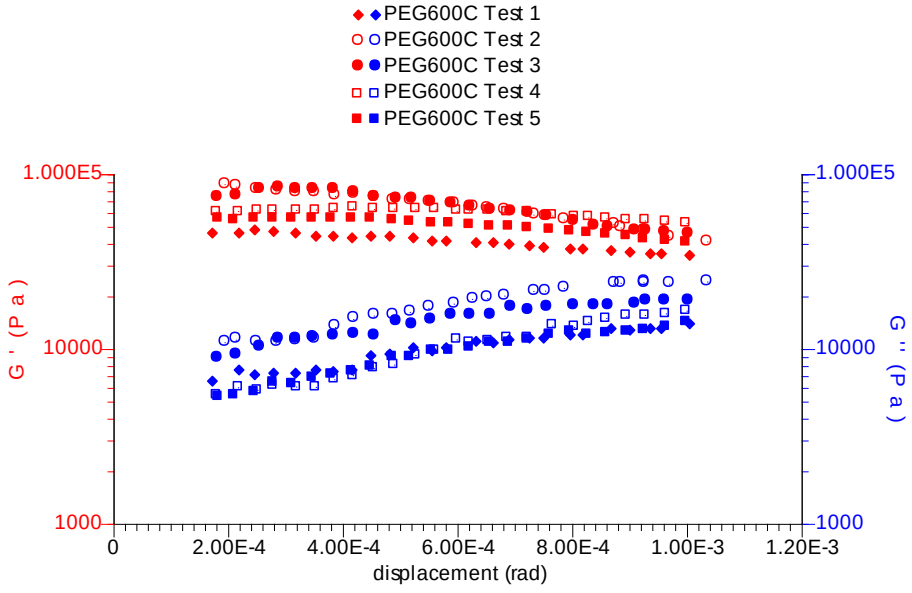

Strain sweep plot for PEG600 C hydrogels

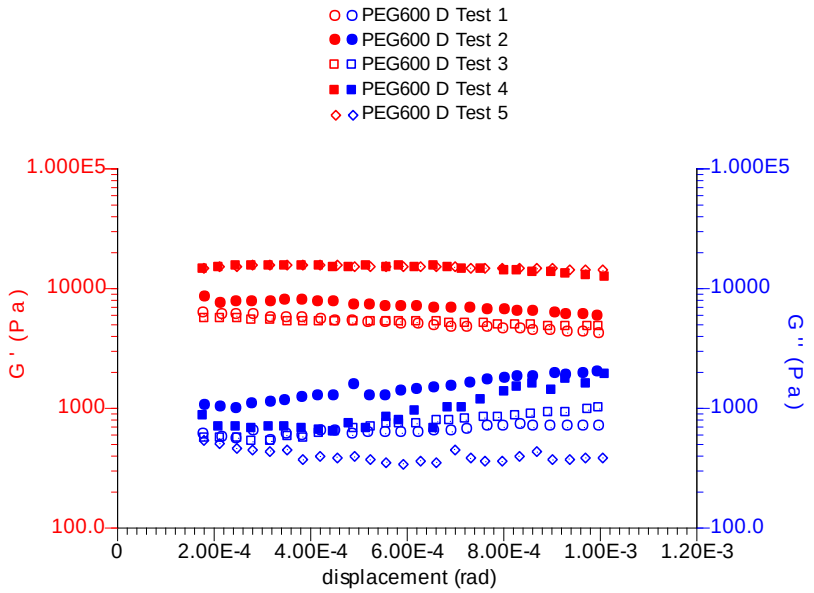

Strain sweep plot for PEG600 D hydrogels

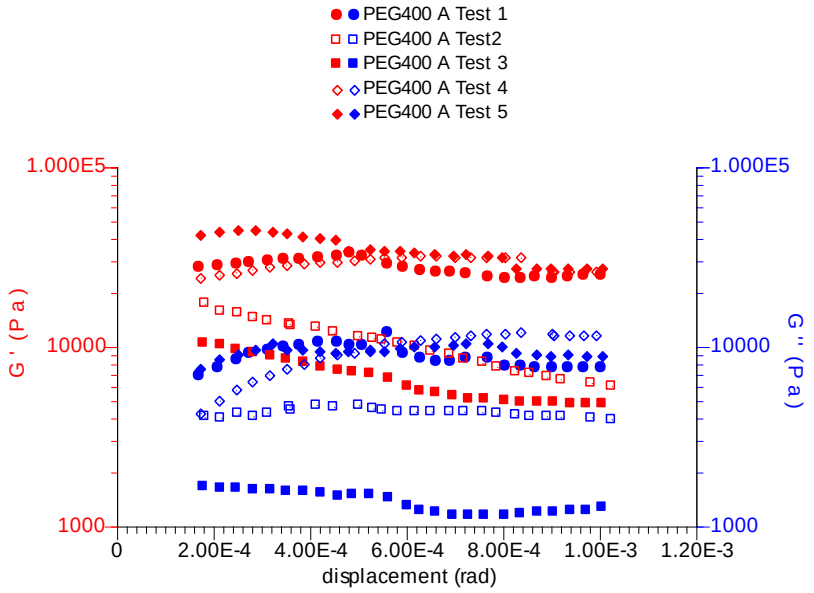

Strain sweep plot for PEG400 A hydrogels

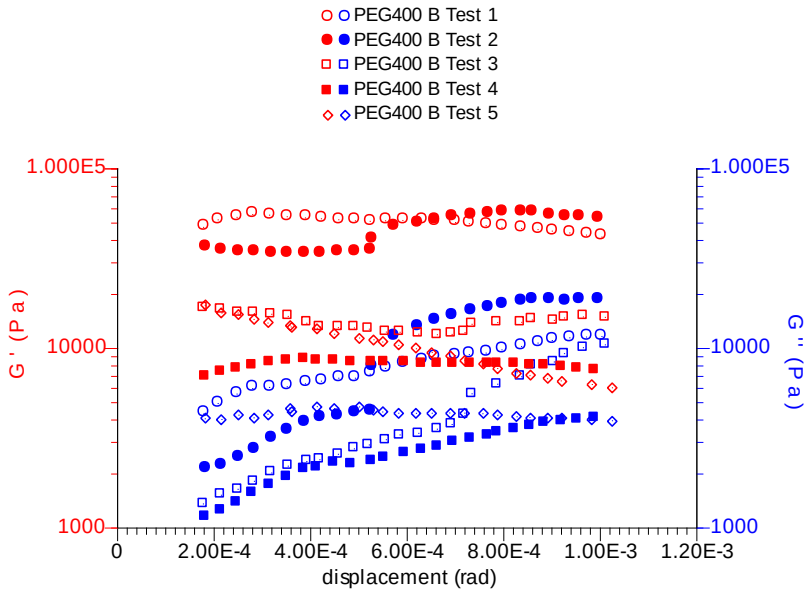

Strain sweep plot for PEG400 B hydrogels

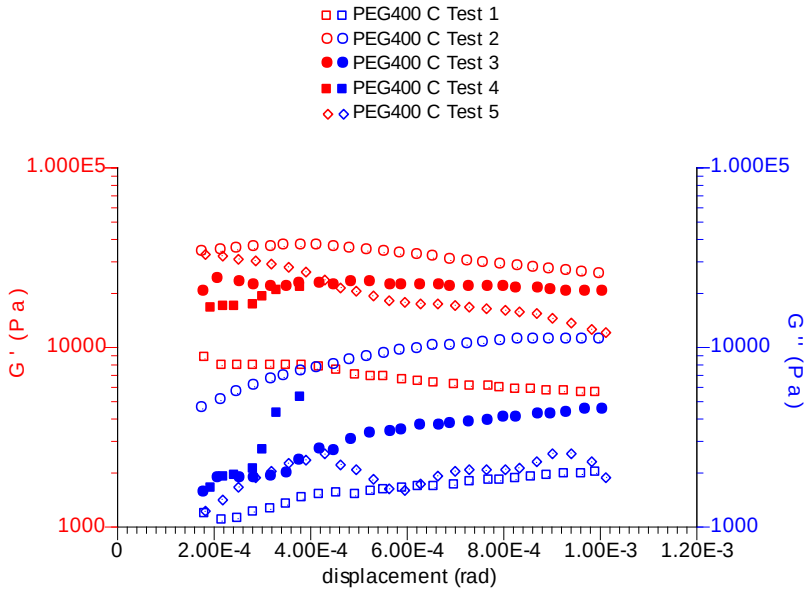

Strain sweep plot for PEG600 C hydrogels

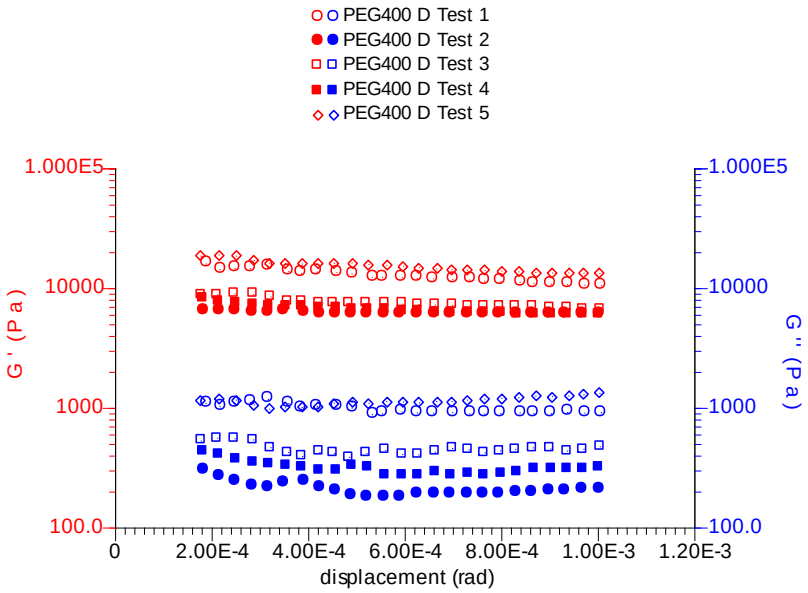

Strain sweep plot for PEG400 D hydrogels

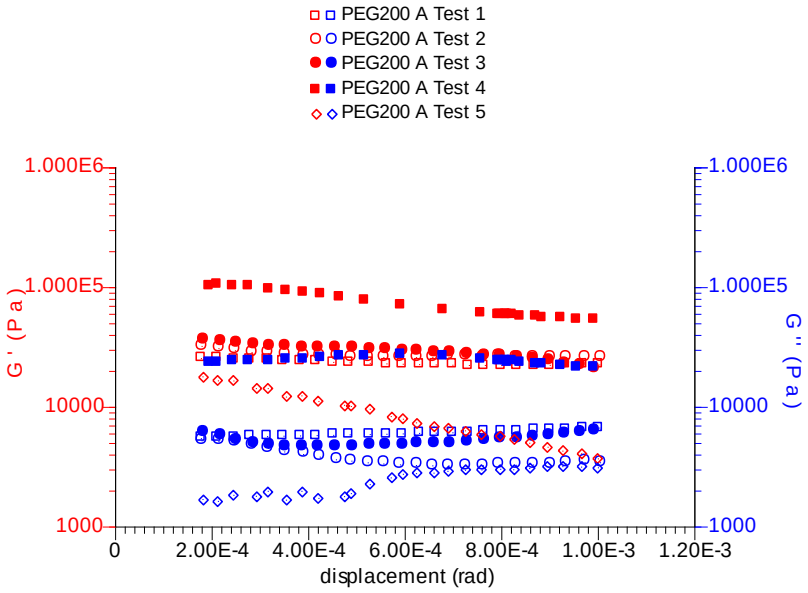

Strain sweep plot for PEG200 A hydrogels

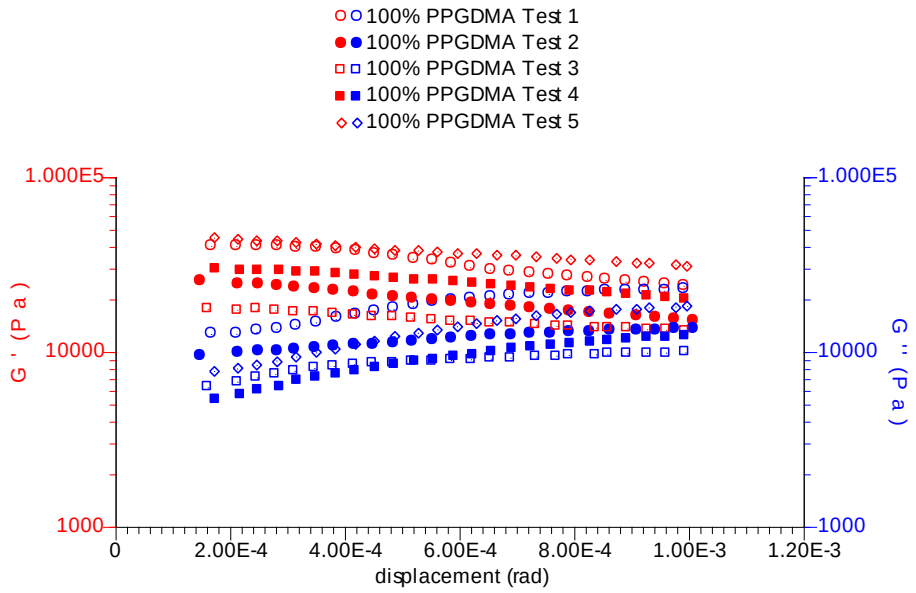

Strain sweep plot for 100% PPGDMA hydrogels

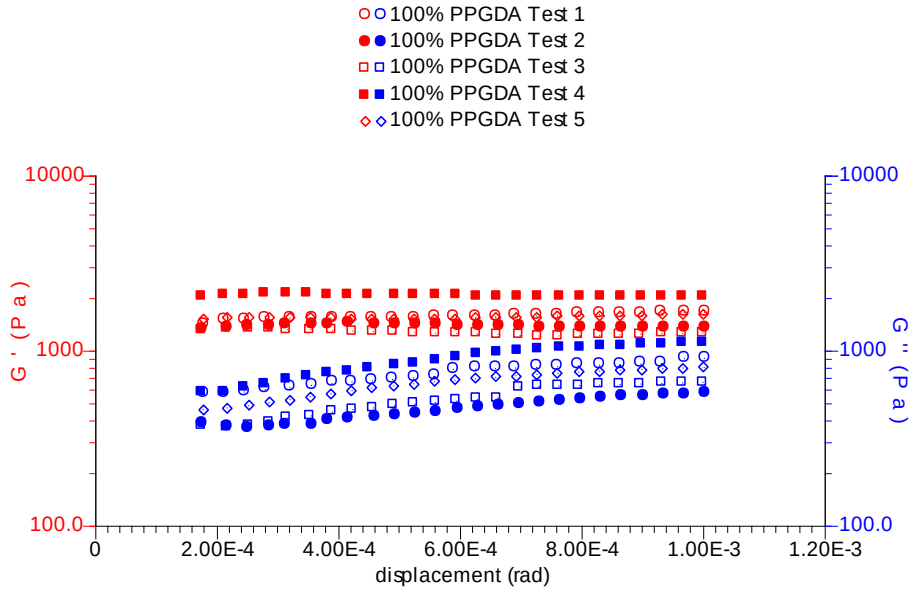

Strain sweep plot for 100% PPGDA hydrogels

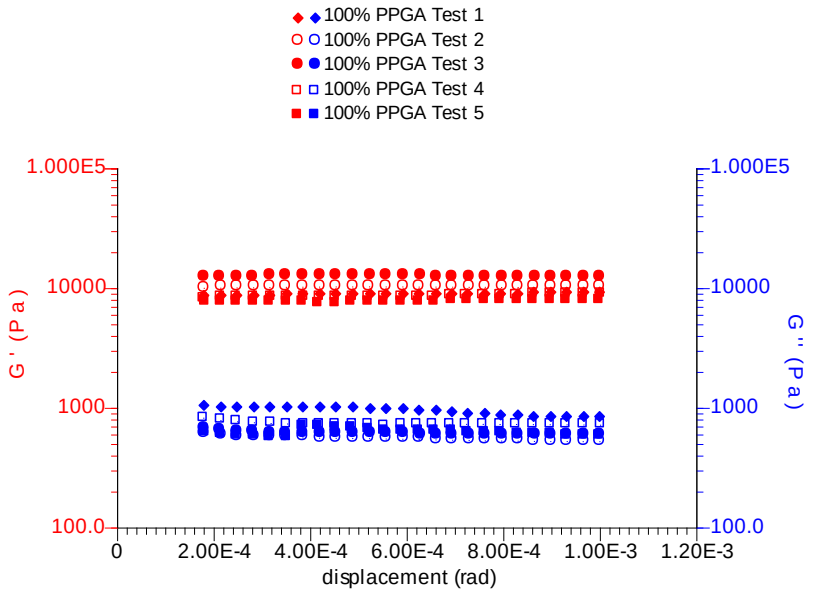

Strain sweep plot for 100% PPGA hydrogels

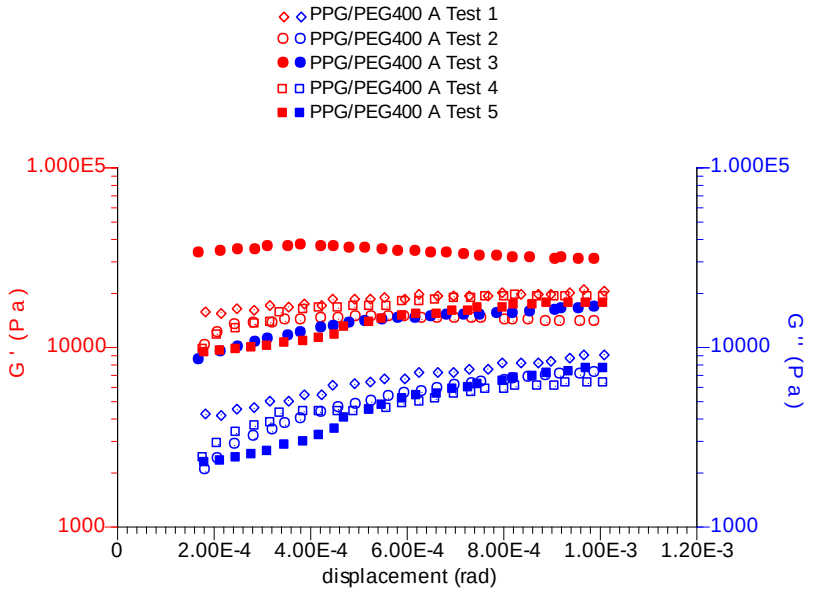

Strain sweep plot for PPG/PEG400 A hydrogels

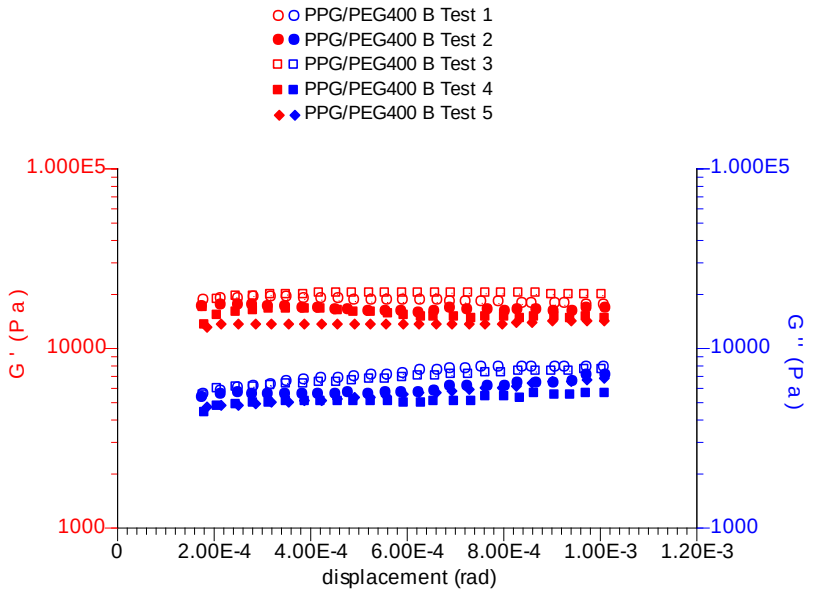

Strain sweep plot for PPG/PEG400 B hydrogels

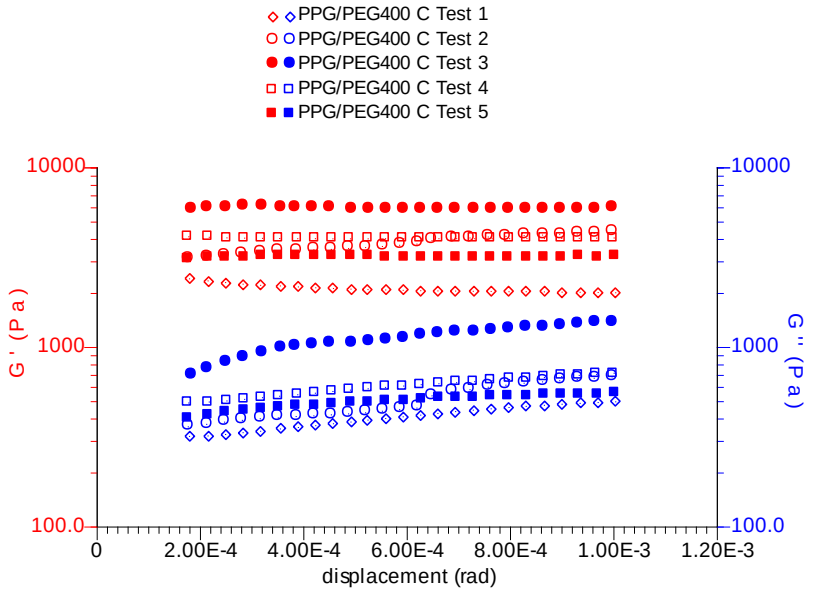

Strain sweep plot for PPG/PEG400 C hydrogels

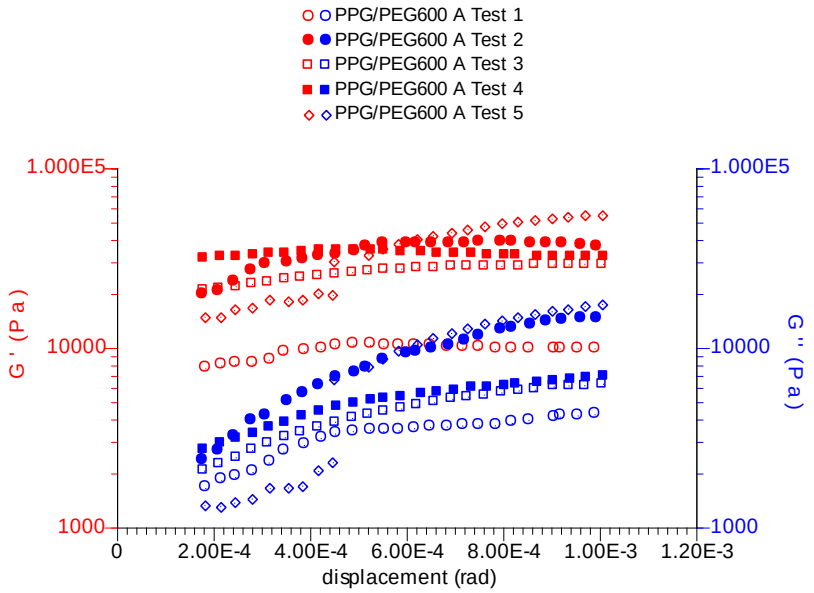

Strain sweep plot for PPG/PEG600 A hydrogels

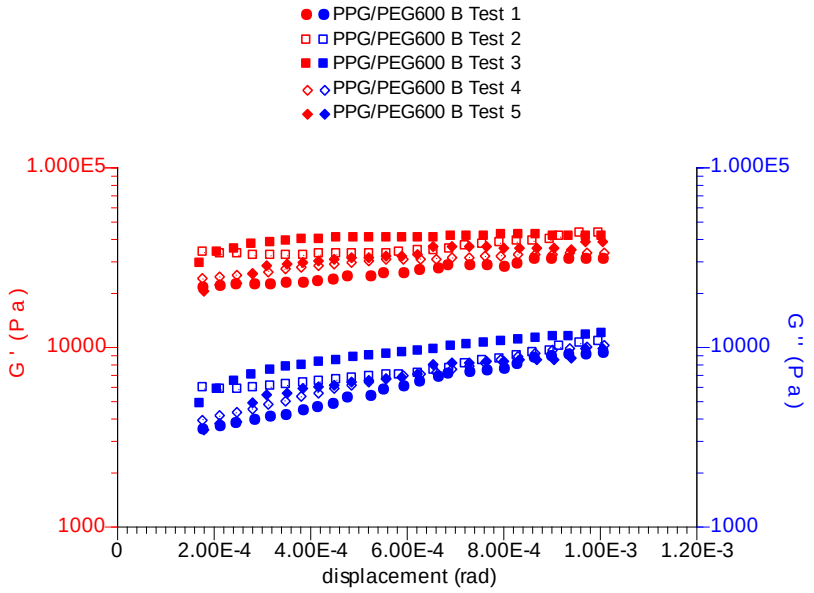

Strain sweep plot for PPG/PEG600 B hydrogels

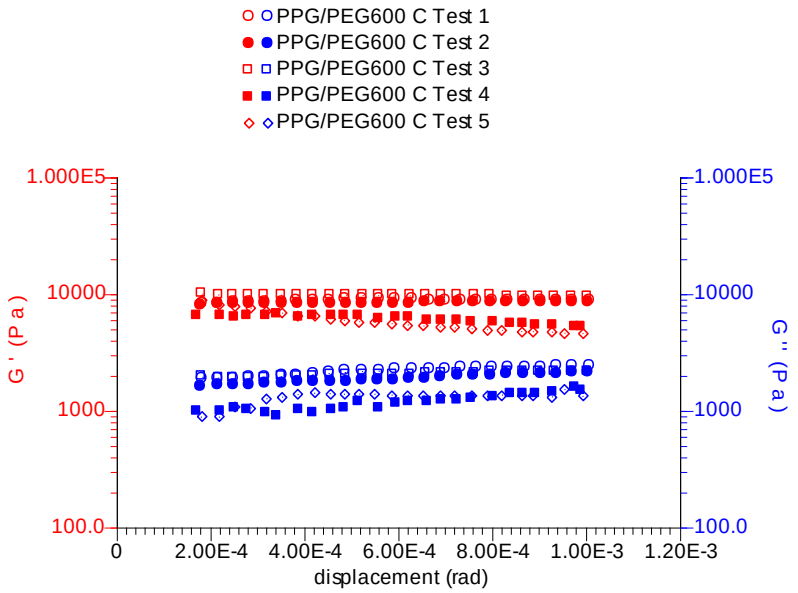

Strain sweep plot for PPG/PEG600 C hydrogels

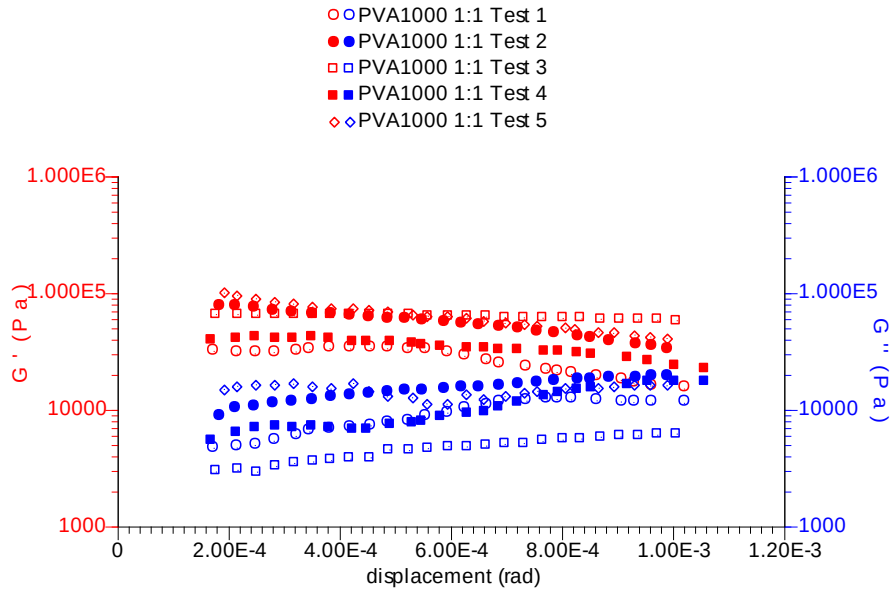

Strain sweep plot for PVA1000 1:1 hydrogels

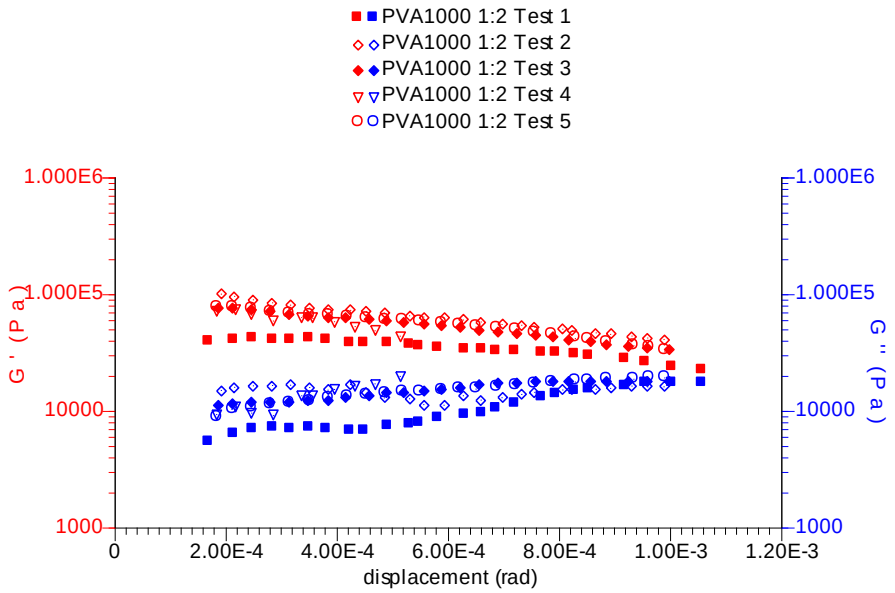

Strain sweep plot for PVA1000 1:2 hydrogels

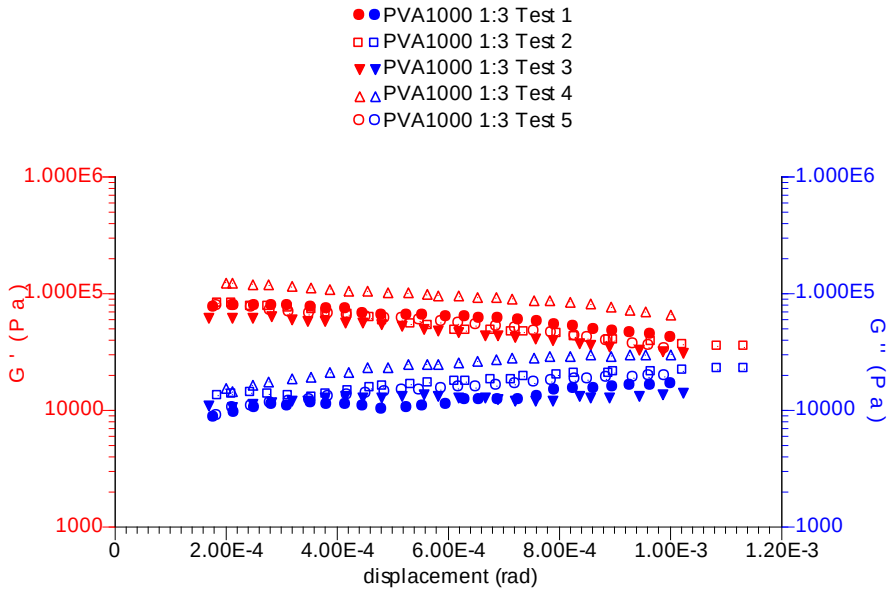

Strain sweep plot for PVA1000 1:3 hydrogels

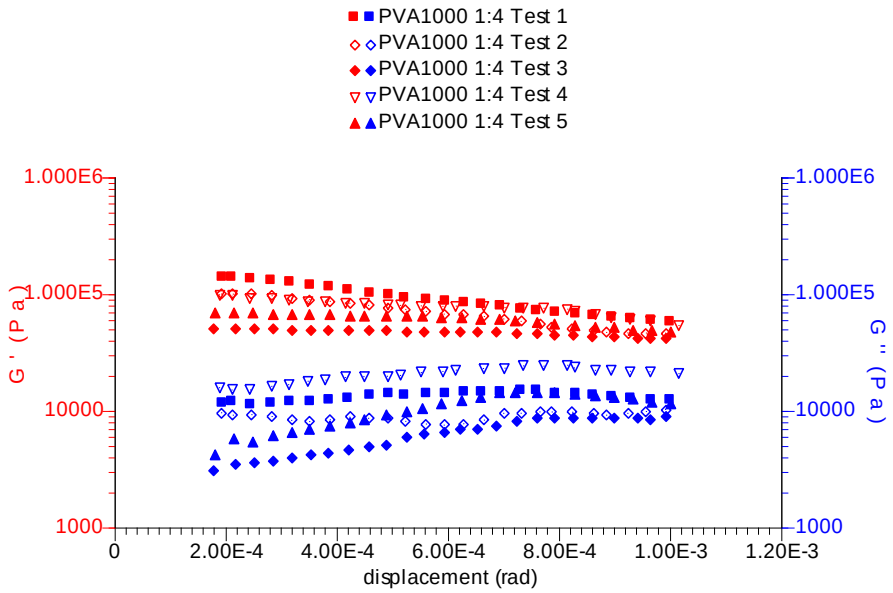

Strain sweep plot for PVA1000 1:4 hydrogels

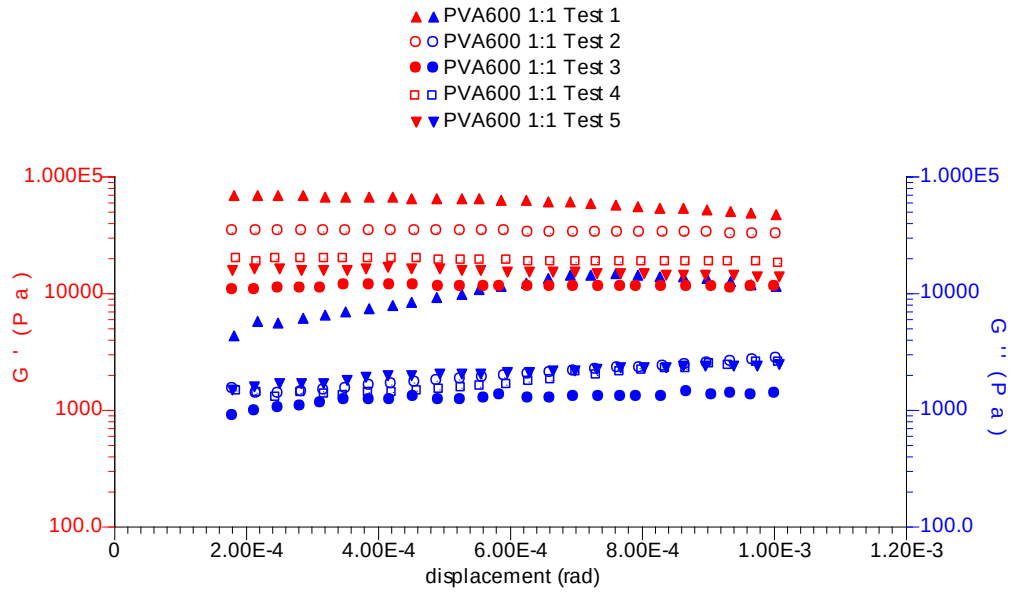

Strain sweep plot for PVA600 1:1 hydrogels

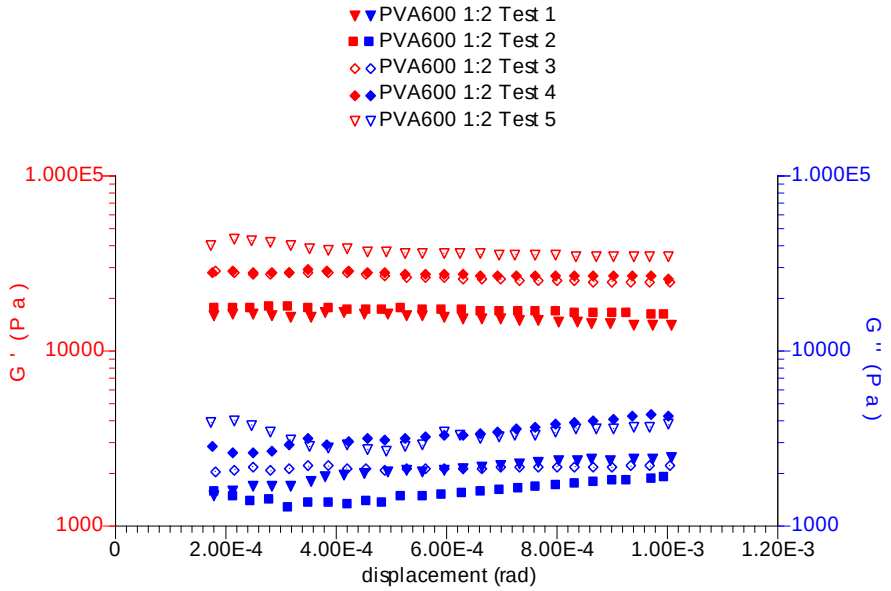

Strain sweep plot for PVA600 1:2 hydrogels

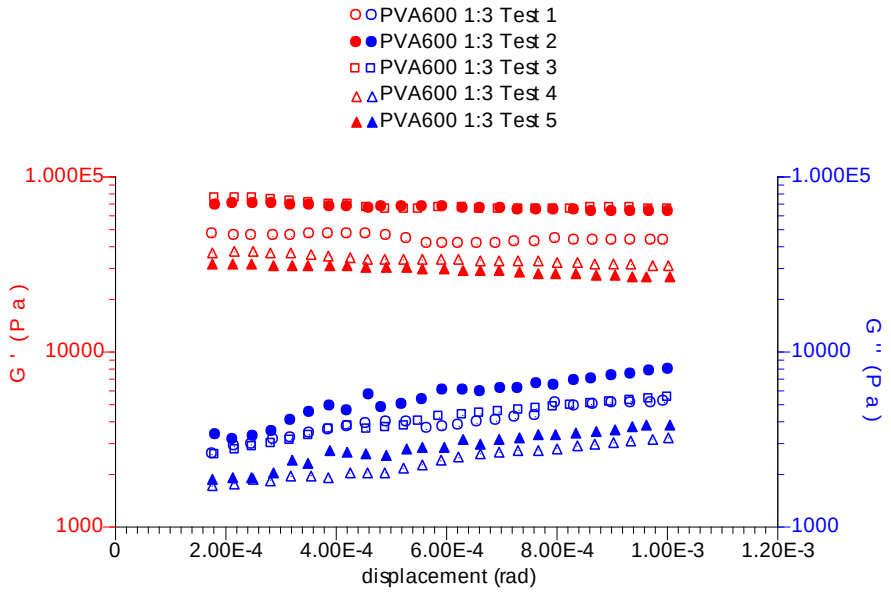

Strain sweep plot for PVA600 1:3 hydrogels

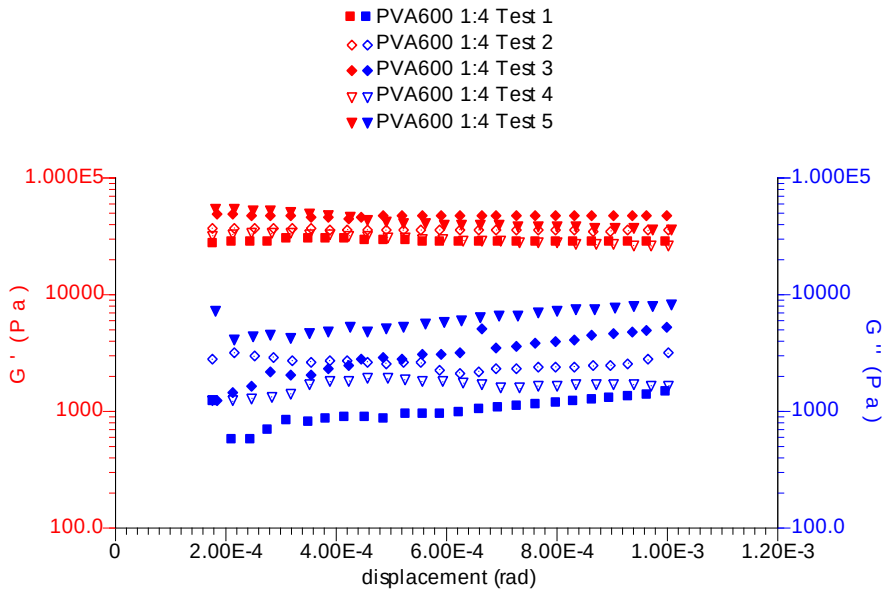

Strain sweep plot for PVA600 1:4 hydrogels

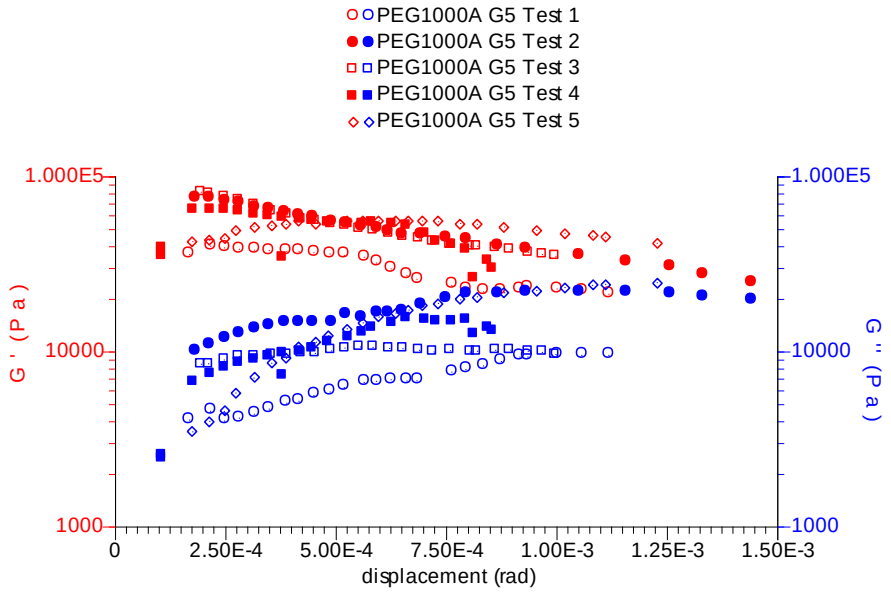

Strain sweep plot for PEG1000A G5 hydrogel based composites

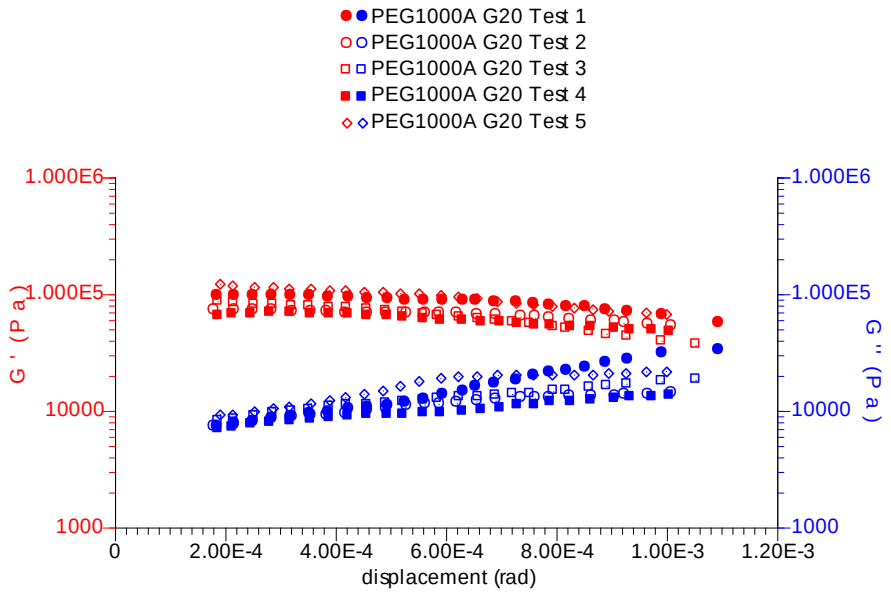

Strain sweep plot for PEG1000A G20 hydrogel based composites

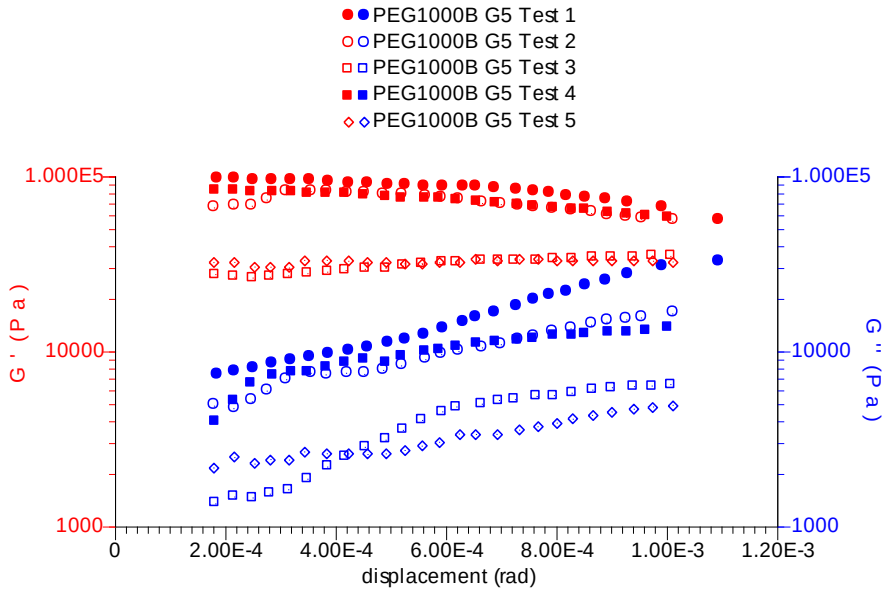

Strain sweep plot for PEG1000B G5 hydrogel based composites

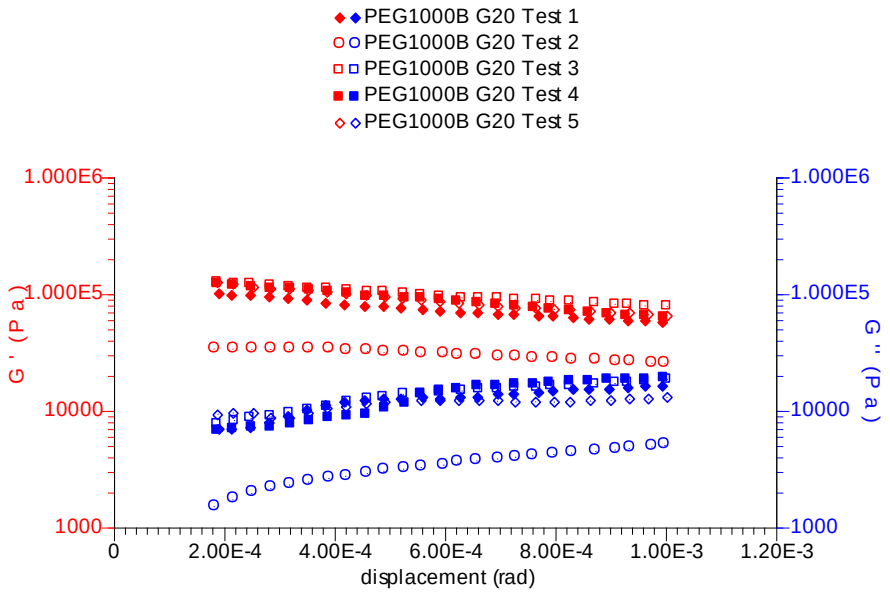

Strain sweep plot for PEG1000B G20 hydrogel based composites

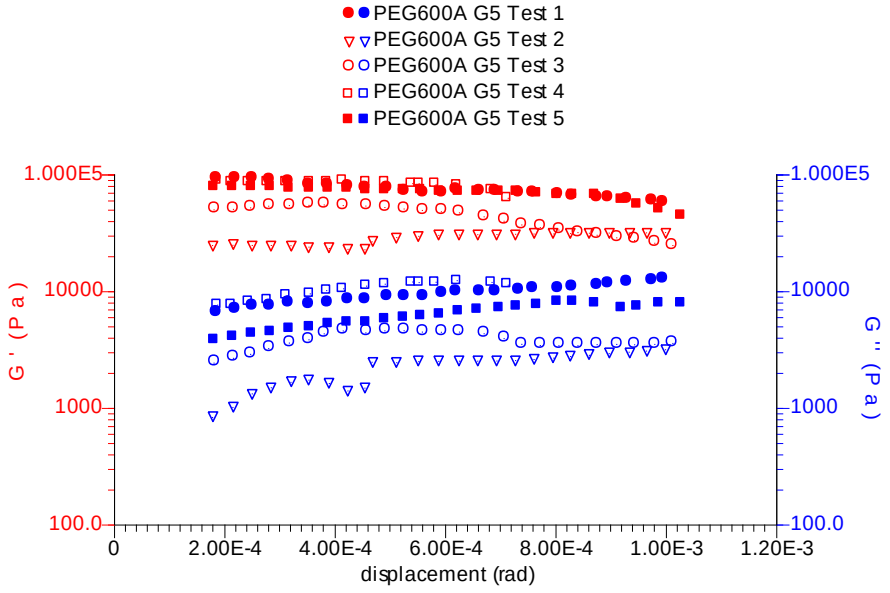

Strain sweep plot for PEG600A G5 hydrogel based composites

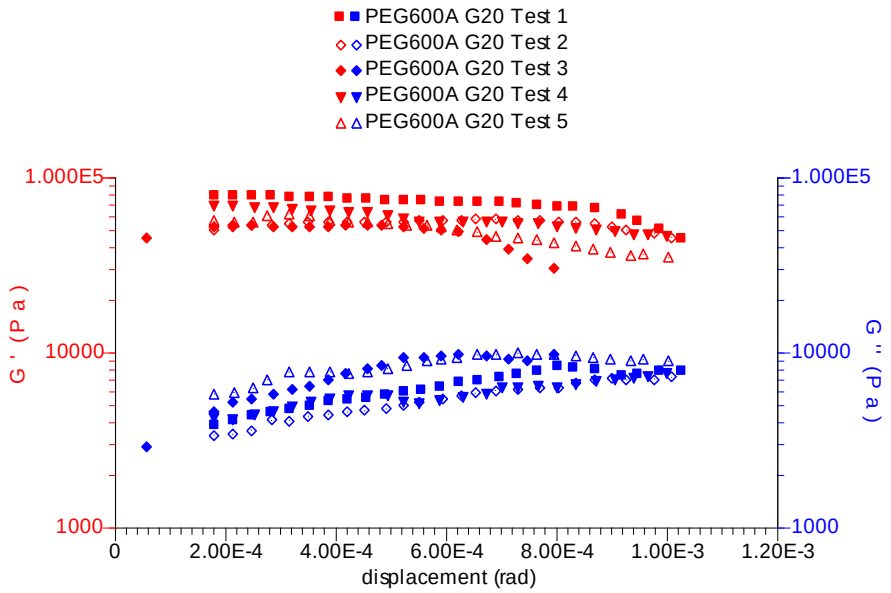

Strain sweep plot for PEG600A G20 hydrogel based composites

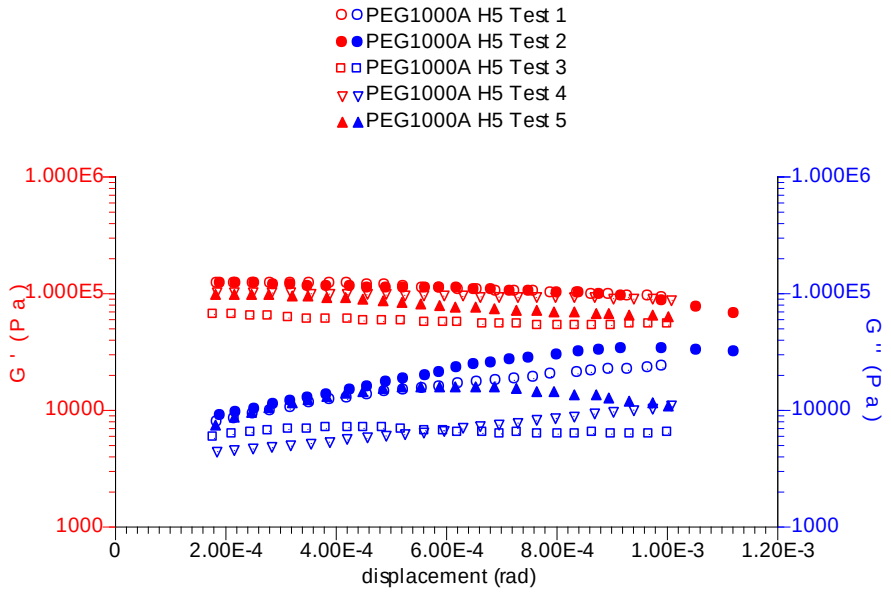

Strain sweep plot for PEG1000A H5 hydrogel based composites

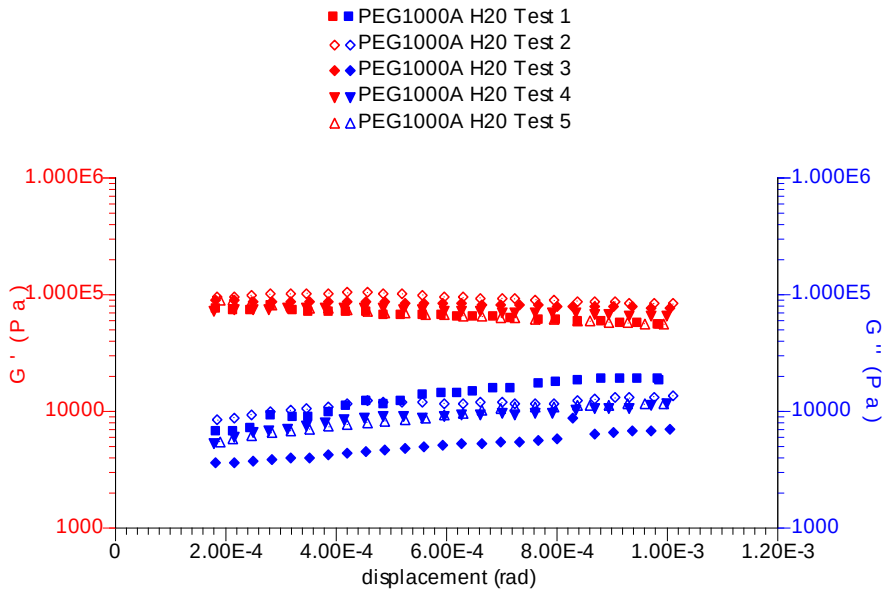

Strain sweep plot for PEG1000A H20 hydrogel based composites

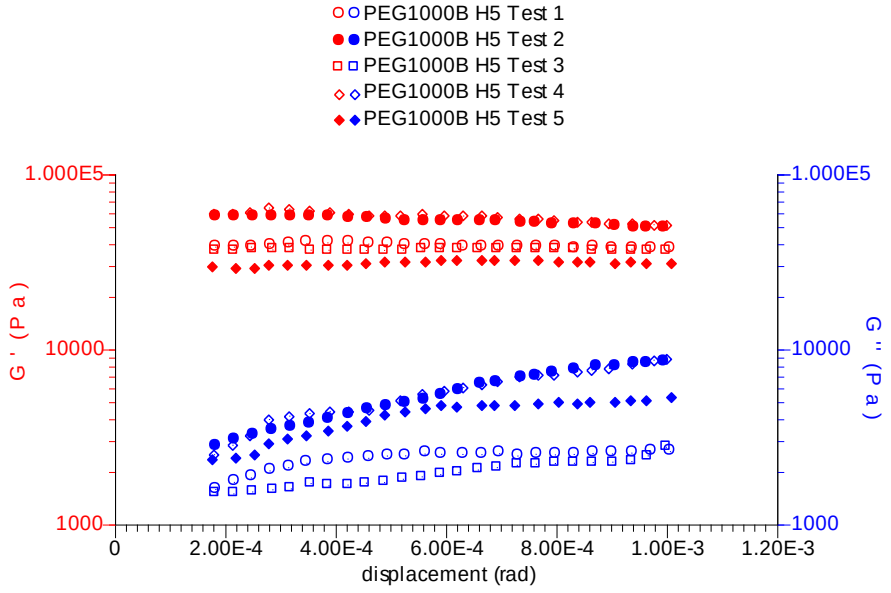

Strain sweep plot for PEG1000B H5 hydrogel based composites

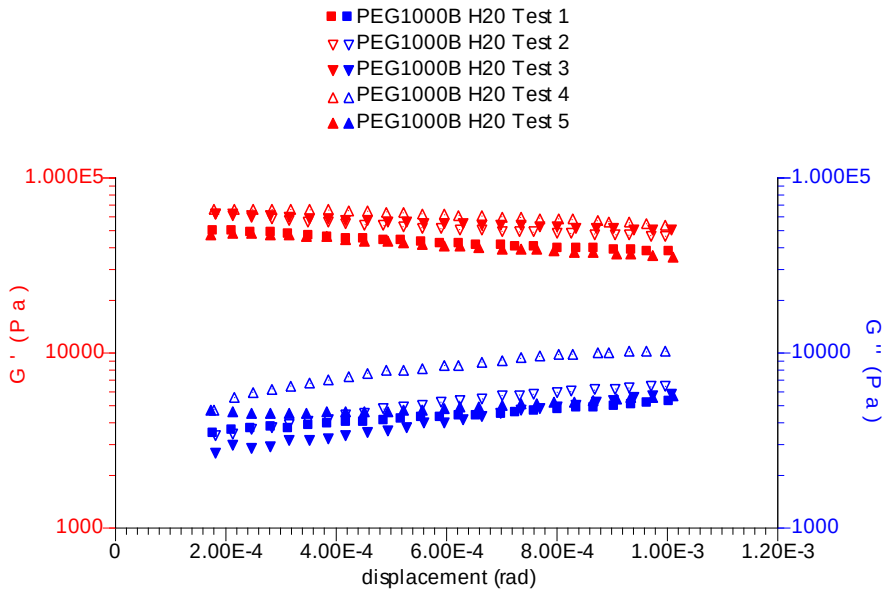

Strain sweep plot for PEG1000B H20 hydrogel based composites

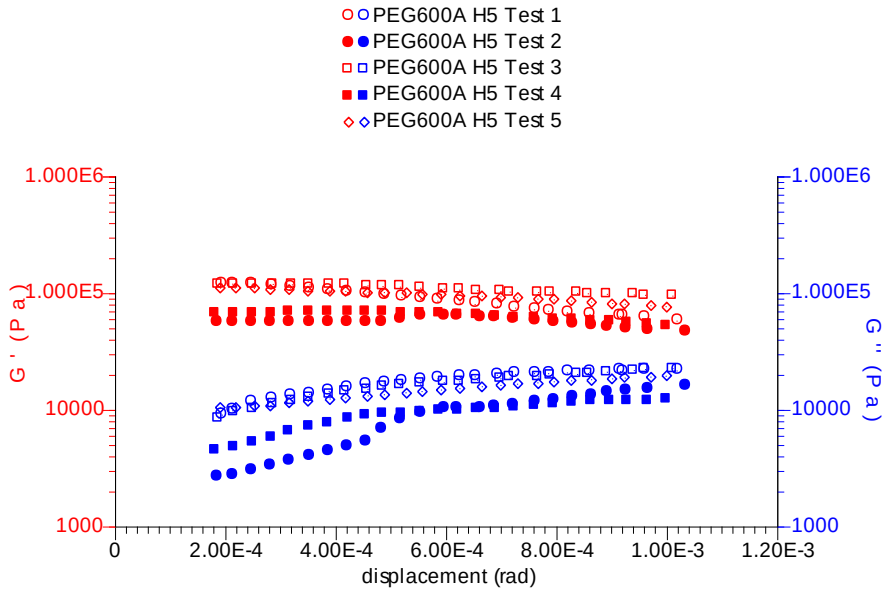

Strain sweep plot for PEG600A H5 hydrogel based composites

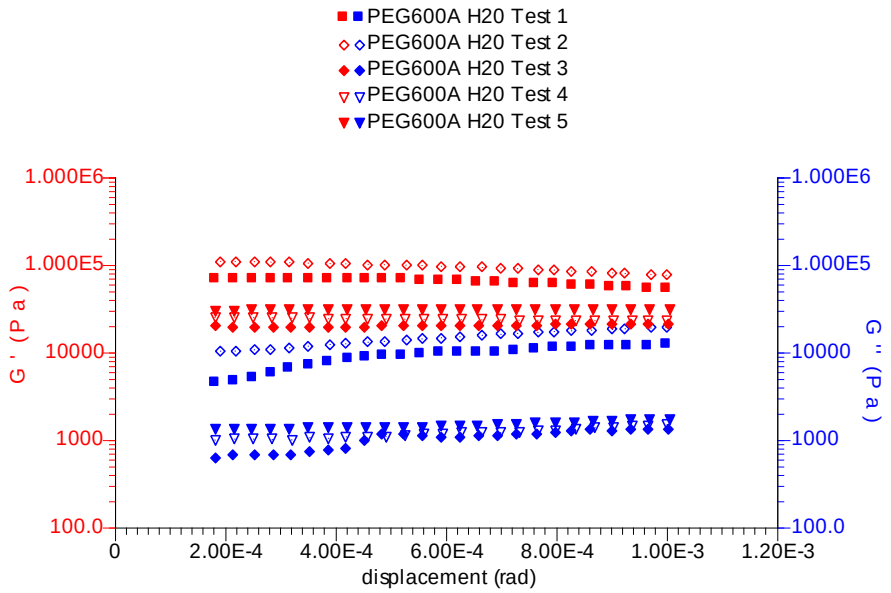

Strain sweep plot for PEG600A H20 hydrogel based composites

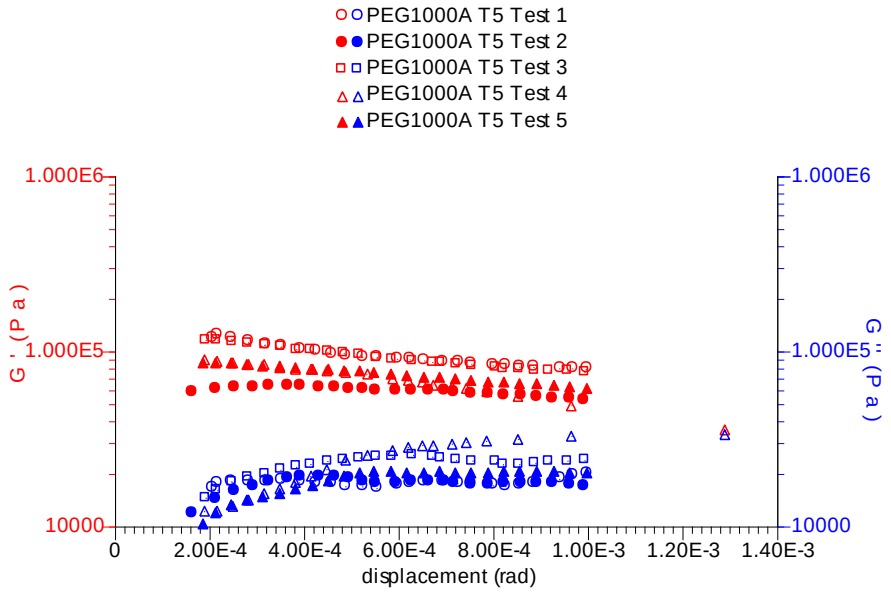

Strain sweep plot for PEG1000A T5 hydrogel based composites

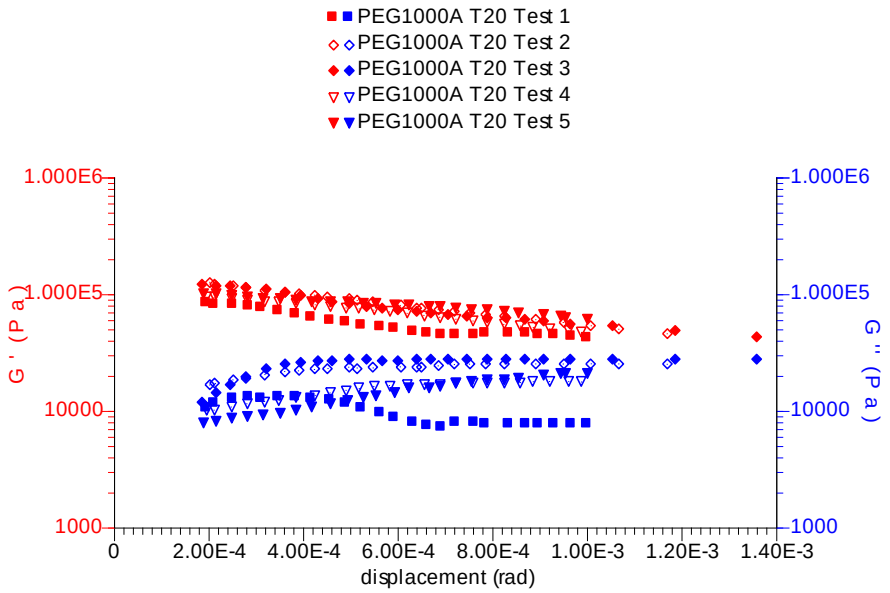

Strain sweep plot for PEG1000A T20 hydrogel based composites

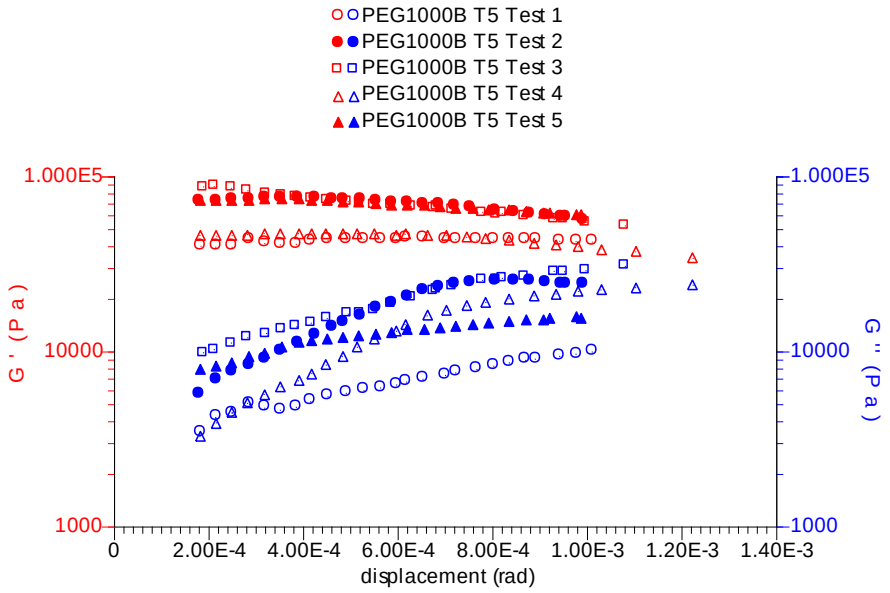

Strain sweep plot for PEG1000B T5 hydrogel based composites

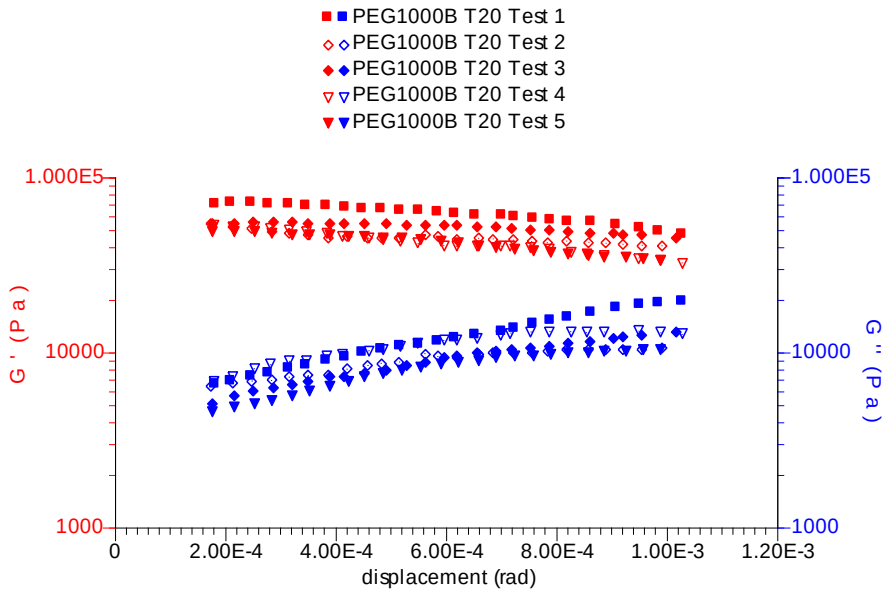

Strain sweep plot for PEG1000B T20 hydrogel based composites

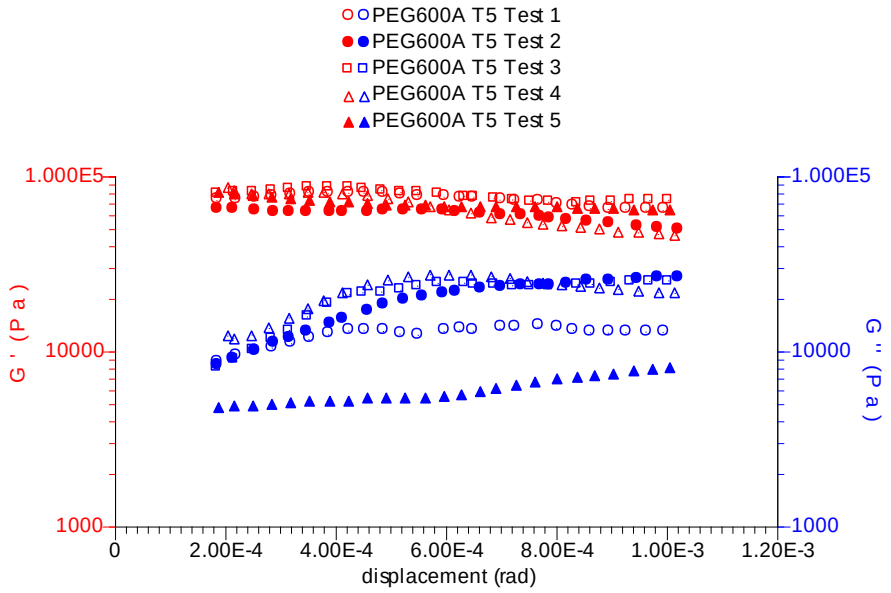

Strain sweep plot for PEG600A T5 hydrogel based composites

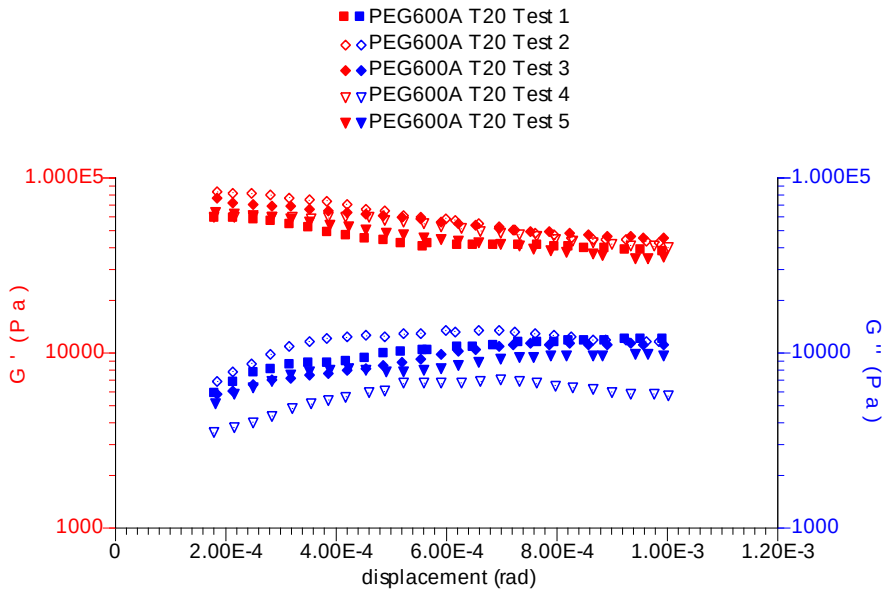

Strain sweep plot for PEG600A T20 hydrogel based composites

Publications

Papers published

I. Killion *et al*. (2011) Mechanical properties and thermal behaviour of PEGDMA hydrogels for potential bone regeneration application. Journal of the Mechanical Behaviour of Biomedical Materials, 4 (7) pp. 1219-1227.

II. Killion *et al*. (2012) Modulating the mechanical properties of photopolymerised polyethylene glycol–polypropylene glycol hydrogels for bone regeneration. Journal of Materials Science, 47 (18) pp. 6577-6585.

III. Killion *et al*. (2013) Hydrogel/Bioactive Glass Composites for Bone Regeneration Applications: Synthesis and Characterisation. Material Science and Engineering: C 33 (1) pp. 4203-4212

IV. Killion *et al*. (2013) Development Of Synthetic Alternatives For Bone Tissue Engineering. Australian Journal of Basic and Applied Sciences. 7(5) 150-156.

V. Killion *et al*. Compressive strength and bioactivity properties of photopolymerisable hybrid composite hydrogels for bone tissue engineering. International Journal of Polymeric Materials (in press).

VI. Killion *et al*., Fabrication and *in vitro* biological evaluation of hydroxyapatite hydrogel composites for bone regeneration. Journal of Biomaterials Applications (in press).

Book Chapter

I. Geever L., Killion *et al.* (2012). The role of hydrogels in the development of artifical bone substitutes Superscript: Hydrogels Synthesis Characterisation and Applications. Italy: Nova Biomedical. 53-92.

Oral presentations

I. Killion *et al*. (2010), A Study Into The Mechanical Properties And Thermal Behaviour Of PEGDMA Hydrogels For Potential Bone Regeneration

Application, Materials Ireland Annual Conference, Dublin, Ireland, December 13-14, 2010.

II. Killion *et al*. (2012), Synthesis and Characterisation of Hydrogel Based Composites for Bone Regeneration, International Malaysia-Ireland Joint Symposium, Kuala Lumpar, Malaysia, June 18-19, 2012.

Conference preceedings

I. Killion *et al*. (2011), Synthesis and Characterisation of Photopolymerisable Hydrogels for Application in Bone Regeneration, International Malaysia-Ireland Joint Symposium, Athlone Ireland, June 9-11, 2011.

II. Killion *et al*. (2011), Mechanical Properties, Thermal and Drug Release Behaviour of PEGDMA Hydrogels for Potential Bone Regeneration Application, European Society of Biomaterials, Dublin, Ireland, September 4-9, 2011.